

**Western Australia School of Mines
Department of Exploration Geophysics**

**Inversion of multiple geophysical data sets
using petrophysical constraints**

Duy Thong Kieu

**This thesis is presented for the Degree of
Doctor of Philosophy
of
Curtin University**

January 2018

This work is dedicated to my family.

DECLARATION

“To the best of my knowledge and belief this thesis contains no material previously published by any other person except where due acknowledgment has been made. This thesis contains no material which has been accepted for the award of any other degree or diploma in any university.”

Signature:

Date: 15/01/2018

ABSTRACT

Geophysical methods provide a powerful tool to investigate the earth subsurface by turning raw data into earth model representative of the earth's characteristics. Accordingly, the models are interpreted for different purposes such as geological maps, geotechnical design, guiding further exploration or locating further drill holes. A critical issue in the inversion process is a non-unique solution, in that are many models that adequately explain the measured data. Thus, my thesis focuses on reducing the ambiguity of the inversion solution and simultaneously building a geologically plausible model.

I have improved existing damped least squares inversion algorithms that invert a single dataset by utilising fuzzy cluster based constraints and integration of prior information via fuzzy clustering techniques. As the subsurface is mostly comprised of distinct rock units that are likely formed in the same geological conditions the properties of units should be fairly uniform, with sharp changes at the boundaries between the units. Hence, an inversion process that builds "blocky" models is sought and the fuzzy cluster method lends itself naturally to perform this task. I have used the fuzzy cluster methods as an extra constraint that in the inversion objective function that assists the inversion to build a model with characteristics more relatable to geology. In addition, fuzzy clustering introduces 'soft constraints' within the inversion, so there is more tolerance of errors in the constraints and dealing with unclear situations in the geology. By applying different variants of the fuzzy c-means clustering, my inversion approach can incorporate both petrophysical statistics and spatial distribution of parameter information. Specifically, my work focuses on the inversion of post stack seismic reflection and magnetotelluric (MT) data, both as separate inversion processes and as a co-operative technique.

Two co-operative strategies have been designed: sequential and parallel cooperative inversion of MT and seismic data based on fuzzy clustering coupling. In the sequential process, the two inversion processes run in sequence without any sharing of information during the iterative inversion process: MT inversion is run first, and then the inversion of seismic data follow using the low frequency spatial information supplied by the MT inversion. The parallel cooperative inversion approach is

executed by running MT and seismic inversion independently, but are coupled by a common earth model with shared parameters generated by the fuzzy clustering process. A crucial aspect of my approach is flexibility; the inversion processes can run with and without conversion between elastic and geoelectrical models, and it is applicable without known relationships between two model properties.

The fuzzy cluster based inversion schemes were tested with both synthetic and real data. The results of synthetic data show that inversion with clustering constraints recovers the true model better than inversion with only a smoothness constraint even with significant Gaussian noise added. Application to real data demonstrates very clearly the benefits of my approach as the inversion of difficult data sets were able to generate models that provide insights that other efforts with the data were not able to perform. The dataset acquired in the Carlin gold district (USA), demonstrates very well how the fuzzy cluster constrained co-operative inversion delivers benefits from interpreting the membership results. The good correlation between mechanically weak zones mapped by the co-operative MT and seismic inversion with zones of prospective mineralisation zones is an example of how my approach can guide exploration. A second dataset, acquired at the Kevitsa mine site, in Northern Finland, shows that by adopting fuzzy clustering in the geophysical context, I can integrate diverse borehole data types to assist the seismic inversion. Fuzzy clustering is used to fill the missing values of the borehole data to generate a good initial model that then enabled the inversion process to integrate both petrophysical, geochemical and spatial distribution information from boreholes into the inversion. The results from work on both real data sets are shown to be able to assist with geological interpretation and future exploration. Additionally, the fuzzy cluster method makes extracting geophysical information for geotechnical purposes a straightforward process allowing many geophysical data sets to be life-of-mine products beyond exploration.

ACKNOWLEDGMENTS

I gratefully acknowledge Australian Awards Scholarship (AAS) for granting me the scholarship of my PhD.

I would like to express my sincere gratitude to my supervisor Prof. Anton Kepic for his inspiration, encouragement and outstanding supervision. I greatly benefited from his experience and scientific insights throughout my PhD. Besides my supervisor, I would like to thank the rest of my thesis committee: Prof. Boris Gurevich, Asc. Prof. Brett Harris, Dr. Eric Takam, Dr. Anousha Hashemi for their insightful comments and encouragement, but also for the hard question that pushed me to widen my research from various perspectives.

Throughout my PhD studies I got support and valuable knowledge through discussions with my colleagues and staff in Exploration Geophysics Department. My sincere thanks goes to Dr. Michael Carson, Dr. Andrew Pethick, Dr. Hoang Nghia Nguyen for their help. My gratitude to Le Van Anh Cuong and Conny Kitzig for discussions and contributions to my research. Specific mention should go to Robert Verstandig for proofreading my thesis.

This work has been supported by the Deep Exploration Technologies Cooperative Research Centre (DET CRC) whose activities are funded by the Australian Government's Cooperative Research Centre Program. This is DET CRC Document 2018/1080. I would like to acknowledge Barrick Gold for the use of their comprehensive geophysical datasets from Nevada. I also thank First Quantum and Boliden for access to the Kevitsa dataset. I express thanks to Aleksandar Dzunic and Sasha Ziramov for processing seismic data of Kevitsa dataset that improves my work. I have much appreciation to Seong Kon Lee, Korea Institute of Geoscience and Mineral Resources, Korea for using his 2D MT inversion code in my implementation. I would like to express gratitude to CGG Veritas and MathWorks for providing the Hampson Russell and Matlab software, respectively.

Finally, I would like to thank all my friends and colleagues, but special thanks to Le Van Anh Cuong, Mateus Góes Castro Meira, Conny Kitzig, Ida Hooshyari Far, and Snežana Petrović for sharing the office and hallway with over the years.

LIST OF PUBLICATIONS

Journal articles

Kitzig, M. C., A. Kepic, and D. T. Kieu. 2016, Testing cluster analysis on combined petrophysical and geochemical data for rock mass classification. *Exploration Geophysics*, doi: <http://dx.doi.org/10.1071/EG15117>.

Journal articles in review or accepted for publication

Kieu D. T., M. C. Kitzig, and A. Kepic, Prediction of sonic velocities from other borehole data: An example from the Kevitsa mine site, Northern Finland. (Geophysical Prospecting)

Kieu D. T., A. Kepic, Seismic impedance inversion with fuzzy clustering constraints. (Geophysics)

Journal articles in preparation

Kieu D. T., A. Kepic, Fuzzy clustering for magnetotelluric inversion with petrophysical and structural constraints.

Conference paper (invited)

Kieu, D. T., A. Kepic, and V. A. C. Le. 2017, Integration of Borehole and Seismic Data into Magnetotelluric Inversion: Case Study over The Kevitsa Ultramafic Intrusion, Northern Finland. In *Exploration '17*. Toronto, Canada.

Expanded abstracts published in conference proceedings

Kieu, T. D., and A. Kepic. 2015, Seismic Impedance Inversion with Petrophysical Constraints via the Fuzzy Cluster Method. In *24th International Geophysical Conference and Exhibition*. Perth, Australia: ASEG.

Kieu, T. D., A. Kepic, and C. Kitzig. 2015, Classification of Geochemical and Petrophysical Data by Using Classification of Geochemical and Petrophysical Data by Using Fuzzy Clustering. In *24th International Geophysical Conference and Exhibition*. Perth, Australia: ASEG.

Kieu, T. D., and A. Kepic. 2015, Incorporating Prior Information into Seismic Impedance Inversion Using Fuzzy Clustering Technique. In *SEG International Exhibition and Annual Meeting*. New Orleans, USA: Society of Exploration Geophysicists.

- Kieu, D. T., A. Kopic, and V. A. C. Le. 2016, Fuzzy Clustering Constrained Magnetotelluric Inversion-Case Study over the Kevitsa Ultramafic Intrusion, Northern Finland. In Near Surface Geoscience 2016-First Conference on Geophysics for Mineral Exploration and Mining. Barcelona, Spain: EAGE.
- Kieu, D. T., M. C. Kitzig, and A. Kopic. 2016, Estimation of P-wave Velocity from Other Borehole Data. In Near Surface Geoscience 2016 - First Conference on Geophysics for Mineral Exploration and Mining. Barcelona, Spain: EAGE.
- Kieu, D. T., A. Kopic, and A. M. Pethick. 2016, Inversion of Magnetotelluric Data with Fuzzy Cluster Petrophysical and Boundary Constraints. In 25th International Geophysical Conference and Exhibition. Adelaide, Australia: ASEG.

Abstract

- Kieu, T. D., and A. Kopic. 2015, A new co-operative inversion strategy via fuzzy clustering technique applied to seismic and magnetotelluric data. Paper read at EGU General Assembly Conference Abstracts.

NOMENCLATURE

AI	Acoustic impedance
CI	Co-operative inversion
FCM	Fuzzy c-means
MT	Magnetotellurics
Vp	P-wave velocity

Contents

List of Tables	iv
List of Figures	v
Chapter 1: INTRODUCTION	1
1.1. Motivation.....	1
1.1.1. Constrained inversion	4
1.1.2. Including prior information in the inversion	4
1.1.3. Inversion of multiple data sets	5
1.2. Objectives	6
1.3. Thesis arrangement.....	6
Chapter 2: FUZZY CLUSTERING IN THE CONTEXT OF GEOPHYSICAL INVERSION.....	8
Summary.....	8
2.1. Introduction	8
2.2. Fuzzy c-means technique.....	9
2.2.1. Fuzzy c-means clustering algorithm.....	9
2.2.2. Fuzziness and cluster number	11
2.2.3. Membership degree and centre values in the context of inversion.....	12
2.3. FCM as a tool to create pseudo-lithology maps.....	14
2.4. FCM as a platform to include prior information in the inversion	16
2.4.1. Constraining centre values of FCM	16
2.4.2. Constraining the membership degree of FCM	19
2.5. FCM as a means to link multiple data sets.....	22
2.5.1. Working with incomplete data sets.....	23
2.5.2. FCM as a linker of multiple geophysical models	24
2.6. Conclusions	25
Chapter 3: METHODOLOGY OF GEOPHYSICAL INVERSION	26
Summary.....	26
3.1. Introduction	26
3.2. Inversion with smoothness constraint	30
3.3. Including fuzzy c-means into the inversion.....	32
3.4. Inversion scheme.....	35

3.5. Seismic model-based inversion	37
3.5.1. Forward modelling.....	38
3.5.2. Prior information	40
3.5.3. Regularization parameters.....	42
3.5.4. Inversion of a section	43
3.6. Inversion of magnetotelluric data	48
3.6.1. Synthetic model.....	49
3.6.2. Inversion with constraints upon the number of clusters.....	50
3.6.3. Inversion with constraints in petrophysical and boundary information	52
3.7. Co-operative inversion of multiple geophysical datasets.....	56
3.7.1. Co-operative inversion workflow	56
3.7.2. Synthetic example of co-operative inversion with FCM	57
3.8. Conclusions	61
Chapter 4: CO-OPERATIVE INVERSION OF MAGNETOTELLURIC AND SEISMIC DATA.....	62
Summary.....	62
4.1. Introduction	63
4.2. Strategies of co-operative inversions	66
4.2.1. Sequential co-operative inversion strategy	68
4.2.2. Parallel co-operative inversion strategy	69
4.3. Application to real data	71
4.3.1. Geological setting	71
4.3.2. Data sets.....	71
4.3.3. Prior work on the data	77
4.3.4. Sequential co-operative inversion of magnetotelluric and seismic data.....	78
4.3.5. Parallel co-operative inversion of magnetotelluric and seismic data.....	94
4.4. Converting the geophysical model into a pseudo-lithological map	97
4.5. Conclusions	100
Chapter 5: INTEGRATION OF BOREHOLE DATA IN SEISMIC INVERSION	102
Summary.....	102
5.1. Introduction	103
5.2. Kevitsa mine site.....	104
5.2.1. General geology setting	104

5.2.2. Data sets.....	105
5.2.3. Workflow of data analysis.....	107
5.3. Borehole data analysis.....	108
5.3.1. Quality of the data sets.....	108
5.3.2. Preconditioning the data.....	110
5.3.3. Estimation of missing values	110
5.3.4. Establishing a relationship between the seismic data and rock properties....	114
5.4. Integrating borehole information in the seismic inversion	115
5.4.1. Building the initial models.....	115
5.4.2. Integration procedure for borehole data.....	117
5.4.3. Inversion of seismic with constraints from borehole information	121
5.5. Transfer the 3D seismic model into other features.....	126
5.6. Conclusion.....	130
Chapter 6: CONCLUSIONS	132
6.1. Contributions of my thesis.....	133
6.2. Future work.....	136
REFERENCES	138
APPENDICES	146
Appendix A: Borehole data used in Chapter 4.....	146
Appendix B: Borehole data analysis used in Chapter 4.....	148
Appendix C: Data and misfit of the MT inversion in Chapter 4	151
Appendix D: Error data of seismic inversion in Chapter 4.....	153
Appendix E: Lithology in Chapter 5	154
Appendix F: Prediction of sonic velocities, Kevitsa mine, Northern Finland	155
Appendix G: Filling missing values of the whole boreholes	167
Appendix H: Open source code used in this thesis	168
Appendix I : Copyright consent	169

List of Tables

Table 2.1: Membership values of FCM clustering results without boundary information (UN_1 and UN_2) and with boundary information (U_1 and U_2).	22
Table 3-1: Combinations of seismic and MT data	60
Table 4-1: MT inversion strategies	79
Table 4-2. Seismic inversion strategies	87
Table 5-1: Summary borehole data.	107
Table 5-2: Rock quality characterisation based on RQD (After Deere (1988))	114

List of Figures

Figure 1-1: Schematic of dividing a section into rock units.	3
Figure 2-1. An example of using FCM to define rock units based on P-wave velocity (V_p) and density.	10
Figure 2-2: The cartoon represents the mechanism of sorting an item into different clusters.	12
Figure 2-3: A cartoon demonstrates the approach of the use FCM in geophysical inversion.	13
Figure 2-4: Workflow of clustering borehole data to define rock units	14
Figure 2-5 A comparison between schematic geology section (This geological section is adapted from Rex Minerals Ltd.) and clustering results (filled circles) at the hole HDD-064 section 4400N, Hillside.	15
Figure 2-6. Flowchart illustrates the use of FCM to define prior centre values from borehole data, which is used in constraint inversion approach of geophysical data.	16
Figure 2-7. Effect of prior centre values on the clustering results.	18
Figure 2-8. The earth model is divided into cells and two domains A (light blue) and B (orange). Cells [a1, b1] and [a2, b2] have same values but belong to different rock units.	21
Figure 2-9. Membership degree of two clusters applying FCM to the data in Figure 2-8.	21
Figure 2-10: The different between MT and seismic model domains, which may cause problems for joint and co-operative inversion of MT and seismic data	23
Figure 2-11. Workflow of using fuzzy c-means (FCM) clustering.	24
Figure 3-1: Workflow illustrates the inversion scheme.	36
Figure 3-2: (a) A 2-D model comprising four mediums.	39
Figure 3-3: Inversion results with various η values. $\eta=0.0$ (red); 0.25 (green); 0.50 (blue) and 0.75 (black).	40
Figure 3-4: Inversion with different numbers of clusters: 2 (black), 3 (red), 4 (blue) 5 (green) and 6 (purple).	41
Figure 3-5: Inversion results (red lines) with inaccurate prior centres values (blue lines).	42
Figure 3-6: Objective function factors in equation ((3.12)) of inversion trace number 80 vary with regularization parameters β and γ .	43
Figure 3-7: Inversion results of trace 80 with various weighting values of β and γ .	43
Figure 3-8: Inversion results obtained from (b) our method and (c) HRS from (a) the initial model.	44

Figure 3-9: Histogram of the inverted AI from (a) our method and (b) HRS.	45
Figure 3-10: Comparison of the inversion results between our program (red lines) and HRS (blue lines).	45
Figure 3-11: Inverted models (b) and (d) from (a) homogeneous initial model and (c) smoothed initial model, respectively.	46
Figure 3-12: Inverted AI models in depth domain; (a) our method and (b) HRS from models in time domain (Figure 3-8b and c respectively). Dashed black lines mark boundaries of the true model.	47
Figure 3-13: Classification results of using FCM for the inverted AI models of (a) our method and (b) HRS.	47
Figure 3-14: (a) 2-D geoelectrical models. Inversion results using (b) smoothness constraint only and (c) included FCM, which demonstrates that FCM can assist inversion to build a better model than the use of smoothness only.	50
Figure 3-15: The boundaries B1, B2 and B3 (Figure 3-14a) divides the section into different media.	51
Figure 3-16: Inverted results with various prior information cases.	53
Figure 3-17: Inverted results with prior petrophysical information: (a) correct boundary information B2, (b and c) uncorrected locations of B2 (red lines).	54
Figure 3-18: Histogram of resistivity from inverted models using different constraints.	55
Figure 3-19: Workflow of the co-operative inversion.	56
Figure 3-20: Synthetic models of seismic and MT.	58
Figure 3-21: MT synthetic data.	59
Figure 3-22: Seismic synthetic data.	59
Figure 3-23: Inversion results of co-operative inversion for four data combination C1-C4.	60
Figure 4-1: A schematic of the sequential co-operative inversion of seismic and MT data.	70
Figure 4-2: The workflow for parallel co-operative inversion..	70
Figure 4-3: Geological and lithological columns of wells W1 and W2.	72
Figure 4-4: (a) Position of 18 MT stations located at the north-east of the 3D seismic survey area. Wells W1 and W2 are in the vicinity of the MT profile. (b) Seismic slice at the depth of 500 m. (c) Seismic section allocated with MT profile.	75
Figure 4-5: Comparison between normalised resistivity and P-wave velocity from the well logs of W1 and W2.	76
Figure 4-6: Wireline logs of the two wells W1 and W2. The histograms (a and b) show that the two parameters, resistivity and P-wave velocity, are higher in W2 than in W1.	76

Figure 4-7. MT mesh (grey lines) is divided into three regions: A, B and C, by the two boundaries (red dashed lines) that are defined by seismic data (Figure 4-4d).	81
Figure 4-8. Inversion results with different constrains (Table 4-1). The triangles on the top of the section mark MT stations.	83
Figure 4-9. Comparison between the inversion model and borehole data in the two wells (a) W1, and (b) W2.	84
Figure 4-10: Inversion results of the trace at the well location.	86
Figure 4-11: (AI0_1) Initial models generated from the borehole data using the HRS, (AI0_2) migrated velocity model, and (AI0_3) from MT inversion.	89
Figure 4-12: Inversion sections of AI using HRS from three different initial models (Table 4-2).	90
Figure 4-13: Inversion sections of AI using our code from three different initial models (Table 4-2).	91
Figure 4-14: Comparison between borehole data and inversion results using three initial models: (a) borehole data, (b) migration velocity, and (c) the MT model. The lithology keys are shown in Figure 4-3.	93
Figure 4-15: Parallel co-operative inversion results: (a) MT model and (b) the seismic model.	95
Figure 4-16: Comparison between inversion models and borehole data in the well W1.	96
Figure 4-17: Pseudo-lithology sections derived by applying FCM clustering to the inverted models of resistivity and AI models from (a) sequential co-operative inversion and (b) parallel co-operative inversion.	98
Figure 4-18: Comparison between the model AI_FCM_3 (AI) and assay data of Gold (Au), Arsenic (As), Mercury (Hg), and Antimony (Sb).	99
Figure 4-19: Core photos illustrate three abnormal zones in Figure 4-18	99
Figure 5-1: (a) Geological map adapted from Malehmir et al. (2012). (b) Map of borehole and seismic data locations.	106
Figure 5-2: Data analysis workflow	108
Figure 5-3: "Fill missing values" test results in the hole KV28.	111
Figure 5-4: (a) The consistency between estimated and measured acoustic impedance demonstrates that the Vp estimation can be used in the seismic inversion process.	112
Figure 5-5: (a) Cross plot between average values (circles) and error bars of Vp at each of the values of RQD. (b) The cross plot average of Vp, RQD. (c) The cross plot average of Vp, RQD	115
Figure 5-6: Initial model of AI built from both sonic logs and prediction from other borehole data.	116
Figure 5-7: Validation of the initial AI model by comparison between predicted and measured data in the hole KV28	117

Figure 5-8: Wireline logs of P-wave velocity (V_p) versus density (blues crosses) Dashed black lines show the constant values of AI.	118
Figure 5-9: Clustering results from the data sets Co#, Ni# and lithology.	119
Figure 5-10: Schematic shows the concept of including borehole information in the seismic inversion process.	120
Figure 5-11: The certainty of including borehole data in the seismic inversion process is calculated using equation (5.4)	121
Figure 5-12: Inversion results without the clustering constraints from the assay data.	122
Figure 5-13: Inversion results with cluster constraints from the borehole data. The upper figure shows the 3D AI model and the lower figure is AI along section AA' (Figure 5-1b). A, B, C and O mark the low AI zones.	123
Figure 5-14: Comparison of inversion models and borehole data in the KV28 borehole.	125
Figure 5-15: (a) Comparison between clustering results using only acoustic impedance and (b) acoustic impedance plus results of clustering from lithology and Co#, Ni# in the KV28 borehole.	126
Figure 5-16: (a) Geological section along the profile AA' (Figure 5-1b) taken from Koivisto et al. (2015). (b) Migrated seismic data along the section AA'. (c) Clustering (pseudo-lithology) model from the inverted model Inv#2.	128
Figure 5-17: Converted RQD model from the Inv#2 AI model.	129
Figure 5-18: The RQD less than 50% of the borehole is calculated from the Inv#2 inversion in vicinity of the open-pit (black oval line).	130
Figure 6-1: (a) A model of resistivity comprised of both well-defined and fuzzy boundary. (b) Result of MT inversion using smoothness constraint only. (c) Result of MT inversion using smoothness and FCM constraints.	137

Chapter 1: INTRODUCTION

1.1. Motivation

Geophysical methods play important roles in the investigation of the earth subsurface. However, surface geophysical data do not directly image the subsurface. An extra step or process is needed to convert the geophysical data to an earth model with a distribution of physical properties. This process is defined as inversion. Typically, it is this inverted model that is used for geological interpretation, where the petrophysical properties are interpreted or mapped to lithological units. The critical issue of inversion processes is the uncertainty of solutions. The uncertainty of the inversion is caused by many factors (Fernández-Martínez et al. 2013): noise in data, incomplete data coverage, ill-conditioning because the physical assumption of forward modelling is simpler than the real geology and numerical approximation of forward problem, and the resolution of geophysical methods. Nearly all 2D and 3D problems are fundamentally underdetermined as the model is broken into many cells resulting in many more parameters to be estimated than data. Hence, the inversion process must deal with a solution search with multiple solutions to choose between.

Reduction of the uncertainty analysis usually requires a high cost of forward computation (Fernández-Martínez et al. 2013). Moreover, the uncertainty analysis may not be completed because of the accuracy and completeness of the forward modelling plus noise in the measured data. To date, it has been build impossible to build a *natural* subsurface model by a purely mathematic approach; the forward modelling process, often cannot reproduce the real data (Landa and Treitel 2016). In geophysical processing, data noise characteristics are assumed. For example, noise is independent from measurement-to-measurement, zero mean, stationary process (time invariant with statistical parameters), or estimates of variance/noise level may be used. But this assumption is not necessarily true. Producing an inversion solution is significantly more efficient if the inversion process can reduce model space to be explored (Fernández-Martínez 2015). Thus, my thesis focuses on methods that reduces the inversion solutions, and limits the search space to solutions that honour both the data and structures that are geologically reasonable from shallow crustal

investigations. That is, the inverted model solutions should have a similarity to geological maps or conceptual models produced by a geologist.

There are several works published that attempt to reduce the non-uniqueness of the inversion by using constraints of within the inversion process. These constraints come from internal and external information sources. The internal information is based on assumptions about the model parameters; for example, a spatial smoothness constraint on the model (Constable, Parker, and Constable 1987) assumes that the “best” solution is the smoothest model. External information comes from prior information, typically borehole data, and interpretive products from other geophysical methods. When prior information is available, it can assist significantly to remove unreasonable solutions of the inversion process (Jackson 1979, Tarantola and Valette 1982, Meju 1994, Li and Oldenburg 2000, Farquharson, Ash, and Miller 2008, Lelièvre, Oldenburg, and Williams 2009, Johnson et al. 2007). Another approach to condense the number inversion solution possibilities is to use data from multiple geophysical methods. Each geophysical method senses specific physical properties and structures of the earth; thus, using complementary information from multiple geophysical methods should enable the building of a more reliable model (Vozoff and Jupp 1975, Lines, Schultz, and Treitel 1988, Haber and Oldenburg 1997, Bosch and McGaughey 2001, Gallardo and Meju 2004, Paasche and Tronicke 2007, Sun and Li 2011, Zhou et al. 2014, Sun and Li 2015, Zhou, Revil, and Jardani 2016, Heincke et al. 2017).

A robust inversion scheme should integrate both internal information based upon conceptual-geological assumptions and external information to obtain geologically plausible models. Constable, Orange, and Key (2015), Landa and Treitel (2016) claim that the solutions of geophysical inversion, in reality, are neither accurate nor complete. Therefore, a good inversion process should produce an interpretable model in geological perspectives. Geological interpretation process usually divides the geophysical models into areas with relatively homogeneous geophysical parameters. Since rock units formed in the same geological conditions often share similar physical properties due to shared mineralogy this is a reasonable assumption in most cases. Accordingly, the question of how this interpretation step may be integrated more explicitly into the inversion process arises. In the mineral resource exploration and development industry geologists greatly outnumber geophysicists, and unfamiliarity with interpreting petrophysical data is a risk to efficiency. Geologist will not use

methods or data they do not understand or feel comfortable in translating. Again, the question is how can initial information be included in the inversion to produce a result that is more interpretable by a geologist?

Other challenges for a single geophysical method are to produce an incomplete geological model because of each geophysical method senses different geological structures and minerals due to physical contrasts in properties in the subsurface and structures. Where such contrasts do not, or partially, exist an incomplete model result. For example, the reflection seismic method senses elastic properties changes in media. So, this method provides high resolution information about the boundaries of acoustic impedance, but not about the properties within the boundaries directly. In contrast, electromagnetic methods may have lower resolution, but they can provide a geo-electrical model of the whole media. Thus, a combination of the multiple geophysical data in the one inversion approach should be able to build a better geological model. The question is how we can combine the multiple data sets to make earth models that leverage off the desirable aspects of each method?

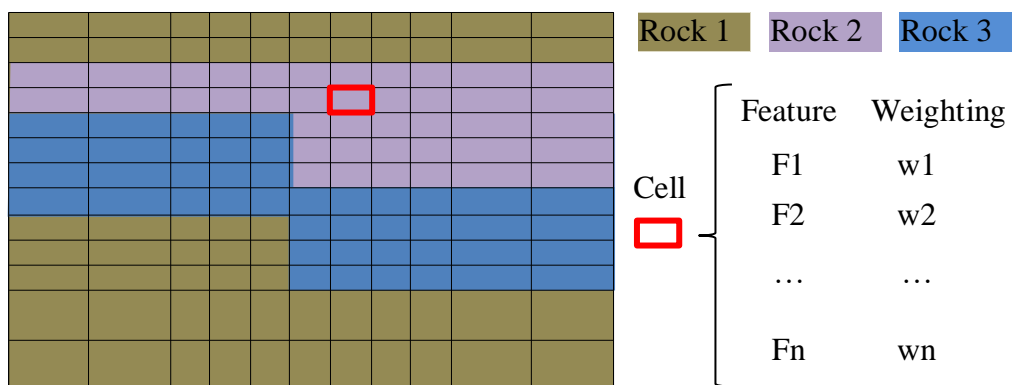


Figure 1-1: Schematic of dividing a section into rock units. Assuming that the subsurface comprises of cells, each cell have n features F ($F1, F2, \dots, F_n$) that may physical properties such as P -wave velocity, resistivity, and density or categorical data such as lithology. Putting the cells in the rock units should consider two aspects (1) all features should be included but with different weighting depending on the certainty of features and purpose of the separation process. It, therefore, needs weighting values $W(w1, w2, \dots, w_n)$ to qualify how much each feature contribute to the separation process. (2) The unclear situation when we have to decide which rock unit the cell should set in.

Figure 1-1 shows an example geological interpretation process based on quantitative features of the subsurface. Assuming that the model is divided into cells, each cell has

constant physical properties. The geological interpretation process should consider the various features-properties with different weighting values depending on the certainty of the features-properties and purposes of the separation. Hence, building the rock unit models by accounting for the weighting of features-properties is a good approach for the inversion constraints to assist in building a geologically plausible model. It is difficult for a formal quantitative method such as geophysical inversion to produce results similar to those that are sometimes considered “an art”, or from expert processes. However, that is the challenge: to deliver inversion results in an unbiased manner that are more amenable to expert processes and require less expertise to interpret.

1.1.1. Constrained inversion

Smoothness constraint is commonly used in the geophysical inversion. However, this constraint creates artefacts because in reality geological boundaries are sharp rather than diffusive. In other words, the parameters should smoothly change inside of a rock unit domain but sharply vary at the boundaries between units. Thus, smoothness constraint is not enough to build a reliable model, and an extra constraint is needed. The nature of rock units should be a good assumption to account for the inversion constraint. The question is how we can divide the data samples into groups. One of the most common clustering algorithms is fuzzy c-means clustering (Bezdek, Ehrlich, and Full 1984a). While hard clustering techniques (e.g., the K-means technique) allocates a term to one group only, soft clustering algorithms (e.g., FCM) put every data point in several clusters with different membership degrees. Soft clustering analysis appears more suitable to the geological environment than hard clustering due to the variability of physical properties for any particular rock type. It is commonly used in geological environments where the physical properties of different rock units are both separated and overlaid. Thus, I adopted the use FCM clustering as an extra constraint of the inversion supposed by Sun and Li (2011).

1.1.2. Including prior information in the inversion

Including prior structural and petrophysical information can reduce the ambiguity of the inversion. Lelièvre, Oldenburg, and Williams (2009) stated an approach to include

prior physical properties and structural information into deterministic inversion. Zhang and Revil (2015) used petrophysical relationship within each unit regarding facie to constrain inversion of gravity and electrical resistivity data. The same approach of Sun and Li (2016), they divide the inversion domain into subdomains, each area has a different clustering approach. Their work based on the idea that the subsurface is usually separated into units of the nearly uniform of physical properties that may relate to rock groups. In this study, I include the prior information into the inversion based on the unit assumption (Figure 1-1) through fuzzy clustering.

1.1.3. Inversion of multiple data sets

Geophysical methods acquired in the collocated location usually provide different subsurface images because they are sensitive to different physical properties and different resolutions. The inversion of multiple data sets likely produce a better geological model than the inversion of single dataset (Vozoff and Jupp 1975, Lines, Schultz, and Treitel 1988, Haber and Oldenburg 1997, Gallardo and Meju 2003, Paasche and Tronicke 2007, Farquharson, Ash, and Miller 2008, Jegen et al. 2009, Doetsch et al. 2010, Moorkamp et al. 2011, Lelièvre, Farquharson, and Hurich 2012, Zhou et al. 2014, Sun and Li 2015, Wang et al. 2017). The crucial issue of the inversion of multiple data sets is how we link the different models. The different models can be coupled by structural or petrophysical information. In the structural link approach, the inversion tends to minimise the structural difference between the models (Haber and Oldenburg 1997) or using a cross-gradient (Gallardo and Meju 2004). The petrophysical process based on the physical relationships to link the models, which usually are experimental definitions (Lines, Schultz, and Treitel 1988, Heincke et al. 2017).

It is better when we can link the model to both structural and petrophysical information because we need both spatial and physical information to build the inversion models. In my approach, the inversion allows imposing both petrophysical and structural coupling through clustering process.

1.2. Objectives

My study objective is to reduce non-uniqueness of the inversion using constraint from internal and external information to construct geologically plausible models. Specifically, my research focuses on utilising fuzzy c-means (FCM) clustering in the inversion with following purposes:

- Adapting FCM clustering to analyse the prior information and to convert the models into more interpretable formats.
- Adding FCM as an extra constraint in the inversion.
- Adapting FCM clustering to be a platform including prior information in the inversion.
- Designing mechanisms of co-operative inversion of multiple data sets based on FCM clustering link.

1.3. Thesis arrangement

My thesis comprises six chapters.

Chapter 1 presents motivation and the objectives of my research.

Chapter 2 describes the fuzzy c-means (FCM) techniques in the context of implementation in geophysical inversion. The fundamental aspects of FCM are described and how this technique can be adapted for inversion purposes.

Chapter 3 describes the methodology of the inversion with simple synthetic test examples to demonstrate the effectiveness of this methodology. Specifically, the focus is on model-based inversion of seismic reflection and magnetotelluric data with the ultimate aim of providing a framework to conduct co-operative inversion. A new scheme of co-operative inversion of multiple geophysical data sets is demonstrated with a synthetic 1-D example of seismic and magnetotelluric data. This is the scheme is used upon real data in Chapters 4 and 5

Chapter 4 demonstrates the robustness of a co-operative inversion approach to data from the Carlin-style gold districts, Nevada, USA. The inversions of seismic and magnetotelluric data are run with two processes: sequential and parallel co-operative inversion.

Chapter 5 provides another example from data from (Kevitsa) Finland to further illustrate the robustness of using fuzzy clustering techniques in the inversion plus show what can be done with an environment rich with borehole data. In this chapter, FCM clustering techniques and the inversion results are adapted to build a more reliable earth models and to extract information that has not been done before.

Chapter 6 concludes my thesis and recommends future research

Chapter 2: FUZZY CLUSTERING IN THE CONTEXT OF GEOPHYSICAL INVERSION

Summary

Fuzzy c-means (FCM) clustering is an unsupervised learning method. The algorithm has been applied to various data types and to automatically define the groups of samples based on the similarity of their attributes. In my work, this technique plays four roles. First, it is a tool to analyse prior information. Second, it is an additional constrained term of the inversion, and in this manner, FCM is a platform to include prior information into the inversion. Third, it is a link of co-operative inversion process. Fourth, it is a tool to convert the inverted models into pseudo-lithological maps that may assist the interpretation process better than using physical models. This chapter presents the basic algorithm of the FCM clustering techniques and the application of FCM clustering in an inversion context. I first describe how FCM parameters, namely the fuzziness index and the cluster number, influence the inversion process. I then will discuss the membership degree and centre values. The next part illustrates the use of FCM to define pseudo-lithology. Finally, I will describe the approach of including prior information into inversion and co-operative inversion using FCM.

2.1. Introduction

In geology, the subsurface is usually divided into rock units that are characterised by different physical properties. However, each of these properties may have overlapping values (un-sharp boundaries) for different rock types. Fuzzy sets theory can deal with classifying data with un-sharp boundaries (Zadeh 1965). Fuzzy c-means (FCM) clustering is an unsupervised learning algorithm based on the fuzzy sets theory (Bezdek 1981). It is a useful tool to explore data structures and is applied in many areas such as neural networks, data clustering, image analysis and structural analysis of algorithms (Nayak, Naik, and Behera 2015). There are many variants of the FCM clustering algorithm (Gosain and Dahiya 2016), with applications in the fields of

image analysis and pattern recognition and geochemistry (Kieu, Kepic, and Kitzig 2015, Kitzig, Kepic, and Kieu 2016).

FCM clustering is also applied in many areas of geophysics. Dekkers et al. (2014) demonstrated that FCM clustering results could identify rock units of distinct rock magnetic properties due to differing geological conditions. FCM enables us to define pseudo-lithology from geophysical data (Paasche and Eberle 2011, Kieu, Kepic, and Kitzig 2015, Kitzig, Kepic, and Kieu 2016). It can be applied independently to subsurface images obtained from geophysical inversion (Paasche et al. 2006, Paasche, Tronicke, and Dietrich 2010, Paasche et al. 2014, Ward et al. 2014b).

Moreover, FCM has been included in the geophysical inversion process as a constraint term in the inversion objective function (Carter-McAuslan, Lelièvre, and Farquharson 2015, Kieu, Kepic, and Le 2016, Kieu, Kepic, and Pethick 2016, Kieu and Kepic 2015c, Lelièvre, Farquharson, and Hurich 2012, Li and Sun 2016, Sun and Li 2011, 2013a, b, 2014, Sun and Li 2015). In this manner, model parameters are divided into clusters based on their similarity. Each cluster may reflect a rock unit. In another application, FCM is utilised as a link in the joint inversion process (Lelièvre, Farquharson, and Hurich 2012, Sun and Li 2011) or in co-operative inversion process (Paasche and Tronicke 2007).

In this study, I use FCM as a constraint term in the inversion objective function as in the work of Sun and Li (2011) and as a link to the geophysical model in the co-operative inversion process (Paasche and Tronicke 2007). Further detail of the inversion algorithm is described in the next chapter. In this chapter, I will present the basic FCM algorithm and the variants of this technique that can be later used with the geophysical inversion process.

2.2. Fuzzy c-means technique

2.2.1. Fuzzy c-means clustering algorithm

FCM is a clustering method that classifies N items of a dataset $\mathbf{Z}(z_1, z_2, \dots, z_N)$ into C clusters based on their similarities by minimising the following objective function:

$$J_{FCM} = \sum_{j=1}^N \sum_{k=1}^C u_{jk}^q d_{jk}^2, \text{ subject to } \sum_{k=1}^C u_{jk} = 1, \quad (2.1)$$

where q is the fuzziness parameter, $q > 1$. The membership degree matrix \mathbf{U} ($u_{jk} \in [0, 1]$), whose u_{jk} represents the degree to which data point j th belongs to cluster k th. d_{jk}^2 is the Euclidian Norm distance from data point j th to centre k th (equation (2.2)).

$$d_{jk}^2 = \|z_j - o_k\|_2^2, \quad (2.2)$$

where $\mathbf{O}(o_1, o_2, \dots, o_c)$ are the centre values.

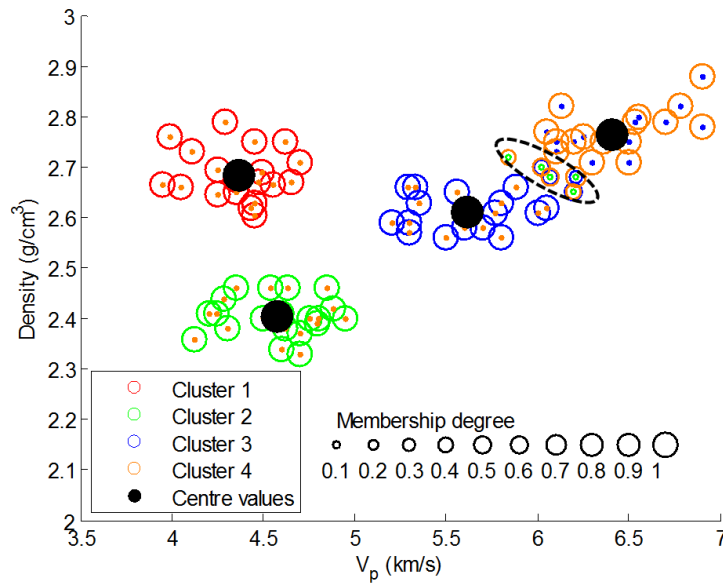


Figure 2-1. An example of using FCM to define rock units based on P-wave velocity (V_p) and density. Cluster 1 and Cluster 2 are well separated. There is an overlapping area, marked by dashed ellipse, between Cluster 3 and Cluster 4. These data points belong to both Clusters with different membership degree. The membership grade illustrates the possibility of the objects belonging to either clusters.

The equations (2.1) and (2.2) show that the FCM objective function J_{FCM} provides a weighted summation error by membership degree when we replace the data points with centre values. J_{FCM} is minimised with respect to membership degree and centre values by an iterative approach (Bezdek, Ehrlich, and Full 1984a). One iteration of updating a centre value o_k is performed as follows:

$$o_k = \frac{\sum_{j=1}^N u_{jk}^q z_j}{\sum_{j=1}^N u_{jk}^q}. \quad (2.3)$$

One iteration of updating the membership degree u_{jk} is performed as follows:

$$u_{jk} = \left\{ \sum_{i=1}^c \left[\frac{d_{jk}^2}{d_{ik}^2} \right]^{q-1} \right\}^{-1}. \quad (2.4)$$

FCM is different from hard clustering techniques such as K-means by allowing one object to belong to many clusters. Thus, FCM can deal with overlapping feature values that are common in geophysics. Figure 2-1 shows one example of an FCM clustering result. If there are two features: P-wave velocity and density from core measurements then Cluster 1 and 2 are clearly separated from cluster 3 and 4. In contrast, the data points in the overlying area between cluster 3 and 4 show membership degrees approximately to 0.5 that means these data points partly belong to cluster 3 and 4.

2.2.2. Fuzziness and cluster number

The key parameters of FCM clustering are the fuzziness index and cluster number. These parameters are defined by numerical (empirical) experiment based on some cluster validity indexes. The weighting exponent q in equation (2.1) reflects the fuzziness, smaller values of q results in harder cluster boundaries, whilst larger values of q allow fuzzier boundaries of the clusters. It is suggested that the fuzziness index is set between 1.5 and 4.0 (Wu 2012). In geophysical inversion, this parameter is usually set to be 2.0 (Carter-McAuslan, Lelièvre, and Farquharson 2015, Sun and Li 2011). In this study, I also used a value of 2.0 for this parameter. Nonetheless, I believe that in the future, the influence of this parameter on an inversion approach that uses fuzzy clustering as an extra constraint, needs to be investigated further.

The cluster number also significantly influences the clustering process. When prior information is not available, the identification of the optimal cluster number is difficult, and is often found by trial and error. This number is usually found by analysing the data based on cluster validity indexes (Bezdek, Ehrlich, and Full 1984a,

He, Tan, and Fujimoto 2016, Paasche, Tronicke, and Dietrich 2010, Xie and Beni 1991a). The cluster number can significantly influence the inversion results when FCM clustering is included in the objective function of the inversion process (Carter-McAuslan, Lelièvre, and Farquharson 2015). The cluster number for the inversion could be defined by using prior information such as analysing borehole data or lithological information, which would be a better process as it is data driven.

The requirements of FCM clustering are that the elements within each cluster are as similar as possible, and the clusters are as dissimilar from each other as possible. Therefore, if the cluster number is increased, a cluster with a high variation of attributes is separated into different clusters. In contrast, if the cluster number is reduced then clusters with low variation and similar in attribute/property are merged into the one cluster (Figure 2-2). In geophysical circumstances, if the cluster number is larger than the number of rock unit, the rocks with a high variation of the property will tend to be divided into smaller clusters. On the other hand, if the cluster number is smaller than the number of rock units, the rock units with less contrast of parameters are merged into a single cluster (of nearest similarity).

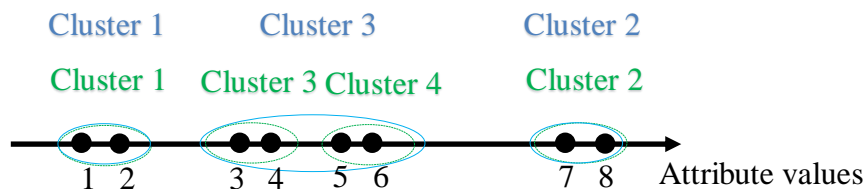


Figure 2-2: The cartoon represents the mechanism of sorting an item into different clusters. There are eight items with values of an attribute varying from low to high. If these items are separated into three clusters, then the items [1, 2] belong to Cluster 1, the items [3, 4, 5, 6] are in Cluster 3 and the items [7, 8] are in Cluster 2. If four clusters are used, then the items [1, 2] and [7, 8] should stay in the same Clusters 1 and 2, but the items [3, 4, 5, 6] now form two Clusters 3 and 4.

2.2.3. Membership degree and centre values in the context of inversion

When applying FCM to geophysical inversion, we can divide the subsurface into elements having uniform physical properties. The elements that have the same values of properties are set into the same cluster, which may correspond to an individual rock unit. The centre values are the “typical” values of clusters; the centre values can be

used to characterise lithological units. The membership degree shows the belonging of the element to the individual clusters.

If the objective function of FCM is minimised, from equation (2.1) and (2.2) we can obtain:

$$z_j \approx \frac{\sum_{k=1}^C u_{jk}^q o_k}{\sum_{k=1}^C u_{jk}^q}. \quad (2.5)$$

Equation (2.3) shows that the centre values are a weighted average of data points or c-mean values. When FCM is included into the objective function of geophysical inversion, the model parameters can be assigned to the input data for FCM clustering. The outputs of FCM are the membership degrees and centre values (Figure 2-3). These centre values, or prototypes, are representative values of the models. From equation (2.5), if we know centre values and membership degree, we can construct the model. Thus, instead of the constraint of the whole model parameters, we can constrain these two variables independently. In the following sections, I present the approaches to constrain these variables and how they can assist the geophysical inversions.

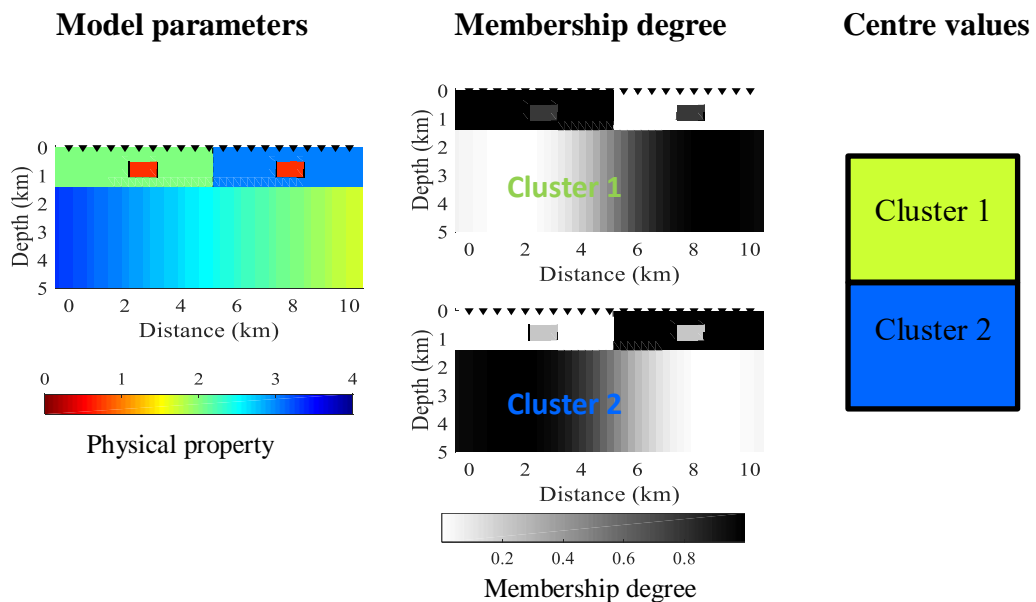


Figure 2-3: A cartoon demonstrates the approach of the use FCM in geophysical inversion. The model parameters of a 2-D geophysical model can be decomposed into membership degree and centre values. Membership degree presents possibility of the model elements belonging to the clusters and it also contains spatial information of the model. The centre values show the presentative values of units.

2.3. FCM as a tool to create pseudo-lithology maps

The objective of FCM clustering is to separate an input data set into groups based on similarity of data features. Elements in the same group should be similar and the groups should be different from each other. Therefore, FCM clustering can define units that have similar physical properties and that may represent different lithology (Dekkers et al. 2014, Kieu, Kepic, and Kitzig 2015, Kitzig, Kepic, and Kieu 2016). In the following, I define the clusters that are identified by FCM clustering that are pseudo-lithological units.

The geophysical model or geophysical data can be used as an input for FCM clustering, and the output of this approach is a pseudo-lithological map that makes the geological interpretation process easier (Paasche and Eberle 2011, Paasche et al. 2006, Sun and Li 2015). In my approach, the inverted models are put in the FCM process and divided into units. Each unit has representative geophysical parameters that are the prototypes, and the membership degree represents the possibility of elements belonging to the clusters (Zadeh 1978).

Here I provide an example of applying FCM clustering to define rock units of real data, which was presented in detail in Kieu, Kepic, and Kitzig (2015). In this work, the FCM clustering method is used as an automatic classifier to define the different lithologies present at the Hillside prospect, Yorke Peninsula, Southern Australia. The algorithm was applied to various combinations of petrophysical and assay data to identify the combination that returned the most accurate result and the smallest combination that provides a nearly identical success identified as the best.

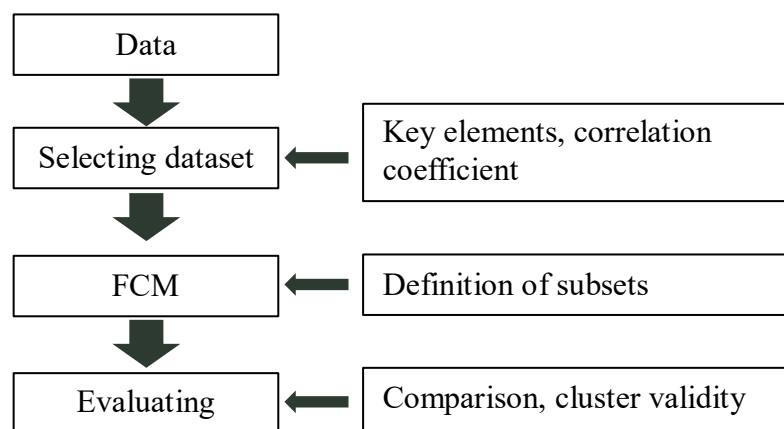


Figure 2-4: Workflow of clustering borehole data to define rock units

Figure 2-4 shows the workflow of the classification process. The first step is to select optimal parameters, using some key parameters and correlation coefficients. For instance, I choose Titanium (Ti) because the proportion of Ti is most indicative of different rock classes in the area, and it correlates with other elements, which assists in reducing the dimensionality of the dataset. Then, any pairs of elements with high correlation values, such as 0.7 or higher, are reduced to one to limit the problems dimension further. Finally, to avoid irrelevant data that might negatively influence the results, data with low correlation coefficient values, such as 0.2 or lower, are excluded. In the second step, FCM clustering is applied to a few different combinations of the data sets to choose the best one.

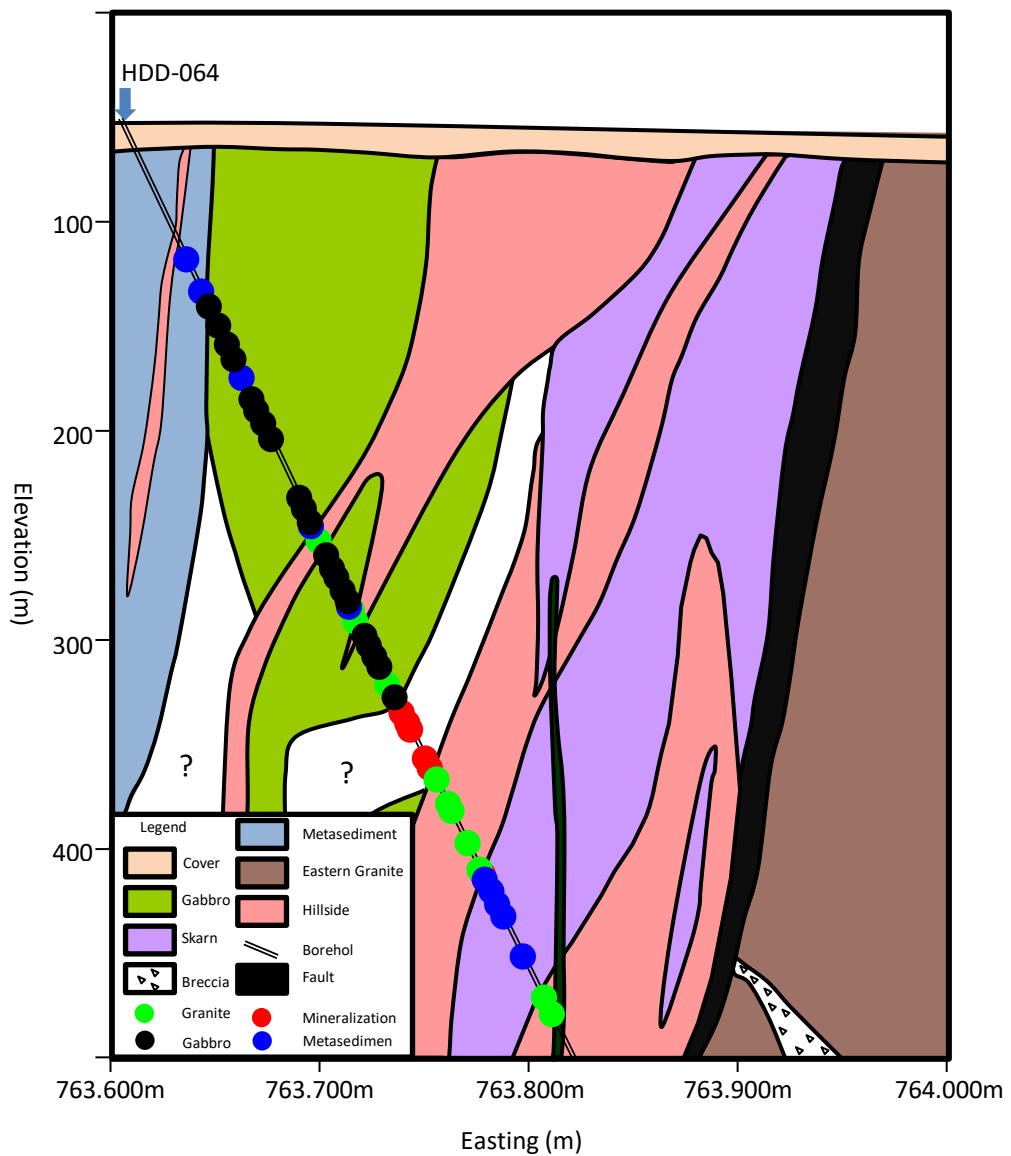


Figure 2-5 A comparison between schematic geology section (This geological section is adapted from Rex Minerals Ltd.) and clustering results (filled circles) at the hole HDD-064 section 4400N, Hillside.

Several combinations of data sets were trailed and compared to a “training” data set. A combination of geochemical and petrophysical data produced the best results, with better than 65% correct. Note there is an additional lithology in the test data set (in Figure 2-5) so the best result the four clusters can achieve is about 75%. However, a dataset with a few common elements and a few petrophysical values can achieve almost the same success rate as the best result (about 63%). The clustering results show a good match with the geological section plotted from the borehole data (Figure 2-5), with most issues at the boundaries and the extra lithology with no cluster mapped to it. This result demonstrates that FCM clustering can be a good tool to automatically classify lithology with little prior knowledge of the local geology. The performance shows that if we can add petrophysics to an optimal elemental analysis suite, then automated lithological classification may work. Also, if we can incorporate such measurement into the drilling process then we can automate geological mapping for exploration and therefore, it should be useful to include this approach in the inversion process.

2.4. FCM as a platform to include prior information in the inversion

2.4.1. Constraining centre values of FCM

If borehole data are available to constrain the geophysical inversion, the question is how this information can be included in the inversion. In my work, I utilised the fuzzy clustering results from borehole data to define prior information, in the form of fuzzy clustering centre values, as the model parameters during the inversion process (Figure 2-6).

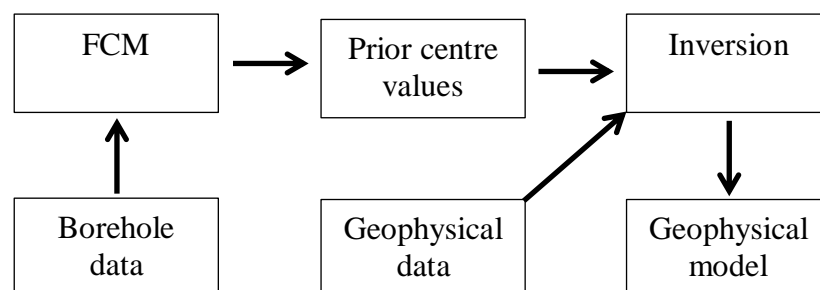


Figure 2-6. Flowchart illustrates the use of FCM to define prior centre values from borehole data, which is used in constraint inversion approach of geophysical data.

The centre values of FCM clustering are constrained by prior information using an algorithms proposed by Berget et al. (2005). The objective function of FCM in equation (2.1) is modified as follows:

$$\begin{aligned} \Phi_{FCM}(U, O) = & (1 - \eta) \sum_{j=1}^N \sum_{k=1}^C u_{jk}^q \|z_j - o_k\|_2^2 \\ & + \eta \sum_{k=1}^C \|o_k - p_k\|_2^2, \end{aligned} \quad (2.6)$$

where η , [0, 1], is a weighting value that represents a certain level of prior information and the $\mathbf{P}=(p_1, p_2, \dots, p_c)$ are the desired values for the clusters.

The centre values, in this case, are updated as in equation (2.7). In this equation, the second factor is the penalty term which finds consonant clusters with prior information. It shows that prior information increasingly dominates the clustering process as the values of η are higher. If η is zero that means we do not have prior information, the centre values in equation (2.7) is the same as in the equation (2.3). When the centre values are fixed as prior information (Carter-McAuslan, Lelièvre, and Farquharson 2015), η is set to 1, from equation (2.7) centre values v_k equals to prior centre values p_k .

$$o_k = \frac{(1 - \eta) \sum_{j=1}^N u_{jk}^q m_j}{(1 - \eta) \sum_{j=1}^N u_{jk}^q + \eta} + \frac{\eta p_k}{(1 - \eta) \sum_{j=1}^N u_{jk}^q + \eta}. \quad (2.7)$$

Figure 2-7 shows an example of the effect of prior centre values on the clustering results. The prior centre values are set as seed values for rock units [A; B; C; D]. When this weighting value is larger, the clustering results change and close to the rock units.

The advantage of using centre values is to exploit the limited information that can constrain the whole geophysical inversion model. This constraint needs an assumption that the geophysical model shares the same prototypes as the prior information. However, we could not exploit more information even if we have a

wealth prior information. To include more of the prior information, I utilised the constraint of membership degree. The membership degree presents the possibility of the items belonging to the groups. In regard to the spatial information of the model, this membership degree also reflects spatial information.

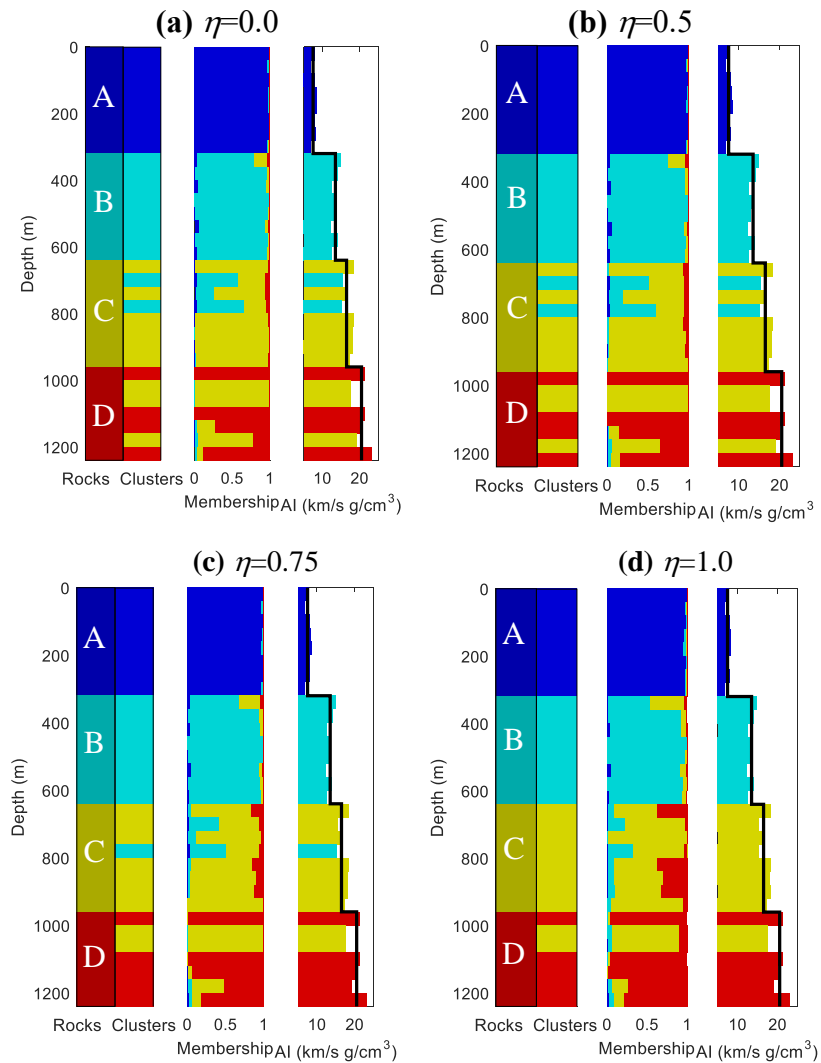


Figure 2-7. Effect of prior centre values on the clustering results. Assuming that we have one borehole with four rock types A, B, C, and D with true AI values [7.5; 13.5; 16.5; 20.52] (km/s g/cm³). The measurement of AI is generated by the prior values (bold black line) plus 15% random Gaussian noise. Running clustering of AI with higher values of η (from a to d) gives a better result matching cluster to rock types. The initial centre values are set same as the true values of the four rocks.

2.4.2. Constraining the membership degree of FCM

Regarding the geophysical inversion, the earth model is usually divided into cells; each cell has a constant physical value (Figure 2-8); the cells may belong to different geological units based on FCM clustering analysis. The membership degree in the equation (2.4) is a measure of grade of belongingness of an element to a cluster. It can also be seen as the possibility of the cell belonging to a certain geological unit (Paasche et al. 2006, Sun and Li 2016). It is worth noting that geophysical measurements can only distinguish between rock units with different physical properties. Thus the term “rock units” or geological unit refers to units defined by differences of their geophysical properties.

My work exploits another aspect of the membership degree, spatial information. The membership matrix of cells in the inversion model contains spatial information (Pham 2001, Rapstine 2015, Paasche, Tronicke, and Dietrich 2010). Therefore, we can constrain the membership degree toward the prior geometrical information that drives the inversion process (Rapstine 2015). My approach is different from previous work. In my algorithm, the spatial information \mathbf{b} is simply treated as a categorical feature data in the fuzzy clustering process (Kim, Lee, and Lee 2004). This feature is combined with the model parameter \mathbf{m} to form the data input $\mathbf{x} = [\mathbf{m} \ \mathbf{b}]$ for FCM clustering. Thus, the distance between item j th to centre k th can be formulated as following:

$$d_{jk}^2 = \|m_j - o_k\|_2^2 + w_k \|b_j - o_k\|_2^2. \quad (2.8)$$

In (2.8), the first factor defines the distance between values of model parameters to the centre values and is calculated by equation (2.2). w_k is the weighting values of domain k th (o_k) to contribute to clustering process. The second factor accounted for the boundary information and defined as follow:

$$\|b_j - o_k\|_2^2 = \begin{cases} 1 & \text{if } b_j = o_k \\ 0 & \text{if } b_j \neq o_k \end{cases} \quad (2.9)$$

I provide an example to address our idea of that the spatial information can be involved in the clustering. Assuming the earth model is divided into units by

boundaries, the physical properties of units are different. Figure 2-8 shows 16 cells of a geophysical model during the inversion process. The cells belonging to two geological domains *A* and *B* should have different physical parameters. Almost all cells in group *A* have physical property values smaller than those in group *B*. Nonetheless, the two cells *a1* and *b1* have the same value 2.6 and the two cells *a2* and *b2* have value of 2.3, they are located in the different domains. It is therefore impossible to distinguish these cells according to their physical properties. Thus extra information is needed to help the inversion process to build a model that separates these cells into different domains. In this case, I exploit the domain as an aspect of clustering process that allows differentiating the cells of the different domain into different clusters.

Table 2.1 shows a comparison between the FCM analysis results without and with boundary information. According to the membership degrees, cells *a1* and *b1* are set in group *B*; cells *a2* and *b2* belong to group *A* if the spatial information is not included in the clustering process. On the other hand, cells *a1* and *a2* are set in unit *A* and cells *b1* and *b2* are set in unit *B* with assistance from further boundary information. As a result, the updating of the model is guided by the prior spatial information to put the cells in the correct domains.

Figure 2-9 shows the membership values of two clusters. The images of the membership present the spatial distribution of the two rock units, in other words, it contains geometric boundaries of the model. Fuzzy clustering results using model parameter only show the cluster 1 and 2 of the cells with low and high physical values respectively and these clusters are different from geological domain *A* and *B* (Figure 2-9). In the case where spatial domain information is involved, cluster 1 and 2 represent domains *A* and *B* respectively.

Moreover, the change of membership degree due to the inclusion of spatial data results different centre values. In this example, the centre values change from 2.08 and 2.90 without boundary information, into 2.05 and 2.82 with boundary information. Therefore, by constraining the membership degree with spatial information, we can change the physical spatial distribution and the values as well. Both geometry and physical properties contribute to the updating model of the inversion process. That means we can put prior geological information into the

inversion process. This information can guide the updating process of the inversion to follow geologic information and to build a geologically interpretable model.

1.5	2.6 a1	2.4	3.2
1.8	2.2	2.6 b1	2.9
2.3 a2	2.0	2.8	3.0
2.8	2.3 b2	3.5	2.6

Figure 2-8. The earth model is divided into cells and two domains A (light blue) and B (orange). Cells [a1, b1] and [a2, b2] have same values but belong to different rock units.

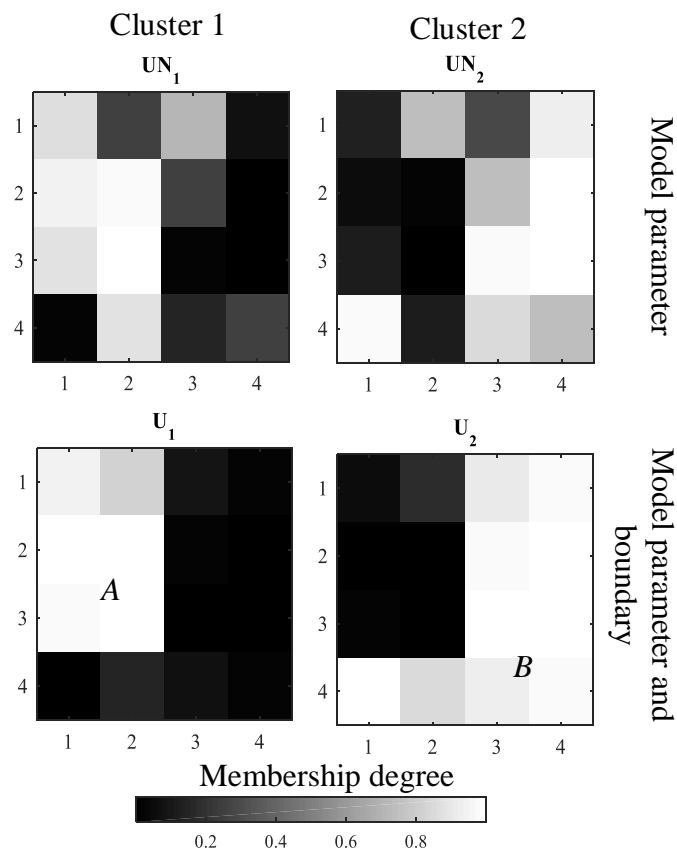


Figure 2-9. Membership degree of two clusters applying FCM to the data in Figure 2-8: cluster 1 (left panel) and cluster 2 (right panel). The upper panel shows clustering results using the model parameter only; the below panel is clustering with the model data and the boundary information.

Table 2.1: Membership values of FCM clustering results without boundary information (UN_1 and UN_2) and with boundary information (U_1 and U_2). Cluster 1 and 2 present rock units A and B respectively. The bold numbers show the cases cells in different rock units but have the same physical values. If boundary information is included in FCM analysis, the cell is set in the correct units.

Without boundary			With boundary			
Data	Membership		Data	Membership		
m	UN_1	UN_2	m	b	U_1	U_2
1.5	0.85	0.15	1.5	A	0.95	0.05
1.8	0.94	0.06	1.8	A	0.98	0.02
2.3	0.88	0.12	2.3	A	0.97	0.03
2.8	0.02	0.98	2.8	B	0.00	1.00
2.6	0.25	0.75	2.6	A	0.83	0.17
2.2	0.97	0.03	2.2	A	0.99	0.01
2.0	0.99	0.01	2.0	A	1.00	0.00
2.3	0.88	0.12	2.3	B	0.15	0.85
2.4	0.71	0.29	2.4	B	0.09	0.91
2.6	0.25	0.75	2.6	B	0.02	0.98
2.8	0.02	0.98	2.8	B	0.00	1.00
3.5	0.15	0.85	3.5	B	0.07	0.93
3.2	0.07	0.93	3.2	B	0.03	0.97
2.9	0.00	1.00	2.9	B	0.00	1.00
3.0	0.01	0.99	3.0	B	0.01	0.99
2.6	0.25	0.75	2.6	B	0.02	0.98

This example also demonstrates that we can include expert knowledge simultaneously in geophysical inversion processes through fuzzy clustering. Since we use fuzzy clustering, it tolerates for imprecision and uncertainty (Zadeh 1994). That means we can introduce ‘soft constraints’ in the geophysical inversion that can deal with inconsistencies between prior information and inverted model better than ‘hard constraints’.

2.5. FCM as a means to link multiple data sets

In geophysical data analysis and inversion of multiple data sets, we usually need to exchange properties of subsurface models. For instance, we may need to calculate one physical property from different data features of the boreholes, which helps build a better model. Or in the co-operative inversion using petrophysical constraints, we

need to transfer parameters of a previous inverted model of one geophysical method, to the initial model of the other method. Conventionally, we usually use an empirical function that correlates the different parameters to exchange data features. However, this function is usually difficult to define and may not be efficient enough to produce a ‘good’ model. That exchange process creates errors and accumulates them into the results. Here I utilize FCM as a tool to exchange data features in data analyses and inversion of multiple geophysical data sets.

2.5.1. Working with incomplete data sets

Our routine of using FCM clustering can flexibly work with multiple model domains which may partially collocate. Figure 2-10 shows one example of MT and seismic model domain that includes three parts: (1) MT model only (M_M), (2) seismic model only (S_S) and (3) overlapping model between MT (M_{MS}) and seismic (S_{MS}). The input data for FCM clustering is simply modified as:

$$\mathbf{Z} = \begin{bmatrix} \mathbf{M}_{MS} & \mathbf{S}_{MS} \\ \mathbf{M}_M & \mathbf{nan} \\ \mathbf{nan} & \mathbf{S}_S \end{bmatrix}, \quad (2.10)$$

where *nan* denotes not a number, which marks we do not have data at that position. This input data can work with the modified FCM clustering algorithms for incomplete data sets. In this work, we applied the modification proposed by Dan, Chongquan, and Jinhua (2012).

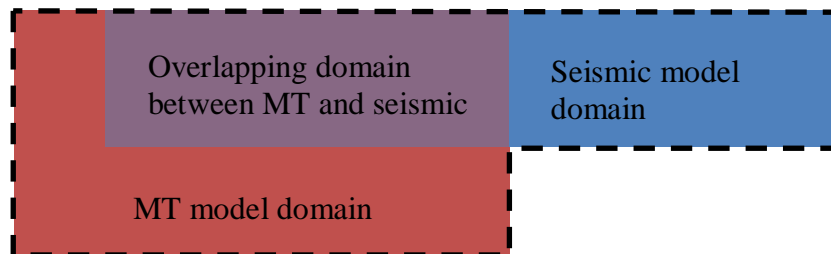


Figure 2-10: The different between MT and seismic model domains, which may cause problems for joint and co-operative inversion of MT and seismic data

2.5.2. FCM as a linker of multiple geophysical models

In a co-operative inversion of multiple geophysical data sets, the key issue is to define the relationship between the geophysical models (Lines, Schultz, and Treitel 1988, Moorkamp et al. 2011). In the conventional approaches, the link is established by empirical relationships. However, this relationship is usually not easily defined, particularly in the hard rock environment. The poor correlation of the physical parameters may generate spurious features (Moorkamp et al. 2011). In my process, I utilized FCM to couple different features. This approach does not need a prior relationship between the models because FCM is an unsupervised learning method, the relationship is automatically defined during the inversion process.

In the conventional approaches (Lines, Schultz, and Treitel 1988), the function of the relationship between models is initially defined, and the function is applied to entire models. This approach may not be robust because the relationship likely varies with geological environment. Therefore, the relationship should be defined locally depending on the geological units (Jegen et al. 2009). In my work, this relationship changes with the clusters that may represent rock units. That means it is more flexible and may define the relationship between the models better than using one function for the entire model.

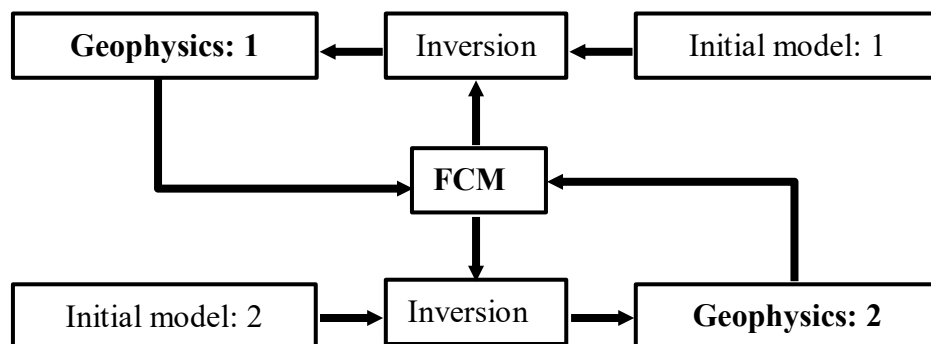


Figure 2-11. Workflow of using fuzzy c-means (FCM) clustering. This is a link between the two geophysical methods in the co-operative inversion process. In the same manner, this workflow can be expanded to an inversion process consists more than two geophysical methods.

The workflow is illustrated in Figure 2-11. The input data of FCM is a matrix $\mathbf{Z} = (z_{ji}, j=1\dots N, i=1\dots M)$, where N is sample number, and M is feature number. In the co-operative inversion of seismic and MT data, N is the number of model cells, and M is both, the acoustic impedance of seismic model and the resistivity of MT model. The outputs of FCM are the centre values, which represent the petrophysical properties of the clusters, and the membership degrees, which contain spatial information of the models. Thus, both, the petrophysical properties and spatial information of MT and seismic models are exchanged during the clustering process.

2.6. Conclusions

Fuzzy c-means (FCM) clustering plays a crucial role in my inversion process. First, it is added as an additional constraint term to the inversion objective function. In this manner, it restricts the geophysical model in numbers of clusters that may represent geological units. Second, FCM clustering is utilised in the inversion regarding both petrophysical and structural constraints by exploiting centre values and membership degree aspects. Centre values are typical value of units, thus they can be a petrophysical constraint term during the inversion process. Membership values play as ‘fuzzy’ or possibility when we assign the elements to groups, which enable us to introduce ‘soft constraint’ in the inversions. Beyond, the membership degree of elements of the earth model, which contains spatial information, can be a structural constraint term in the inversions. Third, in my co-operative inversion approach, the link between geophysical models is defined by FCM clustering. That is more robust than using conventional way and applicable without a prior relationship between models. Fourth, membership degree and centre values obtained by applying FCM clustering to the inversion model can be used to define pseudo-lithology map.

Chapter 3: METHODOLOGY OF GEOPHYSICAL INVERSION

Summary

Geophysical inversion can produce very useful images of the subsurface and make interpretation of complex data sets possible. However, inversion results typically suffer from inherent non-uniqueness; where any subsurface models with different distributions of the physical properties can reproduce the measurements with a given uncertainty (noise level). Hence, extra information about the earth's structure and physical properties is needed to resolve the ambiguity. This extra, or prior, information may be extracted from geological principles, prior petrophysical information from well logs, or complementary information from other geophysical methods. Any technique used to constrain inversion should be able to integrate the prior information and to guide the inversion process regarding the updates to the geological model.

The objectives of my inversion methodology comprise: (1) constrained inversion based on the geological assumption that subsurface is usually divided into distinctive rock units often with characteristic physical properties; (2) constraints that enable me to integrate a wider range of prior information into inversion, including both numerical data such as borehole data and non-numerical data such as boundary information, lithological information or expert knowledge; (3) an inversion process that can be applied for single and multiple geophysical data sets (in a co-operative process).

3.1. Introduction

In general, to resolve ambiguity a model smoothness criteria is added to constrain the inversion (deGroot-Hedlin and Constable 1990). This constraint works to stabilise the inversion process and reduces ambiguity by choosing the smoothest model that fits the data to an acceptable level. However, it also usually tends to produce unrealistic

geological models because both sharp and smooth geological boundaries exist in nature, with sharp boundaries more frequent in shallow crustal environments. To deal with this issue, Groot-Hedlin and Constable (2004) proposed a method of inversion 2D MT structure with sharp resistivity contrasts, but their method requires a sufficiently good initial model that is not easy to obtain in practice. Li and Oldenburg (2000) have incorporated strike and dip information into the inversion of direct current resistivity and induced polarisation data. They divided the earth model into regions with different strikes and dips by including a model objective function into the objective or cost function (to be minimized in the process of inversion). Structural information from high-resolution methods can assist low-resolution methods. For example, GPR data can be used to support direct current inversion (Zhou et al. 2014), or MT inversion is constrained by seismic data (Favetto et al. 2007, Le et al. 2016, Takougang et al. 2015, Bergmann et al. 2014). These approaches are based on the assumption that the changes of geological structures are directly related to the various measured (by the geophysical survey) physical properties of rocks. This assumption is invalid in many geological circumstances, and results in artificial of inversion models (Moorkamp et al. 2011, Moorkamp 2017), particularly with the use of ‘hard constraints’ (forcing localised solutions to a “known” or assumed value) in the inversion.

One approach of integrating petrophysical information into inversion is to use prior information introduced as a reference model. Farquharson, Ash, and Miller (2008) demonstrate that inversion with model constraints from the reference model built by borehole data significantly enhanced the geological consistency of the inverted model. However, this method requires a reasonable number of drill holes, distributed evenly, to create a sufficiently “good” initial model. In practice few mining-resource problems have evenly and consistently measured properties via boreholes. Such conditions are to largely know the solution before solving for it. Interpolation and extrapolation of borehole data to the geophysical model may result in artefacts that drive the inversion to construct an inappropriate earth model (i.e. geologically impossible). As the process of interpolation of point data (from boreholes) to produce a prior model and then constraining the solution not to deviate too far from this model is a de-facto smooth model inversion. Thus, such a scheme is not helpful in recovering distinct boundaries. Where, there is insufficient information to build a good model,

statistical methods such as fuzzy c-means (FCM) clustering technique may be used to incorporate physical data in inversion processes (Sun and Li 2011). Clustering of model parameters assumes that the geological environment is comprised of a few distinctive rock units with differing physical properties linked to belonging to a particular rock unit. An aspect of my thesis investigates is the ability of clustering to provide sharp boundaries without specifying where the boundaries are located exactly. This is a desirable trait in an inversion algorithm, to allow data misfit drive the location of geological boundaries rather than localised prior information (from boreholes). Therefore, FCM clustering provides a platform to constrain geophysical inversion, and should tend to produce models that are more geologically meaningful.

Rock units formed in different geological conditions usually have different physical properties and relationships between physical parameters due to differing mineral assemblages. If the physical properties are characterised correctly, then a formulated set of physical properties in a unit can represent a particular rock unit. For example, an unaltered ultramafic unit is typically denser, more magnetic, acoustically faster, and less radioactive than felsic rocks. In other words, the rock units can be defined based on a group of lithologies with distinct physical characteristics. The question is how to divide the data samples into groups. A common clustering algorithm is fuzzy c-mean clustering (Bezdek, Ehrlich, and Full 1984a). While hard clustering techniques (e.g., the K-means technique) allocates a term to one group only, soft clustering algorithms (e.g., FCM) put every data point in several clusters with varying membership degrees. That is, a data point may have physical values that are similar (or nearby as per norm) to “characteristic values” of several units. Soft clustering analysis appears to be more suitable to creating realistic petrophysical models for the geological environment than hard clustering due to the natural variation of physical properties for any particular rock type. The FCM method is commonly used in geological environments where the physical properties of different rock units overlap, but the actual boundaries for each rock units are relatively distinct (hard). In other words, the boundaries between the various rock units relating to petrophysical properties can be hard, but the physical traits may be fuzzy rather than well defined.

There are several applications of FCM to geophysical inversion, in which FCM is imposed in the objective function as a constraint term. Lelièvre, Farquharson, and Hurich (2012), Carter-McAuslan, Lelièvre, and Farquharson (2015) have used this

approach with tests on synthetic data of seismic topography and gravity. The same process was applied to cross-hole seismic and gravity (Sun and Li 2011, 2013c, Sun and Li 2015, 2016), and gravity and magnetics (Teranishi et al. 2013), both successfully. Another application of FCM, is as a tool to analyse multiple data sets to build a unified geological model (Paasche and Tronicke 2007, Paasche, Tronicke, and Dietrich 2010). Where it may be used to construct a geologic model from geophysical inversion (Ward et al. 2014a). In my thesis, I explore combining both above mentioned aspects: linking the incorporation of FCM constraints into the inversion and then using the clustering results to generate “pseudo” geology models or maps.

A search of recent literature indicates that the use of clustering constraints in inversion of geophysical data appears to be a better approach than using single, localised, petrophysical or structural constraints if we can utilise the both petrophysical and structural information in the inversion process. Lelièvre, Oldenburg, and Williams (2009) proposed an approach to include prior physical properties and structural information into “deterministic” inversion. Zhang and Revil (2015) have used petrophysical relationship within each unit regarding facie to constrain inversion of gravity and electrical resistivity data. A similar approach is used by Sun and Li (2016), where they divide the inversion domain into subdomains and each area has a different clustering approach. Their work is based on the assumption that the subsurface is usually separated into units of the nearly uniform of physical properties that may relate to rock groups. Such an assumption seems to be a reasonable approximation to many mining environments in crystalline rock, which is where the application of my research is mostly directed.

I have adopted the the basic approach of Sun and Li (2011), but despite constraining of petrophysical information through centre values of FCM clustering, FCM clustering has been implemented in a different manner that enables the simultaneous inclusion of petrophysical and structural information the into inversion algorithm. This approach exploits the fuzzy logic technique to implement “soft constraints” on model structures. By “soft” I mean that the inversion is not directed to a particular localised position or petrophysical value directly, but indirectly by the association of membership to a cluster. Thus it enables the algorithm to tolerate miss-matches between prior structural information and the distribution of physical properties of the model versus the “real” model.

3.2. Inversion with smoothness constraint

There are many models that can adequately fit the observation data regarding the statistical uncertainty of best fit due to noise and error. For geophysical surveys that attempt to model in 2D or 3D there are many more parameters than there are measurements. The problem is under-constrained with respect to data. To narrow the solution domain of the inversion process, the inverted model is often chosen as the most smooth model (Constable, Parker, and Constable 1987). The “objective function” of the inversion process is as follows:

$$\phi = \phi_d + \beta\phi_m, \quad (3.1)$$

where ϕ_d and ϕ_m are the misfit and smoothness terms calculated by equation (3.2) and (3.3) respectively. β is the regularization (relative weighting compared to data misfit) parameter balancing between the misfit and the smoothness of the model structure.

$$\phi_d = \|\mathbf{W}\mathbf{d} - \mathbf{W}\mathbf{f}(\mathbf{m})\|_2^2, \quad (3.2)$$

$$\phi_m = \|\tilde{\mathbf{d}}\mathbf{m}\|_2^2, \quad (3.3)$$

where $\|\cdot\|_2$ is the Euclidian Norm, $\mathbf{d}=(d_1, d_2, \dots, d_M)^T$ and $\mathbf{m}=(m_1, m_2, \dots, m_N)^T$ are data and model parameters respectively, $\mathbf{f}(\mathbf{m})$ is a forward modelling operator, it is a nonlinear function, \mathbf{W} is the diagonal $N \times N$ matrix of data variation σ (3.4), and $\tilde{\mathbf{d}}$ is difference operator (3.5)

$$\mathbf{W} = \text{diag}\{1/\sigma_1, 1/\sigma_2, \dots, 1/\sigma_N\}, \quad (3.4)$$

$$\tilde{\mathbf{d}} = \begin{bmatrix} 1 & -1 & & & \\ & 1 & -1 & & \\ & & & \ddots & \\ & & & & 1 & -1 \end{bmatrix}. \quad (3.5)$$

As most geophysical problems I wish to solve are non-linear, I have used an iterative model update approach proposed by Constable, Parker, and Constable (1987). If the forward functional $\mathbf{f}(\mathbf{m})$ can be linearized about a starting vector model $\mathbf{m}_{(1)}$. The first two terms of the Taylor approximation as following:

$$\mathbf{f}(\mathbf{m}_{(1)} + \Delta\mathbf{m}) = \mathbf{f}(\mathbf{m}_{(1)}) + \mathbf{J}_{(1)}\Delta\mathbf{m}, \quad (3.6)$$

where $\Delta\mathbf{m}=\mathbf{m}_{(2)}-\mathbf{m}_{(1)}$ is the adjusted model parameters, and $\mathbf{J}_{(1)}$ is the Jacobian matrix of partial derivatives of $\mathbf{f}(\mathbf{m})$ with respect to the vector model parameter $\mathbf{m}_{(1)}$.

From equations (3.1), (3.2), (3.3), and (3.6), we obtain

$$\phi = \|\mathbf{W}\mathbf{d}_{(1)} - \mathbf{W}\mathbf{J}_{(1)}\mathbf{m}_{(2)}\|_2^2 + \beta\|\tilde{\mathbf{d}}\mathbf{m}_{(2)}\|_2^2, \quad (3.7)$$

where

$$\mathbf{d}_{(1)} = \mathbf{d} - \mathbf{f}(\mathbf{m}_{(1)}) + \mathbf{J}_{(1)}\mathbf{m}_{(1)}. \quad (3.8)$$

If we deviate the objective function in (3.7) subject to the vector model parameters $\mathbf{m}_{(2)}$:

$$\frac{\partial\phi}{\partial\mathbf{m}_{(2)}} = 2[(\mathbf{J}_{(1)}^T\mathbf{A}\mathbf{J}_{(1)} + \beta\mathbf{H})\mathbf{m}_{(2)} - 2\mathbf{J}_{(1)}^T\mathbf{A}\mathbf{d}_{(1)}], \quad (3.9)$$

where $\mathbf{H} = \tilde{\mathbf{d}}^T\tilde{\mathbf{d}}$ and $\mathbf{A}=\mathbf{W}^T\mathbf{W}$,

and set to zero, we can find the model that minimizes the objective function. Substitute equation (3.8) into equation (3.9) and $\Delta\mathbf{m}=\mathbf{m}_{(2)}-\mathbf{m}_{(1)}$, we obtain:

$$\begin{aligned} & [(\mathbf{J}_{(1)}^T\mathbf{A}\mathbf{J}_{(1)} + \beta\mathbf{H})(\mathbf{m}_{(1)} + \Delta\mathbf{m}) - \mathbf{J}_{(1)}^T\mathbf{A}(\Delta\mathbf{d}_{(1)} + \\ & \mathbf{J}_{(1)}\mathbf{m}_{(1)})] = 0, \end{aligned} \quad (3.10)$$

where $\Delta\mathbf{d}_{(1)} = \mathbf{d} - \mathbf{f}(\mathbf{m}_{(1)})$ is the the different between observed and synthetic data from the model $\mathbf{m}_{(1)}$.

Suppose after i th iteration, according to equation (3.10), in the next iteration, the perturbation vector model $\Delta\mathbf{m}_{(i+1)}$ is calculated by the equation (3.11).

$$\Delta\mathbf{m}_{(i+1)} = [(\mathbf{J}_{(i)}^T\mathbf{A}\mathbf{J}_{(i)} + \beta\mathbf{H})^{-1}][\mathbf{J}_{(i)}^T\mathbf{A}\Delta\mathbf{d}_{(i)}], \quad (3.11)$$

where $\Delta\mathbf{d}_{(i)}$ is the error between synthetic data from the model $\mathbf{m}_{(i)}$ and observed data. Equation 3.11 is the “normal equations” for model updates that lead to models that minimise the objective function, and follow the form of non-linear damped least squares with \mathbf{H} substituting for the identity matrix in the basic NLSQ formulation (Constable, Parker, and Constable 1987).

3.3. Including fuzzy c-means into the inversion

Geophysical inversion using the smoothness constraint reduces ambiguity; however, this constraint produces geologically unrealistic models in the environments where the physical properties vary sharply. Such environments are the norm in sedimentary and igneous rock environments. Therefore, I propose to use an extra constraint term that restricts the models to those that restrict model values to a limited small number of clusters (Sun and Li 2011, Kieu and Kepic 2015c). This term assists the inversion to build a “blocky” model, which is more desirable as the inversion tends to place a boundary rather a geophysicist selecting a contour on a gradient (a process prone to bias). Moreover, I utilise FCM as a platform to transfer various prior information into the inversion process. This is to input petrophysical and boundary/spatial information (Kieu and Kepic 2015c, b, Kieu, Kepic, and Le 2016, Kieu, Kepic, and Pethick 2016) to guide the inversion algorithm towards a better model.

The fuzzy c-means (FCM) clustering technique is incorporated as an added constraint term in the geophysical inversion. This fuzzy clustering method is described in Chapter 2. Incorporating FCM clustering provides a bias toward models that cluster (rock units), but still fit the data. The FCM objective function ϕ_{FCM} is imposed in the inversion objective function (3.1) in the same way as a Lagrangian formulation (3.12).

$$\min \{\phi(\mathbf{O}, \mathbf{U}, \mathbf{m}) = \phi_d + \beta\phi_m + \gamma\phi_{FCM}\}, \quad (3.12)$$

where β and γ are the regularisation parameters balance between misfit, model structure and FCM clustering constraint terms. \mathbf{O} represents the cluster centre values, and \mathbf{U} is the membership degree matrix.

When differentiating the objective function (3.12), subject to \mathbf{O} and \mathbf{U} to find a minimum, the first two terms in the objective equation are unrelated to \mathbf{O} and \mathbf{U} ; thus, the partial differential of these terms are zero. Only the third term is dependent upon \mathbf{O} and \mathbf{U} . Therefore, differentiating the objective function (3.12) is similar to the FCM objective function subject to \mathbf{O} and \mathbf{U} , and the solution of this problem is presented in Chapter 2 (Equation (2.3) and (2.4), respectively).

Differentiating the objective function (3.12) subject to \mathbf{m} , in the same maner of finding a solution to the non-linear inverse problem, the partial deviative of the objective function to \mathbf{m}_2 is:

$$\frac{\partial \Phi}{\partial \mathbf{m}_{(2)}} = \frac{\partial(\Phi_d + \beta \Phi_m)}{\partial \mathbf{m}_{(2)}} + \frac{\gamma \partial \Phi_{FCM}}{\partial \mathbf{m}_{(2)}}. \quad (3.13)$$

The first term in right-hand side of equation (3.13) is similar to that in the smoothness constraint process equation (3.9).

The objective function of FCM clustering is presented in equation (2.1). The detail of this function is described in the section 2.2 of Chapter 2. Note that this function omits all the factors that are not dependent on \mathbf{O} , \mathbf{U} and \mathbf{m} , because these factors are zero when differentiating subject to \mathbf{m} .

$$\Phi_{FCM} = \sum_{j=1}^N \sum_{k=1}^C u_{jk}^q \|m_{(2)j} - o_k\|_2^2, \quad (3.14)$$

where q is the fuzziness parameter, $q > 1$. The membership degree matrix $\mathbf{U}=(u_{jk} \in [0, 1])$, whose u_{jk} represents the degree to which data point j th belongs to cluster k th. $\mathbf{O}=(o_1, o_2, \dots, o_C)$ are the centre values.

The second term is solved by:

$$\frac{\partial \Phi_{FCM}}{\partial \mathbf{m}_{(2)}} = \sum_{j=1}^N \frac{\partial \Phi_{FCM}}{\partial m_{(2)j}}. \quad (3.15)$$

Taking the derivative of each element of vector model $\mathbf{m}_{(2)}=(m_{(2)j}, j=1..N)$ we have:

$$\frac{\partial \Phi_{FCM}}{\partial m_{(2)j}} = 2 \sum_{k=1}^C u_{jk}^q m_{(2)j} - 2 \sum_{k=1}^C u_{jk}^q o_k, \quad (3.16)$$

Substituting equation (3.16) in equation (3.15) we obtain:

$$\frac{\partial \Phi_{FCM}}{\partial \mathbf{m}_{(2)}} = 2 \sum_{j=1}^N \sum_{k=1}^C u_{jk}^q m_{(2)j} - 2 \sum_{j=1}^N \sum_{k=1}^C u_{jk}^q o_k. \quad (3.17)$$

In matrix form the expression is:

$$\frac{\partial \Phi_{FCM}}{\partial \mathbf{m}_{(2)}} = 2\hat{\mathbf{U}}\mathbf{m}_2 - 2\mathbf{U}\mathbf{O}, \quad (3.18)$$

where

$$\hat{\mathbf{U}} = \text{diag}\left(\sum_{k=1}^C u_{jk}^q\right)_{N \times N}, \quad (3.19)$$

$$\mathbf{U} = \{u_{jk}^q\}_{N \times C}, \quad (3.20)$$

$$\mathbf{0} = \{0_k\}_{C \times 1}. \quad (3.21)$$

Substituting the equation (3.9) and (3.18) into equation (3.13) and setting to zero yields:

$$2[\mathbf{J}_{(1)}^T \mathbf{A} \mathbf{J}_{(1)} + \beta \mathbf{H} + \gamma \hat{\mathbf{U}}] \mathbf{m}_{(2)} - 2\mathbf{J}_{(1)}^T \mathbf{A} \mathbf{d}_{(1)} + \gamma(2\hat{\mathbf{U}} \mathbf{m}_{(2)} - 2\mathbf{U} \mathbf{0}) = 0 \quad (3.22)$$

Substituting $\Delta \mathbf{m} = \mathbf{m}_{(2)} - \mathbf{m}_{(1)}$ and $\mathbf{d}_{(1)} = \Delta \mathbf{d}_{(1)} + \mathbf{J}_{(1)} \mathbf{m}_{(1)}$ in equation (3.22) produces:

$$\Delta \mathbf{m} = [\mathbf{J}_{(1)}^T \mathbf{A} \mathbf{J}_{(1)} + \beta \mathbf{H} + \gamma \hat{\mathbf{U}}]^{-1} [\mathbf{J}_{(1)}^T \mathbf{A} \Delta \mathbf{d}_{(1)} + \gamma(\mathbf{U} \mathbf{0} - \hat{\mathbf{U}} \mathbf{m}_{(1)})], \quad (3.23)$$

where $\Delta \mathbf{d}_{(1)} = \mathbf{d} - \mathbf{f}(\mathbf{m}_{(1)})$ is the difference between observed and predicted data from the model $\mathbf{m}_{(1)}$

Suppose after i th iteration, according to equation (3.23), in the next iteration, the perturbation vector model $\Delta \mathbf{m}_{(i+1)}$ is calculated as following:

$$\Delta \mathbf{m}_{(i+1)} = [\mathbf{J}_{(i)}^T \mathbf{A} \mathbf{J}_{(i)} + \beta \mathbf{H} + \gamma \hat{\mathbf{U}}]^{-1} [\mathbf{J}_{(i)}^T \mathbf{A} \Delta \mathbf{d}_{(i)} + \gamma(\mathbf{U} \mathbf{0} - \hat{\mathbf{U}} \mathbf{m}_{(i)})], \quad (3.24)$$

where $\Delta \mathbf{d}_{(i)}$ is the error between synthetic data from the model $\mathbf{m}_{(i)}$ and observed data.

One method of including prior information is to use any prior information to constrain FCM clustering. For example, statistical means of petrophysical parameter distributions to constrain centre values, or on constraints on neighbouring memberships to incorporate boundary information. Since the FCM objective function is directly incorporated into the inversion objective function, the prior information is transferred into model building process via FCM. The inclusion of prior information

to constrain FCM is presented in the section 2.4 of Chapter 2. The prior information is invariant in the inversion process. Thus it does not influence any partial derivatives of the inversion objective function. Therefore, the formula to calculate model perturbation of inversion is equation (3.24). Assuming that we have a model with N elements $\mathbf{m}=(m_j, j=1, \dots, N)$, and the prior information of C centre values $\mathbf{P}=(p_1, p_2, \dots, p_C)$. Then the membership degree $\mathbf{U}=(u_{jk} \in [0, 1], j=1, \dots, N; k=1, \dots, C)$ and centre values of FCM clustering $\mathbf{O}=(o_1, o_2, \dots, o_C)$ are calculated by the equations (3.25) and (2.7).

Membership degree calculation:

$$u_{jk} = \left\{ \sum_{i=1}^C \left[\frac{m_j - o_k}{m_i - o_k} \right]^{\frac{2}{q-1}} \right\}^{-1}. \quad (3.25)$$

Centre values calculation:

$$o_k = \frac{(1 - \eta) \sum_{j=1}^N u_{jk}^q m_j}{(1 - \eta) \sum_{j=1}^N u_{jk}^q + \eta} + \frac{\eta p_k}{(1 - \eta) \sum_{j=1}^N u_{jk}^q + \eta}. \quad (3.26)$$

In equations (3.25) and (2.7), q is the fuzziness parameter and is set to 2.0 in this work (See detail in section 2.2.2 of Chapter 2). η [0, 1] is a weighting value that represents a certain level of prior information (See detail in section 2.4 of Chapter 2).

3.4. Inversion scheme

Figure 3-1 shows the workflow of the inversion process. In the block “prior information”, we need to define an initial model \mathbf{m}_0 . Regularisation parameters β , γ , and η can be adjusted during inversion processes as per Sun and Li (2015), but they also mention that the interaction among these parameters are complex. Therefore, I have fixed these parameters (in the iterations) in my inversion process for simplicity. I have not found any good reason to construct a more complex process of adjusting the regularisation parameters during iteration. Borehole data can be used to define the prior centre values, \mathbf{P} , and cluster number, C . These may be found from basic statistical analysis of the distributions of physical properties. The fuzziness factor q

is set to 2.0 as this appears to work and there appears little benefit from deviating from this value. If geological information such as lithology or litho-boundary information is available, it may be directly incorporated into the FCM cluster structure (e.g. number of clusters), as other features (a prior cluster model structure-spatial distribution), or as a parameter to be inverted with other inverted model parameters.

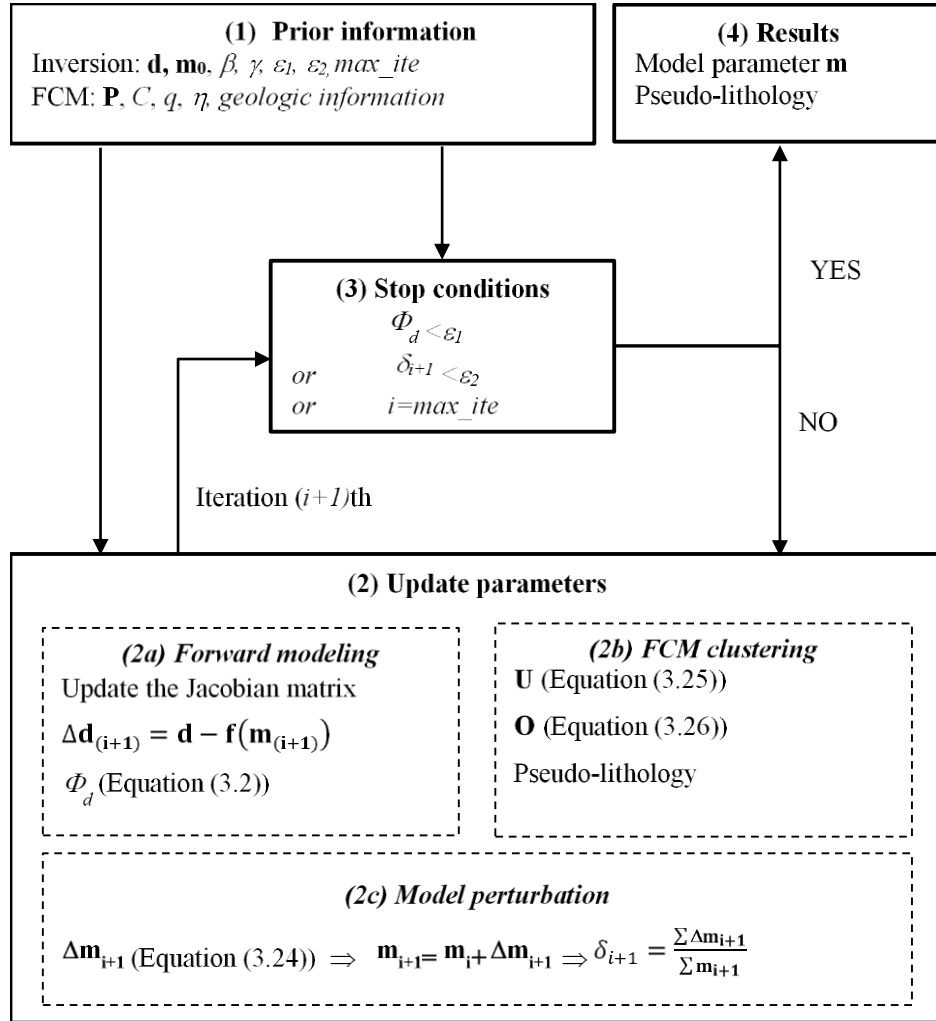


Figure 3-1: Workflow illustrates the inversion scheme. The scheme includes four main blocks (1), (2); (3); and (4). Index i represents iteration. In prior information block, \mathbf{d} and \mathbf{m}_0 are data and prior model respectively, β and γ are regulation parameters (equation 3.24), ε_1 , ε_2 are small numbers and max_ite is maximum iteration number they are stop conditions of inversion process, \mathbf{P} is prior centre values, C and q are cluster number and fuzziness respectively and η is weighting of prior centre values. In block (2b), we can obtain membership and centre values of the models, and based on this information we can define pseudo-lithology.

In the “update parameters” block, two processes are executed simultaneously/parallel: forward modelling and FCM clustering. The forward modeling block calculates data misfit, the difference between synthetic and observed data, and updates the Jacobian matrix. The FCM clustering block, calculates a membership matrix and may update new centre values. Analysing membership and centre values, we may obtain a pseudo lithological image of the inverted model.

The inversion process finishes when one of three stop conditions are satisfied: misfit reaches desired level; relative model update is smaller than a threshold value; or the iteration count is equal to the maximum number. The output of inversion results is the inverted model and pseudo-lithological (cluster membership of each cell) information.

3.5. Seismic model-based inversion

In geophysical exploration, the seismic reflection method offers many advantages over other standard mineral exploration methods as it has higher resolution with depth than potential field or electromagnetic methods, and penetrates far deeper than GPR. However, the resulting stacked seismic image only determines boundaries between contrasting regions of acoustic impedance (AI). This limitation can be overcome by performing an AI inversion process that converts the seismic data into AI intervals. Using the AI results should provide better interpretation products than the stacked image data alone. Various seismic impedance inversion algorithms have been published, such as model-based inversion (Cooke and Schneider 1983), nonlinear inversion (Ma 2001, Oliveira et al. 2009, Zhang, Shang, and Yang 2007) and seismic inversion based on the L1-norm (Zhang, Dai, and Liu 2014). Model-based inversion is the most commonly used because it allows the integration of low-frequency information in a straight forward manner, providing a result that is more reliable and often with higher resolution (Russell and Hampson 1991).

In general, seismic inversion techniques are non-unique, as are nearly all inversion techniques (Cooke and Schneider 1983) and bandlimited (ten Kroode et al. 2013, Ghosh 2000). Consequently, the inversion result is ambiguous and often depends strongly on the initial model (which is my experience in using commercial software, where a good example is in Chapter 4). One solution to the non-uniqueness problem

is to use constraints. Conventionally, smoothness criteria are added (Pilkington and Todoeschuck 1992) to generate a unique solution, which may be regarded as an average of most likely solutions. However, the smoothness criteria tends to produce an undesirable model because sharp rather than smooth boundaries are common in the geological environment. It also defeats much of the advantage of using seismic reflection data, which is to recover boundaries at depth with precision. Using global constraints, as in the work of (Ma 2001) may produce a reliable model, but it is computationally time-consuming. To deal with bandlimited seismic data, an efficient approach in constructing a reliable model is to include complementary information such as petrophysical well logs and core measurements. Several algorithms integrate this information into the inversion process comprising: bound and trend constraints (Lelièvre, Oldenburg, and Williams 2009); a reference model and statistical data (Sun and Li 2013c, González, Mukerji, and Mavko 2008, Bosch et al. 2009).

In this study, I adopt the use of FCM as a constraint term in the objective function (Sun and Li 2011). However, my algorithm is different in the manner of exploitation the FCM concept. The work of Sun and Li used only petrophysical data in parameter domains to constrain the inversion. Whereas, the approach in this thesis is to utilise both petrophysical and spatial (boundary) information to construct the model that fits the seismic data and the geometry of identified subsurface boundaries and petrophysical values. This approach reduces the non-uniqueness of the AI model and produces a more geologically reasonable/interpretable result.

3.5.1. Forward modelling

The forward model of seismic trace is generated by convolution between a source wavelet $\mathbf{w}(t)$ and reflection coefficient $R(t)=(r_1, r_2, \dots, r_N)$ equation (3.27).

$$\mathbf{S}(t) = \mathbf{w}(t) * \mathbf{R}(t). \quad (3.27)$$

The j th reflection coefficient is calculated as follows:

$$r_j = \frac{AI_{j+1} - AI_j}{AI_{j+1} + AI_j}, \quad (3.28)$$

where $AI_j = \rho_j \times v_j$ is acoustic impedance, a product of density ρ_j and velocity v_j of the j th layer.

If the reflection coefficient series and an AI (e.g. at the first layer) are known, then acoustic impedance (AI) of all layers are calculated by the recursive equation (3.29) (Cooke and Schneider 1983)

$$AI_j = AI_1 \prod_{i=2}^{j-1} \frac{1+r_i}{1-r_i}, \quad (3.29)$$

A two-dimension synthetic test model (Figure 3-2a) consists of four media which have constant AI within each unit. Figure 3-2b shows synthetic data that is generated by a convolution of calculated reflectivity from the 2D model with a Ricker wavelet, which has a dominant frequency of 40Hz (which is a typical centre frequency of relatively shallow land seismic data, pers. comm. with HiSeis Pty Ltd representatives). Random Gaussian noise is added to the synthetic traces with a signal-to-noise ratio ($SNR=1.5$) calculated by equation (3.30) (Dahl and Ursin 1991). The distance between two successive traces is 25m. Each trace has 501 samples with an interval of 2ms. There are two wells located at trace positions of CDP numbers 21 and 81 respectively.

$$SNR = \left(\sum_i s_i^2 / \sum_i n_i^2 \right)^{1/2}, \quad (3.30)$$

where s_i and n_i are signal and noise respectively.

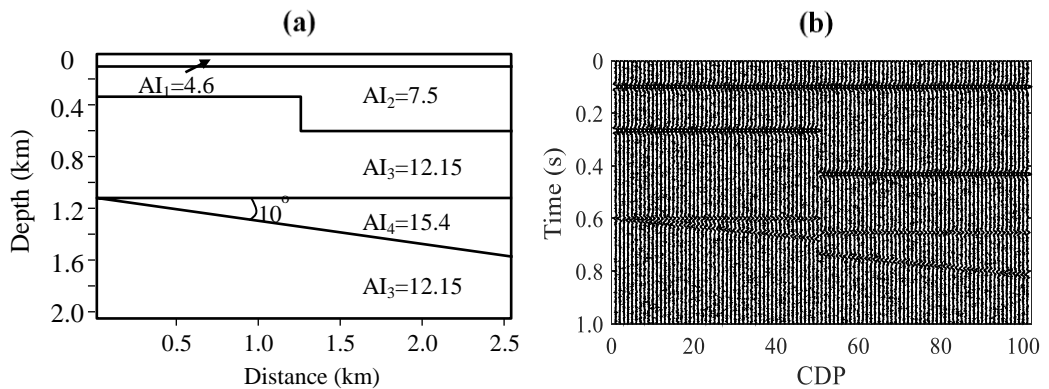


Figure 3-2: (a) A 2-D model comprising four mediums. Each medium has a constant of AI (km/s g/cm^3). (b) Seismic data generated by convolution of reflectivity calculated from model (a) with a Ricker wavelet, a dominant frequency of 40Hz, plus random Gaussian noise ($SNR=1.5$).

In order to evaluate the goodness of fit the Misfit criteria given by equation (3.2) is used. In the case of synthetic data, I also define a model error (*MER*) as follows:

$$MER = 100\% \sqrt{\frac{1}{M} \sum_{j=1}^M \left(\frac{AI_j - AI_j^t}{AI_j^t} \right)^2}, \quad (3.31)$$

where *AI* and *AI'* denote the inverted and the true AI, respectively and *M* is the number of model parameters. This error can be used to evaluate the quality of the recovered model with respect to the “true” AI model.

3.5.2. Prior information

The FCM algorithm will be tested on scenarios where the prior information is variable with differing credibility. We can vary the impact of the prior information by setting different weighting values of η in equation (2.7). If the prior information uses the true (cluster centre values for AI) model values, $\mathbf{P}=[4.6, 7.5, 12.15, 15.4]^T$ (km/s g/cm³) the result of inversion of trace number 80 is shown in Figure 3-3. These results demonstrate that our algorithm is stable: the Misfit decreases steadily with each iteration, and the inverted model is closer to the true model with increasing η .

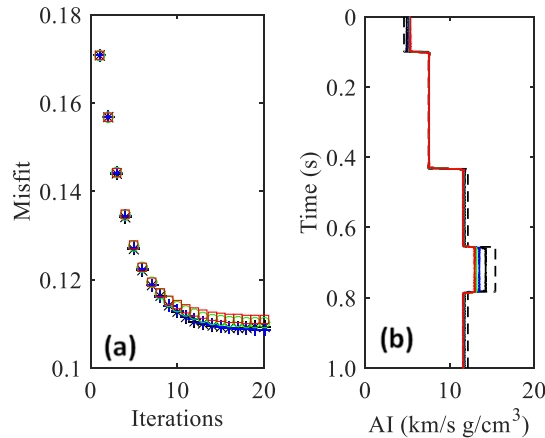


Figure 3-3: Inversion results with various η values. $\eta=0.0$ (red); 0.25 (green); 0.50 (blue) and 0.75 (black). (a) The misfit is inversely proportional to η ; (b) AI models. The inverted model using $\eta=0.75$ is closest to the true model (dashed black line), whilst lower values for η result in inferior models.

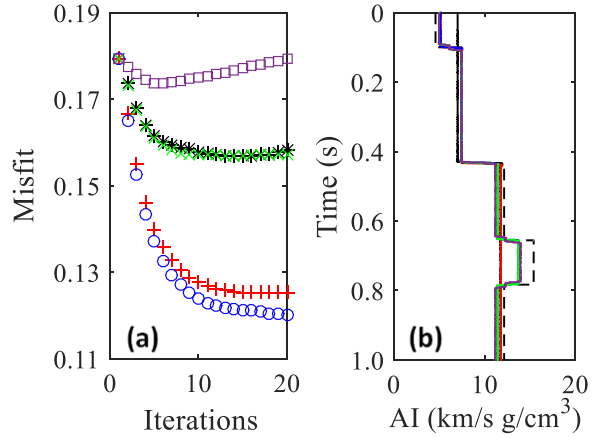


Figure 3-4: Inversion with different numbers of clusters: 2 (black), 3 (red), 4 (blue) 5 (green) and 6 (purple). (a) The misfit is smallest when using the correct number of clusters (4); (b) Comparison between inverted AI models and the true AI (dashed black line).

The number of clusters C (for the inversion to choose from) is a critical parameter for the FCM method. This number can be chosen by analysing any prior information or using numerical experiments (Paasche and Tronicke 2007). Figure 3-4 displays the inversion results with various C values. If C is chosen correctly (4 clusters), the inversion produces the best model. If C is smaller than the true number, the inverted model combines layers. On the other hand, if C is larger than the true number, there may be extra layers created. The inverted models differ little from the optimal case.

Carter-McAuslan, Lelièvre, and Farquharson (2015) state that wrongly defined prior centre values causes incorrect inverted results. However, it is worth noting that in their work, the centre values are predefined and fixed during the inversion process. To test the response of inversion to poorly chosen prior centre values, we define the vector prior centre values \mathbf{P} in equation (2.7) by:

$$\mathbf{P} = \mathbf{AI}^t(1 + \alpha \times \text{rand}). \quad (3.32)$$

where \mathbf{AI}^t denote the true model values, α is a factor that defines how much the vector \mathbf{P} varies from the true model, and rand is the random vector.

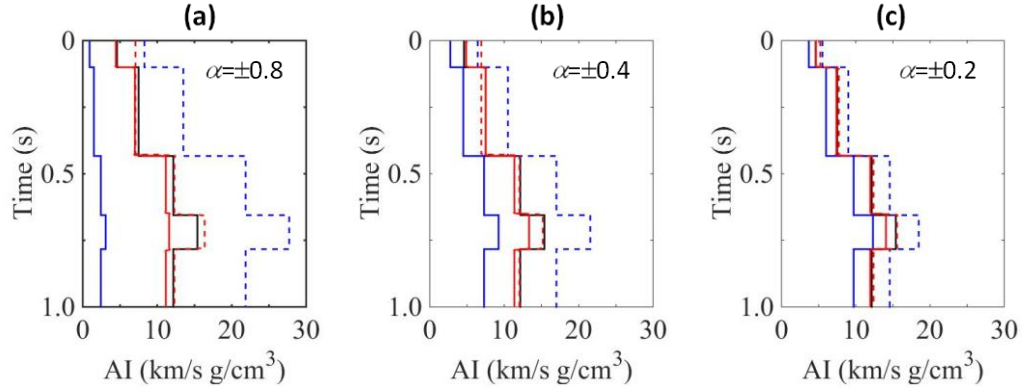


Figure 3-5: Inversion results (red lines) with inaccurate prior centres values (blue lines). In (a), (b) and (c), the black line is the true model; the solid and dashed lines present the cases for negative and positive values of factor α respectively.

To test whether allowing the FCM inversion to predict the FCM centre values with poor initial values there scenarios were created: very inaccurate centre values ($\alpha=\pm 0.8$), moderately inaccurate centre values ($\alpha=\pm 0.4$), and slightly inaccurate centre values ($\alpha=\pm 0.2$). In the case of very inaccurate prior centre values (Figure 3-5a), some parts of the inversion model are incorrect, the fourth layer for $\alpha=-0.8$ and the first layer for $\alpha=0.8$. When the prior centre values approach the true model values (Figure 3-5b, c), the inversion almost always recovers the true model well. In general, it would appear that allowing the FCM inversion to invert for cluster centre values is better than fixing to known or expected values.

3.5.3. Regularization parameters

Figure 3-6 and Figure 3-7 show the experimental results of tracking objective function factors in equation (3.12) of the inversion of trace number 80. Conventionally, the damping factor β is given a large value at the beginning and is then allowed to decrease with each iteration (Lelièvre, Farquharson, and Hurich 2012) to balance between misfit convergence rate versus overshoots until close to the local minima. If the value of γ is too small, the inversion process is unstable, and the inverted results are unreliable (Figure 3-6). The inversion process tends to stabilise with increasing γ , and as expected the inverted model becomes less smooth and forms compact clusters (Sun and Li 2015). In order to optimise the smoothness and clustering parameters, a numerical experiment was conducted. Figure 3-7 shows that the objective function

value is smaller when β is smaller and it is mainly dominated by β . On the other hand, the model error MER , equation (3.31), depends on both β and γ . The regularization parameters β and γ are empirically defined, but their range is wide enough to flexibly choose the optional couple values.

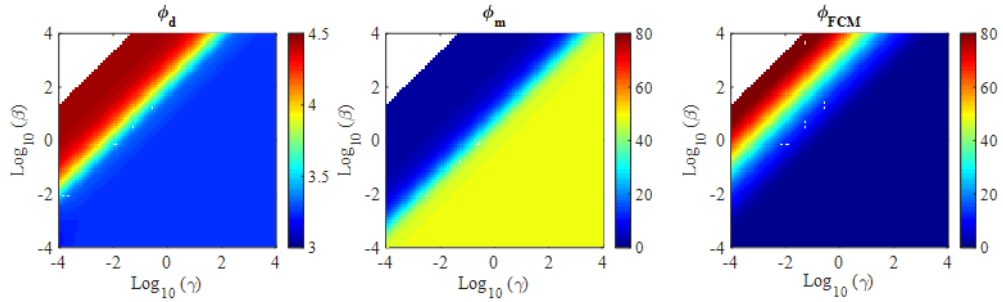


Figure 3-6: Objective function factors in equation ((3.12)) of inversion trace number 80 vary with regularization parameters β and γ . The trend in the misfit Φ_d is similar to the objective function of FCM, Φ_{FCM} and different from the smoothness term Φ_m . The scales of Φ_m and Φ_{FCM} are the same since they both relate to the model parameters.

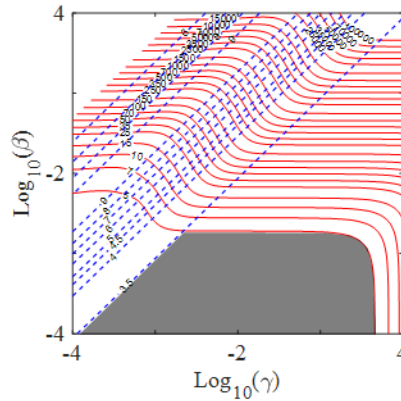


Figure 3-7: Inversion results of trace 80 with various weighting values of β and γ . The solid red contour lines show objective function values and the dashed blue contour lines show the model error. The grey area marks the optimal values of β and γ .

3.5.4. Inversion of a section

In order to maximize the prior information, both prior petrophysics from well-log and/or core measurement and the spatial information that is usually available in seismic data are included in the inversion process through FCM. Prior petrophysical data is input via initial cluster centre values in the clustering process, as in the work of (Sun and Li 2011). Boundary information is incorporated into the inversion process

by attributing media as a feature of FCM input by imposing/weighting for a change of cluster membership near the boundaries as part of the constraints. This process is described detail in the section 2.4.2 of Chapter 2.

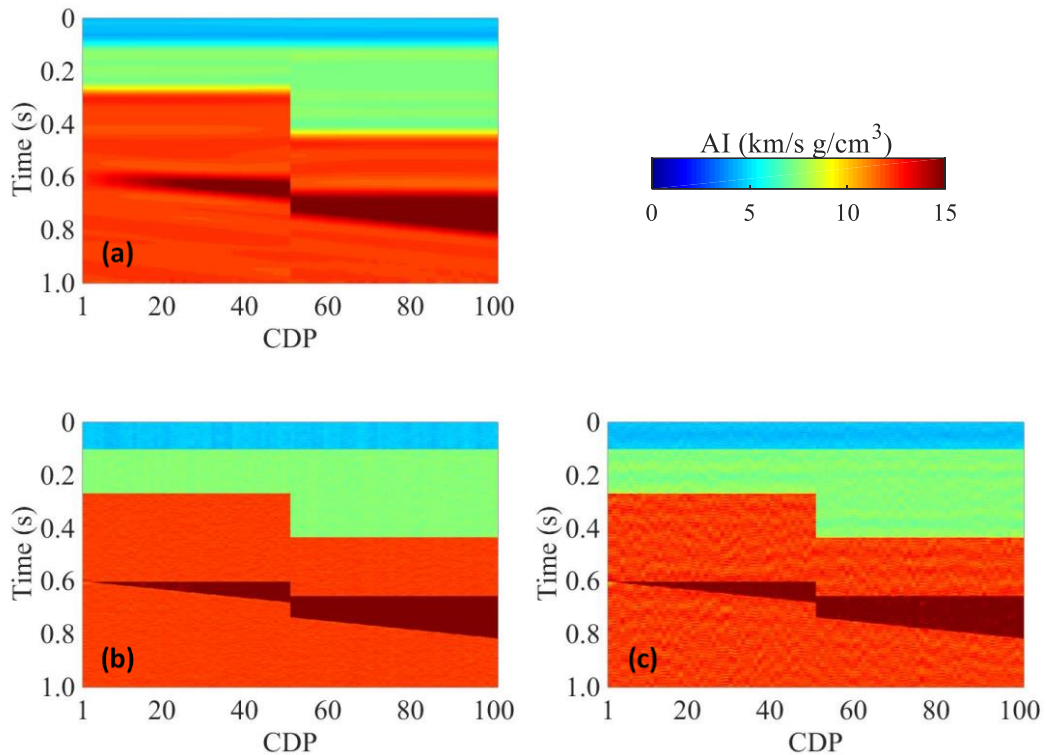


Figure 3-8: Inversion results obtained from (b) our method and (c) HRS from (a) the initial model.

My Matlab coded program (namely FCM inversion) was tested with an initial model generated by Hampson-Russell (HRS) software using two wells located at trace numbers 21 and 81 and with the petrophysical values of the true model, and four horizons picked from the seismic section (Figure 3-8a). After application of the abovementioned coded inversion to the synthetic data from the initial model and prior information (including petrophysics with $\eta = 0.5$ and horizons) a good AI model (Figure 3-8b) results. In comparison with the inversion results of HRS (Figure 3-8c), which uses model-based inversion with the option of hard constraints (maximum impedance change) and lower and upper bounds of 100%, the FCM inversion produces a better model, closer to the true model. The histograms of AI from the resulting models in Figure 3-8b, and c shown in Figure 3-9, indicate that the FCM inversion method recovers the true values better, especially in the second and the third medium. In more detail, the inversion results of two traces, numbers 20 and 80 (next

to the position of the wells), are compared and shown in Figure 3-10. Again, the FCM derived models are closer to the true model than that of the HSR result and clearly less affected by the Gaussian noise.

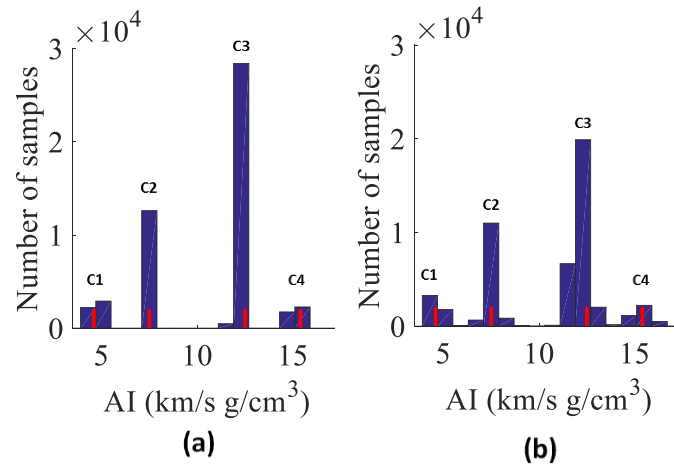


Figure 3-9: Histogram of the inverted AI from (a) our method and (b) HRS. The red colour bars mark positions of the true model values which correspond to the four clusters from C1 to C4.

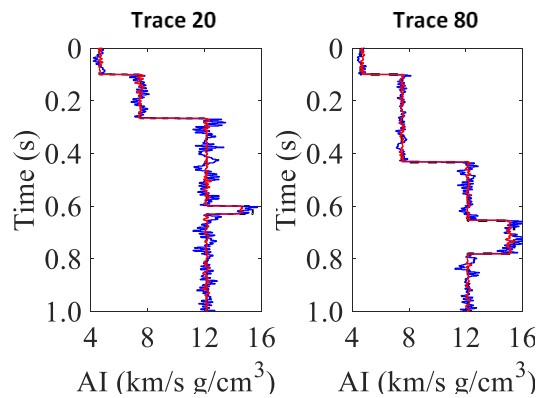


Figure 3-10: Comparison of the inversion results between our program (red lines) and HRS (blue lines).

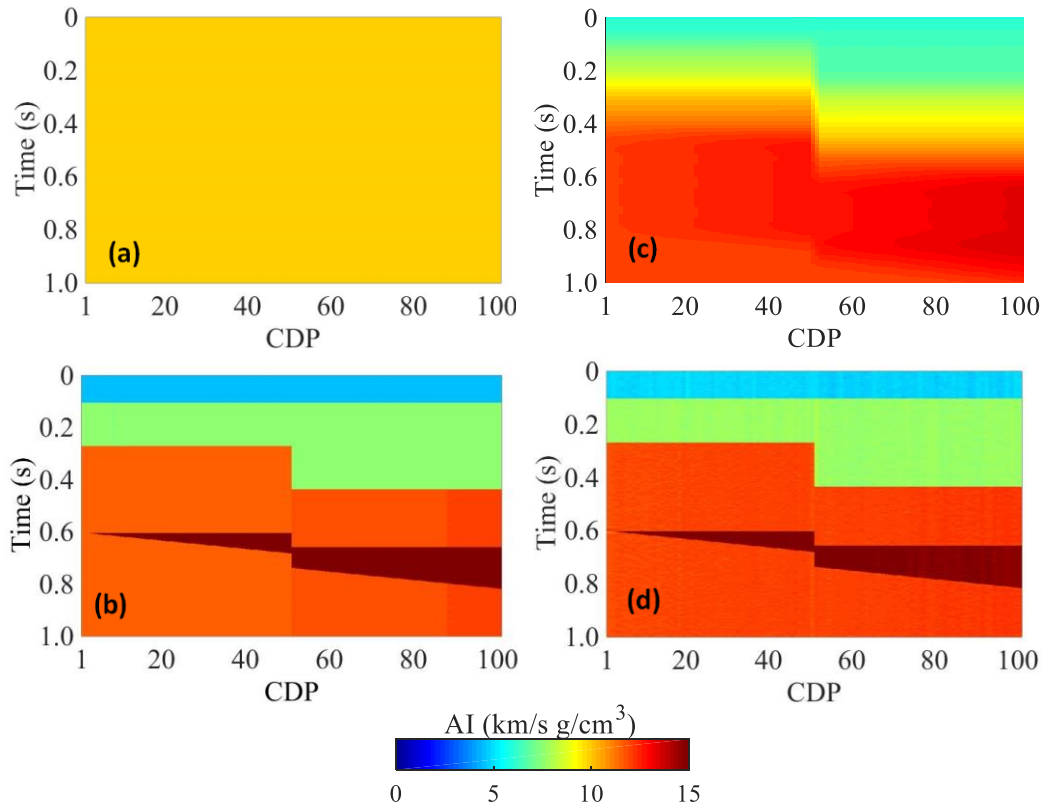


Figure 3-11: Inverted models (b) and (d) from (a) homogeneous initial model and (c) smoothed initial model, respectively.

In a second test, the FCM inversion code was applied to a homogeneous initial model AI of 10 km/s g/cm^3 (Figure 3-11a). Running the inversion with prior petrophysical information weighting of $\eta=0.5$ and without any boundary information did not allow the true model to be recovered. However, if prior boundary information is integrated into the inversion, the results improve considerably. The true model is almost completely recovered, but required 500 iterations (Figure 3-11b) to achieve this result. Computation times can be significantly reduced if we use the initial model in Figure 3-11c which is a smoothed version of the model result in Figure 3-8a. The inversion result after only 20 iterations (Figure 3-11d) is better than that obtained with the homogeneous initial model (after 500 iterations).

To compare the inverted model in time (seismic reflection data are inverted in time to allow the wavelet to be extracted correctly) with the true model, the AI is converted from the time domain into the depth domain. If we assume that the densities of the different rock units of the model are well-known then a velocity model is calculated from the AI model. This velocity model allows the mapping from time-to-depth.

Figure 3-12 shows the inversion results of the FCM inversion algorithm and HRS; both are close to the true model shown in Figure 3-2a.

Finally, FCM is used to group the units of each inverted model into clusters. The number of clusters was chosen to be five (Figure 3-13), which includes four clusters from C1 to C4 that represent the units of the true model. With different colours assigned to each cluster it is evident that the cluster map may be used as a pseudo-lithology section for geological interpretation. When the petrophysical values are subtle between clusters, the cluster maps draw greater distinction to the changes that may be geologically significant.

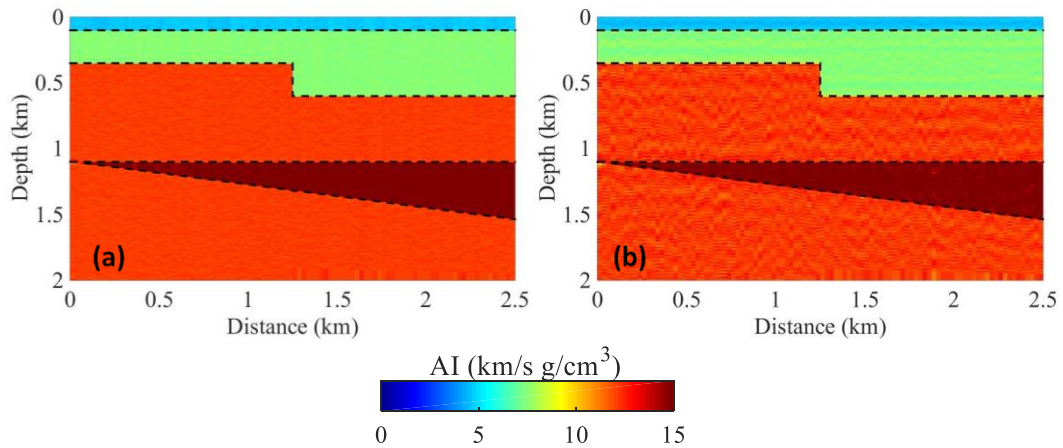


Figure 3-12: Inverted AI models in depth domain; (a) our method and (b) HRS from models in time domain (Figure 3-8b and c respectively). Dashed black lines mark boundaries of the true model.

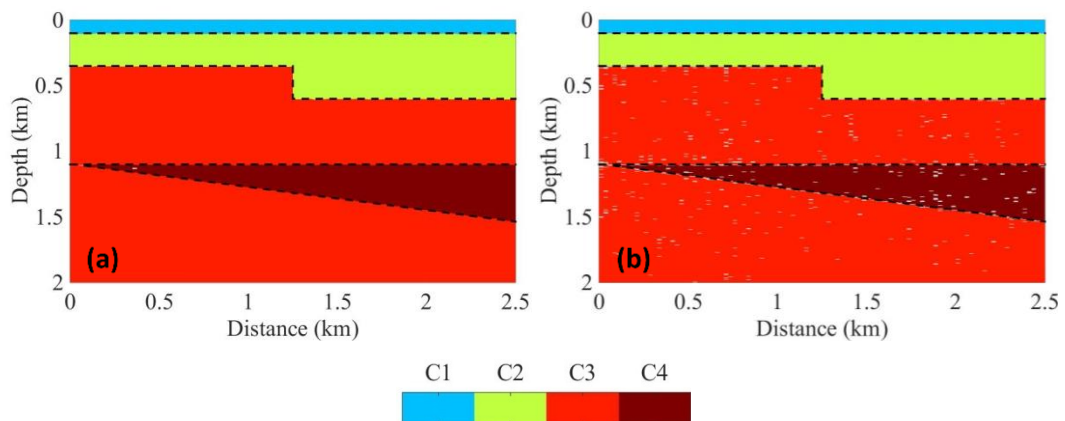


Figure 3-13: Classification results of using FCM for the inverted AI models of (a) our method and (b) HRS. The cluster from C1 to C4 present four mediums (Figure 3-2a). Dashed black lines mark the boundaries of the true model.

3.6. Inversion of magnetotelluric data

Inverting magnetotelluric (MT) data can image the distribution of conductivity beneath earth surface. However, it is a solution ill-posed problem, and often strongly so. Multiple models of conductivity distributions may generate the same electromagnetic signature, especially at depth where sensitivity to changes are low. Thus, extra information is essential to reduce the ambiguity of the MT solution. The source of additional information may come from the prior/anticipated structure of the model and/or locally known values of conductivity. Conventionally, smoothness criteria are added to constrain the MT inversion (deGroot-Hedlin and Constable 1990). This constraint may stabilise inversion process and reduce ambiguity by choosing the smoothest model. However, it also usually produces unrealistic geological models because most significant geological boundaries in the top 5 km of the crust are not gradational, and nearly all geological maps encountered show sharp boundaries not smooth transitions.

The MT method is based on diffusive EM fields as it utilise relatively low-frequency electromagnetic waves (generally less than 1 kHz) and are most sensitive to conductive environments (Simpson and Bahr 2005). Therefore, the MT method loses resolution and ‘sharpness’ with depth, and it is also relatively insensitive to resistive units (the absence of conductive material provides less anomalous response than an excess of conductive material). Resolution and boundary ‘sharpness’ can be improved with appropriate constraints, for example, by incorporating prior information. This prior information comes from borehole data, geological information, or other geophysical methods with higher resolution (e.g. seismic reflection).

In this thesis petrophysical information from boreholes combined with seismic reflection data is used to constrain MT inversion via FCM clustering. The MT derived resistivity from inversions is biased to values measured from borehole to assist in building models that are more reliable. If the boundaries derived from seismic data are co-incident with changes in resistivity then these may be introduced into MT inversion via the FCM method outlined previously. This approach has been demonstrated to significantly enhance the inverted MT data results (Kieu, Kepic, and Pethick 2016).

3.6.1. Synthetic model

The FCM MT inversion code with petrophysical and boundary constraints was initially tested with a synthetic model (Figure 3-14a). This work was partly presented in Kieu, Kepic, and Pethick (2016). The 2D geoelectrical model comprises four layers, and there are two local objects superimposed into the second and third layer. It is worth noting that it is a significant challenge for the MT method to define object O2 and boundary B3. O2 is located right beneath a conductive layer and B3 separates the basement rock units and the upper layer where the media is low in conductivity contrast and has high resistivity values.

The inversion process was run on several prior initial condition scenarios: the typical petrophysical values of the media (i.e., the centre values) $\mathbf{P}=[100; 30; 300; 1000] \Omega\text{m}$ are included, and the combination of both the prior boundaries and petrophysical information. The number of distinct resistivity media in the model is five; this is different from the number clusters in the inversion process. In this case, we assume that we do not know about object O2 (Figure 3-14a). The three boundaries may be included in inversion processes creating three scenarios (Figure 3-15). First, B1 is used, it divides the section into two layers; second, if we know information about B1 and B2, the section is separated into three layers; and the last case, all the three boundaries information that define the four layers of the section are included. The media classes are category features (non-numerical data) and are to be inverted along with the model parameters to put in FCM cluster. Through the clustering process, model updates are guided by boundary information.

The purpose of the synthetic test is to determine the importance of each prior initial condition within the inversion process. Also, the FCM inversion approach is tested to check if the resulting conductivity distribution better reflect the true model. Particularly, the ability to differentiate between the basement rock units and the upper layer will be difficult task due to the low conductivity contrast and high resistivity values. The FCM inversion uses modified the 2D MT inversion code from Lee et al. (2009) while retaining the original forward solution. An inversion of the synthetic data is performed with the same regularisation parameters β and γ (0.1 and 0.01 respectively). The initial model is set homogeneously to 400 Ωm , although it would

be better and more correct to set to an initial 1-D smooth model based upon the average MT sounding curve.

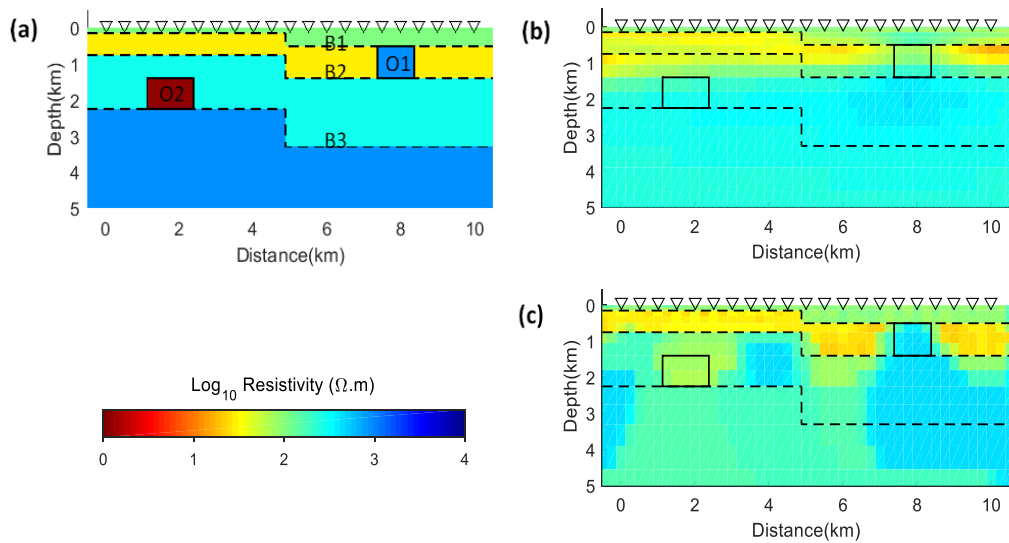


Figure 3-14: (a) 2-D geoelectrical models. The three boundaries B1, B2 and B3 (dashed lines) divides the section in four layers. The two objects O1 and O2 (rectangles) are superimposed in the second and the third layer respectively. The triangles on the top profile mark the position of MT stations. Inversion results using (b) smoothness constraint only and (c) included FCM, which demonstrates that FCM can assist inversion to build a better model than the use of smoothness only.

3.6.2. Inversion with constraints upon the number of clusters

In the basic scenario, when petrophysical and boundary information are unknown, and only the number of units are estimable the FCM inversion method is shown in Figure 3-14c. The FCM constrained result is significantly better than the approach that uses a smoothness constraint only (Figure 3-14b). This result demonstrates the power of directing the inversion algorithm to pick a limited number of petrophysical properties to construct a model. Such direction also leads to a model more representative and interpretable for mineral exploration as it produces discrete targets/units that are not as open to interpretation.

3.6.3. Inversion with constraints in petrophysical and boundary information

Figure 3-16 shows the inverted models when constraints in the petrophysical values and some upper boundary information are included after ten iterations. The inversion results show that boundaries B1, B2 and the objects O1, O2 are recovered well. When

some petrophysical information is known, but the boundary information is unknown (Figure 3-16a), the resulting geoelectrical model is significantly improved. Improvements in resolving the lower units are made by the inclusion of shallow unit boundaries within the inversion as prior information (Figure 3-16b-d). Such a situation is not uncommon as there may be previous drill holes in the area, but not penetrating fully to the depths of interest. When the shallowest boundary B1 is included as an inversion constraint, the basement is significantly better recovered (Figure 3-16b). Similar results are encountered for scenarios when the boundary B2 and B3 are utilised respectively. Particularly, in the case where all three boundaries are included in the inversion (Figure 3-16d), the inversion almost recovers the true geo-electrical distribution. Note that knowing the location of the uppermost boundary offers the greatest improvement. Thus, if we were to combine seismic reflection data to guide MT inversion, it is perhaps more important to gather information about the shallow boundaries rather than using seismic data to constrain deep boundaries alone.

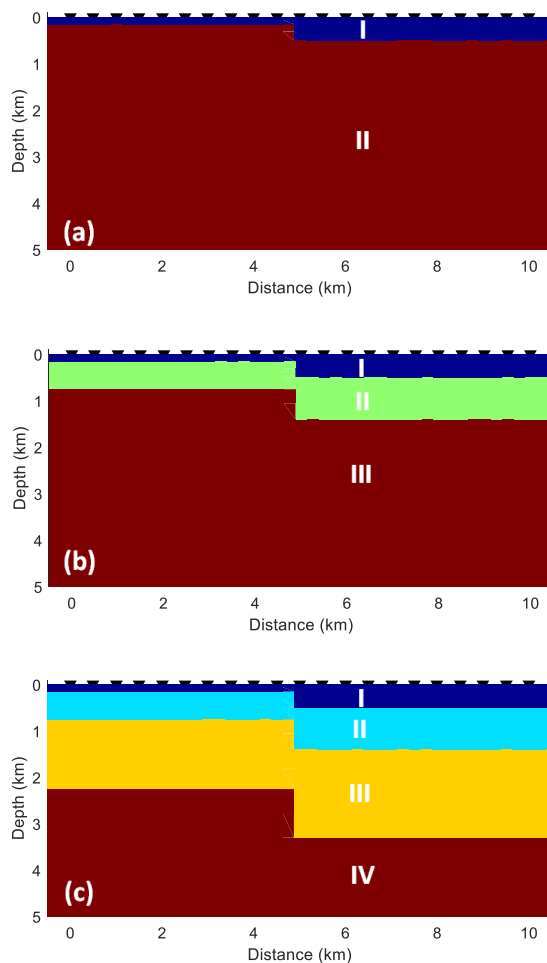


Figure 3-15: The boundaries B1, B2 and B3 (Figure 3-14a) divides the section into different media. (a) The section is divided in two areas I and II by boundary B1. (b) B1 and B2 separate the section into three areas I, II and III. (c) B1, B2 and B3 separate the section into four areas I, II, III and IV.

To evaluate the tolerance of the FCM guided algorithms with incorrect boundary locations, which is possible as geological boundaries or seismic boundaries may not be geo-electrical boundaries. Figure 3-17 shows the FCM inversion results with three cases when boundary information B2 is included into the FCM inversion. In the case of correctly locating the boundary, the inverted model (Figure 3-17a) shows significant improvement in comparison to the result without boundary information (Figure 3-16a). If the location of boundary is inaccurate, the results of FCM inversion (Figure 3-17b and c) are still acceptable and better than without boundary any information (Figure 3-16a).

These synthetic inversion tests demonstrate that fuzzy clustering can be included successfully, and significantly enhance MT inversion. In comparison with the approach of constraining inversion using smoothness constraints only (Figure 3-14b), the inverted models from FCM constraint (Figure 3-14c) are closer to the true model (Figure 3-14a). The first and second layers are clearly seen in the inversion results using FCM as an extra constraint. As a posed to the results in the inversion with smoothness constraints. The two objects (O1 and O2) are clearly identifiable in the FCM inversion results. However, the objects, O1 and O2, are not apparent in the smooth inversion results. These objects are clearly too small and smeared out by the smoothness constraint. Whereas, FCM assists in forming distinct units with sharp boundaries as so does much better in preserving the identity of such small anomalies. Examining the histograms of inverted resistivity model parameters from smoothing (Figure 3-18a) and FCM (Figure 3-18b) constraints shows the differences in approach. We can see that for the smoothing constraint, the model is divided into three groups: the first two groups are not well separated, and as a result it could not recover the highest resistivity media. With the assistance from FCM, the FCM constrained inverted resistivity model is divided into four clusters. The first two groups are well defined, which is better than the smoothing results. However, the FCM guided inversion is not able to recover the correct values of the true model in the two-last media.

The prior petrophysical data can be exploited to bias the centre values of the FCM clustering. By this manner, the physical properties of the inverted model are tied to prior information. When comparing results without (Figure 3-18b) and with (Figure 3-18c) prior petrophysical information, the use of prior petrophysics estimates the

resistivities of the units significantly better, which is expected. The two clusters with higher resistivity are significantly improved with respect to accurately recovering resistivity. Whereas, the two distributions (units) with lower resistivity are reasonably recovered without prior petrophysical constraints. The improvements in the resistivity distribution also improves the structure of the model, as the model with prior petrophysical information (Figure 3-16a) is closer to the real model than the model without the prior information (Figure 3-14c).

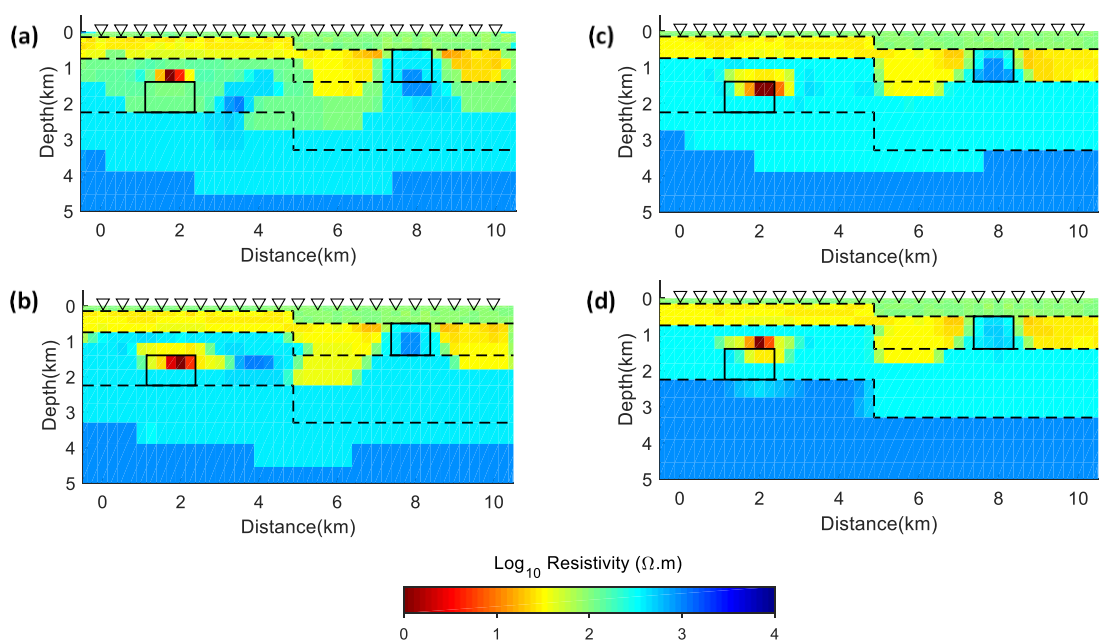


Figure 3-16: Inverted results with various prior information cases: (a) petrophysics only; both information of petrophysical and boundary information (b) B1, (c) B1 and B2, and (d) B1, B2 and B3. The dashed lines mark the three boundaries and two objects locations are presented by the two rectangles. Boundary information, particularly in the case all of three boundaries are included in the inversion, the true model is almost fully recovered.

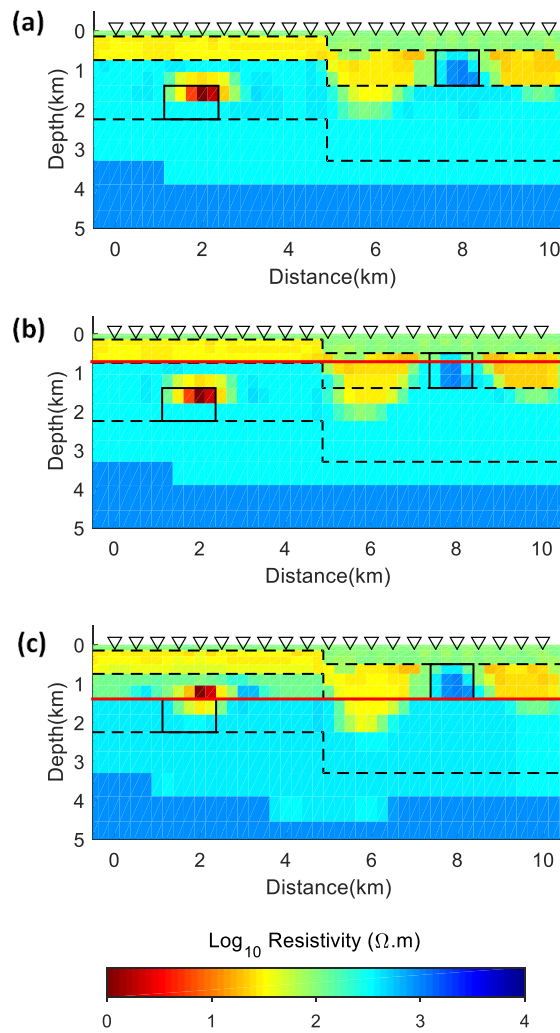


Figure 3-17: Inverted results with prior petrophysical information: (a) correct boundary information B2, (b and c) incorrected locations of B2 (red lines). In general, these both results almost are similar with the result when the boundary are correctly defined and significantly better than the inversion result without any boundary information (Figure 3-14a).

When petrophysical and spatial information are combined to assist the inversion process the results are significantly improved (Figure 3-16 and Figure 3-18). Since the MT method is not sensitive to geometry information, it is very beneficial if the spatial-boundary information is put into the inversion process even though the geometry may not be accurate the inversion still produces better results than without any of this information (Figure 3-17). In the example provided when boundary information B1, B2, and B3 are included into inversion process the inverted models (Figure 3-16b, c, and d) are closer to the actual model than inversion without any boundary information (Figure 3-14a). Interestingly, incorporating shallow boundaries B1 and B2 in the example significantly improved the results in the deeper part of the

section. This situation is common in geophysical exploration where we often have shallow information from borehole data or other geophysical methods with high resolution, but limited in depth. As the geometry of the model is enhanced the physical properties of the inverted model become more accurate as the uncertainty in one aspect is reduced so are related aspects. The histogram of inverted model resistivity (in Figure 3-16a, b, c, and d are shown in Figure 3-18c, d, e, and f respectively) demonstrate that improving of the model geometry improves the resistivity distributions.

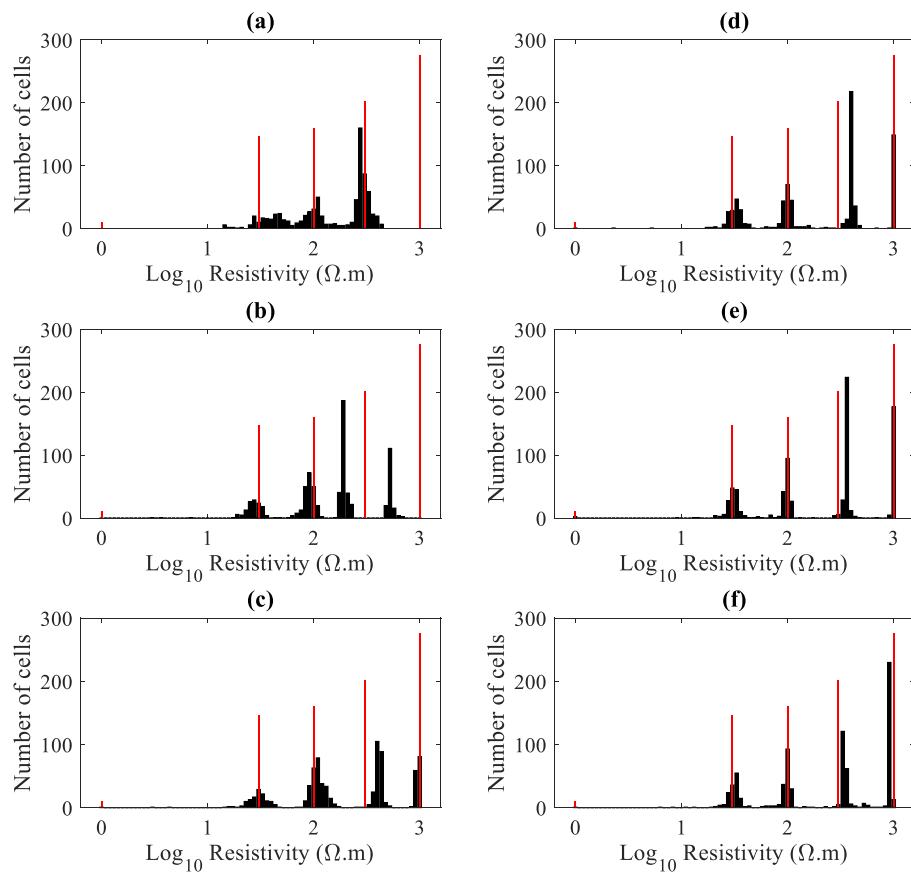


Figure 3-18: Histogram of resistivity from inverted models using different constraints: (a) smoothness, (b) FCM clustering, (c) FCM clustering and petrophysics, (d) FCM clustering, petrophysics and boundary B1, (e) FCM clustering, petrophysics and boundary B1 and B2, and (f) FCM clustering, petrophysics and boundary B1, B2 and B3. The red bars are resistivity of the true model.

3.7. Co-operative inversion of multiple geophysical datasets

3.7.1. Co-operative inversion workflow

Figure 3-19 presents the workflow of a co-operative inversion (CI) scheme. In this scheme, the individual data is separately inverted, and the models are updated simultaneously. The exchange of information between models is executed by FCM clustering analysis. In this process, all model parameters and prior information of all methods are put into FCM clustering, the output of this process including membership matrix and centre values are utilised for calculating perturbation models (equation (3.24)) for any of the inversion processes, which run in parallel. This approach is a form of “common earth” model for inversion, but the common earth is the FCM cluster model. Thus, the FCM process also allows a methodology for co-operative inversion strategies with multiple geophysical data.

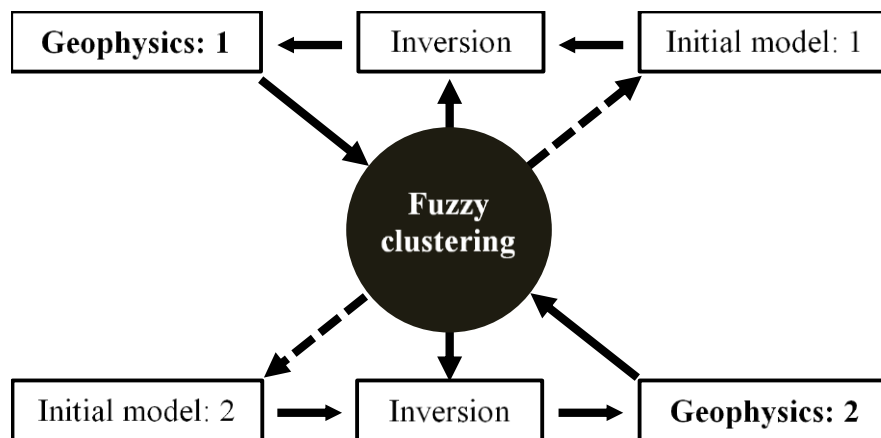


Figure 3-19: Workflow of the co-operative inversion. To couple the models using petrophysical relationship by mean of FCM clustering, I exploit FCM clustering in two approaches. Firstly, FCM is a function to convert one geophysical model into another model. Secondly, FCM is a platform sharing information between the geophysical models.

As previously, the prior information comprising both petrophysical and spatial information can be exploited to constrain inversion. In this manner, FCM plays a role of guider; it uses the prior information to drive the generation model that honours both observed data and prior information. Using the synthetic example of seismic and MT data demonstrates that this co-operative FCM inversion process works to produce reliable models.

The information of the two models is shared through the FCM process. From equation 3.23, we can obtain the adjustment model in separate (3.33) and co-operative (3.34) inversion processes, respectively.

$$\Delta \mathbf{m}_{sep} = [\mathbf{J}_{(1)}^T \mathbf{A} \mathbf{J}_{(1)} + \beta \mathbf{H} + \gamma \widehat{\mathbf{U}}_{sep}]^{-1} [\mathbf{J}_{(1)}^T \mathbf{A} \Delta \mathbf{d}_{(1)} + \gamma (\mathbf{U}_{sep} \mathbf{O}_{sep} - \widehat{\mathbf{U}}_{sep} \mathbf{m}_{(1)})], \quad (3.33)$$

$$\Delta \mathbf{m}_{coo} = [\mathbf{J}_{(1)}^T \mathbf{A} \mathbf{J}_{(1)} + \beta \mathbf{H} + \gamma \widehat{\mathbf{U}}_{coo}]^{-1} [\mathbf{J}_{(1)}^T \mathbf{A} \Delta \mathbf{d}_{(1)} + \gamma (\mathbf{U}_{coo} \mathbf{O}_{coo} - \widehat{\mathbf{U}}_{coo} \mathbf{m}_{(1)})]. \quad (3.34)$$

In equation (3.33) and (3.34) the subscript ‘sep’ and ‘coo’ refer to separate and co-operative process. In my inversion algorithm, the adjustment of the models in next iteration (Equation 3.33) relates to membership degree and centre values that are obtained by applying separately fuzzy clustering to the each model parameter of previous iteration. In the co-operative inversion routine, the membership and centre values relating to the updating model parameters (Equation 3.34) are define by the parameters of the both models. Thus, the sharing information of the two models is computed via fuzzy clustering.

3.7.2. Synthetic example of co-operative inversion with FCM

A synthetic example will be used to demonstrate the co-operative FMC inversion method, and that this method efficiently recovers an accurate earth model. The co-operative inversion of seismic and MT data will be used to demonstrate that seismic data increases the effective resolution of MT data and in turn, seismic impedance models benefit from the lower frequency data in the MT model. Both MT and seismic reflection are often used together for deep exploration.

The 1-D model includes six layers (Figure 3-20), whose velocity and resistivity are functions of density. Co-operative inversion using empirical relationships between the geophysical parameters can produce a good result if these functions are properly defined (Heincke et al. 2017). A poor result can be expected when an inappropriate

relationship is put into co-operative inversion (Moorkamp 2017). This is because the relationship between geophysical parameters forms a very strong, de-facto constraint. To demonstrate this issue, model MT#2 is almost the same as model MT#1, the resistivity is generally a function of density, but the resistivity in layer 6th departs from the function. The simulated MT and seismic data are shown in Figure 3-21 and Figure 3-22 respectively. The effect of the different resistivity between MT#1 and MT#2 in layer 6 is observable in the MT curves.

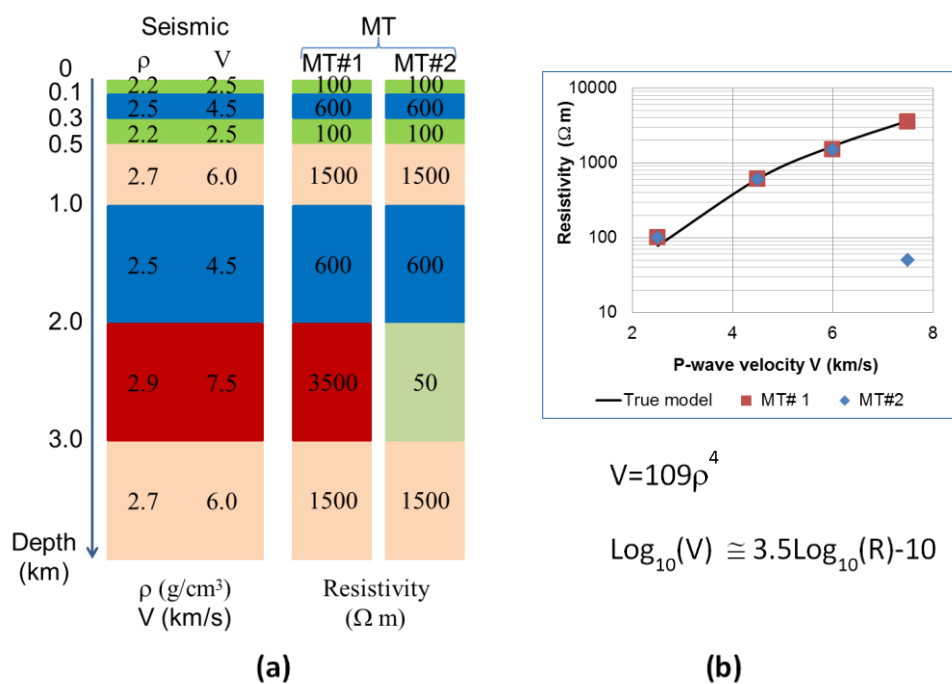


Figure 3-20: Synthetic models of seismic and MT. (a) 1D model of density ρ (g/cm³), velocity V (km/s) and Resistivity R (Ωm), the numbers in each layer present parameter values of the layer. (b) relationship between the parameters, velocity and resistivity of true model is functions of density. Resistivity of the model MT#1 approximately equal to the true model. The model MT#2 is almost the same as model MT#1 except 6th layer, the resistivity is 50 Ωm instead of 3500 Ωm as in model MT#1.

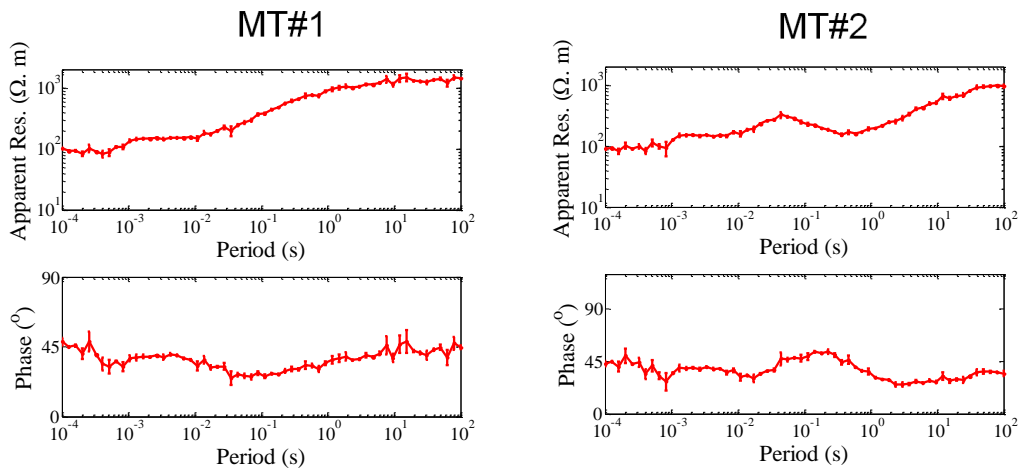


Figure 3-21: MT synthetic data calculated from model MT#1 and MT#2 (Figure 3-20) and added random noise with level of 5 % and 10% for dead band (0.001-0.005 s).

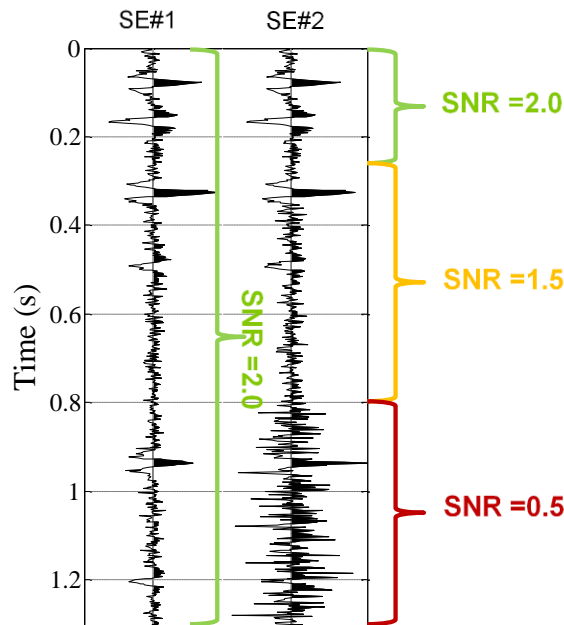


Figure 3-22: Seismic synthetic data generated by convolution reflectivity coefficient computed from the model (Figure 3-20) with Ricker wavelet and added random noise with different ratio SNR (Dahl and Ursin 1991).

Table 3-1: Combinations of seismic and MT data

Relationship \ Data	Good (SE#1)	Noisy (SE#2)
Good (MT#1)	C1	C2
Bad (MT#2)	C3	C4

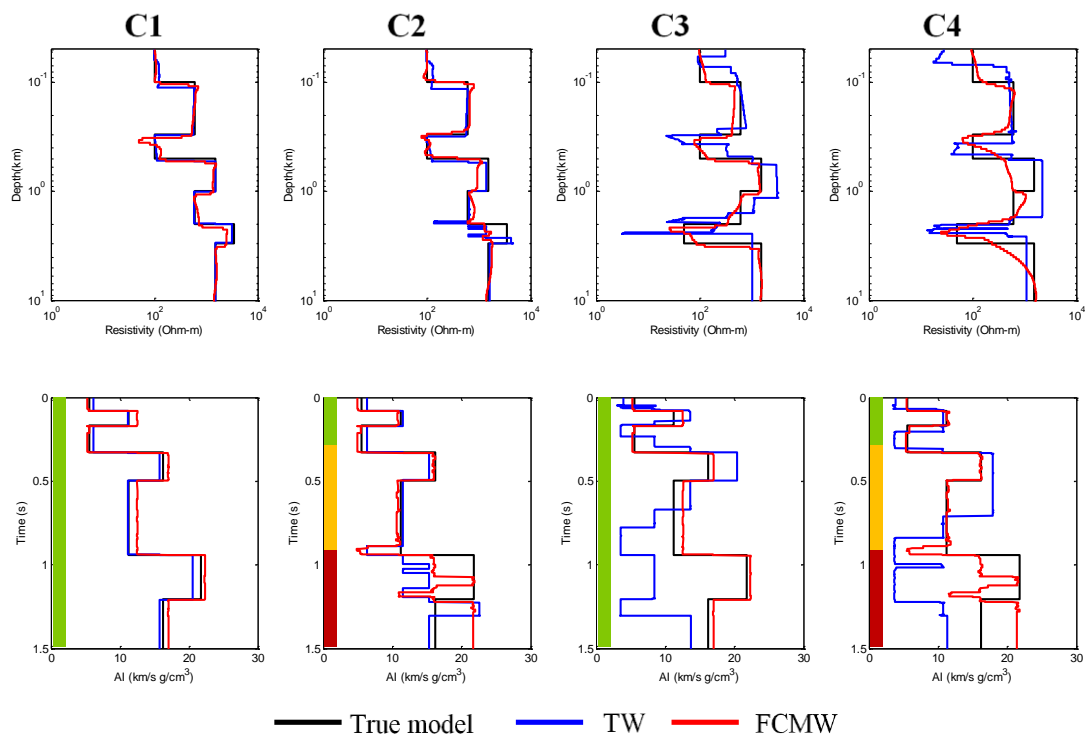


Figure 3-23: Inversion results of co-operative inversion for four data combination C1-C4. The inversion result of using my workflow (FCMW) is closer to true model than using translation workflow (TW). The colour column in low panel represent noise level of seismic data (Figure 3.22).

Four scenarios of combination data between MT and seismic data C1, C2, C3 and C4 (Table 3-1) are examined. MT data from the model MT#1 that follows a function of density is named a “Good” relationship, on the other hand, model MT#2 has an exception in the 6th layer that is not a function of density is named “Bad” relationship (Table 3-1). Seismic data with a relatively low noise level, SE#1, is “Good” data.

Meanwhile the data with noise that increases with depth SE#2 is the “Bad” data from seismic (Table 3-1).

Figure 3-23 compares co-operative inversion results of two schemes, which perform as expected. The conventional workflow (Translation workflow) using a function to convert the inverted model of one method to a prior model of the other method produces magnificent results in the case of C1. However, in the other cases, the results are poorer due to the incorrect exchange of parameters. The FCM workflow produced good models in all cases without knowing or needing to define an explicit relationship between resistivity and velocity. Thus, the FCM approach tends to establish relationships between various physical properties and this provides a very powerful means to perform co-operative inversion of multiple data.

3.8. Conclusions

It is demonstrated how FCM may be incorporated in both separate and co-operative inversion strategies. Prior information comprising both petrophysical and spatial information can be exploited to constrain inversion with FCM clustering. In this manner, FCM plays a role of guider; it uses the prior information to drive the generation model that honours both observed data and prior information. Using synthetic examples of seismic and magnetotelluric data demonstrates that the presented algorithms and workflows create inversion processes that well in producing reliable models.

Chapter 4: CO-OPERATIVE INVERSION OF MAGNETOTELLURIC AND SEISMIC DATA

Summary

In this chapter, application of the co-operative FCM inversion algorithms is applied to a real dataset. This dataset comprises of magnetotelluric (MT), 3D seismic reflection and borehole data acquired over an area prospective Carlin-style gold deposits, Nevada, USA. The main target of the exploration is mineralised zones containing gold, which are primarily hosted in Palaeozoic basement rock. The mineralised zones usually occur along with the faults through the process of hydrothermal alteration, forming weakened rocks with low resistivity. Hence, these zones are likely to be detectable by seismic and electromagnetic methods directly as relative low velocity and conductive if they have sufficient volume. However, the mineralisation zones are usually small and located at great depths within the basement, which presents challenges for both MT and seismic methods. Therefore, my study utilises a mechanism of co-operative inversion, which enables the integration of additional prior information into the model creation process. This provides a better result than using just a single dataset for this process. The aim of this work is to build a model that maps the main geological features of the section of interest, and possibly some signatures relating to possible mineralisation itself.

Two schemes of co-operative inversion (CI) are tested, sequential and parallel. In the sequential co-operative method, MT inversion is run first with boundary constraints from the seismic imaging data, followed by seismic inversion with the MT model assisting to build a starting acoustic impedance (AI) model through a shared cluster model in one variant. The MT models show significant improvement with the assistance of prior information and seismic data. The seismic inversion is trialled with three initial models, which are generated from borehole data, a migrated velocity model and the MT model. The results demonstrate that even though the FCM algorithm reduces the dependence on an initial model, there are limitations if the initial models are poorly defined due to the lack of low-frequency band information in the reflection seismic data. Running the seismic inversion with an initial model

generated from the conversion of the MT model resulted in an outcome that shows the main structure of the faults best and assists to define the possible mineralised zones.

The parallel co-operative inversion approach is executed by running the MT and seismic inversions independently but coupling them simultaneously through the fuzzy clustering process. The results of this process are comparable with the borehole data and produces model results almost same as those produced by sequential co-operative inversion. Nonetheless, there is a difference between the two due to the coupling process. The link in parallel co-operative inversion imposes less constraint than the sequential co-operative inversion as there is no conversion of the model parameters. Consequently, the MT model has lower resolution than the sequential co-operative inversion modelling approach. Nevertheless, the parallel co-operative inversion can reduce the bias inherent in an improper relationship between the two models' parameters.

Finally, the MT and seismic models are processed by fuzzy c-means (FCM) clustering to build a pseudo-lithological model. These images should assist in the interpretation process, making it much easier than by using just the inverted models created from MT and seismic images alone.

4.1. Introduction

Data acquired using geophysical methods in the same location usually provides different subsurface images because they are sensitive to different physical properties and different resolution. Integrated models from multiple geophysical data will likely produce a better geological model (Paasche et al. 2006, Bedrosian et al. 2007, Ogaya et al. 2016). This process attempts to reduce the model uncertainty by exploiting complementary information from the multiple geophysical models. However, this process does not maximise the use of the complementary information from the data sets explicitly to narrow the solution domain of the geophysical inversion. Since the inversion is non-unique, the inverted models from the different methods cause ambiguity or even contradiction in geological interpretation. Thus, it is more efficient to narrow the solution domain by using the complementary information explicitly via an algorithm during the inversion of multiple data sets than in a post inversion process

of the inversion of a single dataset (Vozoff and Jupp 1975, Lines, Schultz, and Treitel 1988, Haber and Oldenburg 1997, Gallardo and Meju 2003, Paasche and Tronicke 2007, Farquharson, Ash, and Miller 2008, Jegen et al. 2009, Doetsch et al. 2010, Moorkamp et al. 2011, Lelièvre, Farquharson, and Hurich 2012, Zhou et al. 2014, Sun and Li 2015).

There are two main inversion schemes for multiple geophysical data, co-operative and joint inversion. While joint inversion involves simultaneously processing multiple geophysical data sets with a single algorithm and often a single multi-physics forward algorithm, the co-operative inversion approach implies individual application of different inversion techniques to a single dataset and /or a common earth model with linked parameters. There are advantages and disadvantages to both techniques. The joint inversion process exploits the complementary information of individual methods to directly build the petrophysical models (Gallardo et al. 2012) simultaneously. Nevertheless, there are several drawbacks of the joint inversion strategy (Heincke et al. 2017). The most problematic occurs when dealing with the weighting of the different geophysical methods, as there are different responses and resolutions to the model (Lines, Schultz, and Treitel 1988, Heincke et al. 2017). On the other hand, co-operative inversion, using the output of one method as part of the prior information for the next method, avoids the difficulties of the joint inversion scheme, but may not keep the complementary information. For instance, if we convert the seismic inversion results into the initial MT model, the resolution of the seismic data may be destroyed by the MT inversion and the MT model output might not be suitable for further use by the seismic inversion method. In this work, a hybrid scheme of joint and co-operative inversion processes take advantage of both these schemes and avoid most limitations. In this approach, individual data is run separately; and, the link and updating of the model is simultaneous via a shared FCM constructed model.

Setting up the relationship between the different models is an essential issue of joint or co-operative inversion. There are two coupling categories, structural and petrophysical. The structural link is based on the assumption that the models have similar structures (i.e. boundaries between changes in properties and the uniformity within each rock unit are similar). This approach to inversion tends to minimise the structural differences between the models (Haber and Oldenburg 1997) or the cross-

gradient (Gallardo and Meju 2003, 2004, 2007, 2011) method that requires that when property changes the other should too. The petrophysical process is based on using physical relationships describe with a mathematical function to link the models, which are usually empirical definitions (Lines, Schultz, and Treitel 1988, Jegen et al. 2009, Giraud et al. 2016, Heincke et al. 2017, Bosch and McGaughey 2001).

Petrophysical coupling can produce better results than structural linking (Lines, Schultz, and Treitel 1988, Moorkamp et al. 2011), since the petrophysical constraints establish a strong interaction over the whole model domain. On the other hand, structural constraints, such as cross-gradient, only impose the strong interactions at the discontinuity (Stefano et al. 2011). When petrophysical relation is not likely to be valid for the whole model and using an improper relationship to exchange models will result in spurious models (Moorkamp et al. 2011, Moorkamp 2017). To overcome this limitation, Heincke et al. (2017) proposed a flexible strategy by using adaptive relationships. Their work demonstrates that by separating the entire relation function into multiple functions for different regions of the models results in a significant improvement at the expense of significant added complexity. The empirical functions are not easy to identify because the crosscorrelation between the two physical properties often has considerable scatter (Moorkamp 2017).

Bosch and McGaughey (2001) proposed a robust tool to deal with the correlation scatter issues; they defined the petrophysical relationship for each lithological unit by using a mean of the geostatistical model, which can work well where the physical properties of the units show granular relations. However, in geophysics we usually have initially unclear, separated and unlabelled units, which may cause issues when using co-operative inversion under the constraints.

Several authors have proposed fuzzy clustering to link the models (Paasche and Tronicke 2007, Sun and Li 2011, Lelièvre, Farquharson, and Hurich 2012, Sun and Li 2015). This technique is based on fuzzy logic; thus, it enables us to deal with ‘unclear’ situations. Moreover, this technique can automatically define units, which allows the models to be linked with very little prior information, such as the cluster number. The use of fuzzy clustering needs the least restrictive means of coupling models while still honouring the individual data sets.

I chose to use fuzzy c-means clustering as the means of coupling in the co-operative inversion schemes as in Paasche and Tronicke (2007). Nonetheless, my approach is different from previous works (Paasche and Tronicke 2007, Lelièvre, Farquharson, and Hurich 2012, Sun and Li 2015) in the way the FCM is modified and utilised in the co-operative inversion process. My approach allows imposing both petrophysical and structural coupling in the inversion processes.

4.2. Strategies of co-operative inversions

The purpose of the co-operative inversion is to exploit complementary information from each member method to build more reliable models than using a single dataset model. The co-operative inversion of seismic reflection and MT data can utilise the high resolution of seismic data to support the low resolution of MT data and vice versa; the seismic reflection model, which lacks low-frequency information, benefits from the MT model. Nevertheless, the FCM method allows both the MT model and borehole prior data to be integrated with major changes to the algorithm as the MT data assist in setting the spatial distribution of parameters (in a low-frequency sense) and the borehole information provides information about the cluster number and statistical distribution of parameters away from the borehole.

The crucial issues of the co-operative inversion are “over constraint” or bias (Moorkamp 2017) and convergence issues. The prior information may drive the inversion process too much, which may make the inversion unstable, and likely divergent. Or the inversion simply does not change much from the initial model. Lelièvre, Farquharson, and Hurich (2012) stated that the convergence issues might be avoided if the level of coupling between the models is slowly increased during their joint inversion of seismic travel times and gravity data. I also found that the inversion procedure is stable and the convergence of the process is reliable if the effect of cooperation coupling is raised slowly during the inversion process. Thus, other implemented FCM co-operative inversion strategy runs iteratively with the increasing integration level with iteration.

Two co-operative inversion strategies were tested: sequential and parallel. In the sequential routine, each dataset is processed in order and the final model of the first dataset is used to constrain the inversion of the next dataset. In the parallel strategy,

the inversions of all data sets use parallelised processing. The inversion process stops when the prior conditions are met. The stop conditions in my inversion include three terms: threshold value of misfit between synthetic and real data, the threshold value of relative perturbation model, and maximum iterations (these conditions are described in section 3.4, Chapter 3).

It is worth reinforcing that the inversion process utilises FCM clustering to couple the models. This technique is based on fuzzy logic; thus, it can introduce ‘soft constraints’ from parameter statistics/distributions into the inversion process. This soft constraint approach can tolerate inaccurate and unclear situations better, which are very common in geology. With “hard” model constraints the confidence in the accuracy in space and in the accuracy of measurement limit the weighting. Plus, the borehole measurements may not be representative only a few metres away from the borehole. Moreover, if the prior information is not available, the FCM routine is still applicable and works. Since FCM clustering is an unsupervised learning method, it enables the automatic definition of the relationship between the model parameters during the inversion process. For instance, the cluster centre values are sought as part of the inversion process, whereas having borehole information allows the use of measured average values (at least as a starting point). If the prior information is available, it can then be used to convert between model parameters as described in the following process:

Assuming that the two models include N cells $\mathbf{M}(m_j, j=1, \dots, N)$ of MT and $\mathbf{S}(s_j, j=1, \dots, N)$ of seismic. The prior centre values can be defined (e.g., by borehole data), $\mathbf{V}_0[\mathbf{V}\mathbf{m}_0, \mathbf{V}\mathbf{s}_0]$. We run MT inversion first and obtain the model \mathbf{M} . Then, we convert MT model into an initial seismic model: $\mathbf{S}_0(s_{0j}, j=1, \dots, N)$. This approach is modified from equation (2.5):

$$s_{0j} = \frac{\sum_{k=1}^C u_{jk}^q v_{s_{0k}}}{\sum_{k=1}^C u_{jk}^q}, \quad (4.1)$$

where C and $\mathbf{V}\mathbf{s}_0(v_{s_{0k}}, k=1, \dots, C)$ are cluster number and centre values of the seismic model parameter, respectively, which are defined initially. q is fuzziness. Membership degree $\mathbf{U}(u_{jk}, j=1 \dots N, k=1, \dots, C)$ is computed by model \mathbf{M} and centre values $\mathbf{V}\mathbf{m}_0$ equation (4.2).

$$u_{jk} = \left\{ \sum_{i=1}^c \left[\frac{m_j - vm_{0k}}{m_i - vm_{0k}} \right]^{\frac{2}{q-1}} \right\}^{-1}. \quad (4.2)$$

In the co-operative inversion routine, we use FCM clustering as a platform to share information between the MT and seismic models. In this case, the separate inversions are performed independently and the coupling process comes from the FCM clustering. The input to FCM clustering is from both of the seismic-MT models' parameters. As a result, the membership degree and centre values are influenced by both geophysical data sets. This information is subsequently transferred into subsequent inverted models through the membership and centre values, which contribute to updating a new model during the inversion process (More detail of this updating process can be found in Chapter 3). For instance, to include the seismic model into the inversion of MT via FCM, we use the seismic model (**S**) along with MT model (**M**) to form the input data of FCM as **Z**=[**M**, **S**]. Accordingly, the membership degree and the centre values of the MT model are also influenced by the seismic model, in other words, the seismic information contributes indirectly to the MT model via the FCM clustering process because each cell in the 2D or 3D model has physical parameters and membership degrees to the clusters (which have characteristic physical parameters)

Multiple data sets with different resolutions, cause another issue for the inversion. For instance, if we use the inverted model of a seismic method to build an initial model for MT inversion, the process of MT inversion may degrade the resolution of the initial model. By processing the seismic model using a common FCM cluster model of the earth, that information is then used to update the MT model implicitly via the cluster update, but does not explicitly change the resistivity values using seismic acoustic impedance values.

4.2.1. Sequential co-operative inversion strategy

In the sequential co-operative inversion, the inverted result of one method is usually converted to an initial model for another method. It is robust if the transfer process is properly executed, otherwise, it may cause problems for the inversion (Lines, Schultz, and Treitel 1988). This process does not guarantee to keep the resolution of the

previous method. For instance, the MT inversion may not keep the resolution of the seismic data. In this work, we use FCM clustering without little smoothing to resolve these issues and incorporate readily identifiable boundaries in the seismic data as a “soft” constraint via weighting the cluster membership degrees. This technique can automatically define relationships between the model parameters and is applicable in cases where the relationship parameters are scattered. Moreover, this inversion scheme enables us to keep the resolution of the seismic in MT inversion.

Figure 4-1 displays a flowchart of the sequential inversion process, which comprises of three main blocks: (A) seismic inversion, (B) transferring models using FCM clustering, and (C) MT inversion. The separate inversions of both models are the same, including the four blocks from (1) the initial prior information, (2) update parameters, (3) stop condition and (4) the final model. The initial information comes from two sources: the external inversion process (e.g., borehole data), and the internal inversion process, from member methods through FCM clustering. The initial information constrains the update model parameters, and then the stop conditions determine whether the inversion process continues to update the model or stops with the final model. Both the MT and seismic models is put in the transferring block using FCM clustering. The membership, centre values, and an initial model for the next inversion method, are set for next the inversion iteration.

4.2.2. Parallel co-operative inversion strategy

Figure 4-2 presents the workflow of the parallel co-operative inversion. This strategy is almost same as the sequential inversion strategy where the individual data is separately inverted and the exchange information between models is analysed using FCM clustering. The critical difference between this scheme and the sequential process is that the models are updated simultaneously. In this process, all model parameters and prior information of all methods are input to FCM clustering. The output of this process, including membership, centre values and initial models, are utilised for updating models at each iteration of the inversion.

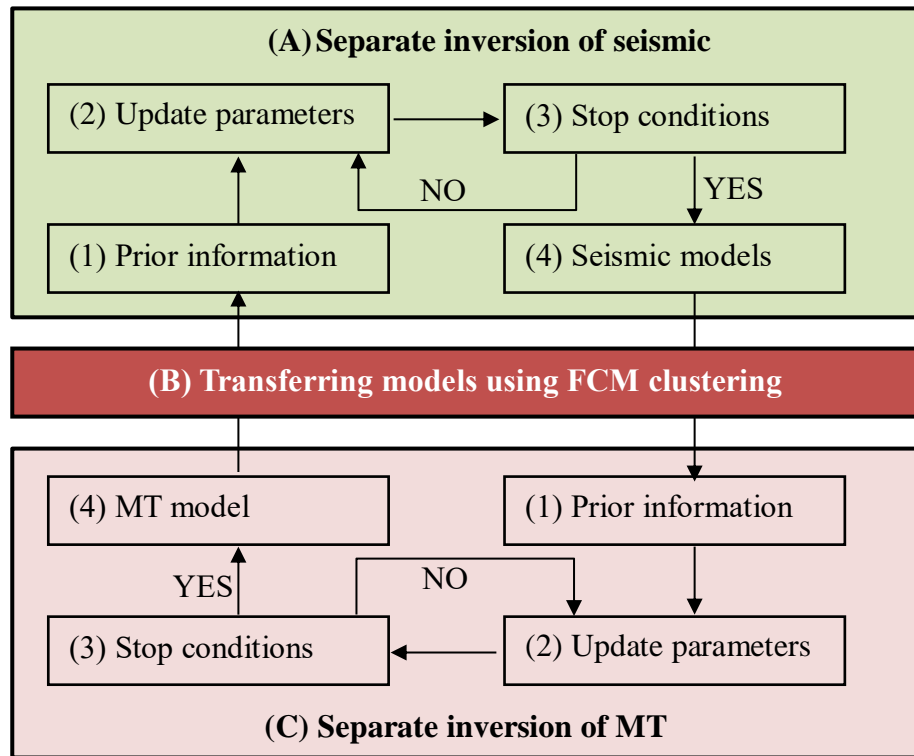


Figure 4-1: A schematic of the sequential co-operative inversion of seismic and MT data. MT inversion results can provide the low-frequency band for seismic data by using FCM clustering to convert the MT model into an initial seismic inversion model. In turn, coupling the acoustic impedance and resistivity models via FCM clustering during MT inversion can improve the high resolution of the seismic inversion in the resistivity model.

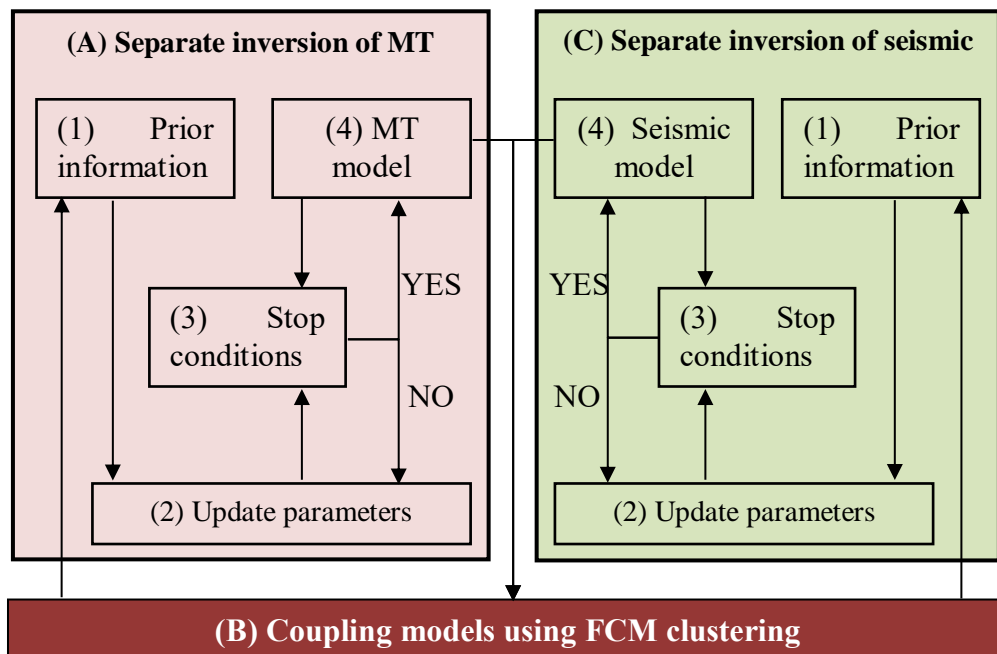


Figure 4-2: The workflow for parallel co-operative inversion. The inversion of MT and seismic data run in parallel and the coupling model parameters are processed using FCM clustering.

4.3. Application to real data

4.3.1. Geological setting

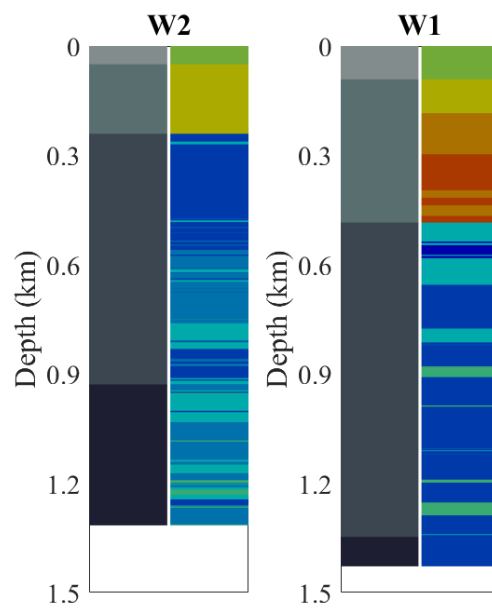
The data were acquired in the Carlin gold district, within the Basin and Range, Nevada, USA, by Barrick Gold Corporation. The main gold deposits are found in Paleozoic rocks (Cline et al. 2005, Muntean et al. 2011). Based on a previous geologic study nearby (Cline et al. 2005, Muntean et al. 2011, Large, Bull, and Maslennikov 2011), the geologic setting can be divided into three layers (Figure 4-3): a cover layer of the Quaternary alluvial formation, the middle layer is rocks of the Tertiary Carlin formation, and the basement is rocks of the Valmy Ordovician and Comus Ordovician formation, which are older sediments and carbonates with some volcanics interlain, metamorphised, and faulted. The three layers are apparent in the seismic section (Figure 4-4c) where they are separated by two horizons, H1 and H2. Takougang et al. (2015), Le et al. (2016) stated that the upper layer has higher conductive values than in the basement, particularly in the second layer, which comprises interbedded (younger) sedimentary rock with a high proportion of clay. This is consistent with high values of Potassium found in the assay logs (See Appendix A).

Both the seismic and MT data detect and image the major fault in this area (Figure 4-4). Figure 4-5a and b show that the major fault has divided the basement into two parts and separating the region into two zones: high and low resistivity and velocity on the left and right-hand side respectively.

4.3.2. Data sets

The data sets investigated include data from 18 MT stations (Figure 4-4) acquired along with a 2D seismic section extracted from the 3D seismic survey (aligned with the MT stations) and the two boreholes in the vicinity of the MT and seismic profile (Figure 4-4). This data set was described by Takougang et al. (2015), Le et al. (2016). The seismic section and MT profile in this work is Line 14 from the work of Takougang et al. (2015). The major tectonic feature in this area is a large fault zone (Figure 4-4b), is also the primary geoelectrical strike. The MT induction arrows that point towards anomalous internal concentrations of current (Parkinson 1959) at a 0.0011 s period, point toward a different direction, but at the longer 0.1449 s period, they point perpendicular to the fault trend as expected. The amplitudes of the

induction arrows at the north-west side of the fault are larger than that from the south-east side, showing that the resistivity is higher towards the north-west than in the south-west. In the basement, a comparison resistivity histogram of two boreholes located on each side of the major fault (Figure 4-5) confirms that the resistivity of the north-west section is higher than in south-east, which is consistent with expectation when interpreting the seismic reflection data.



Formation keys

QAL	Quaternary alluvium
TC	Tertiary Carlin
OV	Ordovician Valmy
OC	Ordovician Comus

Lithology keys

Layer 1	QAL	Alluvium
	TG	Rhyodacite volcanic-tuffaceous silt and clay
Layer 2	TS	Tuffaceous silt
	TV	Glassy volcanic
	TUF	Tuff, lapilli tuff marker bed
Layer 3	SBM	Siliceous mudstone, siliceous mudstone with tuff
	BMT	Mudstone, mudstone with tuff, limestone
	BAS	Basalt
	QTZ	Quartzite

Figure 4-3: Geological and lithological columns of wells W1 and W2. The geological section can be divided by three main layers: Layer 1 is the cover layer relating to QAL; Layer 2 is young sediment of TC formation; and Layer 3 is the basement of OV and OC formations

The challenges of using this dataset for the inversions are:

- (1) The wireline resistivity logs and sonic P-wave velocity are only available below the young sedimentary layer (due to steel casing to keep the hole open). Thus, we do not have reference data to validate our process within the cover layers. Moreover, seismic model-based inversion requires a 'good' prior model that is normally obtained from borehole sonic data; hence, lacking this information can cause a major issue in any impedance inversion process.
- (2) The cover layer was identified as the conductive environment (Takougang et al. 2015, Le et al. 2016). The electromagnetic energy is absorbed when the MT fields propagate through this layer. Consequently, the MT signal at long periods/low frequency that provide information about the basement is weak; therefore, MT inferences about the basement are limited by noise and unknown near-surface effects.
- (3) The poor correlation between P-wave velocity and resistivity (Figure 4-5c and mentioned by Takougang et al. (2015), and despite reservations inversion was performed) causes problems for co-operative inversion when using an empirical relation strategy.
- (4) Although seismic data show good quality in the sedimentary layers, it also has low signal-to-noise in the basement, which is the main target medium for gold exploration in the area.

The advantages of this dataset for my inversion strategies are:

- (1) The FCM petrophysical constrained inversion utilises the centre values of clusters; we may assume that the patterns of the cluster locally obtained at borehole position are also valid for the whole survey area. It is not an unreasonable assumption, and in the absence of alternatives is worth attempting. The character of the reflections in the seismic reflection image (Figure 4-4c) also reinforces the expectation that assuming that physical characteristics measured in the boreholes are translatable else. According to the geological setting and reinforced in seismic image data, the whole section is apparently separated into three environments: overburden,

young sediment and basement, and there are no significant factors that may change the patterns of the physical properties of the rocks. Therefore, the assumption that the cluster centres obtained by statistically analysing borehole data seem valid for the whole section, is reasonable.

- (2) The consistency between the variation in the geoelectrical and elastic models. Both the resistivity and acoustic impedance models appear to share two common main boundaries that separate the section into three geological environments (Takougang et al. 2015, Le et al. 2016). Hence, we may use the seismic boundaries to constrain MT inversion.
- (3) The resistivity and P-wave velocity of the borehole data show poor correlations (Figure 4-5c), but the pattern overall shows better relationship within the units (See Appendix B). Figure 4-6 illustrates two main patterns of P-wave velocity and resistivity: (1) low P-wave velocity and low resistivity relating to fracture zones and high concentrations of minerals and/or fluid due to porosity (Smith 2010); (2) high resistivity and high P-wave velocity relating to the stronger rock zones. Note that there is no direct information on a relationship between P-wave velocity and resistivity within the cover layers, but based on geological information provided via DET CRC partnership with Barrick and previous studies (Takougang et al. 2015, Le et al. 2016) we can define the pattern in this medium as low P-wave velocity and low resistivity.

FCM inversion objectives with this data are:

- (1) Maximum exploitation of the prior information from the borehole data to assist with the inversion.
- (2) Using complementary information of MT and seismic data to optimise the co-operative inversion to build a viable earth model with the main focus on mapping the basement media for prospective zones.

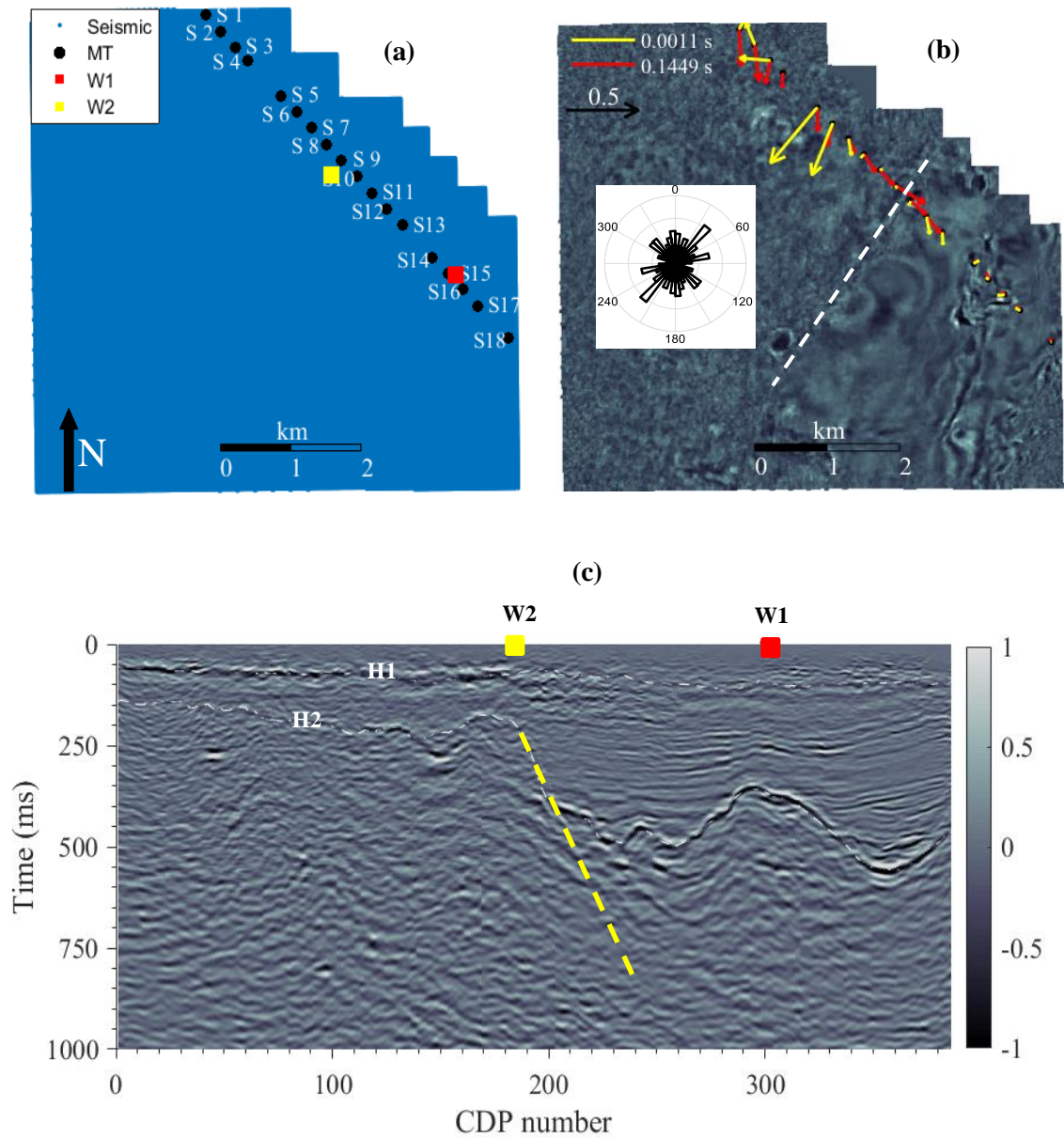


Figure 4-4: (a) Position of 18 MT stations located at the north-east of the 3D seismic survey area (blue area). Wells W1 and W2 are in the vicinity of the MT profile. (b) Seismic slice at the depth of 500 m. The main fault can be seen (dashed white line). The rose diagram shows the geoelectric strike; the main direction is along the direction of the fault. The arrows represent the real component of the induction arrow (Parkinson convention). (c) Seismic section allocated with MT profile. Two squares show the projection of wells W1 and W2 on the profile. The dashed white lines represent the two horizons H1 and H2. The dashed yellow line marks the major fault.

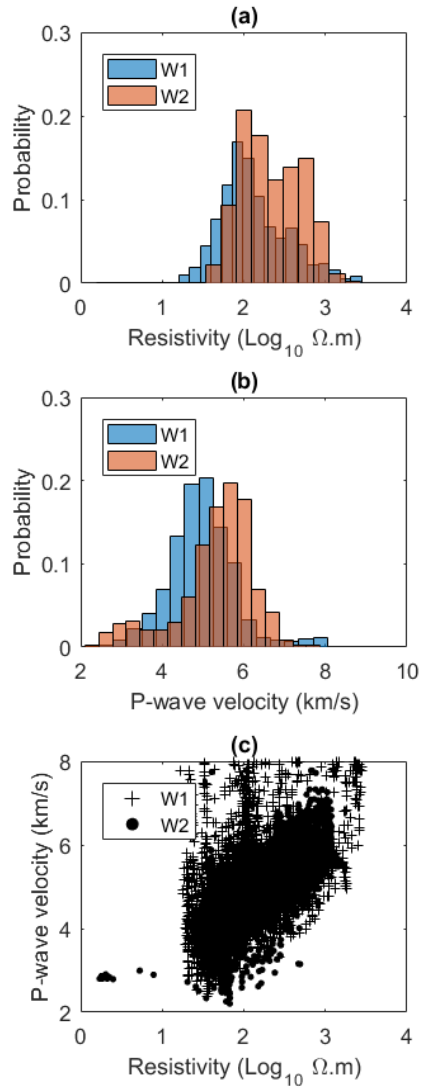


Figure 4-5: Wireline logs of the two wells W1 and W2. The histograms (a and b) show that the two parameters, resistivity and P-wave velocity, are higher in W2 than in W1. Note that the velocity in W1 is acquired at a depth of about 500 m. The cross plot (c) between these parameters illustrates poor correlation.

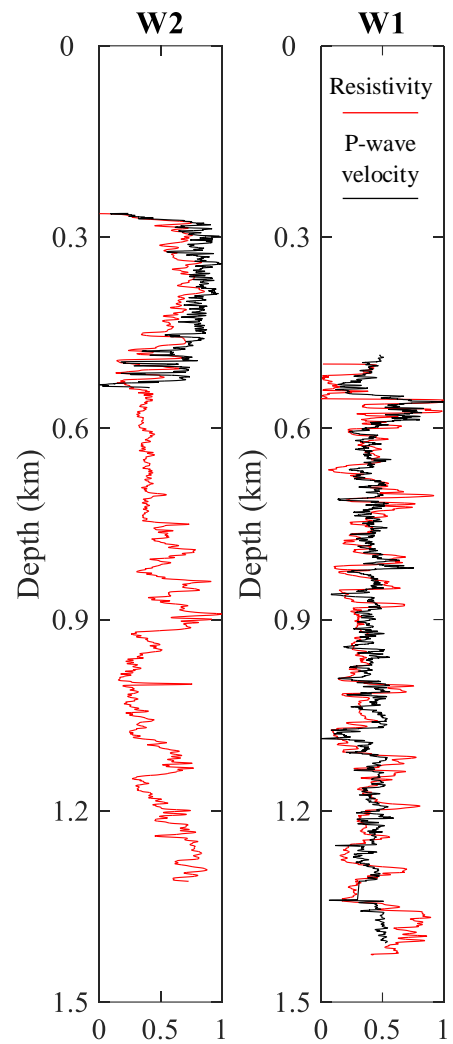


Figure 4-6: Comparison between normalised resistivity and P-wave velocity from the well logs of W1 and W2. The high correlation between the variation of resistivity and P-wave velocity provides evidence that the rock fractures may be filled with conductive material that has a low resistivity and low velocity. This demonstrates that seismic signature can support MT inversion and vice versa.

4.3.3. Prior work on the data

The same data sets used by Takougang et al. (2015), Le et al. (2016), who both trialled co-operative inversion methods. I also run co-operative inversion process, however, my inversion method differs significantly to their efforts regarding inversion algorithms, the performance of incorporating data sets and the presented results. Both previous attempts tended to rely on MT data, with the seismic playing mainly a secondary role in constraining the MT inversion where it had difficulty with the basement. No serious attempt was made to invert the seismic data. Le et.al. (2016) used seismic attributes to condition the MT inversion and assist with defining boundaries. The result of neither study was able to make meaningful interpretation of the prospective basement rocks.

The use of fairly strong smoothness constraint in the inversion in both works may not have been helpful for the issue at hand: finding small mineralised traps in the basement. According to Muntean et al. (2011) and prior geophysical information from nearby borehole data, the structures in the basement in this area should be blocky rather than smooth. A modified model covariance can help the inversion process make the resultant model “sharper” at a known discontinuity; but, the model covariance is empirically chosen and fixed in the inversion process, in other words, it is a “hard constraint”. This constraint is restricted to prior information and can drive a poor updating process if the prior information is incorrect or has errors. By including FCM clustering as an extra constraint in the inversion process, the clusters tend to naturally build a blocky model. This FCM constraint has two key characteristics: (1) the process is based on fuzzy logic; thus, it accepts the imperfection of prior information; (2) fuzzy clustering automatically defines the patterns; hence, it enables the constraints to vary during the inversion process according to the model.

The dissimilarity is in the way the data sets were used. FCM clustering establishes relationships between properties-features of the models automatically; therefore, it is still applicable in cases where the prior information is not available, or there is an incomplete dataset as is the case here. One of the key problems in the work of Takougang et al. (2015) is the reliance upon empirical functions between elastic and geoelectrical properties. As previously mentioned (in Chapter 3 about co-operative inversion methods) this only works well when medium dependent relationships are used to exchange information between the seismic and MT models. Apart from the

poor correlations between the known properties in this data, the borehole properties were only acquired in the basement. The significantly different geological setting in the upper layers should form different relationships than those in the basement. Therefore, application of the function obtained from basement information and used across all media will produce untrustworthy results. In the work of Le et al. (2016), only the seismic information within the cover layers showed significant effects on the MT inversion process where the borehole information could not be used to constrain the inversion usefully.

Lastly, after the differences in inversion approach does produce a difference in the final results compared to Takougang et al. (2015) and Le et al. (2016). The FCM cluster approach produces better results where it is needed, in the basement rocks. My final product from the inversion process is a map of the clusters, namely a “pseudo-lithology” map, which can help with interpretation. This output is easier to use for interpretation than the inverted petrophysical models.

4.3.4. Sequential co-operative inversion of magnetotelluric and seismic data

4.3.4.1. Magnetotelluric inversion

As the quality of prior petrophysical information is different from the basement and the cover layers the clusters in the respective regions have different weighting values with respect to the use of prior information constraints. The weighting value of the prior centre value, η (used in equation 3.26, Chapter 3) is set to 0.5 for the basement and 0.3 for the cover layers. A value 0.5 of η means that the cluster centre values have equal input from prior information and the inversion updated model parameters. The credibility of prior information within the basement from borehole data is set higher than the cover layers, where the information comes indirectly from other sources (Takougang et al. 2015, Le et al. 2016). The regularisation parameters of structure β and FCM γ , in the inversion objective function (used in equation 3.24, Chapter 3) are set up according to the empirical-numerical experiments. I tested two strategies. First, β and γ are decreased with iteration, similar to the work of Lelièvre, Farquharson, and Hurich (2012). Second, β and γ are fixed through the inversion process. I decided to fix these (β and γ) parameters because this strategy is considerably simpler, and more

stable than varying β and γ with each iteration. A homogeneous starting model of 100 Ωm was used for all inversions.

The inversions were run with four scenarios listed in Table 4-1 to try various implementations of FCM constraints.

Table 4-1: MT inversion strategies

Inversion names	Constraints
RES_1	Cluster number
RES_2	Petrophysics
RES_3	Petrophysics + Boundary from seismic
RES_4	Petrophysics + Seismic inverted model

a. MT inversion with cluster number constraints

Only MT data is available is the basic case, as in the early stages of an exploration project. FCM clustering inversion requires an initial cluster number. This number is not difficult to define based on the general area geological information and the previous works Takougang et al. (2015) and Le et al. (2016), or we may experiment using a few numbers and choose the one that produces the smallest misfit. Figure 4-8 illustrates the inversion result RES_1; it creates a model with a district boundary between the basement and the cover layers and the major fault. This divides the basement into two parts: high and low resistivity at the left- and right-hand sides of the profile respectively.

b. MT inversion with petrophysical constraints

The histogram of resistivity in the boreholes (Figure 4-5a) shows that the basement is separated into two major geoelectrical units. Histogram analysis of parameter frequency from the well-log data defines the optimal number of clusters and centre values (See Appendix B). Using FCM to analyse the resistivity values within the boreholes, centre values [52.4; 90.0; 249.6; 584.0] Ωm are obtained. According to

Takougang et al. (2015), Le et al. (2016), the uppermost layer resistivity is approximately 50 Ωm and the second layer is comprised of two geoelectrical units: a very conductive unit of about 7 Ωm , and superimposed in the middle is less conductive media of approximately 15 Ωm . Finally, the initial petrophysical constraints are set to seven groups of geoelectrical units [50; 7; 15; 52.4; 90.0; 249.6; 584.0] Ωm .

The inverted model RES_2 (Figure 4-8) shows the main structural features of the section. The conductive layer in the shallow parts of the section shows the young sedimentary rock of the Alluvium (QLA) and Tertiary Carlin (TC) formations. The basement of more resistive media is comprised of Ordovician (OV and OC) rock formations, which are separated by the fault in two parts. The right-hand side of the section is more conductive than in the left-hand side.

c. MT inversion with petrophysical and boundary constraints

In this variation the seismic boundary is used to constrain MT inversion. The seismic horizons (Figure 4-4c) appear to divide the section into three parts: Quaternary overburden, young Ordovician sedimentary rocks, and the older altered basement rocks. The young sediment layer is usually conductive and the cover and basement layers are most likely resistive. Thus, the two horizons split the section into three geoelectrical media, namely A, B and C (Figure 4-7), and this information is included in the inversion process (Kieu, Kepic, and Pethick 2016).

The model RES_3 (Figure 4-8) shows the inverted model using petrophysical and boundary constraints. The resulting geoelectrical model is similar to the inverted model without the boundary information. Nevertheless, the section is sharply divided into three main layers as a result of the inclusion of the boundary information. The cover relating to the unconsolidated rock of the QLA formation shows the heterogeneous nature of this medium. The conductivity of the TC layer/unit layer is highest, particularly from stations 11 to 17. The conductive media reasonably represent as sedimentary environment with high shale content (Le et al. 2016) or saline water. In the basement, the resistivity of the media is greater than in the covers and is also laterally separated in two main parts by the fault. The conductive zones seen in Figure 4-8 may represent the fluid/porosity in the fault zones.

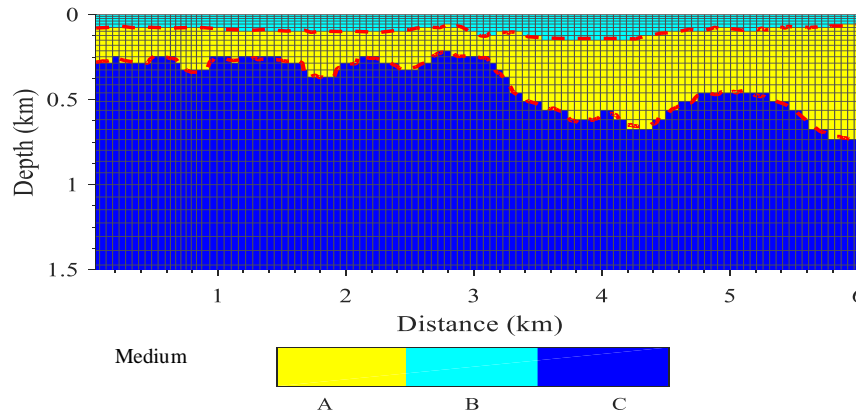


Figure 4-7. MT mesh (grey lines) is divided into three regions: A, B and C, by the two boundaries (red dashed lines) that are defined by seismic data (Figure 4-4d).

d. MT inversion with petrophysical and seismic model constraints

The MT inversion results using both petrophysical and seismic boundary constraints demonstrates significant improvements when compared to results without boundary inclusion. Nonetheless, the nature of the MT method is that it is low resolution in comparison with seismic method. Thus, the resolution of the MT model is enhanced with assistance from the seismic model. In this work, I used the AI model created by seismic data inversion to constrain the MT inversion. The RES_4 model (Figure 4-8) shows that the MT geoelectrical model still keeps the major features that can be seen in the MT inversion with boundary constraints; however, this model shows higher resolution results from the use of the seismic data.

e. Discussion of MT inversion

In terms of convergence and final data misfit comparisons between inversion strategies, the analysis of errors between synthetic data from the inverted model and real data indicates that the global misfit decreases steadily with the number of iterations and the misfit is acceptably small (see Appendix C) for all strategies tested. The inversion results from MT inversion with cluster number constraints RES_1, using only the basic information of the cluster numbers (Figure 4-8), detected/imaged the major boundaries and the presence of the fault. However, as the nature of the MT method is diffusive; it is difficult for MT data to recover the resistive basement that overlaid by conductive layers. The comparison between the inverted model and wireline logs (Figure 4-9) illustrates that the inverted model matches geological

boundaries and the overall trend of borehole data. Nonetheless, the resistivity of the inverted model at the well W1 is considerably less than that of the measured borehole data. This likely caused by the impact of the low resistivity of the upper layers. This blanket effect demises as the thickness of the layers reduce and the resistivity increases; hence, the inverted resistivity model is closer to the measured data from well W2.

The MT inversion with petrophysical constraints (RES_2 in Figure 4-8), shows considerable improvement (it looks more geologically reasonable) compared to the inversion without prior petrophysical information. It matches the seismic image better, particularly on the right-hand side of the section, where the inverted model captures the boundary between young sedimentary and basement rocks. The borehole comparison (Figure 4-9) confirms that the prior information helps to recover the resistivity of the basement closer to the borehole data.

The inclusion of seismic horizons in MT inversion with petrophysical and boundary constraints (RES_3) assists in building a reasonable MT geoelectrical model (Figure 4-8). The basement is obviously separated by a young sedimentary rock covering. This conductive zone was also described in the works of (Takougang et al. 2015, Le et al. 2016). Nevertheless, the inversion of 3D MT including seismic information (Takougang et al. 2015) is almost homogenous in the basement; the main fault is invisible. The use of seismic attributes to build a “good” initial model and set a covariance matrix for 3D MT inversion (Le et al. 2016) might produce more apparent fault structures. However, in comparison with the resistivity wireline logs in the two boreholes, the geoelectrical model of the basement is almost homogeneous. This geoelectrical model matches the borehole data well and is much better than the inversion without the boundary constraints (Figure 4-9).

The MT inversion, with assistance from the seismic model through FCM clustering, enables an increase the resolution of the MT geoelectrical model. The inverted model RES_4 (Figure 4-8), can define the interbed layers within young sediment on the right-hand side of the section. It is impossible for MT alone to image these layers with confidence. In the basement, the inverted result also has substantial agreement with the borehole data and provides higher resolution than the other inverted models.

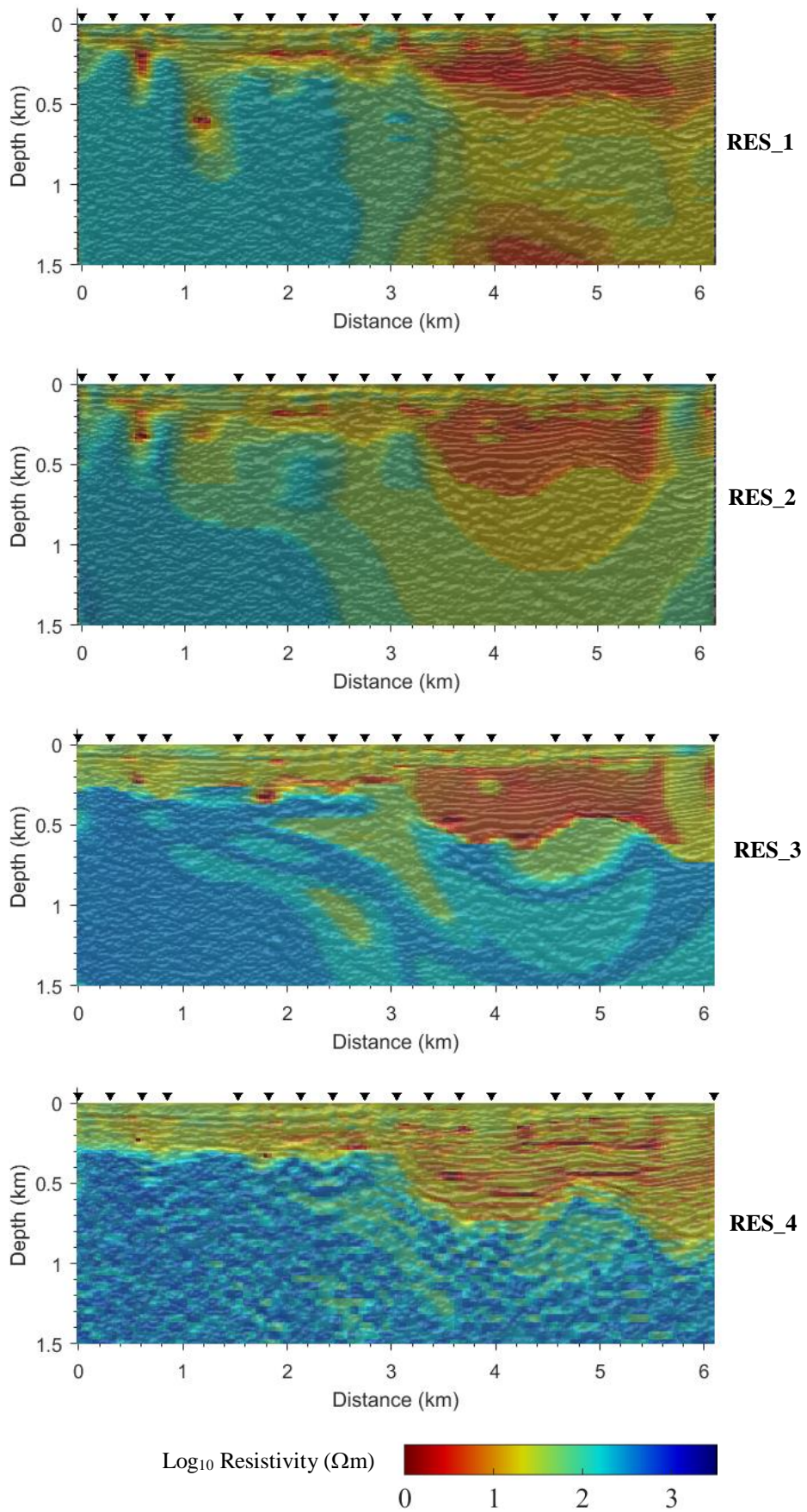
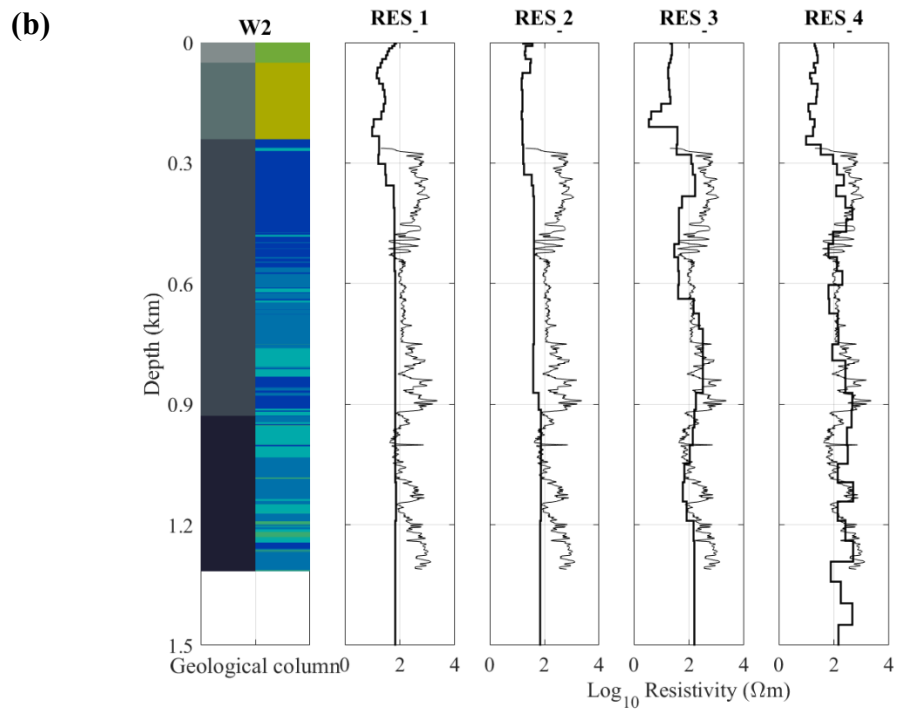
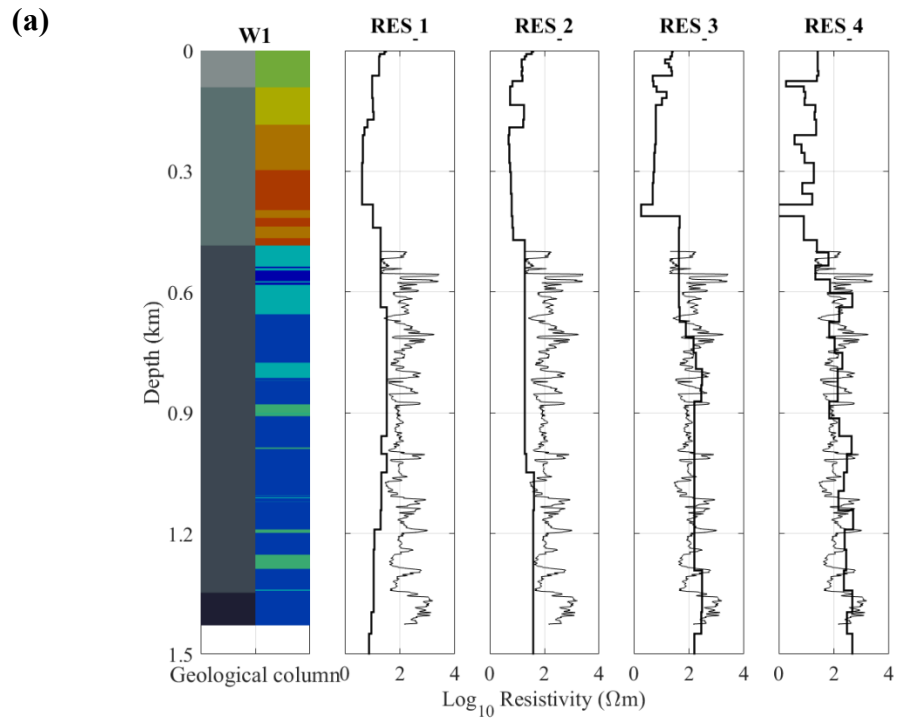


Figure 4-8. Inversion results with different constrains (Table 4-1). The triangles on the top of the section mark MT stations.



Formation QAL TC OV OC — Inversion models

Lithology QAL TG TS TV TUF SBM BMT BAS QTZ — Wireline logs of resistivity

Figure 4-9. Comparison between the inversion model and borehole data in the two wells (a) W1, and (b) W2. The abbreviation of the formation and lithology can be seen in Figure 4-3. From left to right of the figures, the inversion is increasing from basic to more advance and the inverted models are closer to the borehole data.

Note that using the seismic model to enhance the resolution of MT should be performed after very careful consideration of the relationship between resistivity and acoustic impedance (AI). Naturally, MT data does not contain high-frequency band information; this high resolution in the model is biased by the seismic information. If the seismic and electrical information are not well linked then the seismic data may push the results too much. Fortunately, in this area and in the data the relationship between resistivity and P-wave velocity seems to be consistent, as found in borehole data analysis (Figure 4-6). This also may explain the reason the automatic cooperative inversion strategy of Le et al. (2016), using a seismic attribute to build an initial model of MT inversion, achieved a ‘surprising’ result.

4.3.4.2. Seismic model-based inversion

a. Creating an initial model for the inversion

The first layer is defined as unit 1 and the second as unit 2. The basement clusters are defined based on analysis of the well-log data. For the shallow section, the velocity of the first layer is 1.676 km/s and comes from vertical seismic profile (VSP) data acquired near this area. The velocity of the next layer is 2.93 km/s, which is calculated from interval velocities of traces at the well location and compared to the migrated velocity model as a cross-check. From the seismic section, the boundaries in the time domain between the two top layers and basement can be determined and wireline measurements from the deeper part from the well logs (which could not be run in the alluvium sequence) provides the set of the velocity information. An AI inversion is run on the single trace (from the post stack seismic data) at the well location and compared to the result of the well-log data in the deeper layer to choose the most suitable inversion parameters (Figure 4-10).

The cluster number is set by analysing the prior information (See Appendix B) and in this case seven clusters were chosen. We prior (starting values for) centre values of the seven clusters C1 to C7, [4.2, 7.76, 7.76, 10.43, 13.13, 13.96, 15.48]^T (km/s g/cm³). Note that the first three clusters are based on the result of inversion of the trace at the well location, and have lower certainty due to a lack of actual well-log data; therefore, the weighting values are set lower for the upper section. The weighting values are set similar as with the MT inversion, 0.5 for basement and 0.3

for the cover layers. These seven clusters can be reduced to five if the seismic inversion is run alone; the centre values of the second and the third are the same and the difference between the fifth and sixth values are very small. Seven clusters were set so as to be comparable with the co-operative inversion performed later.

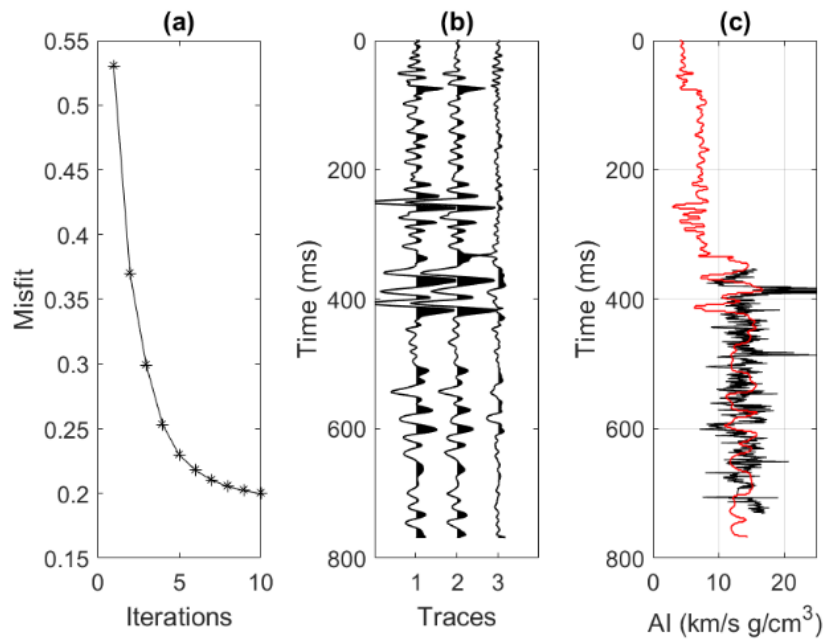


Figure 4-10: Inversion results of the trace at the well location. (a) Misfit gradually decreases with iterations. (b) The synthetic seismic (trace 2) is almost identical to the real seismic data (trace 1), which results in a small residual (trace 3). (c) Acoustic impedance from the inverted model (red line) is consistent with the well-log data (black line).

The initial models are generated from borehole data, migrated velocity data and the MT inversion model (Figure 4-11). First, the borehole information is extrapolated along the section using the Hampson-Russell Software (HRS). Secondly, the migrated velocity model is multiplied with an average density from core measurement, 2.65 g/cm^3 , to form another initial model. Thirdly, the MT inversion model is converted to an initial AI model using FCM clustering.

b. Model-based inversions

The inversion process was run with three prior models using the well-known commercial software, Hampson-Russell software and my Matlab code (Table 4-2).

In this work, only the information gathered from well W1 is used to compare with the inversion results because the sonic logs only are available within a small proportion of well W2.

Table 4-2. Seismic inversion strategies

Data to generate initial model methods	Initial model	Inversion models	
		HRS software	Our code
The borehole	AI0_1	AI_HRS_1	AI_FCM_1
Migrated velocity model	AI0_2	AI_HRS_2	AI_FCM_2
MT model	AI0_3	AI_HRS_3	AI_FCM_3

Firstly, the impact of the different starting (or initial) models are tested on the inversion results by running inversion with the prior models (Figure 4-11). In my routine, the inversion is constrained by information from the borehole analysis and the horizons, H1 and H2 (Figure 4-4c). In the first initial model AI0_1, there is only one borehole and the data is only available from the basement of the section; for the upper parts, the information comes from different sources. The initial model is formed by extrapolating the borehole data along the section. In the Hampson-Russell software, it assumes a layer cake geology and the various physical changes are conformal to the horizon H2. This causes artefacts in the resulting inversion model because the seismic data used is severely band-limited (it is suspected that an AGC to normalize the traces before stacking may be the issue) and the starting model influences the AI inversion result strongly. In the case of using the migrated velocity model obtained by seismic reflection processing, the initial model is notably different to the known geological setting as it illustrates the smooth change of velocities with space instead of three distinct layers corresponding to the known geological units. The solution for this situation is to use complementary information from other geophysical methods. In this work, we can exploit the inversion of MT data. Moreover, the use of FCM clustering allows us to preserve the ‘blocky’ model so that it realistically resembles the geological changes. The FCM clustering parameter is defined by analysing the data of nearby boreholes. Hence, our FCM-based inversion

enables us to incorporate both MT and borehole data in the acoustic impedance inversion.

Takougang et al. (2015) stated that the MT model might provide low-frequency band information for seismic data inversion. In their work, the MT inversion model is converted to the AI initial model by means of an empirical relationship between resistivity and AI. Nonetheless, the poor correlation between resistivity and P-wave velocity and density causes problems for the inversion. In our work, we utilise FCM clustering to convert the MT model into an initial AI model. In the clustering process, the variation of features, or in other words, the similarities and differences of petrophysical features, plays a vital role to define the group rather than actual petrophysical values from the geological features. Figure 4-6 shows a good match between standardised resistivity and P-wave velocity, which means that the clustering of resistivity and velocity should consistently domain the geology. Consequently, the conversion between the seismic and geoelectrical models by using the mean petrophysical property of the fuzzy cluster is more robust than using a deterministic empirical function alone (see Appendix B).

The three prior initial models result in quite different inversion models when using the HRS (Figure 4-12) and our code (Figure 4-13) due to the lack of a low-frequency band in the seismic data. Our algorithm can further exploit petrophysical and boundary information to reduce the impact of the initial model as it is further prior information (the starting model is itself prior information). For example, comparing the resulting inversion model with the initial model generated using migrated velocities shows that our result can separate the section into the expected three main parts representing the cover layer, young sediment layer in the middle and the basement. In contrast, the HRS inversion process depends heavily on the initial model; it almost represents the initial model plus reflection seismic data as an overlay as there is not enough extra information given to the HRS algorithm to change the initial model. A comparison of the trace inversion at the well location (Figure 4-14) shows that our inversion is more consistent with geological information and matches the core measurements better than the inversion process of HRS.

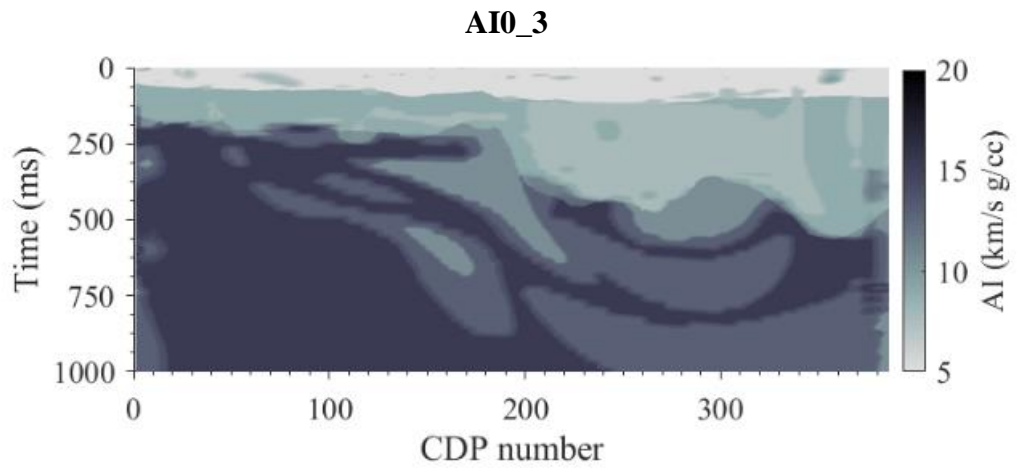
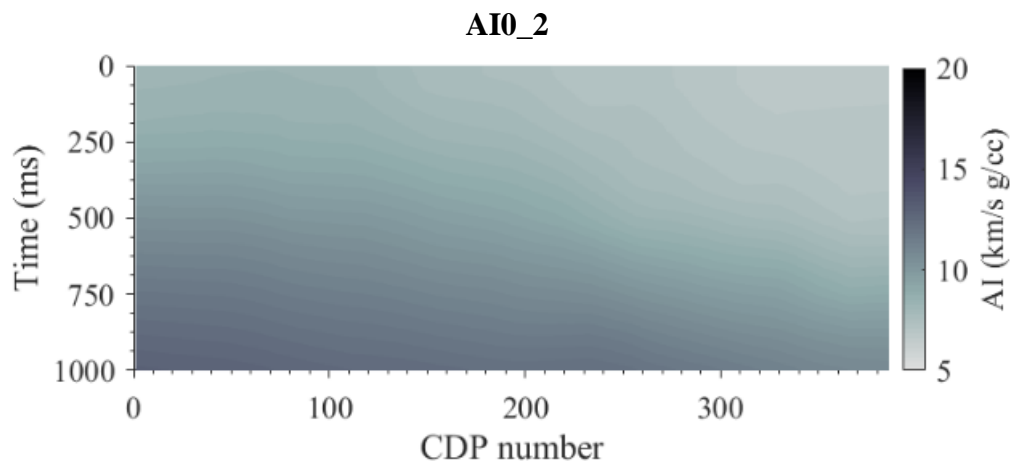
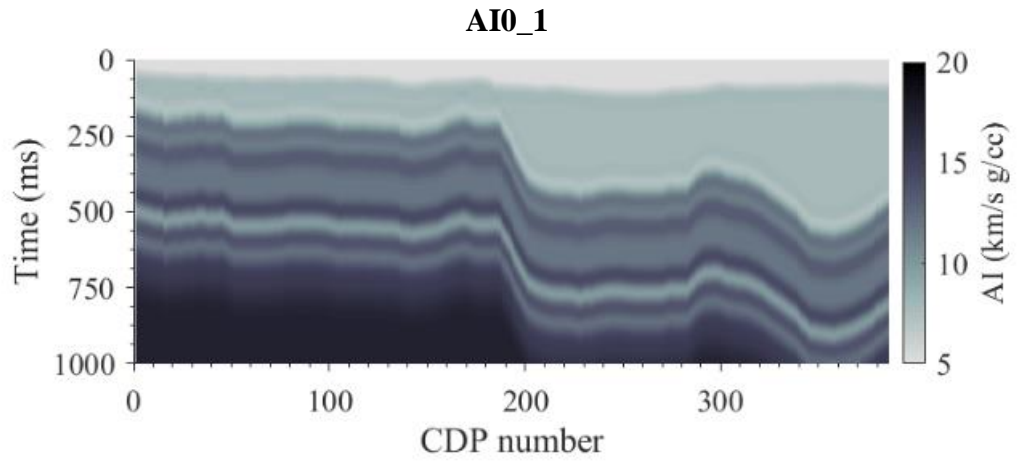
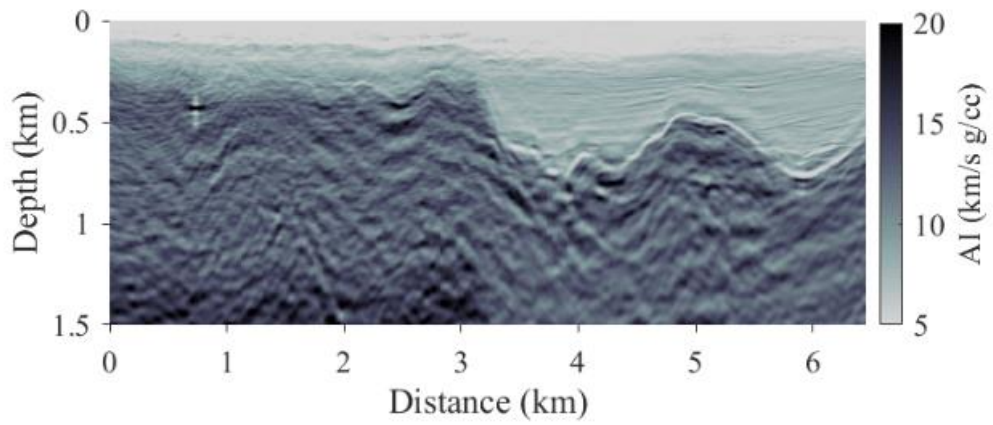
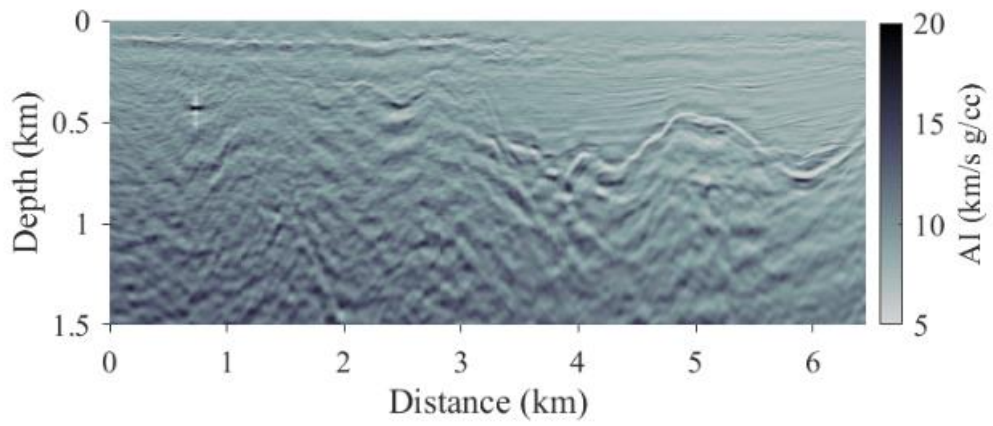


Figure 4-11: (AI0_1) Initial models generated from the borehole data using the HRS, (AI0_2) migrated velocity model, and (AI0_3) from MT inversion.

AI_HSR_1



AI_HSR_2



AI_HSR_3

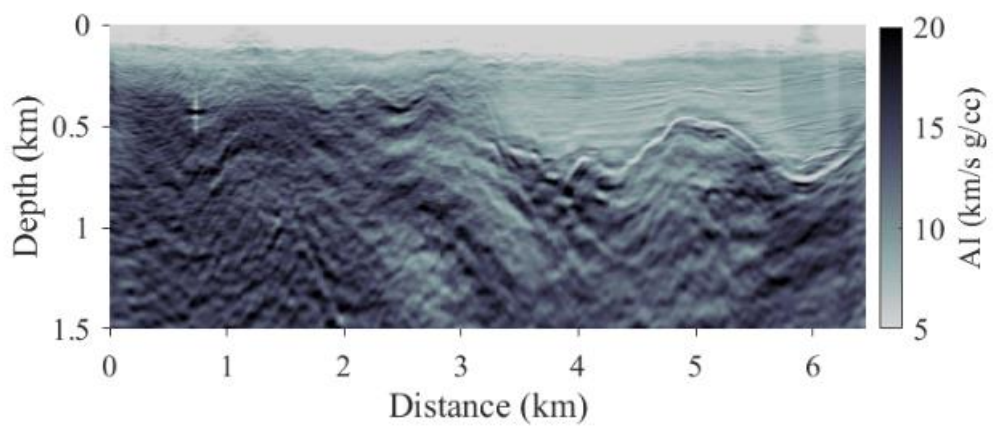


Figure 4-12: Inversion sections of AI using HRS from three different initial models (Table 4-2).

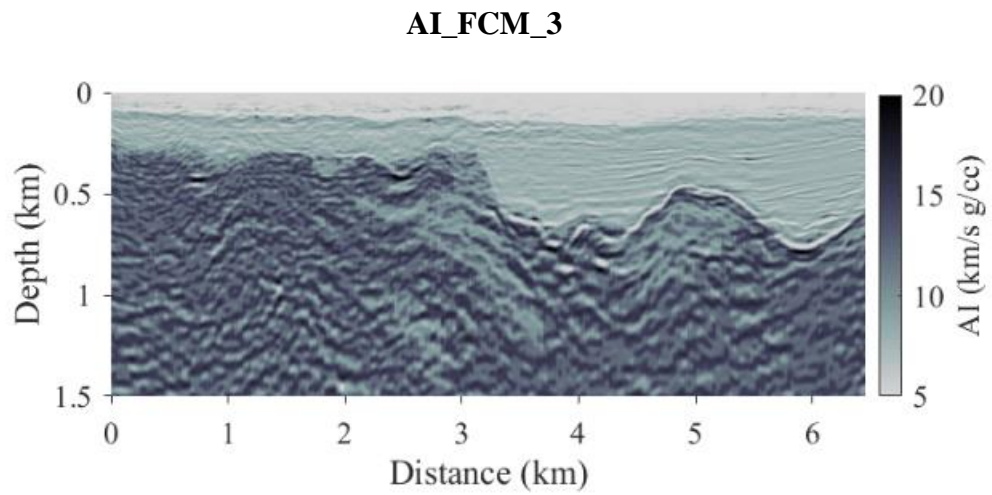
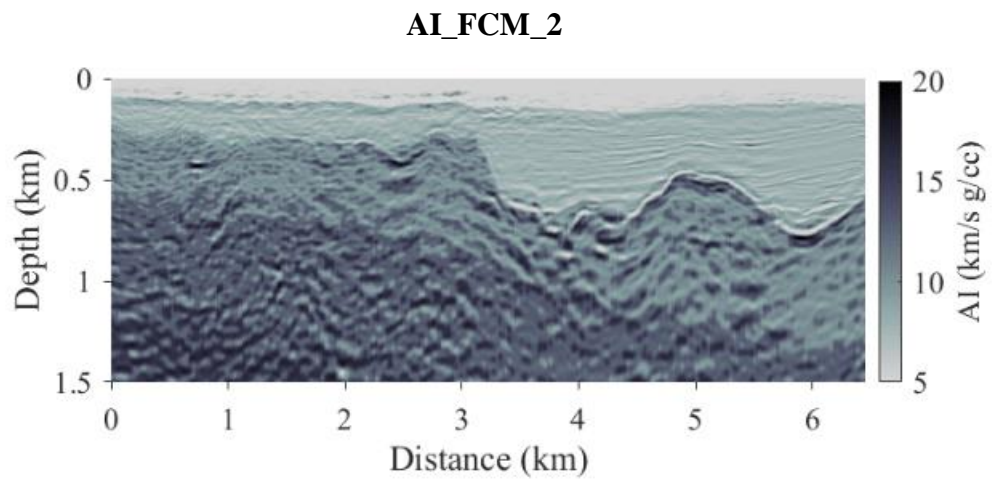
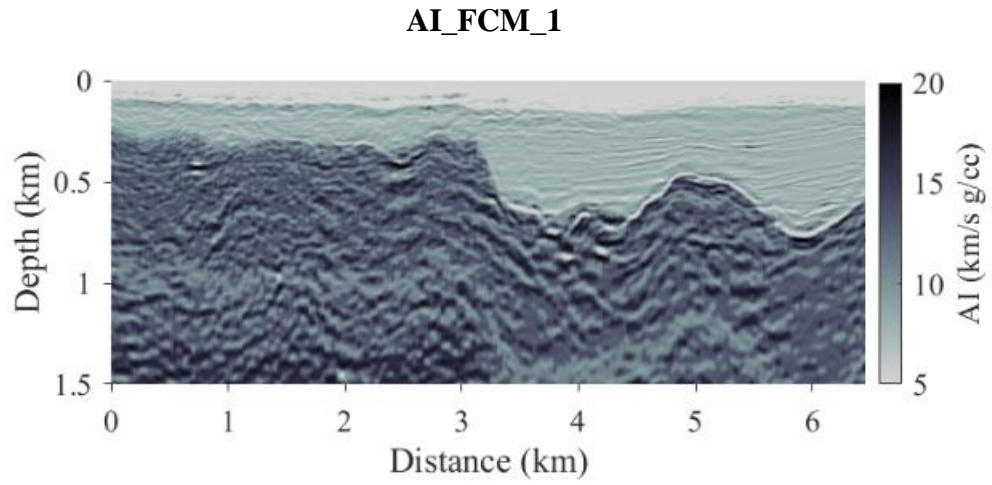


Figure 4-13: Inversion sections of AI using our code from three different initial model: (Table 4-2).

c. Discussion of seismic inversion

The key point of this work is to demonstrate that the FCM inversion strategies produce a more useful product for geological interpretation than the post stack seismic section alone. This methodology provides an effective set of constraints for the inversion that guides the model-generating process toward petrophysical clusters that represent geologic units. Moreover, this technique can be a useful platform for incorporating other prior information into the inversion process. In the most basic situation, if the prior petrophysical information is not available, it is not difficult to define the number of media based on general known geologic information. In this case, we can estimate the number of clusters and run inversion without petrophysical constraint. In the case where the prior petrophysical data are available, the inversion result is more accurate than without petrophysical constraint (Kieu and Kepic 2015c). Boundary information is another useful prior information, which can be derived from the post stack seismic data.

The performance of the FCM algorithm in comparison with the benchmark commercially available Hampson-Russell software AI inversion is that my approach works better in this environment and data set, with some advantages to the HRS in its greater sophistication in performing the AI inversion process (extracting the wavelet for example). The HRS post stack inversion heavily depends on the initial model with poor data, but our algorithm enables us to reduce the impact of the initial model because we can add further constrain information to the inversion process. The inversion result AI_HRS_2 (Figure 4-12) from the initial model AI0_2 demonstrates that the HRS inversion still keeps the initial model trend, whereas, the FCM inversion can refer to the known boundary information to build a model with the three known layers: the cover layer, the middle layer of young sediment, and the basement. The inversion results from initial models AI0_1 and AI0_3 and from the HRS software models AI_HRS_1 and AI_HRS_3 (Figure 4-12) are similar to results for AI_FCM_1 and AI_FCM_3 (Figure 4-13), respectively. Nevertheless, the FCM algorithm was created to address the issues of detecting small zones of alteration/mineralisation in crystalline or hard-rock environments so therefore the emphasis is in not smearing out what may be the target of exploration. In this case, the FCM approach tends to preserve this upside for interpreters with an AI section that better highlights possible small zones of mineralisation than the post stack seismic images. The FCM inverted

models are closer to the borehole data than the HRS inversion (Figure 4-14) in all three scenarios of initial models, which demonstrates that using the petrophysical constraints via FCM cluster processing produces more reliable models.

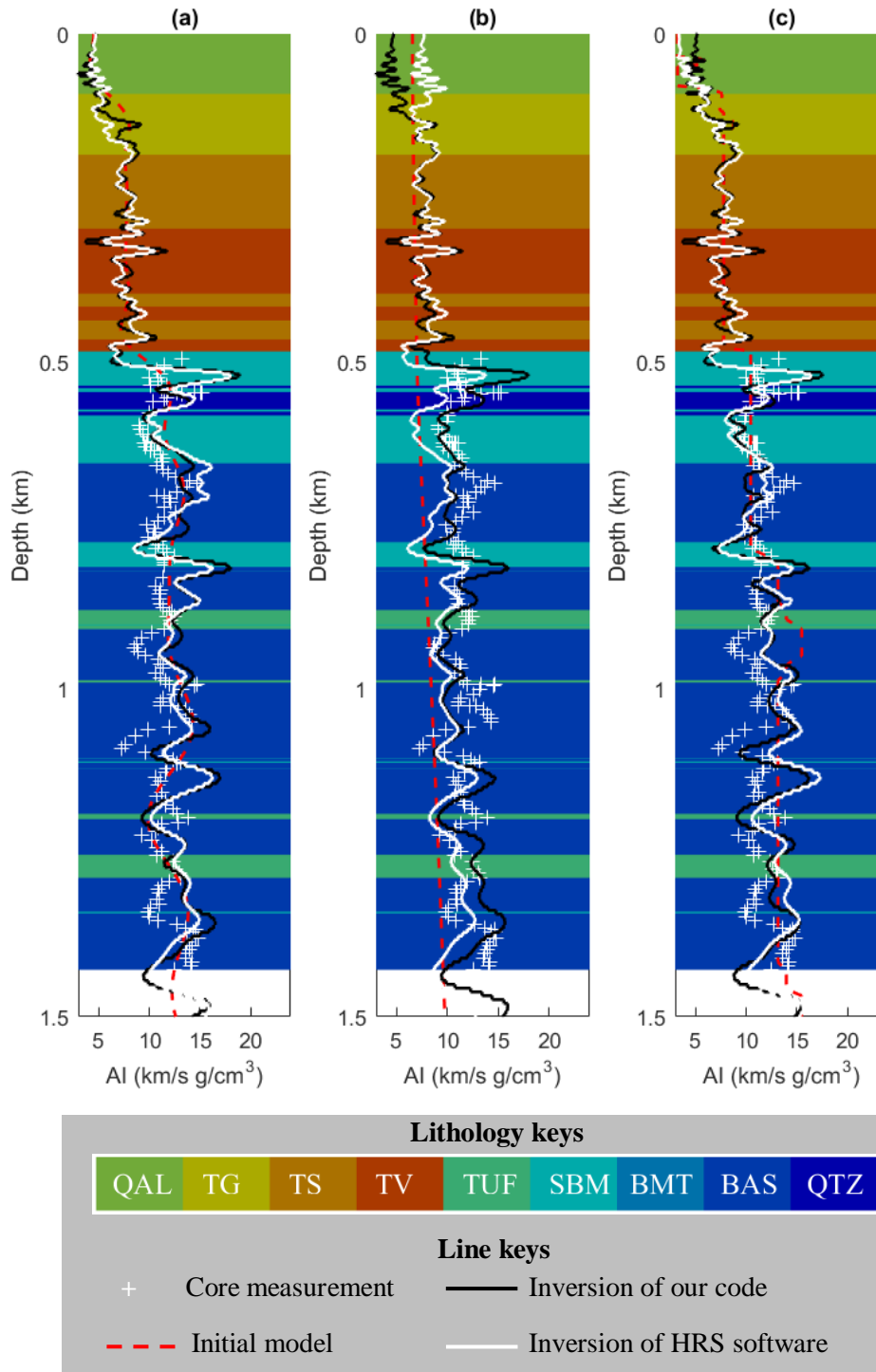


Figure 4-14: Comparison between borehole data and inversion results using three initial models: (a) borehole data, (b) migration velocity, and (c) the MT model. The lithology keys are shown in Figure 4-3.

Although the FCM algorithm can reduce the impact of the initial models by constraints via boundary information that only provides a vertical variation of seismic properties, it cannot recover the lateral change of the section. According to the geological setting of this section, there is one main fault (Figure 4-4b) that may create a lateral change of geophysical properties along the section. The inverted results from the initial models AI0_1 and AI0_2 using HSR, AI_HRS_1 and AI_HRS_2 (Figure 4-12), and the FCM routine, AI_FCM_1 and AI_FCM_2 (Figure 4-13), do not seem to build the models showing these geologic signatures. In the case of initial model AI0_3, the resulting AI inversion models generated by using the MT model, AI_HRS_3 and AI_FCM_3, better represent the geologic setting. For instance, these models have anomalous petrophysics near the main fault. These inversion examples demonstrate that there should be benefits in co-operative inversion of multiple geophysical data.

4.3.5. Parallel co-operative inversion of magnetotelluric and seismic data

To simultaneously couple the models when individually running the seismic and MT inversions, we may run the MT and seismic inversion processes in parallel. The initial MT model is set to a homogeneous value, as previously to 100 Ωm , and the initial seismic model is created by using the migrated velocity model (Figure 4-11b). In this process, the two inversions are run independently. The FCM clustering executes the coupling process after a number of iterations in the inversion process (in this work I set three iterations); this process is more stable than imposing the coupling right at the beginning of the inversion.

Figure 4-15 presents the inverted models. It can be seen that the MT model provides most of the low-frequency spatial information to the seismic model resulting in large scale geological features appearing in both models. This could not be seen in the seismic inversion alone. In turn, the seismic model constrains the MT inversion to significantly enhance the resolution of the MT model. The inversion of both models matches well with the borehole data (Figure 4-16) demonstrating the robustness of the co-operative inversion approach with FCM. This strategy may not impose the strong correlation between MT and seismic models like the conversion process, but

it can mitigate the bias if the relationship between resistivity and acoustic impedance is improperly defined (Moorkamp 2017).

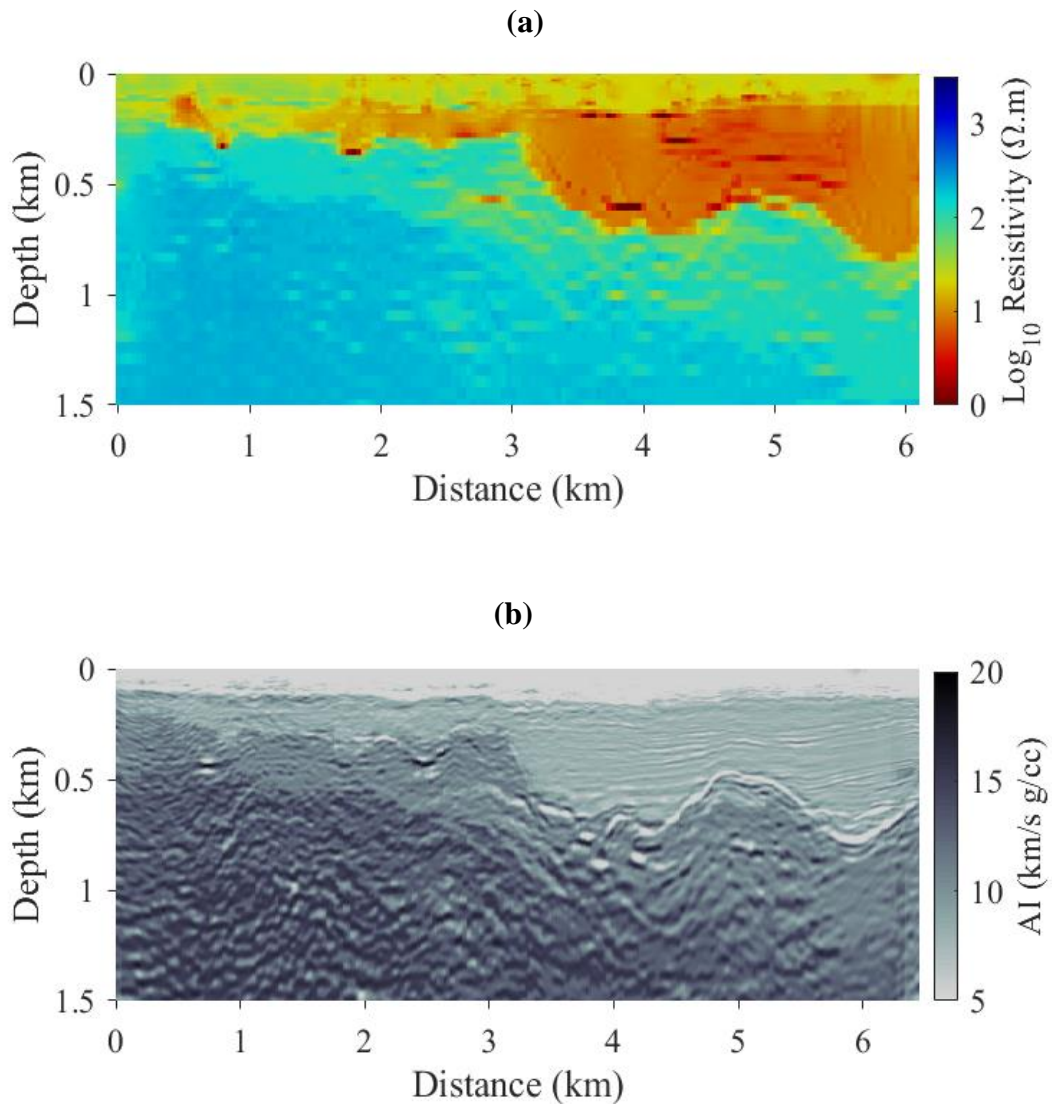


Figure 4-15: Parallel co-operative inversion results: (a) MT model and (b) the seismic model.

The results from the sequential co-operative inversion, RES_4 (Figure 4-16), shows higher resolution and is more consistent with the borehole data than the MT result using the parallel co-operative inversion strategy, while the seismic results of both co-operative inversions are almost the same and consistent with the core measurement. The high resolution of the MT model comes from the seismic data, while the seismic inversion benefits only by the low-frequency band from the MT model. In the sequential co-operative inversion, the AI model obtained by the seismic inversion is fixed and imposes a strong effect on updated MT models. This process

may provide a high-resolution model of the geoelectrical properties, but it may also create artefacts in the MT model. By “softening” the constraints in the parallel co-operative inversion strategy, it also produces good results with less bias.

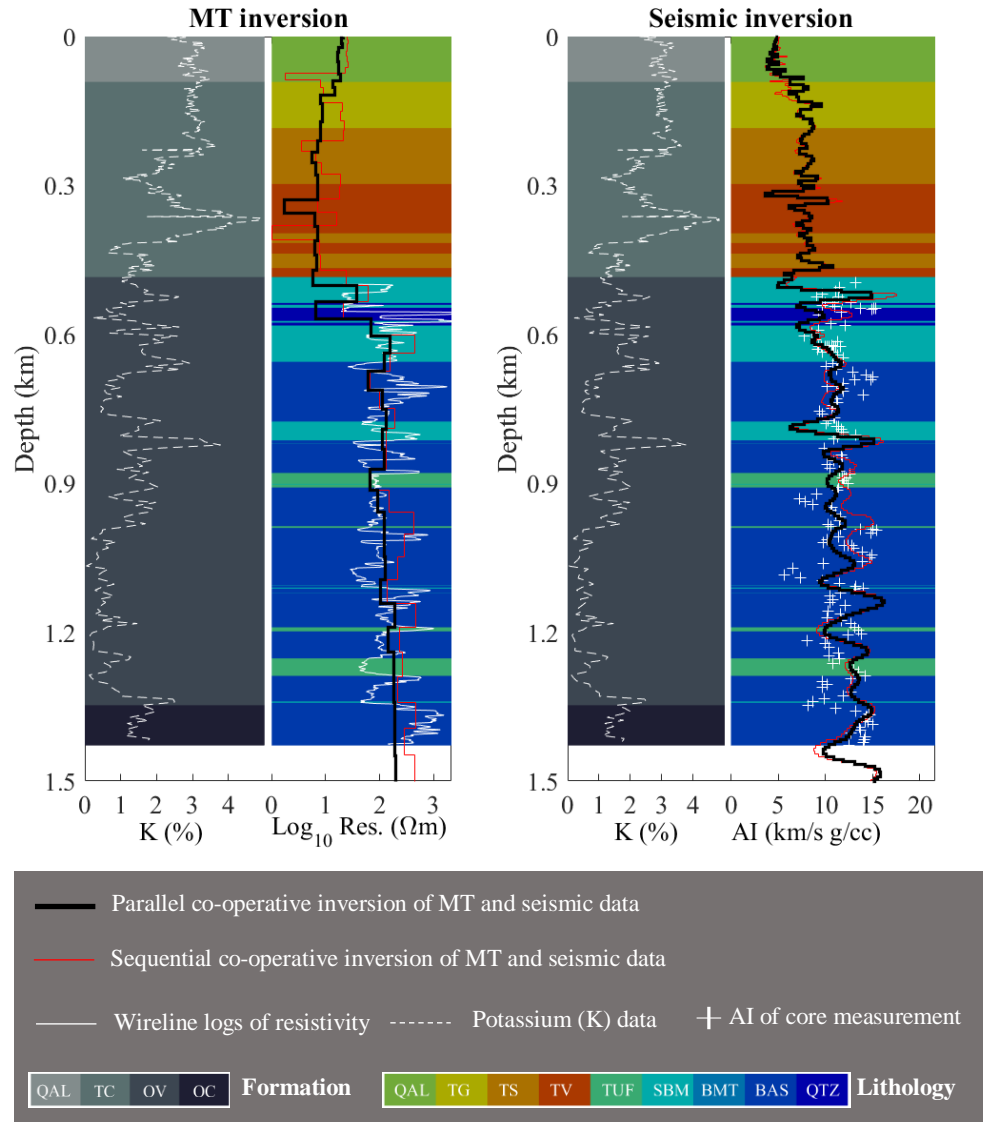


Figure 4-16: Comparison between inversion models and borehole data in the well W1. The sequential co-operative inversion of MT, RES_4 (Figure 4-9) show higher resolution than inverted model of parallel co-operative inversion and is more consistent with borehole data (wireline logs and potassium measurement). The resolution of MT model is attributed to the seismic data. The AI model produced from parallel co-operative inversion is almost the same as the sequential co-operative inversion model, AI_FCM_3 (Figure 4-14), except at depths of about 0.9 to 1.1 km. The AI model produced from sequential co-operative inversion shows a considerably higher resolution than the model of parallel co-operative inversion due to the low-frequency band compensated by MT model. This part also shows a significant difference between the two MT models. The abbreviation of the formation and lithology can be seen in Figure 4-3.

4.4. Converting the geophysical model into a pseudo-lithological map

Applying FCM clustering to an “initial pass” on inverted MT and AI models provides a quicker means to build interpretable images. This results in a pseudo-lithology section based upon the assumed link between petrophysical clusters and geological units. The pseudo-lithology images can assist during the interpretation process better than when using geophysical models alone (i.e., petrophysical property volumes); especially for geologists with little geophysical training. Not all lithologies will be identified with this section, nor will they necessarily be how a geologist would group units. Nevertheless, the pseudo-lithology section does automatically provide the boundaries that geophysicists would interpret, and with less bias. The clustering results from the sequential and parallel co-operative inversions are shown in Figure 4-17. In comparison with the raw seismic data, these pseudo-lithological sections are more interpretable. The signature of minor layers is visible within the sediment in the right-hand side of the section, which may relate to the interbed layers between shale and sandstone. The basement shows zones of shifts/offsets in the pseudo-lithology that can be interpreted as faults associated with horsts and grabens in the basement rocks, which are expected. Additionally, there some zones with “outlier” cluster values that may relate to prospective mineralisation.

The essential idea of imposing FCM into an inversion process is that it may help to highlight mineralisation zones. In this geological setting, numerous gold deposits are often found in old altered carbonate rocks. Prospective areas are where there might be traps for the gold bearing fluids, which often alter the rock significantly by substantially weakening them or by increasing their stiffness due to silica replacement. Thus, we should be able to identify such areas in the cluster map of Figure 4-17 and check assay data from any boreholes that intersect these areas. Inspection into the horst feature of Figure 4-18 reveals three zones where there is anomalously low impedance, which indicates rocks weakened from alteration (at depths of about 550 m, 620 m and 770 m). The elemental assay data for gold (Au) and gold pathfinder elements (As, Sb and Hg) indicates that these zones are in fact anomalous in geochemistry and highly altered. Figure 4-14 illustrates three zones relating low AI values that also have peaks in the Au, As, Hg and Sb. The weak zones are also identifiable in core photos (Figure 4-19) that further confirm the acoustic impedance models produced by our method. It should be noted that inversion models

were produced first, and then supporting core and assay data from the nearby drill hole were examined to test the interpretation. Additionally, the three zones identified are the three most fractured rock cores and have the highest elemental anomalies; thus, it is more than coincidence and it supports the contention that the pseudo-lithology (cluster map) of Figure 4-17 provides a better starting point to interpret the seismic reflection image displayed in Figure 4-4c.

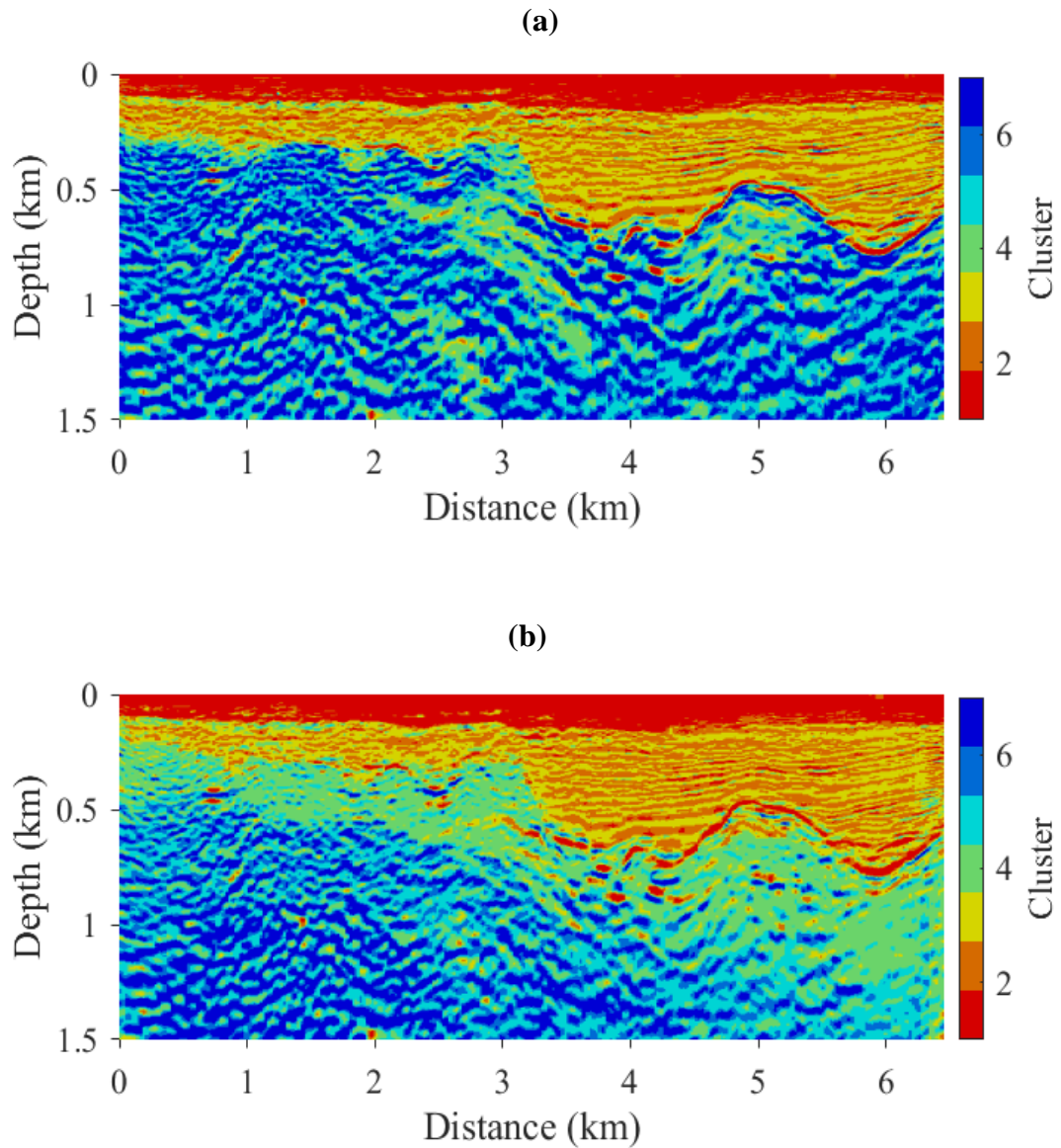


Figure 4-17: Pseudo-lithology sections derived by applying FCM clustering to the inverted models of resistivity and AI models from (a) sequential co-operative inversion and (b) parallel co-operative inversion.

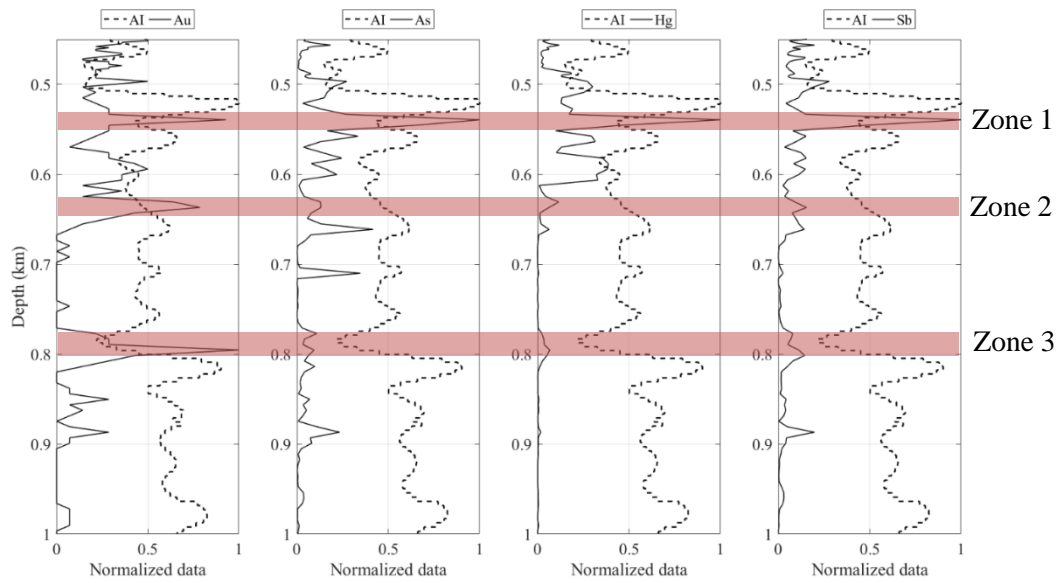


Figure 4-18: Comparison between the model AI_FCM_3 (AI) and assay data of Gold (Au), Arsenic (As), Mercury (Hg), and Antimony (Sb). All the data is normalised in the range of [0, 1]. The red zones indicate abnormal assay zones relating low AI zones.

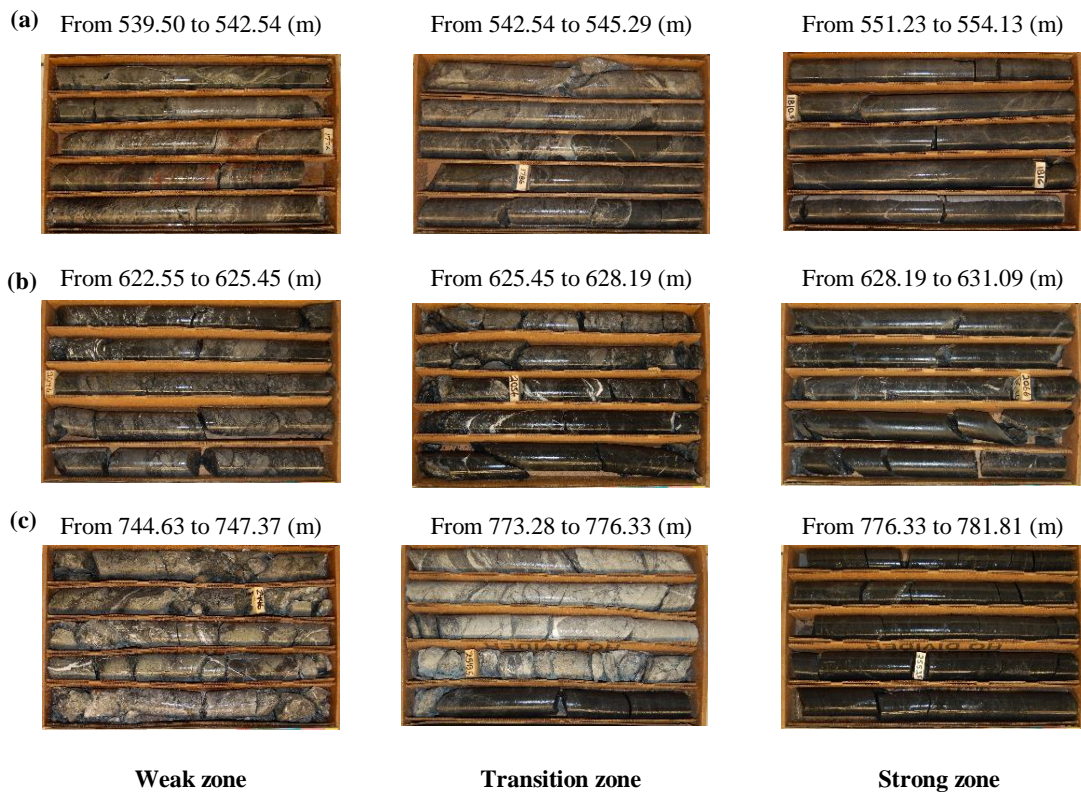


Figure 4-19: Core photos illustrate three abnormal zones in Figure 4-18: (a) Zone 1, (b) Zone 2, and (c) Zone 3. Weak zones relate to low values of AI and high values of assay data; in contrast, strong zones show high values of AI and usually low values of assay data.

4.5. Conclusions

A challenging data set in a mineral exploration environment was used to test novel methods of integrating prior and complementary information from another method into a co-operative inversion schemes are proposed by exploiting the advantages of the fuzzy c-means clustering technique.

Where there is little prior information such as cluster number, the algorithm was successfully run as a conventional inversion process. Inclusion of some borehole information allowed the number of clusters and centre values to be better defined, which also improved both the MT and seismic AI inversion processes. Spatial information from boundaries identified with the seismic data improved the MT results, and low frequency information from MT was also beneficial to producing good seismic AI inversion. Putting all the elements together with FCM created better models that match reasonably well with the ground truth such as borehole data. This was not achieved in previous work (Takougang et al. 2015, Le et al. 2016) with these data.

The FCM constrained seismic model-based inversion illustrates that this methodology is robust and the results are comparable with current benchmark commercial software (e.g., the Hampson-Russell Software, CGG Veritas). The algorithm and methodology dealt with various difficult scenarios. In particular, this inversion process deals with the challenges of inadequate borehole information better than the commercial software and with more flexibility in incorporating various prior information.

The co-operative inversion of seismic and MT data demonstrated the use of multiple geophysical methods to build better models than those created from a single dataset, even when using a better inversion algorithm. The MT data can provide the low-frequency spatial components for seismic data; in turn, seismic data can provide high resolution spatial information for MT. This significantly enhances the resolution of the MT model. Importantly, the FCM inversion approach to real (imperfect and noisy) data can work well where a conventional approach will not. The inversion model matches the well data and the known/expected geology reasonably well. The resulting models and cluster maps may be interpreted to find zones of mechanical weakness and fracture. Such weak zones are expected to be prospective for gold exploration in

the area, and geochemical analysis of recovered from core supports this link to weak zones (identified in the impedance section). Hence, my approach could lead to better exploration outcomes in this world-class gold district.

Lastly, to reinforce the message: this was a not just a demonstration with real data, but a demonstration with really difficult data. And the FCM inversion method worked very well despite the difficulty.

Chapter 5: INTEGRATION OF BOREHOLE DATA IN SEISMIC INVERSION

Summary

Seismic data provide useful information for both exploration and geotechnical purposes. However, reflection seismic data only provides information for the relative variation of acoustic impedance (AI) between different geological entities. Hence, geological interpretation using 3D seismic data is an intensive task and highly uncertain, particularly in hard-rock environment where geological structures are often complex. Moreover, it is usually impossible to directly transfer the seismic data into other formats, such as rock quality designation (RQD) for geotechnical uses. One of solutions for these issues is to convert seismic data into an AI model, for instance, using model-based inversion approaches presented in Chapters 3 and 4. The AI model can provide better quality images for geological interpretation and be more easily converted into other formats. The critical issues for the seismic inversion are the lack of low-frequency band data and non-unique solutions, which can be resolved by including borehole data during processing.

In this chapter, I present an approach of analysing data in a producing mine site, the Kevitsa Ni-Cu-PGE mine, North of Finland. The lack of low-frequency band data can be compensated by the initial model that is often built from borehole data; but it is a difficult task for this particular data set. The velocity in this area has high spatial variability (4 – 7.5 km/s) and these variations may create serious artefacts for an interpolated model from the borehole data if the number of drill holes is not relatively large. Unfortunately, in this case we have only 14 holes with the sonic logs. This numbers of holes is not sufficient to generate a ‘good’ initial model for seismic inversion. Therefore, it is vital to estimate P-wave velocity (V_p) from other borehole data that can build a better initial model. In this work, we utilise aspects of fuzzy clustering techniques to predict acoustic velocity, V_p , from other features of the borehole data. To deal with a non-unique inversion solution, we use both petrophysical and spatial constraints by adapting the borehole data in the context of the inversion.

There are three key outcomes from using this approach: (1) The P-wave velocity model estimated from processing other borehole data may not only help in the seismic inversion process, as in this study, but can also be used in future seismic data reprocessing; (2) the pseudo-lithology model built from clustering the inverted AI model provides more interpretable images when compared to post stack - migrated reflection seismic images, which show boundaries and do not tell much about what is between the reflections; (3) the converted RQD model matches well with the core measurements, which shows that this model could be useful for future mine design and planning.

5.1. Introduction

The Kevitsa Ni-Cu-PGE ore within the Kevitsa mafic-ultramafic intrusion is located in northern Finland (Figure 5-1a). The mine life is forecasted to be about 20 years. In 2012, First Quantum Minerals Ltd. commenced open-pit mining; the depth of the open-pit was at 100 m in 2014 and the planned final depth is about 550 m (Koivisto et al. 2015). This deposit has attracted much research effort because of the wealth of data and the wide availability of this data. It is one of the very few deposits that has both 2D and 3D seismic reflection surveys (another example can be found in (Cheraghi, Malehmir, and Bellefleur 2012)) and other geophysical data, such as airborne EM, gravity, magnetic, IP, DC and MT, and borehole data including both wireline logs and core measurements from 886 holes.

The main objective of the reflection seismic data survey in this area was to map major fault and fracture zones, which may impact on the stability and safety of the mining operation. There are a number of studies of various aspects of the seismic surveys and borehole petrophysics, mostly to assist with defining structural features that could be of interest in the mine planning stage. The 3D reflection seismic data was presented by Malehmir et al. (2012) regarding data acquisition, processing and interpretation. They interpret some of the main structural features, such as vertical faults. The depth to the intrusion basement that hosts the mineralisation is about 1200 m. Notably, they also reported that the challenge when processing the seismic data is the complex geological model and the high variation of velocity. The lateral extents of the intrusion are imaged by 2D seismic data (Koivisto et al. 2012). Combining 2D and 3D seismic

data, Koivisto et al. (2015) built a 3D model of lithological contacts and near-mine structures. The use of multiple data types to build a 3D fracture zone model in the Kevitsa open-pit was conducted by Lindqvist (2014). 3D petrophysical properties were acquired by Steel (2011a) from the borehole data using self-organising maps to see if there could be a means to assist velocity model building for seismic imaging. Neild (2015) mapped aspects of the geology by running seismic inversion and analysing the seismic attributes of the 3D seismic reflection data in an exercise to see what could be done further with the 3D seismic data. Khoshnavaz et al. (2016) imaged the fracture zones by calculating the diffractively in a test of a new imaging technique offered insights.

The major issue of all previous works is the inability to fully exploit both the seismic and borehole data to image the subsurface. The inversion of seismic and seismic attributes (Neild 2015, Khoshnavaz et al. 2016) may better support the interpretation process rather than using just the raw seismic data (Malehmir et al. 2012, Koivisto et al. 2012, Koivisto et al. 2015). Nevertheless, their work does not fully exploit the information from the boreholes. For instance, the seismic inversion by (Neild 2015), only used the thirteen holes where P-wave velocity was available. There are about 900 holes in this area without P-wave velocity data, but that do have other features such as lithology, geochemistry and other downhole geophysical information. This lack of P-wave velocity information can be estimated by the prediction process (Steel 2011a).

In this work, I use both borehole data as the prior information to constrain seismic inversion and the seismic data play as an interpolator to diffuse the borehole data into 3D models. Moreover, analysis of the borehole data can also define links between different features that can be used to convert the seismic model into other formats that are more interpretable.

5.2. Kevitsa mine site

5.2.1. General geology setting

The Kevitsa mine site is located within the mafic-ultramafic Kevitsa intrusion in northern Finland. The main host of the Kevitsa deposit is series of layered intrusions created by igneous activity at about 2.05 Ga (Mutanen 1997). The Kevitsa intrusion

has a roughly oval shape; the long axis is about 7 km and is oriented from the north-east to the south-west.

A geological map is presented in Figure 5-1. Generally, the intrusive rock varies from mafic to ultramafic, comprising of olivine pyroxenite, which dominates the main intrusion, as well as peridotite, gabbro, and granophyre. The mineralisation is lithologically controlled in the ultramafic units (Standing et al. 2009, Gregory et al. 2011). The internal seismic reflectors within the intrusion relate to the pulses of ultramafic flows (which flow with relatively low viscosity when molten), with thickness typically in the order of tens to hundreds of metres (Standing et al. 2009, Gregory et al. 2011). The structure of the intrusion is also dominated by two fault systems, north-west to south-east and north-east to south-west; almost all of the faults are steep (Koivisto et al. 2015). These faults, and the possibly weak zones around faults, were considered a significant risk to the mine plan (pers. comm. with A. Kopic and P. Williams of HiSeis, who helped to plan and implement the seismic 3D survey). So, the proper identification and characterisation of these geological structures and their relationship to rock quality (engineering) was of greater importance than identifying mineralisation.

5.2.2. Data sets

The data sets used for this study are comprised of 3D seismic reflection and borehole data. The location of the seismic acquisition and boreholes is presented in Figure 5-1b. Details of the seismic data are provided by Malehmir et al. (2012). The borehole data includes the wireline logs, assay data, core measurements, and lithological information from 886 holes (Table 5-1). The borehole data was also described by Steel (2011a), Neild (2015).

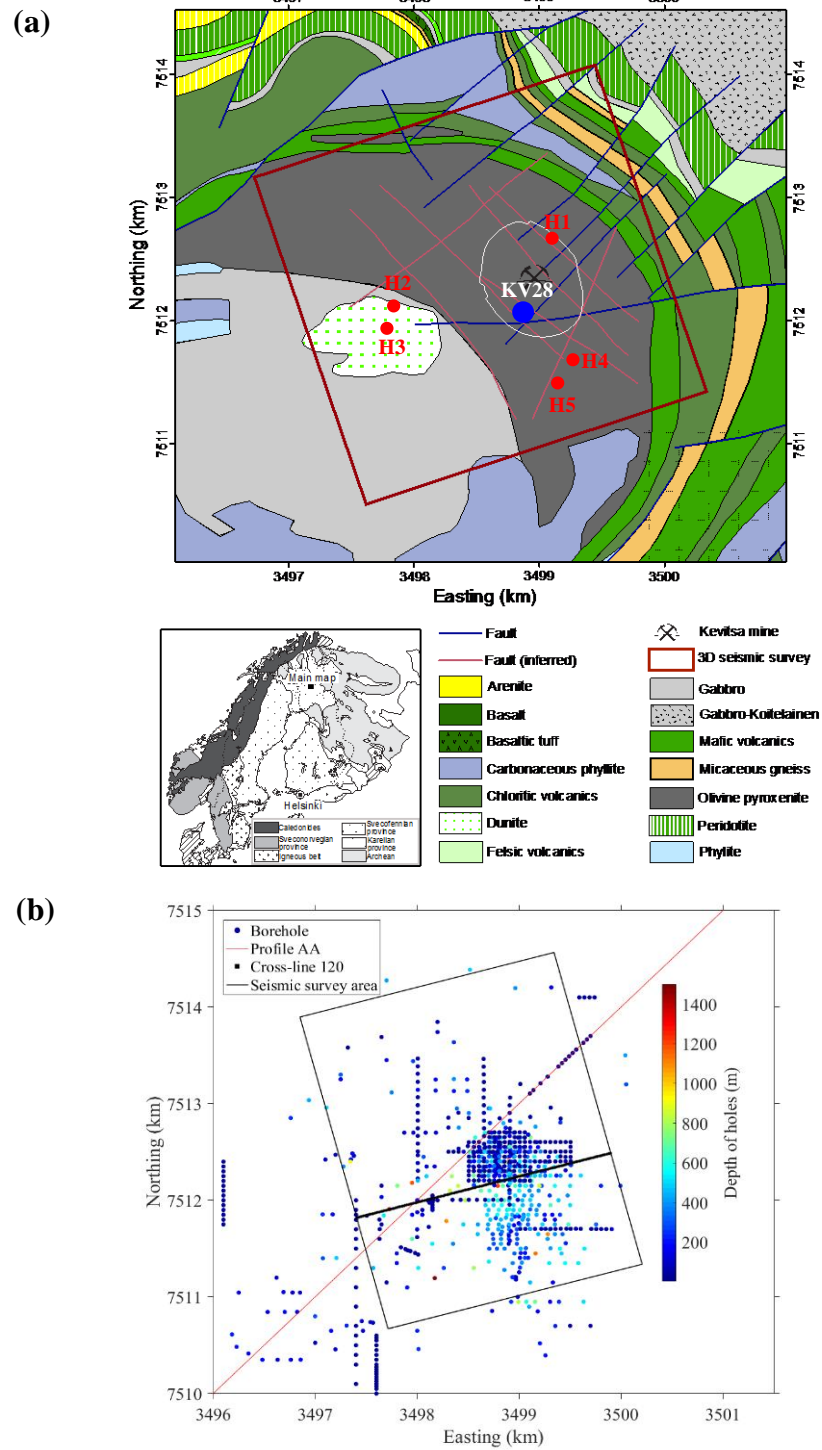


Figure 5-1: (a) Geological map adapted from Malehmir et al. (2012). The solid red circles mark locations of five holes, which are used in P-wave velocity prediction. The solid blue circle is location of the hole, which for validation of the data processing. This is a deep hole with almost full borehole data acquired and is located in the centre of the mine site. (b) Map of borehole and seismic data locations. The colour of the dots shows the depth of hole. The deep holes (>500 m) are located in the centre of mine site, the north of the seismic survey areas show less dense holes, most of which are shallow. The red line marks the location of profile AA' used to compared my results with ones obtained by (Koivisto et al. 2015).

Table 5-1: Summary borehole data.

Wireline logs			Assay			RQD	
Att	Number holes	Length (m)	Att	Number holes	Length (m)	Number holes	Length (m)
V _p	14	11076	Co	442	106458	173	68471
Den	94	42910	Cu	442	106448	Lithology	
NG	93	42871	Ni	442	106456	Number holes	Length (m)
Res	69	33516				886	185035
Mag	83	36396					

Abbreviation: Att - attributes; RQD - Rock quality designation; V_p - P-wave velocity; Den - Density; NG - Natural gamma; Res - Resistivity; Mag - Magnetic susceptibility.

The Rock Quality Designation is a percentage of core recovered in large pieces (pieces greater than 10cm long), which is used to indicate the rock quality for use in engineering structures (Deere 1988). Based on the RQD values, the rock is separated into five classes (Table 5-2) for rock mechanics/engineering purposes. This index is then used to provide important information for mining design, such as will the pit wall tend to collapse under its own weight. In reality, the RQD is measured with core run (usually few meters), however, I assigned the RQD values on point-to-point that makes the comparison with borehole and seismic data to be more convenient.

5.2.3. Workflow of data analysis

Figure 5-2 shows the workflow of the data analysis. The aim of this study is to build a 3D model of features to maximise use for geological interpretation and geotechnical purposes. This workflow has three blocks: DATA, INVERSION and INTEGRATION. In the DATA block, the data set is preconditioned to be inserted into the two remaining blocks. The INTEGRATION block applies the machine-learning algorithms to estimate missing values in the borehole data and to build relationships between the data features. In the INVERSION block, processed data from the DATA and INTEGRATION blocks are utilised to generate an initial model and to constrain the inversion of multiple data types comprising of geophysical,

geological and downhole data. The output of the DATA and INVERSION blocks are used as input for the INTEGRATION block again to build a 3D model of features.

Two essential characteristics of the workflow are: (1) working with both numerical data (such as wireline logs) and surface geophysical data, and categorical data such as lithology, and (2) adapting new information to update the final models. The strategy to deal with mixed data sets is the same as the boundary information and is included in the inversion process as described in the previous chapters. The critical idea of this strategy is the use of fuzzy clustering with mixed data sets (Kim, Lee, and Lee 2004).

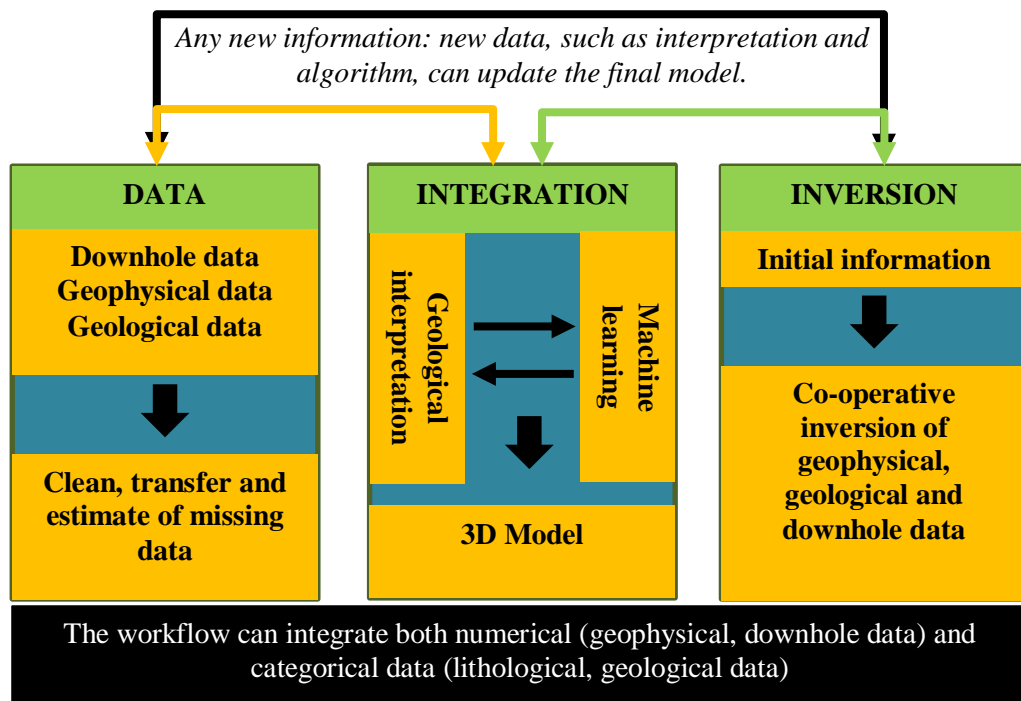


Figure 5-2: Data analysis workflow

5.3. Borehole data analysis

5.3.1. Quality of the data sets

The first essential issue of model-based seismic impedance inversion is wavelet extraction. In this data set, extracting the wavelet is a difficult problem due to the use of two acquisition sources with different characteristics: explosives and Swept Impact vibration (Malehmir et al. 2012). Moreover, the complex velocity model and low quality of the sonic logs also cause difficulties for a well-tie extraction of the wavelet

(Is the log an accurate reference? Sonic logs in fast media often work poorly due to low P-wave amplitudes received, pers. comm. with HiSeis geophysicists at DET CRC annual meetings). The high P-wave velocity in this area (about 4000 to 8000 m/s) that can vary substantially over short distances also may degrade the quality of sonic logging. Hence, the well-tie wavelet extraction shows low cross correlation between synthetic data from borehole information and seismic data (Steel 2011a, Neild 2015). Neild (2015) tested well-tie wavelet extraction with all available sonic logs; the highest cross-correlation is about 51.8%. It should be noted that the seismic data cube is relatively noisy (a lot of “speckle” from scatterers), further reducing correlation numbers. While the statistically extracted wavelets obtain reasonable results, the extraction of the wavelet from the twelve selected holes illustrated is roughly similar in shape (Neild 2015). Therefore, in this study I use the statistical wavelet extraction method for the inversion.

The other crucial issue in the inversion process is to generate an initial model. The initial model is often built from borehole data and we have 886 holes in this data set; however, there are critical problems when using this data. Only 14 of the 886 holes have acquired Vp, which is not sufficient to generate a ‘good’ initial model. Vp varies considerably spatially and interpolation and extrapolation of borehole data into the 3D model poorly represents the 3D distribution. A lack of continuity in the seismic reflectors in the 3D data due to poor signal-to-noise means that it is hard for seismic impedance inversion to “push” any smooth initial model into the proper shape. The initial model would be better in resolution and requiring little interpolation if we can exploit the information from all the boreholes in this area. However, the cross correlation between attributes is poor (Steel 2011a) leading to difficulties in using cross correlation functions to exchange the data features. Therefore, we need to utilise other techniques to estimate the Vp data. In this study, I use fuzzy clustering to predict the missing values (the results are presented in Appendices F and G).

One of the main objectives of this study is exploit the borehole data and use them to constrain the seismic inversion, then convert the inversion results into other formats. This task requires (predictive, or described with a mathematical function) relationships to be established between the features of the boreholes. However, correlations between the physical characteristics of the boreholes and assay data are poor (Steel 2011a, Neild 2015); thus, we can not directly integrate both data in the

same process. Instead, I use the clustering results of borehole data features as a significant constraint inputs for the inversion.

The correlations between P-wave velocity and RQD (Figure 5-5a) is also poor when performed on a point-by-point comparison. As the RQD parameter is calculated by the percentage of the total length of core pieces that is greater than ten centimetres in the total length of the core run and the Vp is measured every 10 centimetres there is a mismatch in scales. Thus, both parameters are extracted from borehole data using their average values over a common scale length (such as 5m) with this adjustment RQD and Vp are clearly strongly related (but not linearly).

5.3.2. Preconditioning the data

Generally, borehole data needs to be preconditioned before it is added to the inversion process. The first step is to remove the outlier data points; for example, negative values or unusually large values. All these values are replaced by “not on a number” values (NaN). To avoid skewness, the data features are transferred into logarithmic scale”. For this study, I use logarithmic scaling for natural gamma, magnetic susceptibility, resistivity, induced polarisation, and all of the elemental assay data.

The sample intervals are then resampled for all holes and measurements; for instance, the different sample rates between wireline logs and core measurements. In this study, I used the sample interval of core measurements as one meter. Therefore, wireline logs with a sample rate equal to 0.01 m is downsampled to the same rate found in the core measurements.

Before the borehole data is added to the inversion process, the data should be smoothed to remove any high frequencies that the seismic cannot preserve. I use a low-pass filter with a window range of 6.5 m, which corresponds to the average travel time distance of one seismic sample, that is, one millisecond multiplied by the Vp average of 6500 m/s.

5.3.3. Estimation of missing values

An overview the main idea of this process of dealing with incomplete and inconsistent data sets follows in this section. However, the full details about the methodology and

the results of this FCM driven process of filling in missing data are presented in Appendices F and G.

$$z_j = \frac{\sum_{k=1}^C u_{jk}^q o_k}{\sum_{k=1}^C u_{jk}^q},$$

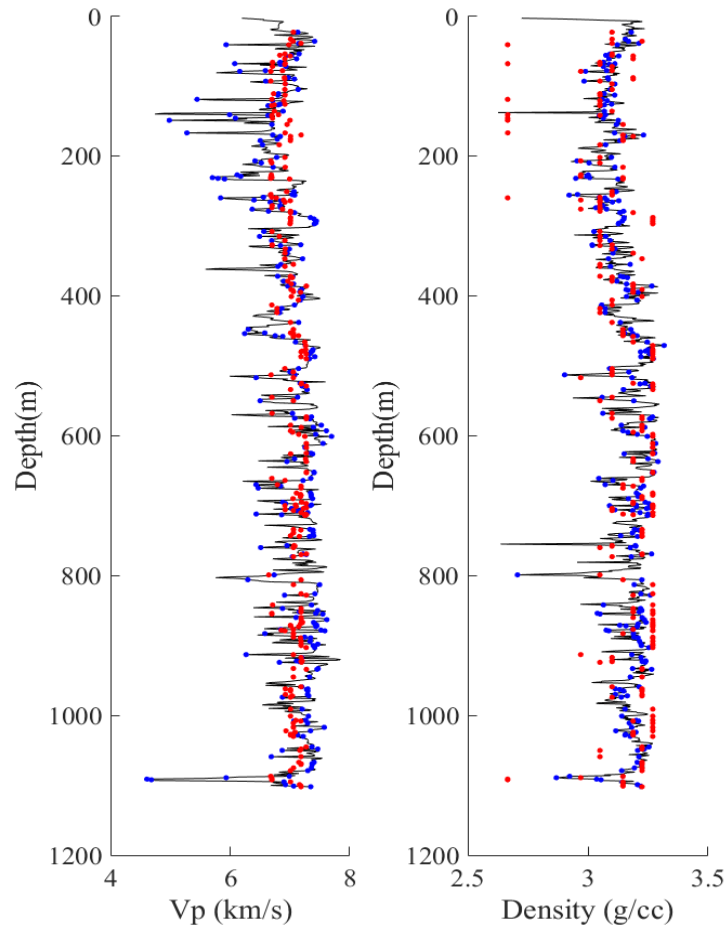


Figure 5-3: “Fill missing values” test results in the hole KV28. The data includes 1100 samples (black lines), 238 samples (about 20%) are randomly replaced by NaN values (blue dots), then running a “fill missing values” programme to estimate the missing data (red dots).

In most mining environments, there are few wireline logs, but many holes with elemental data and often many with geotechnical parameters. The boreholes that have multiple data sets of both wireline and elemental/geotechnical data are used to build up a statistical, or FCM model of the geology. Where the borehole data has at least one or two sets of data the centre values of the clusters and fuzzy c-means clustering are used to replace the other missing property values. Here, I adopt the methods of

Dan, Chongquan, and Jinhua (2012). The main idea behind using FCM clustering here is to assign the weighted average values of the clusters to the missing values, using the equation in Chapter 2 (equation 2.5). Assuming that we can separate N samples of an incomplete data set in C clusters, thus, the membership $\mathbf{U}(u_{jk}, j=1, \dots, N, k=1, \dots, C)$ and centre values $\mathbf{O}(o_k, k=1, \dots, C)$ are defined, then the missing value z_j is calculated by the equation (2.5)

$$z_j = \frac{\sum_{k=1}^C u_{jk}^q o_k}{\sum_{k=1}^C u_{jk}^q}, \quad (5.1)$$

where q is fuzziness. In this work, I set q equal 2 (Bezdek, Ehrlich, and Full 1984b).

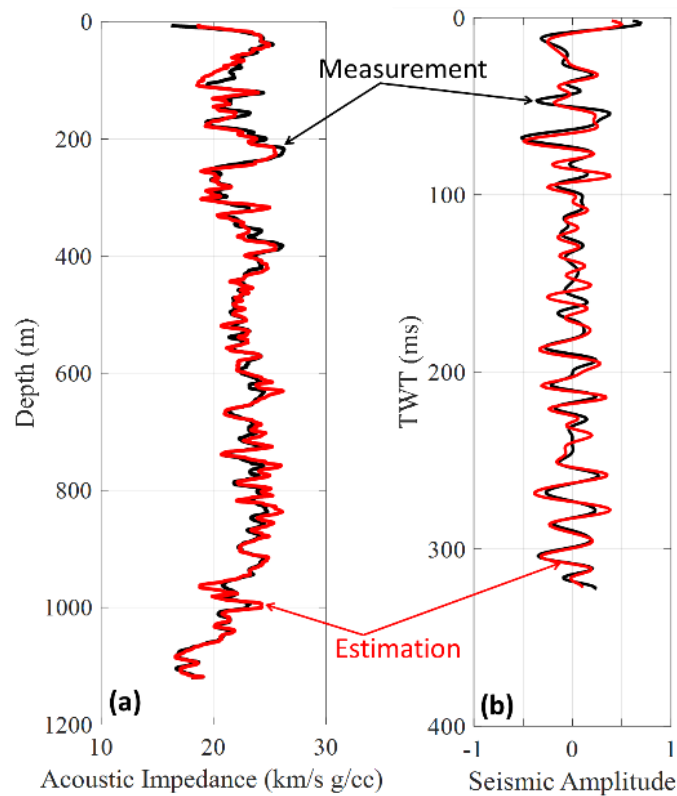


Figure 5-4: (a) The consistency between estimated and measured acoustic impedance demonstrates that the V_p estimation can be used in the seismic inversion process. (b) Comparison of seismograms in the time domain between estimated data and measured data shows that we can use the predicted V_p to build the V_p model for seismic processing.

Figure 5-3 shows results from the KV28 borehole (a test or training data set) when testing the “fill missing values” program. It includes 1100 samples of the feature’s lithology, Vp and density. To use KV28 data only about twenty percent (238 samples) of Vp and Density from this borehole are removed from the training and the algorithm fills these values with the average/cluster centre value from the fuzzy clustering process. After initial setting of cluster centre values (training) the algorithm is tested on another borehole with rich data sets (there are about 7 boreholes with nearly complete and comprehensive data sets of the 880 or so in total). The results demonstrate that the estimated values are not always very close to the true ones; but “on average” they are consistent with the low frequency trends of the true data. What is critically important for the seismic inversion process is not the correlation coefficient, but the lack of bias and provision of low frequency data in the spatial domain, which this process delivers and seismic data completely lacks. As the average values are assigned to the missing values. The low-frequency band or trend of the data is kept rather than the variation in detail. The advantage of this process is that keeps the estimation values with average trend and avoids bias. This estimation process assists the 3D seismic inversion in the low-frequency band data where it needs help the most. This approach avoids trying to fit detail that does not really help answer the principal geological questions.

In cases where properties, such as Vp, are acquired in only a few boreholes, we can predict missing values from other data in a useful way. Figure 5-4a shows the smoothed acoustic impedance product of the estimated and measured Vp and density logs from borehole H4 (Figure 5-1a). In this case, the data from borehole H1, H2, H3 and H5 is used to define a model in the training process and then the model is tested on the data of H4. The prediction process is presented in Appendix F. The data is smoothed by a low-pass filter with a (moving average) window width of 10 m. The trend (the troughs and peaks) and values match well with measured data and demonstrate that the predicted Vp is good to use for seismic impedance inversion purposes.

5.3.4. Establishing a relationship between the seismic data and rock properties

An issue is that RQD is acquired by core measurements and is only available along a borehole trajectory, but it is used in the mining design as volumetric measure of rock quality. It would be much less risky for the mining engineers to have data that is more volumetric (in comparison with localised data of the borehole) and tied to the “known” data in the boreholes. The 3D surface seismic method provides information for the whole survey area volume, but the resolution is much lower than that of the borehole data. Hence, the seismic and borehole data combined may provide a means of de-risk the borehole information for geotechnical studies if we can exploit seismic data as a means of interpolating the “known” borehole data to the whole volume. This relationship between Vp and RQD is well known because both properties/measures are influenced by rock properties such as fracture, alteration and hardness. In this work, we analyse borehole data to establish the relationship between RQD and Vp using the FCM methodology, which is also then used in the seismic impedance inversion process. This relationship is used to convert 3D seismic models that are obtained by co-operative inversion of seismic and borehole data into a 3D model of RQD.

Table 5-2: Rock quality characterisation based on RQD (After Deere (1988))

RQD (%)	Description of rock quality
0 – 25	Very poor
25 – 50	Poor
50 – 75	Fair
75 – 90	Good
90 – 100	Excellent

The relationship between Vp and RQD used to convert the seismic inversion model Vp into a RQD model is presented in Figure 5-5. Not coincidentally, the five clusters applying fuzzy clustering to average values of RQD and Vp (Figure 5-5d) almost correlate very well with the five rock types (Table 5-2). Accordingly, the clusters from 1 to 5 correspond to rock quality from very poor to excellent. Note that AI and Vp are highly correlated, thus, we can link AI produced from seismic impedance

inversion to RQD via V_p and the substantial density information from hundreds of boreholes (whereas only 6 boreholes have trustworthy V_p measurements).

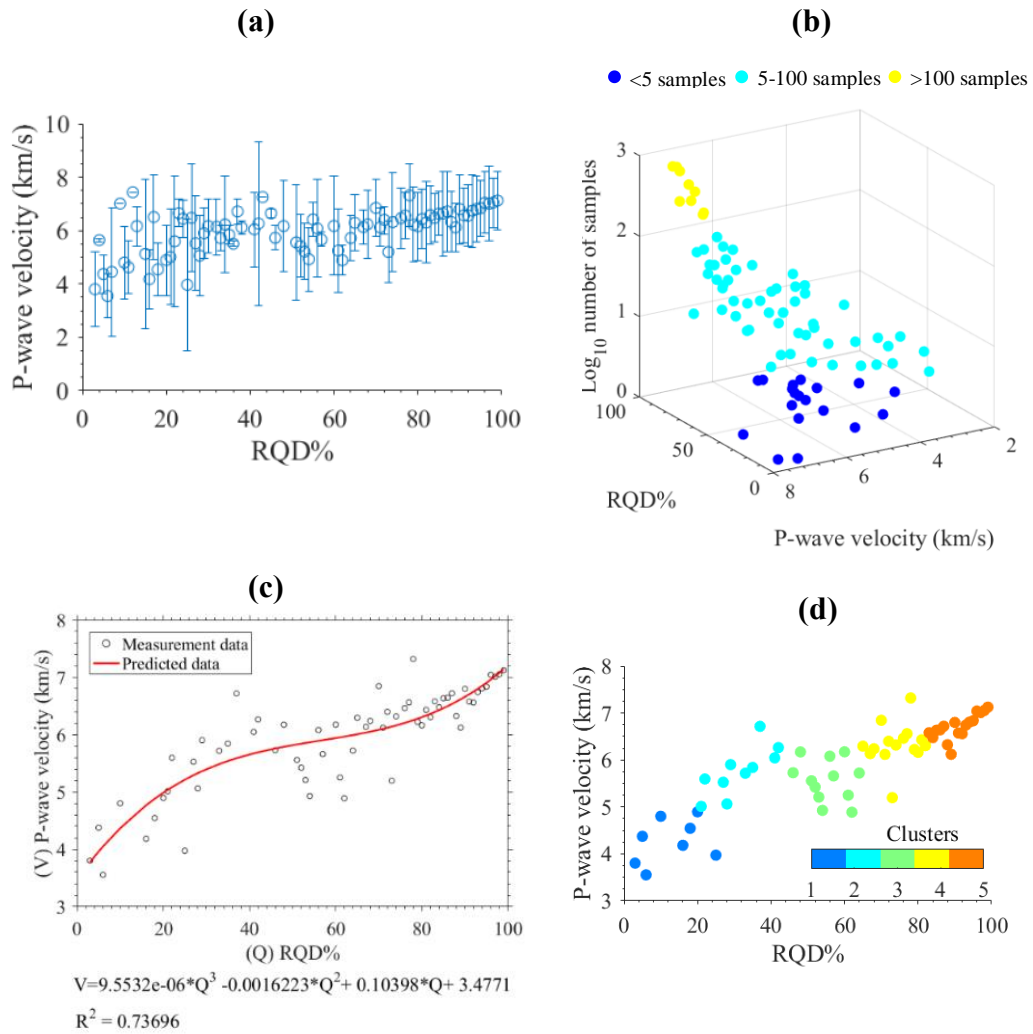


Figure 5-5: (a) Cross plot between average values (circles) and error bars of V_p at each of the values of RQD; the error bars show two times standard deviation. (b) The cross plot average of V_p , RQD with the colour-coded number of samples in each RQD bin. The blue circles with less than five samples are removed because of poor statistics. (c) The cross plot average of V_p , RQD and the least-square function. (d) The cross plot average of V_p , RQD and clustering results. Note that both the function and clustering model can be used to exchange the two parameters.

5.4. Integrating borehole information in the seismic inversion

5.4.1. Building the initial models

The initial seismic inversion AI model is built from the information acquired from all boreholes, including both real and estimated data. The borehole data is interpolated

to cells in a 3D grid of interval of 10 m. This 3D model is then converted into the time domain with an interval of 2 ms, which is the same as the seismic sample interval.

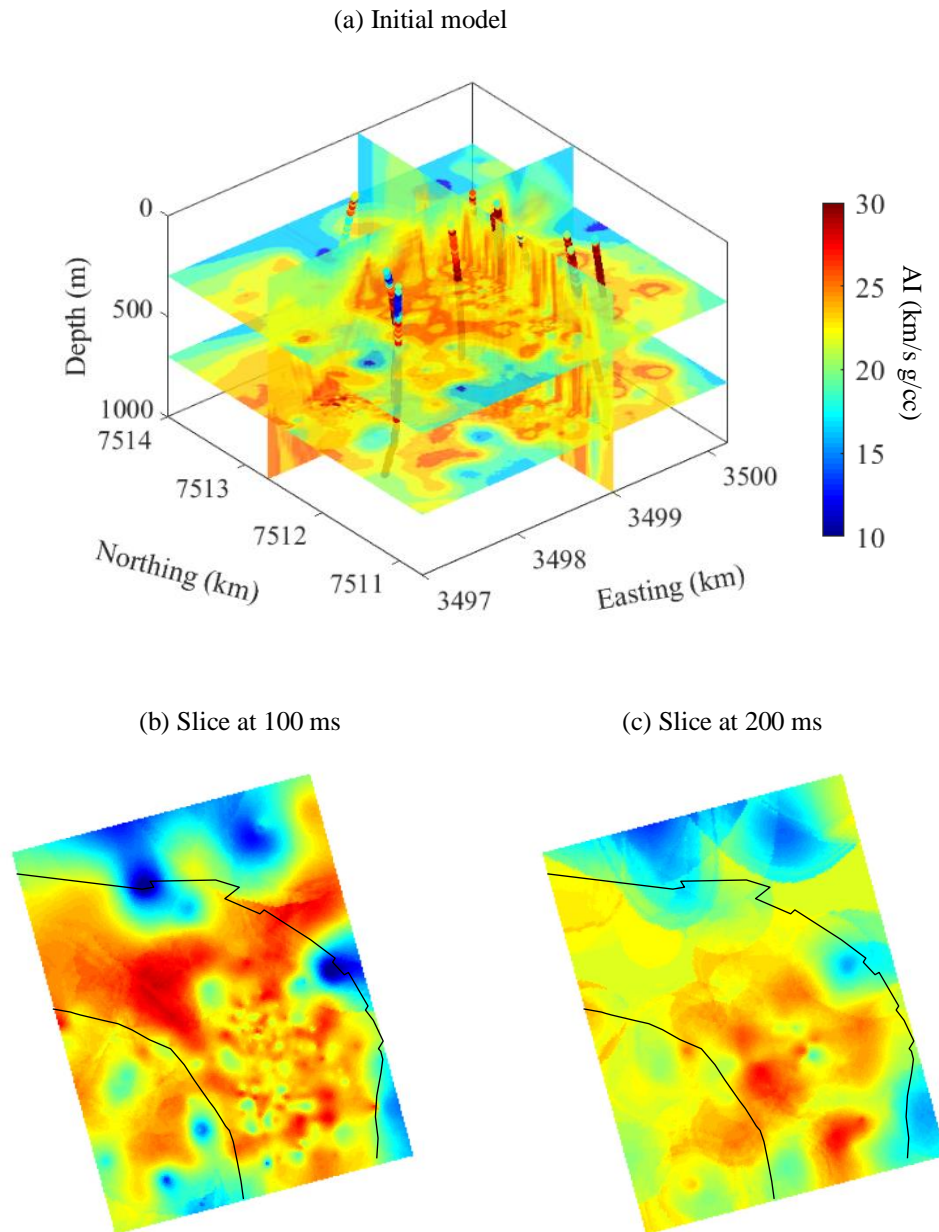


Figure 5-6: Initial model of AI built from both sonic logs and prediction from other borehole data. (a) This model in the depth domain where the sonic logs are used to create the initial model. The initial model is then converted into a time domain using a migration velocity model. (b) and (c) present the slice of the initial model in the time domain at 100 ms and 200 ms, respectively. The black lines mark boundaries between Kevitsa intrusion and country rock.

Figure 5-6 shows the initial AI model in the time domain. Notably, in some areas where deep boreholes are not available (Figure 5-1b), the interpolation process make

a smoother less certain model. For instance, in the part of the northern seismic survey area, there are two sizable low AI zones. This may not be true because there are not enough deep boreholes here from which to acquire good data. In contrast, in the vicinity of the open-pit, the model uncertainty is significantly reduced owing to highly dense information from deep boreholes. Figure 5-7 shows a good match regarding low-frequency data between the estimated model and the real data of the KV28 borehole that is used in a blind test for our process. These results demonstrate that our prior information can be used in the inversion process.

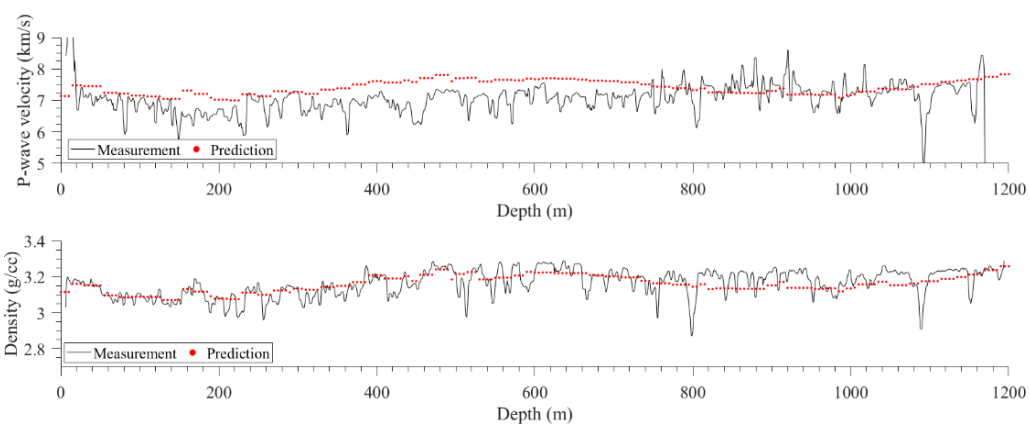


Figure 5-7: Validation of the initial AI model by comparison between predicted and measured data in the hole KV28 that is left out in the training process (Blind test data). The good match in low-frequency information between the borehole data and the initial model illustrates the quality of the initial model for the seismic inversion.

5.4.2. Integration procedure for borehole data

Our inversion algorithm initially requires knowing the number of clusters. A theory is not available to calculate the required number of cluster; however, there are some criterion to judge how well the clustering is likely to perform. The most important aspect of this is the overall “compactness and separation” of clusters; that means where the elements internal to the cluster more similar is better, and the differences between members of other clusters that are more different (or distant as measured by some norm) are better. As described in Chapter 2, the basic idea of FCM clustering is to minimise the error, so the data set is represented by the cluster centre values. Obviously, smaller cluster numbers create a larger separation between clusters, but the error is larger and the homogeneity of elements in the internal cluster is smaller. In contrast, larger cluster numbers produce smaller errors, but the differences between

clusters is also smaller. Therefore, the cluster number definition is a trade-off between the compactness of the internal cluster and separation between clusters. Notably, one important aspect in the application of FCM clustering in the context of geophysics, is that the difference between clusters should be large enough to be detected by the geophysical methods. Hence, the number of clusters is defined by whether it is large enough to produce detectable signatures for the geophysical method used. Figure 5-8 plots the clustering in a manner that indicates that the use of seven clusters is the best option.

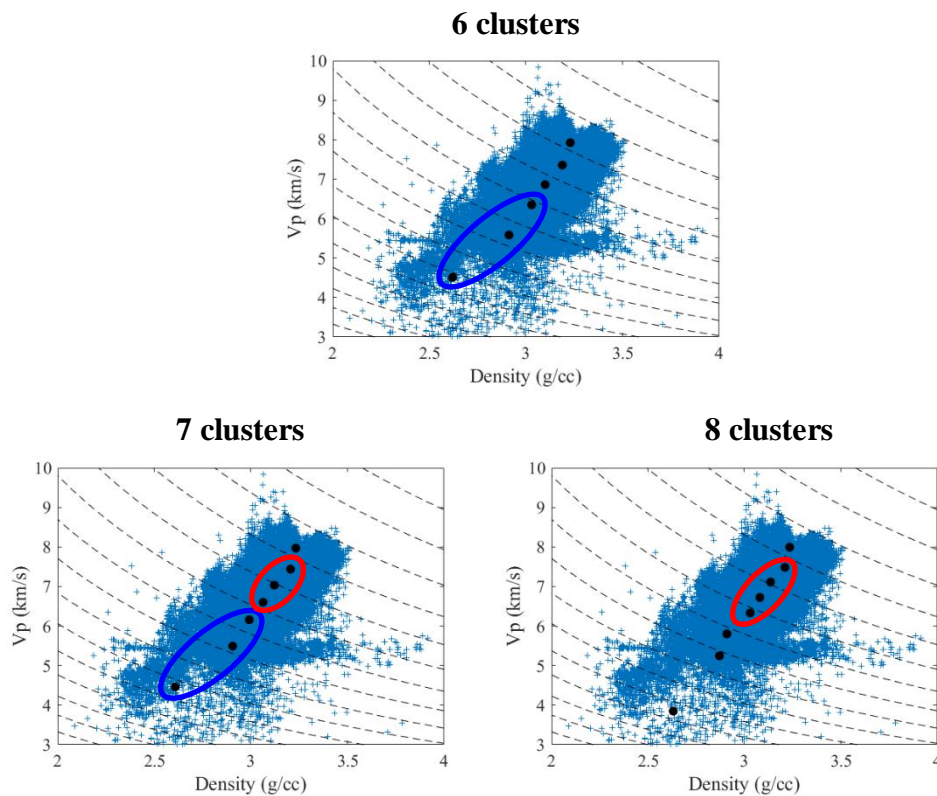


Figure 5-8: Wireline logs of P-wave velocity (V_p) versus density (blues crosses) Dashed black lines show the constant values of AI. A difference between two lines creates a 0.06 reflection coefficient that is usually enough to cause a detectable reflection at a contact between two media (Koivisto et al. 2015). Bold black dots are centre clusters. The distances between six centre clusters show the separation of the first three clusters (blue oval) are too large, and distances between eight centre clusters shows the separation of the clusters (marked by red oval) are too small. Using seven clusters is trade-off and almost agrees with the difference between the two lines from the AI.

The next issue is how to incorporate borehole information into the inversion. In this work, I use the clustering results (Figure 5-9) of borehole lithology plus assay data of Co, Cu and Ni to constrain the seismic inversion. The idea to use this assay combination to help constrain the inversion originates from the work of (Chamanifard

2013), where the author used two parameters calculated from equations (5.2) and (5.3) to discriminate the litho-geochemistry that relates to different magmatic processes in the Kevitsa ultramafic intrusion. The clustering results of the two combinations are presented in Figure 5-9.

$$Ni\# = 100 \frac{Ni}{Ni + Cu'} \quad (5.2)$$

$$Co\# = 100 \frac{Co}{Ni + Co + Cu'} \quad (5.3)$$

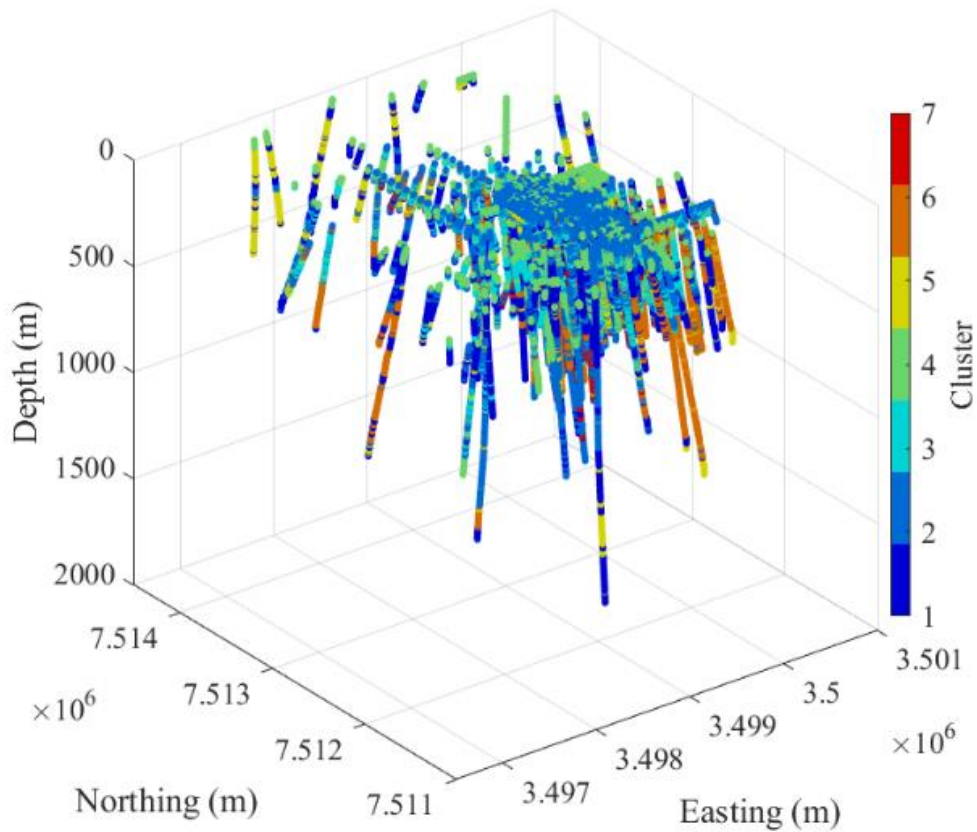


Figure 5-9: Clustering results from the data sets Co#, Ni# and lithology.

The basic idea of how to include borehole data into our inversion procedure is demonstrated in Figure 5-10: assume that with some level of certainty the properties of each seismic sample should be similar to near by borehole samples. In this work, we weigh this certainty according to the following formula:

$$Certainty = \exp\left(-\frac{d}{\alpha}\right), \quad (5.4)$$

where d is the distance from a borehole to the seismic samples and α is a scaling factor that controls the radius of influence of borehole data to the vicinity. Figure 5-11 displays the “certainty” of projected borehole data on seismic samples.

Certainty properties and collaborative clustering can integrate directly with borehole data in the inversion. In this case, the borehole data cluster information plays the same role as spatial information, as described in Chapter 4. The certainty of including borehole data in the seismic inversion process is a form of weighting that can vary with the distances from the boreholes and the seismic sample position (Figure 5-11).

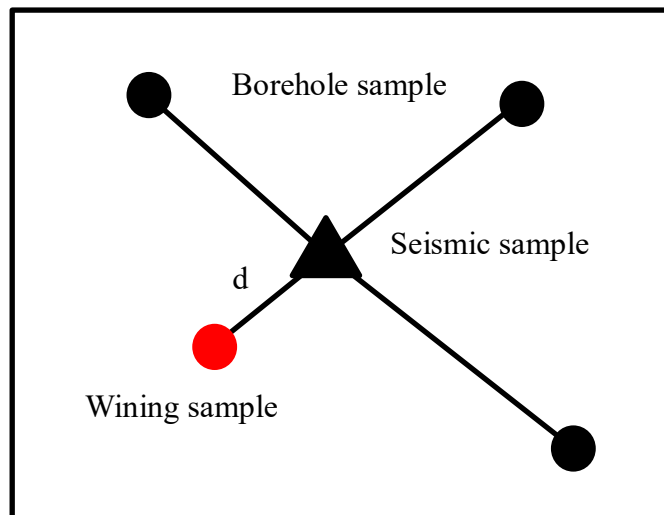


Figure 5-10: Schematic shows the concept of including borehole information in the seismic inversion process. We assume that the seismic sample information is similar to that from the closest borehole sample (namely, the wining sample). The certainty of similarity between the seismic sample and the borehole sample is calculated by the distance, d , between them (Equation (5.4)).

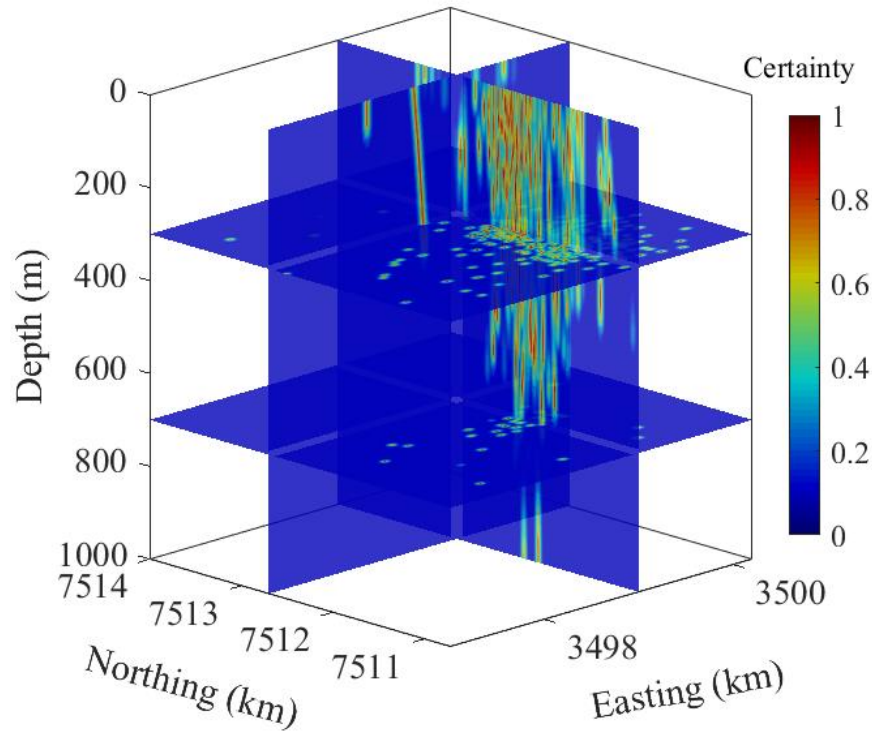


Figure 5-11: The certainty of including borehole data in the seismic inversion process is calculated using equation (5.4)

5.4.3. Inversion of seismic with constraints from borehole information

The seismic inversion routine in this chapter is same as the inversion process described in previous chapters (3 and 4). The difference here is in the manner of how the prior information is included in the inversion. The inversion results without, and with borehole assay data constraints are named Inv#1 (without elemental cluster constraints) and Inv#2 (with borehole assay constraints) respectively. Both of the inversions use the same initial model, which is created from sonic log data and the prediction/estimation processes described in the section of V_p prediction (from missing information). In the later inversion processes (iterations), the lithology and assay data clustering results (Figure 5-9) are included to constrain the inversion with the “level of certainty” (Figure 5-11) weighting factor (i.e. guide solutions towards matching nearby borehole data over ones that don’t). This approach is similar to the inclusion of boundary information in the inversion process, as described in Chapter 4. This certainty-weighting is added to the clustering process as weighting values. The mechanisms of clustering and including this information in the inversion process are presented in Chapters 2 and 3.

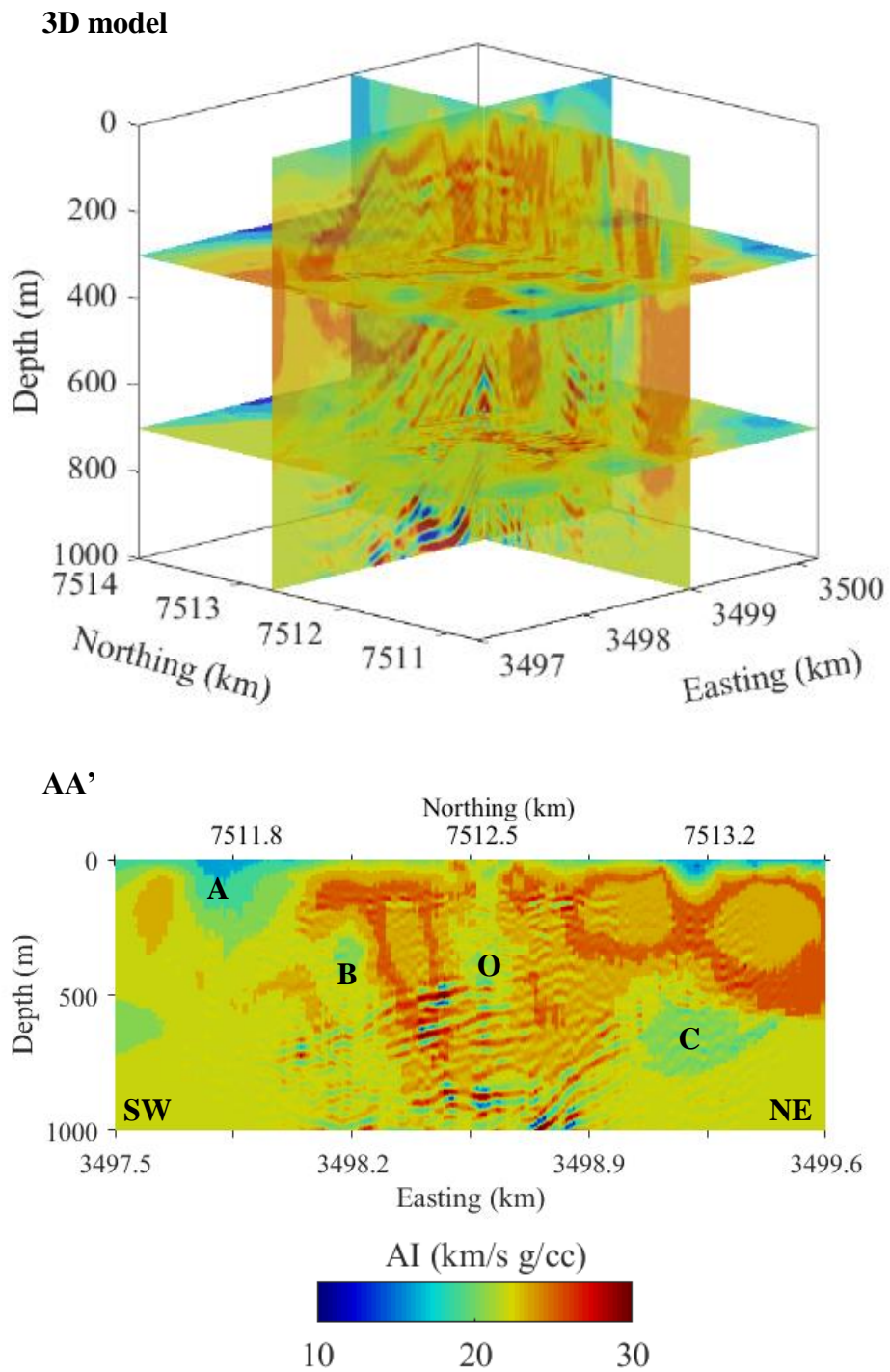


Figure 5-12: Inversion results without the clustering constraints from the assay data. The upper figure shows the 3D AI model and the lower is AI along section AA' (Figure 5-1b). A, B, C and O mark the low AI zones.

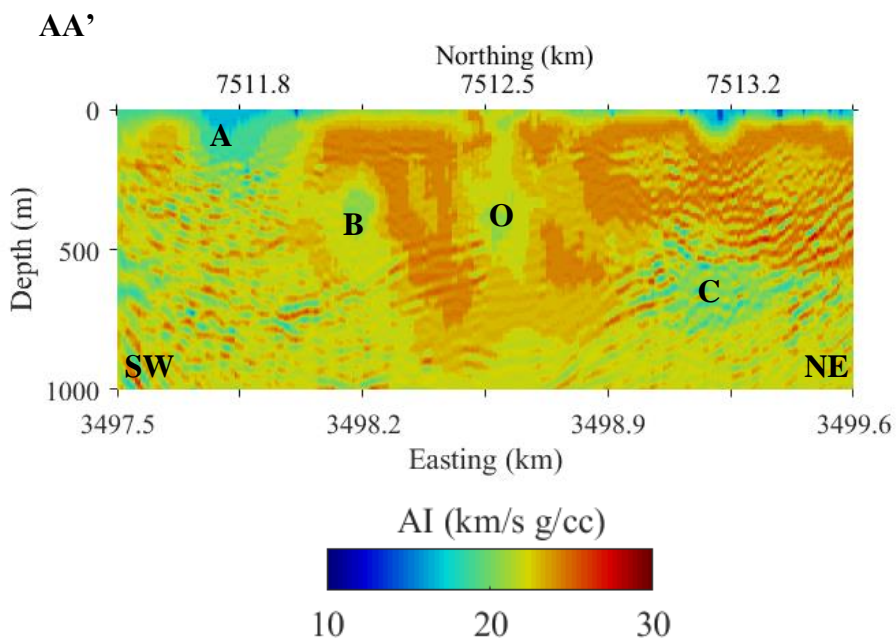
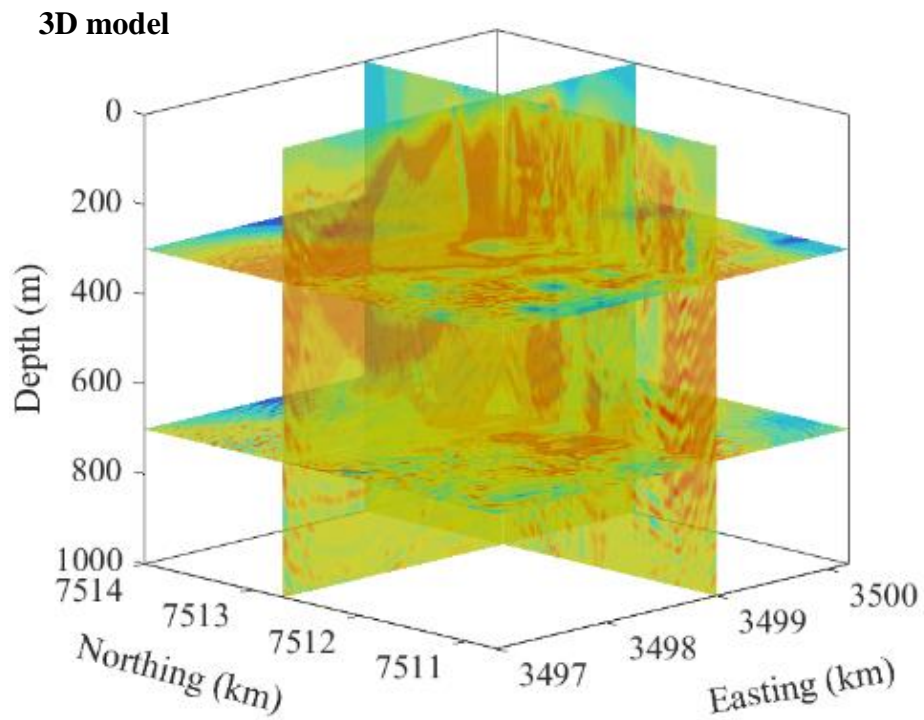


Figure 5-13: Inversion results with cluster constraints from the borehole data. The upper figure shows the 3D AI model and the lower figure is AI along section AA' (Figure 5-1b). A, B, C and O mark the low AI zones.

Figure 5-12 and Figure 5-13 show the inversion results of Inv#1 and Inv#2, respectively. The two models show the same general features, such as the low AI values zones A, B, C and O, because they tend to still keep the main features of the initial model. This could be that the 3D seismic has so little low frequency information that it does not try to force to a different solution than the initial, or that the initial was close and that the seismic data does not need to alter it much. However, there are many subtle differences from the initial model, so the seismic data has steered the results a little, and indicates it is not completely “band-limited”. Also, changes to starting model that are not too great still end up with similar final models, again suggesting that the seismic data still steers the solution and not just the constraints. This is confirmed by comparing the inverted models with the borehole data in the KV28 borehole (Figure 5-14). It can be seen that the general trend of the initial model still exists in the inverted model, but the inverted result of Inv#2 illustrates a better fit to the borehole data than that of Inv#1. Particularly, at depths of 500 to 700 m, the results of Inv#1 shows a high bias compared to the borehole data. This can also be seen in the strong variation in the 3D model and the section AA’ (Figure 5-12). This may be due to overfitting to seismic data where we have a very strong reflection signal caused by previous processing data and imperfect wavelet extraction in the inversion process. Model Inv#2, obtained by including spatial information from the boreholes through projection of the clustering results, has less overfit effects (residual seismic wavelet still in the volume) and appears to produce similar results with less artefacts.

Figure 5-15 illustrates how other aspects can assist the inversion process in building a better geologically model. During the inversion process, if only the acoustic impedance alone is used in the clustering process, the output follows a statistical constraint (i.e. see four clusters get data values that will tend to be close to four parameter values) because the AI varies considerably over a short distance (either due to complex changes in the geology, or measurement noise). This process ignores the spatial (clustering) information that creates the observable geophysical signatures. Therefore, including both the statistical distributions of the physical properties and their spatial distribution properties into this process should build more reliable models. One may argue that we should directly include lithology in the seismic inversion. Using the FCM approach it is possible, just as with boundaries; however, the lithology is subjectively defined and in this data set there are too many categories

with small variations in unmeasurable aspects with wireline and assay data (see Appendix E), which adds to the complexity of the calculation. Therefore, I consider lithology as one additional parameter-feature and include it with the assay data to assist in defining the clusters that are simpler and reduce the subjectiveness of lithological information.

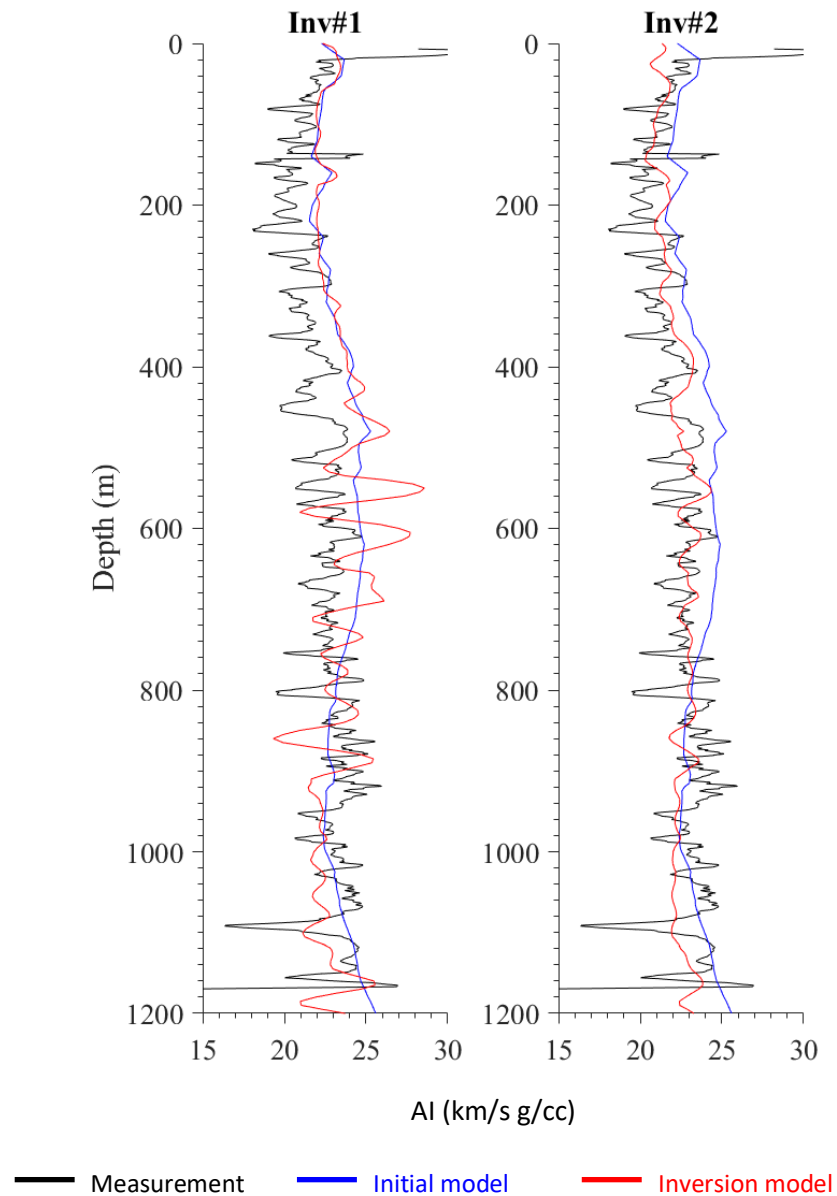


Figure 5-14: Comparison of inversion models and borehole data in the KV28 borehole. Generally, the inversion results match with the borehole data trend. The inclusion of clustering information using the borehole data in Inv#2 results in a better quality inversion than the ones processed without the borehole constraints.

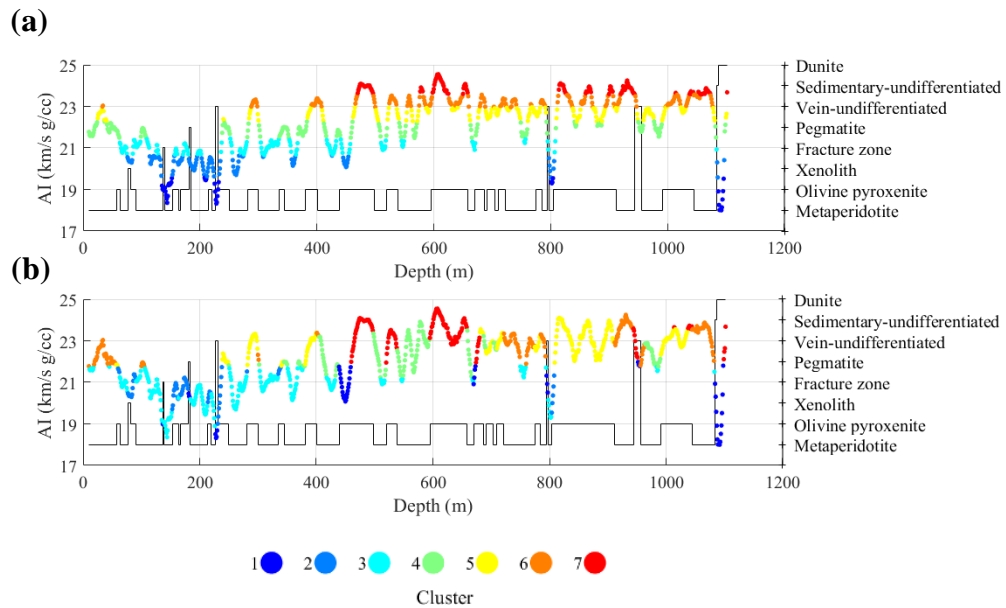


Figure 5-15: (a) Comparison between clustering results using only acoustic impedance and (b) acoustic impedance plus results of clustering from lithology and $Co\#$, $Ni\#$ in the KV28 borehole; the black lines show the variation of different lithologies. Clustering with only AI is inconsistent with the lithology; in contrast, the spatial information resulting from fuzzy clustering of the borehole data can help to build the geological model. For instance, cluster 3 shows low AI and a lithology of Metaperidotite. The low AI values relate to Olivine pyroxenite, which is usually seen in cluster 2. The rocks with high AI values are put in cluster 6 or 7 if they relate to Olivine pyroxenite and in cluster 4 if they are Metaperidotite.

5.5. Transfer the 3D seismic model into other features

Another step after inversion is to convert the geophysical (quantitative) models into other formats for use by geologists and engineering disciplines. Note that in addition to an AI model (or other petrophysical parameter) a cluster model is produced as an outcome of the FCM inversion process. This by-product is a natural product for geological interpretation as it directly incorporates many prior data and the geophysical data to make a unified earth model with many parameters. The two main objectives of converting the geophysical data are: understanding the geology and making the data easier to understand; and to produce volumetric data for geomechanics for future mining production and exploration in this area. Therefore, the inversion results are converted in to a pseudo-lithological model (from the Cluster membership model create during FCM inversion) for geological interpretation, and a RQD model (created from establishing a relationship between V_p and RQD, again via cluster and inversion model results from the FCM inversion process) for geotechnical purposes.

Figure 5-16 compares the pseudo-lithology section derived from the FCM inversion and a migrated seismic section to a interpreted geological section based on the results of 2D and 3D seismic interpretation by Koivisto et al. (2015) along south-west to north-east section (AA'). Clearly, the raw seismic data is more challenging to interpret than the pseudo-lithology section, since the reflection seismic section only contains the boundaries. The interpretation by Koivisto et al. (2015) and others is performed by picking the boundaries first then selecting the rock unit by referring to nearby borehole data. This not too dissimilar to what the FCM inversion process described in this chapter does when the seismic data does not have enough low frequency data to be able to confidently select one model over another. They also state that the continuity of the boundaries is poor and the high velocities with resultant variation in depth-location result in interpretation issues. The boundaries can also be improperly defined because of ambiguity. In contrast, the inverted images tend to produce geological images that should be significantly easier to interpret. For instance, the boundary between the dunite and Kevitsa intrusion (Figure 5-16a) is very ambiguously defined according to the seismic data only (Figure 5-16b), as in the work of Koivisto et al. (2015). This boundary may be redefined based on results (Figure 5-16c) more confidently. The features on the right side of the section need to be interpreted with care due to the artefacts/distortions that may be created by the interpolation of the borehole data when building the initial model that are not corrected by inversion due to lack of data in these regions.

The conversion of RQD from the inverted models is presented in Figure 5-17 and Figure 5-18. The inverted AI model is smoothed by a spatial low-pass filter to avoid extreme values (too high or too low) because the relationship established is with correlation between a running average of Vp and RQD (see in Figure 5-5) over 10 or more metres. Resolving anything less than 10 metres is well beyond the seismic data resolution and meaningless in the context of overall mine pit design. The smoothed AI model is then converted into a Vp model, using the relationship between AI and Vp from the sonic logs. The Vp model is then converted into a RQD model. There are good matches in tests between the converted RQD model, and the core measurement on 100 holes (Figure 5-17 demonstrates this). This shows that our approach is not too bad and the volumetric data adds significantly to information from boreholes.

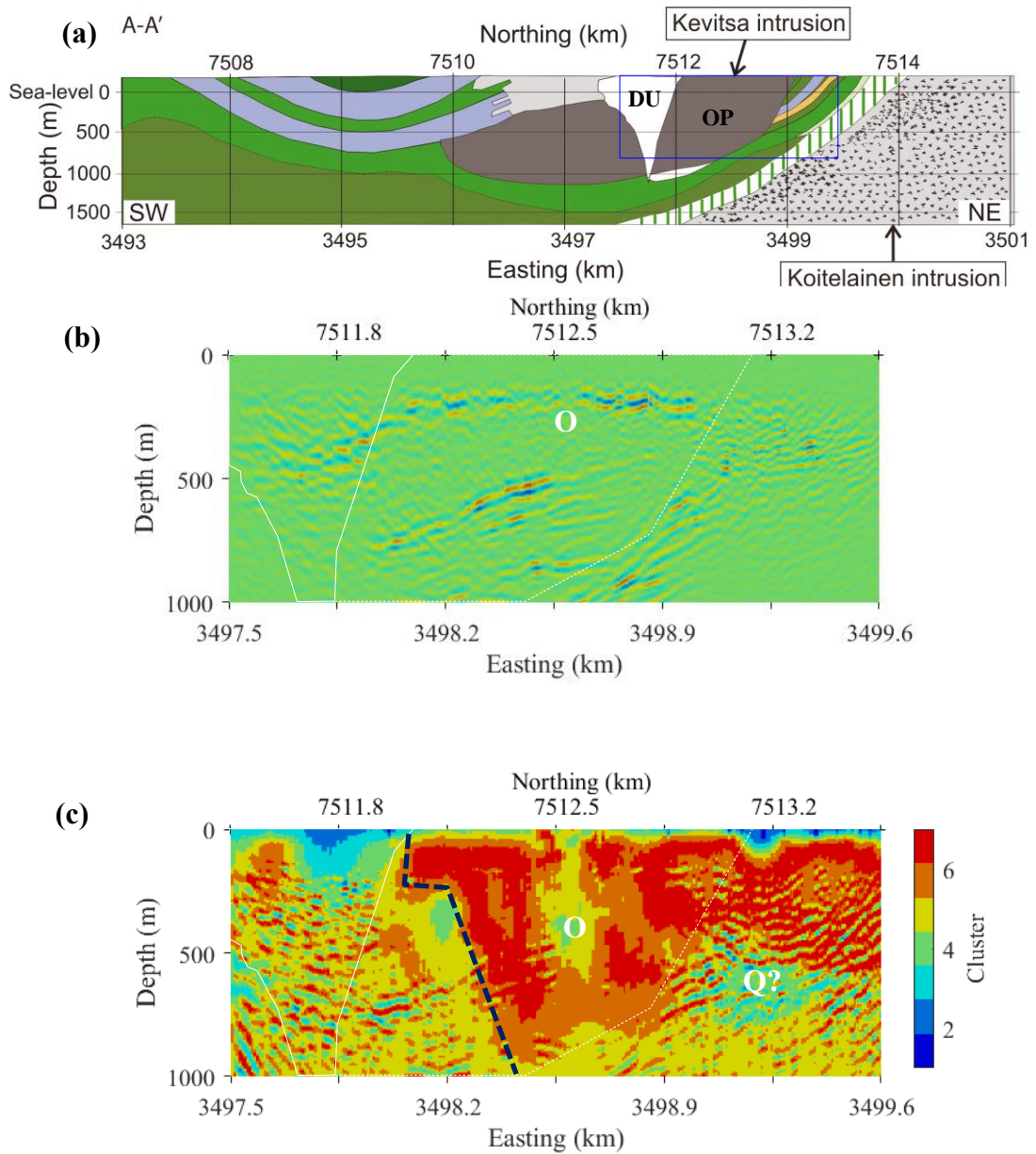


Figure 5-16: (a) Geological section along the profile AA' (Figure 5-1b) taken from Koivisto et al. (2015). The blue rectangle marks the area of our sections. In this interpretation, we concentrate on two areas marked by DU (Dunite) and OP (Olivine pyroxenite). (b) Migrated seismic data along the section AA'. (c) Clustering (pseudolithology) model from the inverted model Inv#2. The dashed and solid white lines show the boundaries of DU and OP zones respectively. The dashed black line is probably a new boundary between DU and OP zones. O marks the ore zone. The Q? zone can relate to Dunite, but this interpretation is highly uncertain because of the lack of deep borehole data from this area.

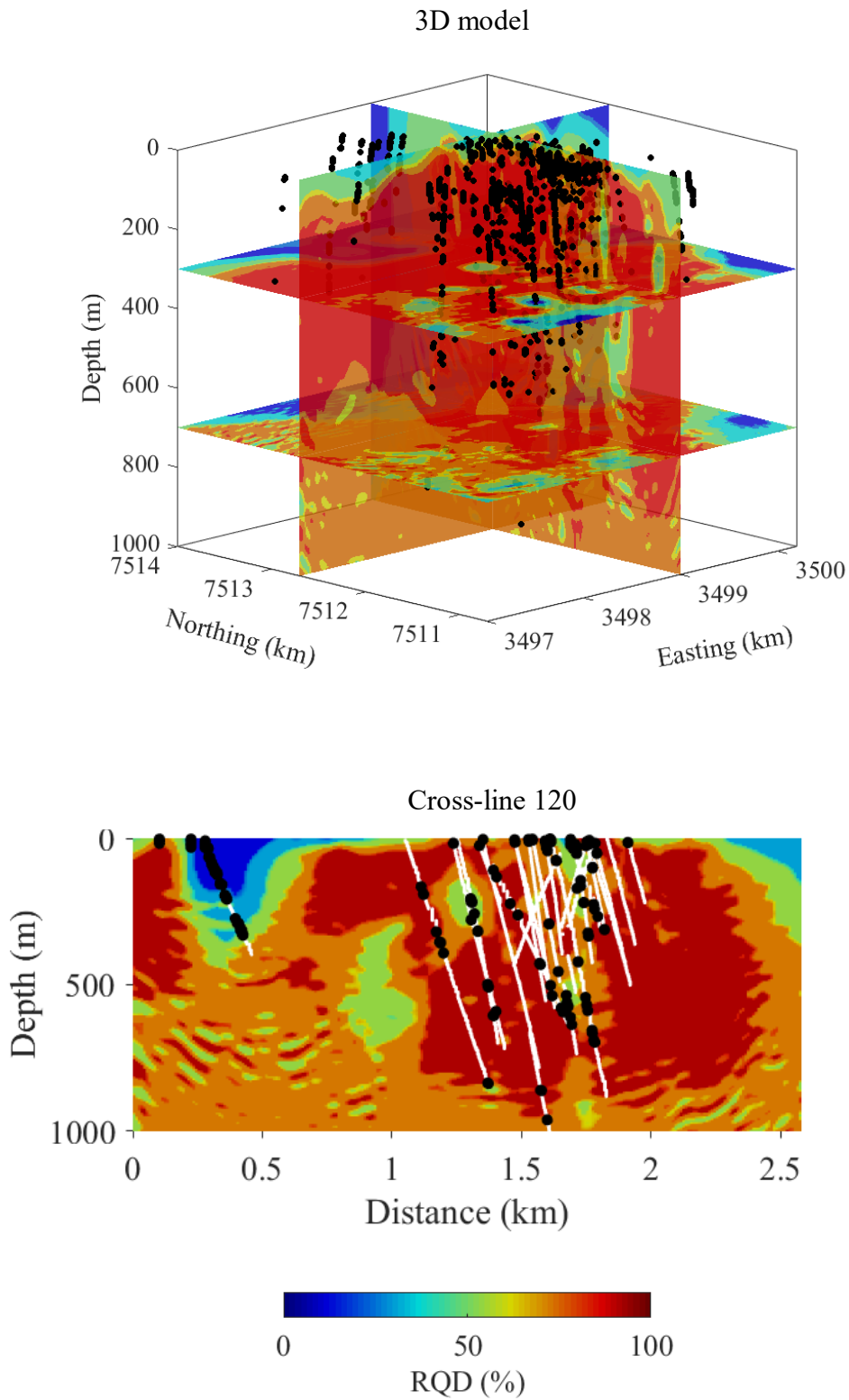


Figure 5-17: Converted RQD model from the Inv#2 AI model. The white lines show trajectory of the projected boreholes in the vicinity of 100 m of the section, and the bold black dots show where the RQD is less than 50% of the core measurements.

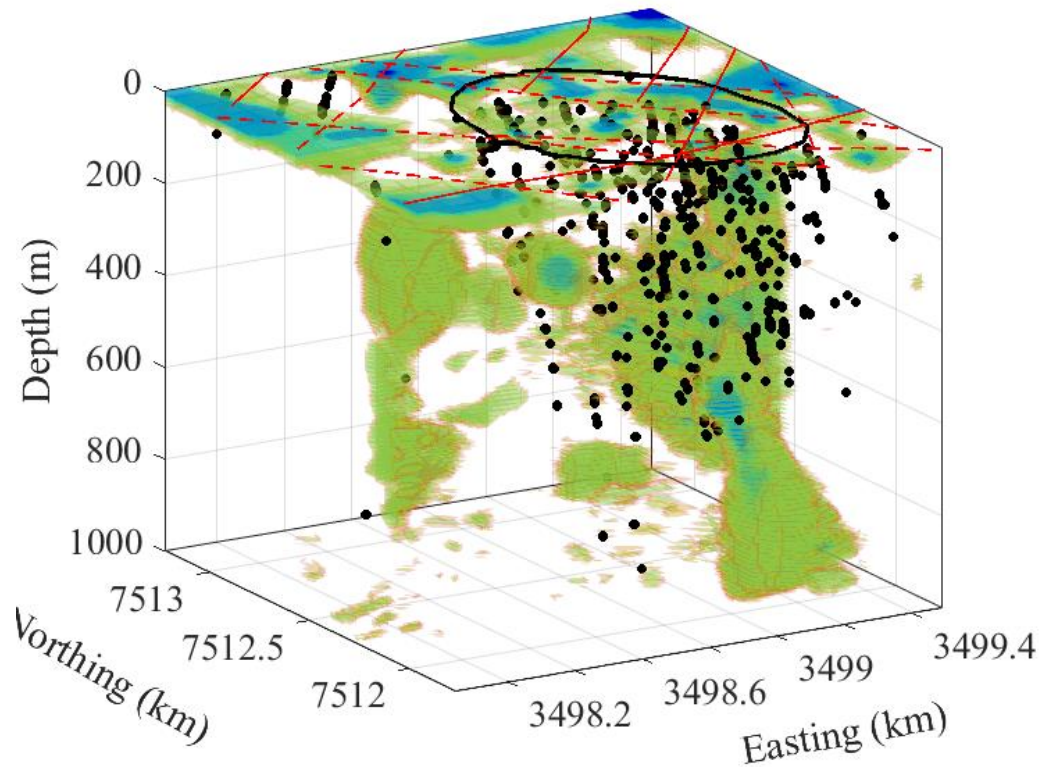


Figure 5-18: The RQD less than 50% of the borehole is calculated from the Inv#2 inversion in vicinity of the open-pit (black oval line). The red lines present projected faults on the surface map (Figure 5-1a). The black dots show the RQD at less than 50% of the core measurements.

5.6. Conclusion

In this chapter, fuzzy c-means techniques were used to estimate missing values and to perform robust extrapolation of parameters between the boreholes. These resulting physical model allowed building of a good initial seismic acoustic impedance model, and to also include the prior information of the borehole data with both parameter statistical and spatial distribution information into the constraints for the seismic inversion process. This FCM process integrated all the available downhole data into the seismic inversion routine, and not just the parameter of interest. The FCM relationship between the data parameters-features were used to convert the inverted parameter model into other models. A pseudo-lithology model created from the FCM cluster map can assist with geological interpretation, and a credible RQD model could provide useful information for designing a mine site. Moreover, the P-wave velocity model could be used to significantly reduce the time to create velocity models in pre-stack depth migration in reprocessing the seismic data with the aim of enhancing the

quality of the data. These inversion, cluster guided interpolation, and relationship strategies should be applicable to other data sets; however, data-rich data sets, like Kevitsa, are needed to properly extract value.

Chapter 6: CONCLUSIONS

In this thesis, I have developed an inversion mechanism that can deal with multiple datasets (co-operative inversion) based on improving existing inversion algorithms that work on a single dataset. The inversion approach is built the adaption of fuzzy logic to generate models more aligned with a geological perspective. As the subsurface is notionally divided into rock units with physical properties sharply changing at boundaries between the units and generally relatively homogeneity (or smoothly varying) inside the units. Hence, the inclusion of clustering criteria as extra constraint assist the inversion build a model that tends to resemble the expected geological model. In addition, the fuzzy clustering based inversion introduces ‘a soft constraint’ in the inversion, which tolerates imperfection and unclear situations better. The algorithms were design for and tested with problems on the inversion of post-stack seismic reflection and magnetotelluric (MT) data. Also, the algorithms are designed for mineral exploration environments and the ideas and concepts tested on data from these environments.

The synthetic examples, presented in Chapter 3, show that inversion with clustering constraints offers superior performances compared to the inversion with just smoothness constraints. The addition of prior information and other geophysical data in the inversion via fuzzy clustering significantly enhances the inversion results.

Data acquired in the Carlin gold districts, Nevada, the USA, presented in Chapter 4, in early stage of an exploration project was trialled succesfully with the FCM inversion method. This data set consisted of surface geophysical data, reflection seismic and MT, and very few drill holes (two holes) with incomplete data acquisition. The results from co-operative inversion worked well and demonstrated the benefit of using the membership dataset for interpretation (the pseudo lithology). These results show that the FCM method with MT and seismic reflection geophysical data might assist further exploration and drilling campaigns in the district. For instance, the good correlation between weak zones mapped by the acoustic impedance inversion with potential mineralization zones (identified with pathfinder elements and Au anomalism).

In the second trial of using FCM inversion, Chapter 5, the dataset acquired in producing mine site of Kevitsa Ni-Cu-PGE ore, North Finland again showed the benefits of using the FCM method with difficult seismic reflection data and extensive prior information. This dataset includes reflection seismic data and numerous drill holes. The challenge was that most of the drillhole data would not be used with conventional approaches as only 0.7% of the many holes had sonic data; normal a prerequisite for acoustic impedance inversion. My approach showed that we can integrate diverse borehole data types to assist the inversion of reflection seismic data. The FCM inversion results provide a way to integrate disparate data to help geological interpretation and future exploration. Additionally, a FCM methodology to extract geophysical information for geotechnical purposes was demonstrated.

6.1. Contributions of my thesis

The use of fuzzy c-means (FCM) clustering in the inversion process

In my work, this technique plays four-fold role and has been incredibly versatile. First, it is a tool to analyze prior information. FCM clustering is applied for analysing borehole data whose results are included to constrain the separate inversion and the co-operative inversion. Particularly, I utilised these techniques to fill missing data or link data features of borehole data that is presented in Chapter 5. Second, it is an extra constraint term and a platform to implicitly include prior information into the inversion. The basic theories and synthetic application are provided and demonstrated in Chapter 3 and then applied to two different datasets in Chapter 4 and Chapter 5. Third, it is a coupling factor in a co-operative inversion process. Fourth, it is a tool to convert the inverted models into pseudo-lithological maps that illustrate the clustering results of the inversion models. These maps assist interpretation process and should be easier to interpret than using physical models.

The idea of using FMC clustering to define lithology is first tested with the borehole data presented in Chapter 2. This example demonstrates that FCM clustering is able to map clusters to lithology from borehole data. Thus, the link between the clusters and geological features is demonstrated. The final results of the inversion in the both real datasets are presented in format of pseudo-lithological maps based upon cluster membership. These maps allow anomalous zones to be significantly easier to pick,

and rather than relying on picking differences and trends in the physical model and raw data with regard interpreting to aid geological interpretation. In particular, the pseudo-lithology obtained by the seismic inversion in Chapter 5 considerably reduced the ambiguity in terms of geological interpretation.

Improving constraint inversion of single dataset

In this study, I have improved the inversion process by exploiting FCM clustering to enable to combine both petrophysical and spatial information from external sources into the inversion. Specifically, I have adapted FCM techniques into the inversion of MT and seismic data. The synthetic examples are illustrated in Chapter 3. The applications to real data are shown in Chapter 4 and 5.

The synthetic examples demonstrate that both seismic and MT inversion benefit from prior petrophysical and spatial information. Specially, including shallow boundary information in the MT inversion we obtain better model recovery at greater depths. Boundary information also assists seismic model-based inversion to recover better the true models and reduce the influences of the initial models. In addition, the fuzzy logic can introduce ‘soft constraints’ in the inversion showing that it tolerates inaccurate prior information with such constraints. The MT inversion with inaccurate boundary information still produced a better result compared to the result with no boundary information constraints.

In Chapter 4, the inclusion of petrophysical information from borehole and structural information from seismic data in MT inversion built a more reliable model with higher resolution rather than MT data only. Seismic inversion enabled detection of anomalous zones in basement that were shown to be the type of zone considered prospective. Two previous studies with the same data were unable to do this. The FCM inversion results are comparable or better than results of the benchmark commercial software, Hampson Russell. Chapter 5 provides an example of how the seismic inversion benefits from borehole data with both petrophysical and structural constraints. Borehole information can build an initial model that is vital for the seismic model-based inversion and further supplies petrophysical constraints during the inversion. Moreover, the important finding of my work is to incorporate spatial information from borehole data to enhance the inversion of surface geophysical data,

and works well even when that borehole information has no measurements of the physical property that is being inverted.

Mechanisms of co-operative inversion

I have presented two schemes of co-operative inversion, sequential and parallel inversion using FCM as coupling means. The main advantage of my schemes are to run co-operative inversion with, and without, conversion between the models. In a conventional scheme, the inversion result of one method is converted in an initial model of another method using an empirical function, which often does not work well without significant complications. The use of FCM clustering appears to deal better with poor correlation between various physical properties, such as in Chapter 4. In particular, my scheme can work without any prior information about the relationships between the petrophysical models because FCM clustering is unsupervised and it automatically finds the relationships between models during the inversion process. Representing these relationships with a cluster with an average value has a risk that is not representative; however, this problem did seem to influence my results, and if it did it was the lessor of many issues.

The synthetic example is demonstrated in the Chapter 3, shows my FCM scheme out performs the exchange scheme. The real test comparison is demonstrated in Chapter 4, where the FCM method performed much better than Takougang et al. (2015). The results of the two schemes show that the inversion of multiple datasets builds a better model than the model from a single dataset, even when one is very dominant in one aspect. The lack of low-frequency information in the seismic data is compensated by the assistance from the model from MT inversion. In turn, the seismic data can provide boundaries to put structure constraints into the MT inversion and the seismic inversion model can enhance significantly the resolution of the MT model via the FCM coupling. The results from both real data sets nicely match borehole information when tested.

6.2. Future work

Although my work shows significant improvement in the application of fuzzy c-means (FCM) clustering based inversion, there are some issues that would benefit from further research.

Firstly, inversion involves many factors that need to be initialised. The question is how we can quantify the impact of these parameters on the inversion results? Of course, this question is somewhat ill-posed in itself as it is likely data dependent. The impact of initial models with the seismic data in Chapter 4 illustrates this issue well. Can we automatically define or identify these factors during the inversion? For instance, updating the weighting values of the structure term and FCM term in the inversion objective function in some way. In this thesis, I defined these parameters based on empirical-numerical experiments on data subsets. However, it would be better if these weighting scaling factors automatically adapted to some goodness criteria.

Second issue is uncertainty analysis. In this thesis, I have focussed on reducing the non-uniqueness, and just making the whole inversion process work. The next step should be to quantify uncertainty. There are three main factors that contribute to model appraisal: (1) data noise, (2) uncertainty of prior information, and (3) the uncertainty of constraint terms, for instance, the uncertainty of fuzzy c-means clustering in my approach may come from cluster number, fuzziness index etc...

Thirdly, the use of fuzzy c-means clustering in the inversion. FCM seems to work pretty well, but the cluster-geological unit assumption will fail in some environments. Therefore, the use of other clustering-classification methods need further investigation and I believe that it depends on datasets and geological environment. For example, Figure 6-1 shows the inversion of MT data from synthetic data. Although, the FCM clustering constraint improves the inversion result versus using a smoothness constraints it is not able to recover the basement where the resistivity parameter is distributed in a diffusive variety. This situation occurs in some sedimentary environments and not uncommonly. Second, we need to deal with a more general problem that both sharp and smooth (or diffusive) boundaries may co-exist rather than only sharp or smooth boundary only (example in Figure 6-1). Thus, how can we incorporate both boundary aspect for the inversion?

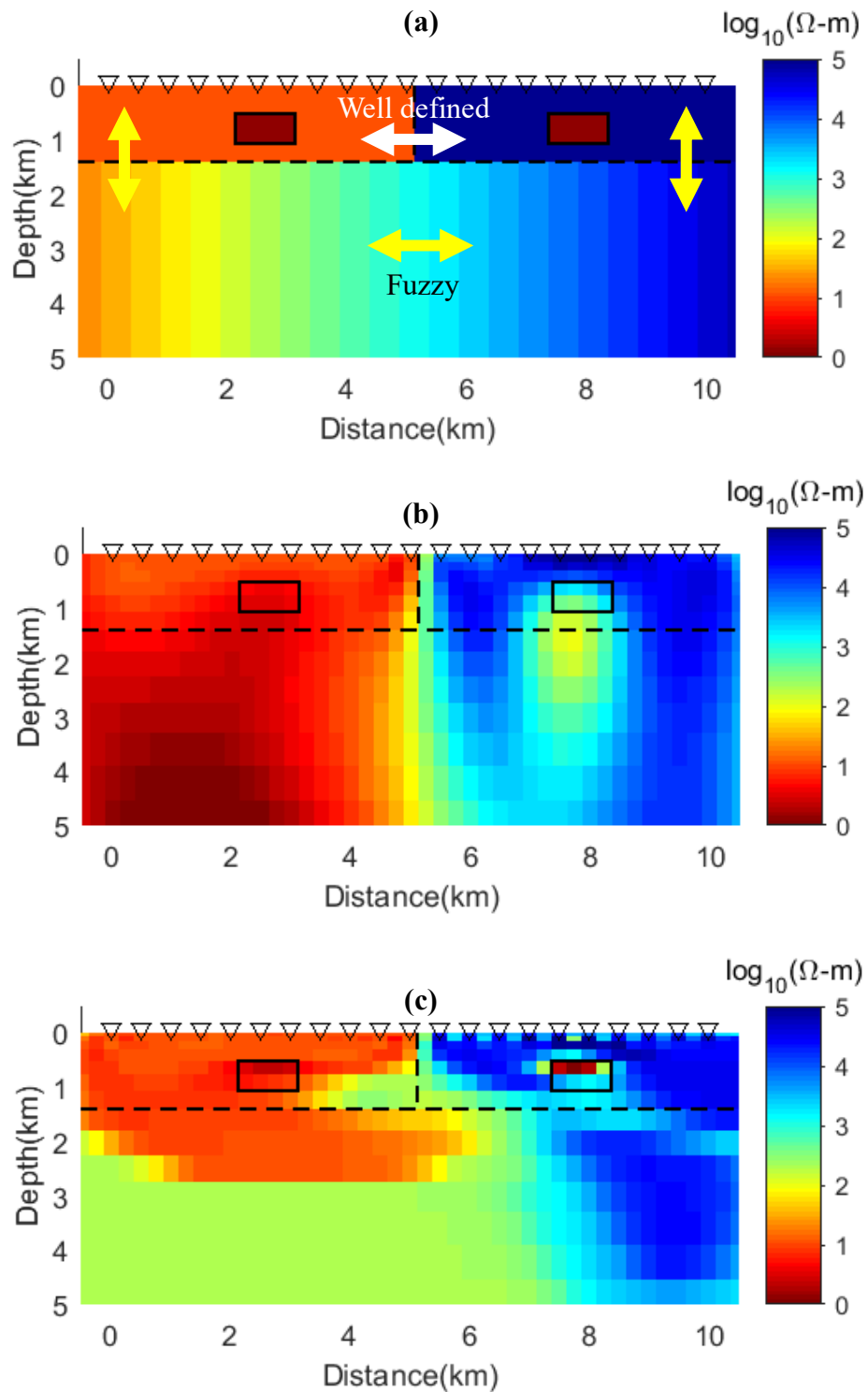


Figure 6-1: (a) A model of resistivity comprised of both well-defined and fuzzy boundary. (b) Result of MT inversion using smoothness constraint only. (c) Result of MT inversion using smoothness and FCM constraints. Even FCM clustering is added to help MT inversion, it is likely unable to recover the fuzzy boundaries.

REFERENCES

- Ahmadi, M. A., S. Zendehboudi, A. Lohi, A. Elkamel, and I. Chatzis. 2013, Reservoir permeability prediction by neural networks combined with hybrid genetic algorithm and particle swarm optimization. *Geophysical Prospecting*, **61**, no. 3, 582-598. doi: 10.1111/j.1365-2478.2012.01080.x.
- Aminzadeh, F. 2004, Soft computing for qualitative and quantitative seismic object and reservoir property prediction. Part 3: Evolutionary computing and other aspects of soft. *First Break*, **22**, no. 6.
- Aminzadeh, F., and P. De Groot. 2004, Soft computing for qualitative and quantitative seismic object and reservoir property prediction. Part 1: Neural network applications. *First Break*, **22**, no. 3.
- Aminzadeh, F., and D. Wilkinson. 2004, Soft computing for qualitative and quantitative seismic object and reservoir property prediction. Part 2: Fuzzy logic applications. *First Break*, **22**, no. 4.
- Asoodeh, M., and P. Bagheripour. 2012, Prediction of Compressional, Shear, and Stoneley Wave Velocities from Conventional Well Log Data Using a Committee Machine with Intelligent Systems. *Rock Mechanics and Rock Engineering*, **45**, no. 1, 45-63. doi: 10.1007/s00603-011-0181-2.
- Bagheripour, P., A. Gholami, M. Asoodeh, and M. Vaezzadeh-Asadi. 2015, Support vector regression based determination of shear wave velocity. *Journal of Petroleum Science and Engineering*, **125**, 95-99. doi: 10.1016/j.petrol.2014.11.025.
- Bedrosian, P., N. Maercklin, U. Weckmann, Y. Bartov, T. Ryberg, and O. Ritter. 2007, Lithology-derived structure classification from the joint interpretation of magnetotelluric and seismic models. *Geophysical Journal International*, **170**, no. 2, 737-748.
- Behn, M. D., and P. B. Kelemen. 2003, Relationship between seismic P-wave velocity and the composition of anhydrous igneous and meta-igneous rocks. *Geochemistry, Geophysics, Geosystems*, **4**, no. 5. doi: 10.1029/2002GC000393.
- Berget, I., B. Mevik, H. Vebø, and T. Næs. 2005, A strategy for finding relevant clusters; with an application to microarray data. *Journal of Chemometrics*, **19**, no. 9, 482-491. doi: 10.1002/cem.954.
- Bergmann, P., M. Ivandic, B. Norden, C. Rücker, D. Kiessling, S. Lüth, C. Schmidt-Hattenberger, and C. Juhlin. 2014, Combination of seismic reflection and constrained resistivity inversion with an application to 4D imaging of the CO₂ storage site, Ketzin, Germany. *Geophysics*, **79**, no. 2, B37-B50. doi: doi:10.1190/geo2013-0131.1.
- Bezdek, J. C. 1981, *Pattern Recognition with Fuzzy Objective Function Algorithms*: Kluwer Academic Publishers.
- Bezdek, J. C., R. Ehrlich, and W. Full. 1984a, FCM: The fuzzy c-means clustering algorithm. *Computers & Geosciences*, **10**, no. 2-3, 191-203. doi: doi:10.1016/0098-3004(84)90020-7.
- Bezdek, J. C., R. Ehrlich, and W. Full. 1984b, FCM: The fuzzy c-means clustering algorithm. *Computers & Geosciences*, **10**, no. 2-3, 191-203. doi: 10.1016/0098-3004(84)90020-7.
- Bosch, M., C. Carvajal, J. Rodrigues, A. Torres, M. Aldana, and J. Sierra. 2009, Petrophysical seismic inversion conditioned to well-log data: Methods and application to a gas reservoir. *Geophysics*, **74**, no. 2, O1-O15. doi: doi:10.1190/1.3043796.
- Bosch, M., and J. McLaughy. 2001, Joint inversion of gravity and magnetic data under lithologic constraints. *The Leading Edge*, **20**, no. 8, 877-881. doi: doi:10.1190/1.1487299.

- Brocher, T. M. 2005, Empirical Relations between Elastic Wavespeeds and Density in the Earth's Crust. *Bulletin of the Seismological Society of America*, **95**, no. 6,2081-2092. doi: 10.1785/0120050077.
- Carter-McAuslan, A., P. G. Lelièvre, and C. G. Farquharson. 2015, A study of fuzzy c-means coupling for joint inversion, using seismic tomography and gravity data test scenarios. *Geophysics*, **80**, no. 1, W1-W15. doi: 10.1190/geo2014-0056.1.
- Chamanifard, E. 2013, Applying Lithogeochemical Discrimination Tools for Nickel-Copper Sulfide Exploration in Northern Finland A Case study of First Quantum Minerals Exploration Targets. Master Thesis, Luleå University of Technology.
- Cheraghi, S., A. Malehmir, and G. Bellefleur. 2012, 3D imaging challenges in steeply dipping mining structures: New lights on acquisition geometry and processing from the Brunswick no. 6 seismic data, Canada. *GEOPHYSICS*, **77**, no. 5,WC109-WC122. doi: 10.1190/geo2011-0475.1.
- Cline, J. S., A. H. Hofstra, J. L. Muntean, R. M. Tosdal, and K. A. Hickey. 2005, Carlin-type gold deposits in Nevada: critical geologic characteristics and viable models. *Economic Geology 100th Anniversary Volume*,451-484.
- Constable, S., A. Orange, and K. Key. 2015, And the geophysicist replied: "Which model do you want?". *Geophysics*, **80**, no. 3,E197-E212. doi: 10.1190/geo2014-0381.1.
- Constable, S. C., R. L. Parker, and C. G. Constable. 1987, Occam's inversion; a practical algorithm for generating smooth models from electromagnetic sounding data. *Geophysics*, **52**, no. 3, 289-300. doi: 10.1190/1.1442303.
- Cooke, D. A., and W. A. Schneider. 1983, Generalized linear inversion of reflection seismic data. *Geophysics*, **48**, no. 6, 665-676. doi: doi:10.1190/1.1441497.
- Cranganu, C., and M. Breaban. 2013, Using support vector regression to estimate sonic log distributions: A case study from the Anadarko Basin, Oklahoma. *Journal of Petroleum Science and Engineering*, **103**,1-13. doi: 10.1016/j.petrol.2013.02.011.
- Dahl, T., and B. Ursin. 1991, Parameter estimation in a one-dimensional anelastic medium. *Journal of Geophysical Research: Solid Earth*, **96**, no. B12, 20217-20233. doi: 10.1029/91JB00419.
- Dan, L., Z. Chongquan, and L. Jinhua. 2012, An attribute weighted fuzzy c-means algorithm for incomplete data sets. Paper read at International Conference on System Science and Engineering, June 30 2012-July 2 2012.
- Deere, D. U. a. D., D. W. 1988, The Rock Quality Designation (RQD) Index in Practice, in Louis Kirkaldie, ed., *Rock Classification Systems for Engineering Purposes*: ASTM International. 91-101.
- deGroot-Hedlin, C., and S. Constable. 1990, Occam's inversion to generate smooth, two-dimensional models from magnetotelluric data. *Geophysics*, **55**, no. 12,1613-1624. doi: doi:10.1190/1.1442813.
- Dekkers, M. J., D. Heslop, E. Herrero-Bervera, G. Acton, and D. Krasa. 2014, Insights into magmatic processes and hydrothermal alteration of in situ superfast spreading ocean crust at ODP/IODP site 1256 from a cluster analysis of rock magnetic properties. *Geochemistry, Geophysics, Geosystems*, **15**, no. 8,3430-3447. doi: 10.1002/2014GC005343.
- Doetsch, J., N. Linde, I. Coscia, S. A. Greenhalgh, and A. G. Green. 2010, Zonation for 3D aquifer characterization based on joint inversions of multimethod crosshole geophysical data. *Geophysics*, **75**, no. 6,53-64. doi: 10.1190/1.3496476.
- Farquharson, C. G., M. R. Ash, and H. G. Miller. 2008, Geologically constrained gravity inversion for the Voisey's Bay ovoid deposit. *The Leading Edge*, **27**, no. 1,64-69. doi: doi:10.1190/1.2831681.
- Favetto, A., C. Pomposiello, J. Booker, and E. A. Rossello. 2007, Magnetotelluric inversion constrained by seismic data in the Tucumán Basin (Andean Foothills, 27°S, NW Argentina). *Journal of Geophysical Research: Solid Earth*, **112**, no. B9,n/a-n/a. doi: 10.1029/2006JB004455.
- Fernández-Martínez, J. L. 2015, Model reduction and uncertainty analysis in inverse problems. *The Leading Edge*, **34**, no. 9,1006-1016. doi: 10.1190/tle34091006.1.

- Fernández-Martínez, J. L., Z. Fernández-Muñiz, J. L. G. Pallero, and L. M. Pedruelo-González. 2013, From Bayes to Tarantola: New insights to understand uncertainty in inverse problems. *Journal of Applied Geophysics*, **98**,62-72. doi: 10.1016/j.jappgeo.2013.07.005.
- Gallardo, L. A., and M. A. Meju. 2003, Characterization of heterogeneous near-surface materials by joint 2D inversion of dc resistivity and seismic data. *Geophysical Research Letters*, **30**, no. 13,1658. doi: 10.1029/2003GL017370.
- Gallardo, L. A., and M. A. Meju. 2004, Joint two-dimensional DC resistivity and seismic travel time inversion with cross-gradients constraints. *Journal of Geophysical Research: Solid Earth*, **109**, no. B3,B03311. doi: 10.1029/2003JB002716.
- Gallardo, L. A., and M. A. Meju. 2007, Joint two-dimensional cross-gradient imaging of magnetotelluric and seismic traveltime data for structural and lithological classification. *Geophysical Journal International*, **169**, no. 3,1261-1272. doi: 10.1111/j.1365-246X.2007.03366.x.
- Gallardo, L. A., and M. A. Meju. 2011, Structure-coupled multiphysics imaging in geophysical sciences. *Reviews of Geophysics*, **49**, no. 1. doi: 10.1029/2010RG000330.
- Ghosh, S. K. 2000, Limitations on impedance inversion of band-limited reflection data. *Geophysics*, **65**, no. 3, 951-957. doi: 10.1190/1.1444791.
- Giraud, J., M. Jessell, M. Lindsay, R. Martin, E. Pakyuz-Charrier, and V. Ogarko. 2016, Geophysical Joint Inversion Using Statistical Petrophysical Constraints and Prior Information. In *ASEG Extended Abstracts 2016: 25th International Geophysical Conference and Exhibition*.
- González, E., T. Mukerji, and G. Mavko. 2008, Seismic inversion combining rock physics and multiple-point geostatistics. *Geophysics*, **73**, no. 1, R11-R21. doi: doi:10.1190/1.2803748.
- Gosain, A., and S. Dahiya. 2016, Performance Analysis of Various Fuzzy Clustering Algorithms: A Review. *Procedia Computer Science*, **79**,100-111. doi: 10.1016/j.procs.2016.03.014.
- Gregory, J., N. Journet, G. White, and M. Lappalainen. 2011, Kevitsa Copper Nickel Project in Finland: Technical Report for the Mineral Resources and Reverses of the Kevitsa Project.
- Groot-Hedlin, C. d., and S. Constable. 2004, Inversion of magnetotelluric data for 2D structure with sharp resistivity contrasts. *Geophysics*, **69**, no. 1,78-86. doi: doi:10.1190/1.1649377.
- Haber, E., and D. Oldenburg. 1997, Joint inversion: a structural approach. *Inverse Problems*, **13**, no. 1,63.
- He, H., Y. Tan, and K. Fujimoto. 2016, Estimation of optimal cluster number for fuzzy clustering with combined fuzzy entropy index. Paper read at 2016 IEEE International Conference on Fuzzy Systems (FUZZ-IEEE), 24-29 July 2016.
- Heincke, B., M. Jegen, M. Moorkamp, R. W. Hobbs, and J. Chen. 2017, An adaptive coupling strategy for joint inversions that use petrophysical information as constraints. *Journal of Applied Geophysics*, **136**,279-297. doi: 10.1016/j.jappgeo.2016.10.028.
- Huenges, E. 1997, Factors controlling the variances of seismic velocity, density, thermal conductivity and heat production of cores from the KTB Pilot Hole. *Geophysical Research Letters*, **24**, no. 3,341-344. doi: 10.1029/96GL02890.
- Jackson, D. D. 1979, The use of a priori data to resolve non-uniqueness in linear inversion. *Geophysical Journal International*, **57**, no. 1,137-157. doi: 10.1111/j.1365-246X.1979.tb03777.x.
- Jang, J. S. R. 1993, ANFIS: adaptive-network-based fuzzy inference system. *IEEE Transactions on Systems, Man, and Cybernetics*, **23**, no. 3,665-685. doi: 10.1109/21.256541.
- Jegen, M. D., R. W. Hobbs, P. Tarits, and A. Chave. 2009, Joint inversion of marine magnetotelluric and gravity data incorporating seismic constraints: Preliminary

- results of sub-basalt imaging off the Faroe Shelf. *Earth and Planetary Science Letters*, **282**, no. 1–4, 47–55. doi: 10.1016/j.epsl.2009.02.018.
- Johnson, T. C., P. S. Routh, T. Clemo, W. Barrash, and W. P. Clement. 2007, Incorporating geostatistical constraints in nonlinear inversion problems. *Water Resources Research*, **43**, no. 10. doi: 10.1029/2006WR005185.
- Khoshnavaz, M. J., A. Bóna, M. S. Hossain, M. Urosevic, and K. Chambers. 2016, Diffraction - Another attribute for the interpretation of seismic data in hard rock environment, a case study. *Interpretation*, **4**, no. 4, B23-B32. doi: 10.1190/int-2016-0023.1.
- Kieu, D. T., A. Kopic, and V. A. C. Le. 2016, Fuzzy Clustering Constrained Magnetotelluric Inversion-Case Study over the Kevitsa Ultramafic Intrusion, Northern Finland. In *Near Surface Geoscience 2016-First Conference on Geophysics for Mineral Exploration and Mining*. Barcelona, Spain: EAGE.
- Kieu, D. T., A. Kopic, and A. M. Pethick. 2016, Inversion of Magnetotelluric Data with Fuzzy Cluster Petrophysical and Boundary Constraints. In *25th International Geophysical Conference and Exhibition*. Adelaide, Australia: ASEG.
- Kieu, T. D., and A. Kopic. 2015a, Incorporating Prior Information into Seismic Impedance Inversion Using Fuzzy Clustering Technique. In *SEG International Exposition and 85th Annual Meeting New Orleans, USA: Society of Exploration Geophysicists*.
- Kieu, T. D., and A. Kopic. 2015b, Incorporating Prior Information into Seismic Impedance Inversion Using Fuzzy Clustering Technique. In *SEG International Exposition and Annual Meeting*. New Orleans, USA: Society of Exploration Geophysicists.
- Kieu, T. D., and A. Kopic. 2015c, Seismic Impedance Inversion with Petrophysical Constraints via the Fuzzy Cluster Method. In *24th International Geophysical Conference and Exhibition*. Perth, Australia: ASEG.
- Kieu, T. D., A. Kopic, and C. Kitzig. 2015, Classification of Geochemical and Petrophysical Data by Using Classification of Geochemical and Petrophysical Data by Using Fuzzy Clustering. In *24th International Geophysical Conference and Exhibition*. Perth, Australia: ASEG.
- Kim, D.-W., K. H. Lee, and D. Lee. 2004, Fuzzy clustering of categorical data using fuzzy centroids. *Pattern Recognition Letters*, **25**, no. 11, 1263-1271. doi: 10.1016/j.patrec.2004.04.004.
- Kisi, O., and M. Zounemat-Kermani. 2016, Suspended Sediment Modeling Using Neuro-Fuzzy Embedded Fuzzy c-Means Clustering Technique. *Water Resources Management*, 1-16. doi: 10.1007/s11269-016-1405-8.
- Kitzig, M. C., A. Kopic, and D. T. Kieu. 2016, Testing cluster analysis on combined petrophysical and geochemical data for rock mass classification. *Exploration Geophysics*, -. doi: <http://dx.doi.org/10.1071/EG15117>.
- Koivisto, E., A. Malehmir, P. Heikkinen, S. Heinonen, and I. Kukkonen. 2012, 2D reflection seismic investigations at the Kevitsa Ni-Cu-PGE deposit, northern Finland. *Geophysics*, **77**, no. 5, WC149-WC162. doi: 10.1190/geo2011-0496.1.
- Koivisto, E., A. Malehmir, N. Hellqvist, T. Voipio, and C. Wijns. 2015, Building a 3D model of lithological contacts and near-mine structures in the Kevitsa mining and exploration site, Northern Finland: constraints from 2D and 3D reflection seismic data. *Geophysical Prospecting*, **63**, no. 4, 754-773. doi: 10.1111/1365-2478.12252.
- Landa, E., and S. Treitel. 2016, Seismic inversion: What it is, and what it is not. *The Leading Edge*, **35**, no. 3, 277-279. doi: 10.1190/tle35030277.1.
- Large, R. R., S. W. Bull, and V. V. Maslennikov. 2011, A Carbonaceous Sedimentary Source-Rock Model for Carlin-Type and Orogenic Gold Deposits. *Economic Geology*, **106**, no. 3, 331-358. doi: 10.2113/econgeo.106.3.331.
- Le, C. V. A., B. D. Harris, A. M. Pethick, E. M. Takam Takougang, and B. Howe. 2016, Semiautomatic and Automatic Cooperative Inversion of Seismic and Magnetotelluric Data. *Surveys in Geophysics*, 1-52. doi: 10.1007/s10712-016-9377-z.

- Lee, S. K., H. J. Kim, Y. Song, and C.-K. Lee. 2009, MT2DInvMatlab-A program in MATLAB and FORTRAN for two-dimensional magnetotelluric inversion. *Computers & Geosciences*, **35**, no. 8,1722-1734. doi: 10.1016/j.cageo.2008.10.010.
- Lelièvre, P., C. Farquharson, and C. Hurich. 2012, Joint inversion of seismic traveltimes and gravity data on unstructured grids with application to mineral exploration. *Geophysics*, **77**, no. 1,K1-K15. doi:doi:10.1190/geo2011-0154.1.
- Lelièvre, P. G., D. W. Oldenburg, and N. C. Williams. 2009, Integrating geological and geophysical data through advanced constrained inversions. *Exploration Geophysics*, **40**, no. 4, 334-341. doi: doi:10.1071/EG09012.
- Li, Y., and D. W. Oldenburg. 2000, Incorporating geological dip information into geophysical inversions. *Geophysics*, **65**, no. 1,148-157. doi: 10.1190/1.1444705.
- Li, Y., and J. Sun. 2016, 3D magnetization inversion using fuzzy c-means clustering with application to geology differentiation. *Geophysics*, **81**, no. 5,WC1-WC18. doi: doi:10.1190/geo2015-0636.1.
- Lindqvist, T. 2014, 3D Characterization of Brittle Fracture Zones in Kevitsa Open Pit Excavation, Northern Finland. Master Thesis, University of Helsinki.
- Lines, L., A. Schultz, and S. Treitel. 1988, Cooperative inversion of geophysical data. *Geophysics*, **53**, no. 1,8-20. doi: doi:10.1190/1.1442403.
- Ma, X. 2001, A constrained global inversion method using an overparameterized scheme: Application to poststack seismic data. *Geophysics*, **66**, no. 2, 613-626. doi: doi:10.1190/1.1444952.
- Malehmir, A., C. Juhlin, C. Wijns, M. Urosevic, P. Valasti, and E. Koivisto. 2012, 3D reflection seismic imaging for open-pit mine planning and deep exploration in the Kevitsa Ni-Cu-PGE deposit, northern Finland. *Geophysics*, **77**, no. 5,WC95-WC108. doi: 10.1190/geo2011-0468.1.
- Maleki, S., A. Moradzadeh, R. G. Riabi, R. Gholami, and F. Sadeghzadeh. 2014, Prediction of shear wave velocity using empirical correlations and artificial intelligence methods. *NRIAG Journal of Astronomy and Geophysics*, **3**, no. 1,70-81. doi: 10.1016/j.nrjag.2014.05.001.
- Meju, M. A. 1994, Biased estimation: a simple framework for inversion and uncertainty analysis with prior information. *Geophysical Journal International*, **119**, no. 2,521-528. doi: 10.1111/j.1365-246X.1994.tb00139.x.
- Moorkamp, M. 2017, Integrating Electromagnetic Data with Other Geophysical Observations for Enhanced Imaging of the Earth: A Tutorial and Review. *Surveys in Geophysics*. doi: 10.1007/s10712-017-9413-7.
- Moorkamp, M., B. Heincke, M. Jegen, A. W. Roberts, and R. W. Hobbs. 2011, A framework for 3-D joint inversion of MT, gravity and seismic refraction data. *Geophysical Journal International*, **184**, no. 1,477-493. doi: 10.1111/j.1365-246X.2010.04856.x.
- Muntean, J. L., J. S. Cline, A. C. Simon, and A. A. Longo. 2011, Magmatic-hydrothermal origin of Nevada's Carlin-type gold deposits. *Nature Geoscience*, **4**, no. 2,122-127. doi: doi:10.1038/ngeo1064.
- Mutanen, T. 1997, Geology and ore petrology of the Aka Danger and Koitelainen mafic layered intrusions and the Keivitsa-Sato Danger layered complex, northern Finland. *Geological Survey of Finland, Bulletin* **395**.
- Nayak, J., B. Naik, and H. S. Behera. 2015, Fuzzy C-Means (FCM) Clustering Algorithm: A Decade Review from 2000 to 2014, in Lakhmi C. Jain, Himansu Sekhar Behera, Jyotsna Kumar Mandal and Durga Prasad Mohapatra, eds., *Computational Intelligence in Data Mining - Volume 2: Springer India*. 133-149.
- Neild, J. 2015, A Multi-Attribute Analysis of Kevitsa 3D Seismic Data. Master Thesis, Curtin University.
- Ogaya, X., J. Alcalde, I. Marzán, J. Ledo, P. Queralt, A. Marcuello, D. Martí, E. Saura, R. Carbonell, and B. Benjumea. 2016, Joint interpretation of magnetotelluric, seismic and well-log data in Hontomín (Spain). *Solid Earth Discuss.*, **2016**,1-27. doi: 10.5194/se-2016-24.

- Oliveira, S., L. Loures, F. Moraes, and C. Theodoro. 2009, Nonlinear impedance inversion for attenuating media. *Geophysics*, **74**, no. 6, R111-R117. doi: 10.1190/1.3256284.
- Paasche, H., and D. Eberle. 2011, Automated compilation of pseudo-lithology maps from geophysical data sets: a comparison of Gustafson-Kessel and fuzzy c-means cluster algorithms. *Exploration Geophysics*, **42**, no. 4, 275-285. doi: 10.1071/eg11014.
- Paasche, H., D. Eberle, S. Das, A. Cooper, P. Debba, P. Dietrich, N. Dudeni-Thlone, C. Gläßer, A. Kijko, A. Knobloch, A. Lausch, U. Meyer, A. Smit, E. Stettler, and U. Werban. 2014, Are Earth Sciences lagging behind in data integration methodologies? : *Environmental Earth Sciences*, **71**, no. 4, 1997-2003. doi: 10.1007/s12665-013-2931-9.
- Paasche, H., and J. Tronicke. 2007, Cooperative inversion of 2D geophysical data sets: a zonal approach based on fuzzy c-means cluster analysis. *Geophysics*, **72**, no. 3, 35-39. doi: 10.1190/1.2670341.
- Paasche, H., J. Tronicke, and P. Dietrich. 2010, Automated integration of partially colocated models: Subsurface zonation using a modified fuzzy c-means cluster analysis algorithm. *Geophysics*, **75**, no. 3, P11-P22. doi: 10.1190/1.3374411.
- Paasche, H., J. Tronicke, K. Holliger, A. G. Green, and H. Maurer. 2006, Integration of diverse physical-property models: Subsurface zonation and petrophysical parameter estimation based on fuzzy c-means cluster analyses. *Geophysics*, **71**, no. 3, H33-H44. doi: 10.1190/1.2192927.
- Parkinson, W. D. 1959, Directions of Rapid Geomagnetic Fluctuations. *Geophysical Journal of the Royal Astronomical Society*, **2**, no. 1, 1-14. doi: 10.1111/j.1365-246X.1959.tb05776.x.
- Pedrycz, W., and H. Izakian. 2014, Cluster-Centric Fuzzy Modeling. *Fuzzy Systems, IEEE Transactions on*, **22**, no. 6, 1585-1597. doi: 10.1109/TFUZZ.2014.2300134.
- Pham, D. L. 2001, Spatial Models for Fuzzy Clustering. *Computer Vision and Image Understanding*, **84**, no. 2, 285-297. doi: 10.1006/cviu.2001.0951.
- Pilkington, M., and J. P. Todoschuck. 1992, Natural smoothness constraints in cross-hole seismic tomography. *Geophysical Prospecting*, **40**, no. 2, 227-242. doi: 10.1111/j.1365-2478.1992.tb00373.x.
- Rajabi, M., B. Bohloli, and E. Gholampour Ahangar. 2010, Intelligent approaches for prediction of compressional, shear and Stoneley wave velocities from conventional well log data: A case study from the Sarvak carbonate reservoir in the Abadan Plain (Southwestern Iran). *Computers & Geosciences*, **36**, no. 5, 647-664. doi: 10.1016/j.cageo.2009.09.008.
- Rapstine, T. D. 2015, Gravity gradiometry and seismic interpretation integration using spatially guided fuzzy c-means clustering inversion, Colorado School of Mines. Arthur Lakes Library.
- Rezaee, M. R., A. Kadkhodaie Ilkhchi, and A. Barabadi. 2007, Prediction of shear wave velocity from petrophysical data utilizing intelligent systems: An example from a sandstone reservoir of Carnarvon Basin, Australia. *Journal of Petroleum Science and Engineering*, **55**, no. 3-4, 201-212. doi: 10.1016/j.petrol.2006.08.008.
- Roubens, M. 1982, Fuzzy clustering algorithms and their cluster validity. *European Journal of Operational Research*, **10**, no. 3, 294-301. doi: 10.1016/0377-2217(82)90228-4.
- Russell, B., and D. Hampson. 1991, Comparison of Poststack Seismic Inversion Methods. 61st Annual International Meeting, SEG, Expanded Abstracts, 876-878.
- Schmitt, D. R., C. J. Mwenifumbo, K. A. Pflug, and I. L. Meglis. 2003, Geophysical Logging for Elastic Properties in Hard Rock: A Tutorial, in David W. Eaton, Bernd Milkereit and Matthew H. Salisbury, eds., *Hardrock Seismic Exploration: Society of Exploration Geophysicists*. 20-41.
- Simpson, F., and K. Bahr. 2005, *Practical Magnetotellurics*: Cambridge University Press.
- Singh, R., V. Vishal, and T. N. Singh. 2012, Soft computing method for assessment of compressional wave velocity. *Scientia Iranica*, **19**, no. 4, 1018-1024. doi: 10.1016/j.scient.2012.06.010.

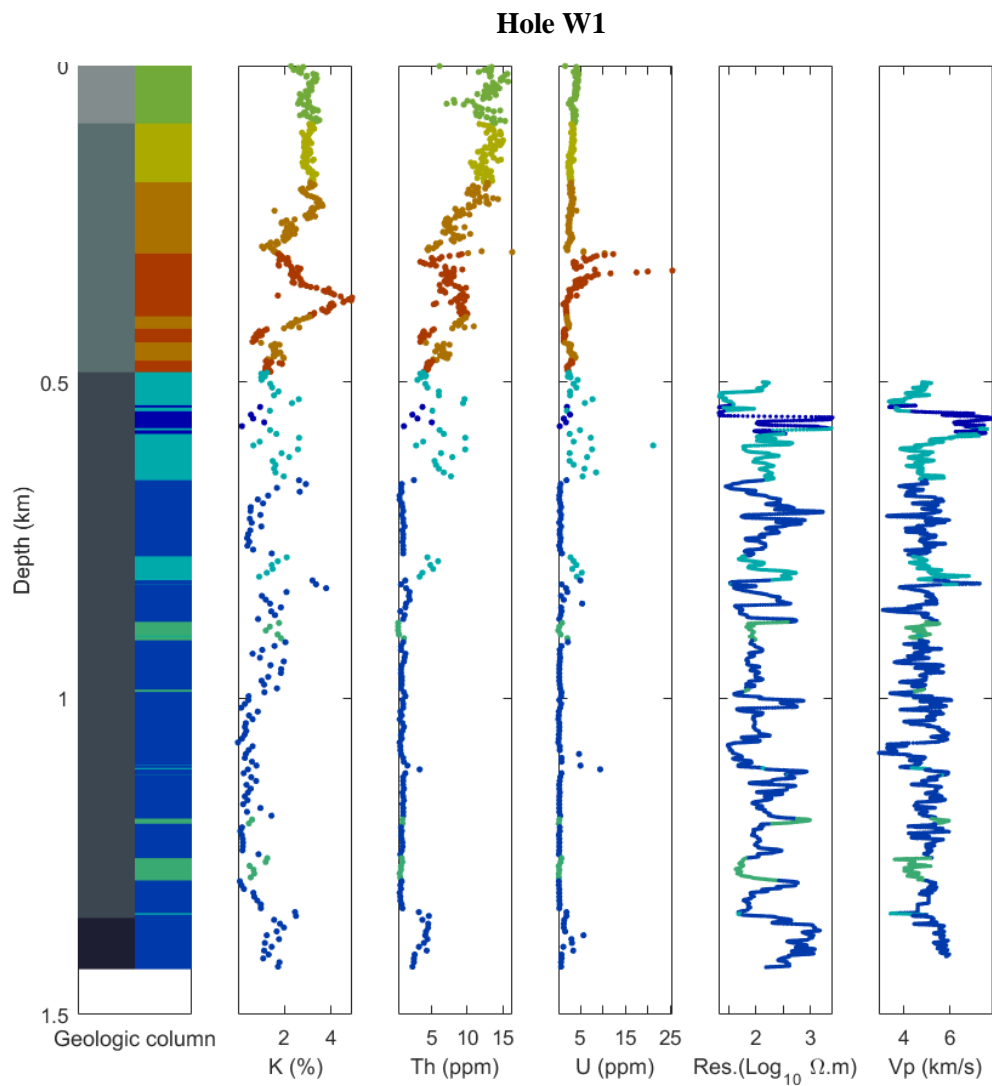
- Singh, T. N., S. Sinha, and V. K. Singh. 2007, Prediction of thermal conductivity of rock through physico-mechanical properties. *Building and Environment*, **42**, no. 1,146-155. doi: 10.1016/j.buildenv.2005.08.022.
- Smith, J. B. 2010, Seismic reflection as a direct detector of gold mineralisation in the Carlin District, USA. BSc. Thesis, Curtin University.
- Standing, J., K. D. Luca, M. Outwhite, M. Lappalainen, C. Wijns, S. Jones, and e. al. 2009, Report and Recommendations From the Kevitsa Campaign, Finland. Confidential Report to First Quantum Minerals Ltd.
- Steel, M. A. 2011a, Petrophysical modelling using self-organising maps. Master Thesis, Curtin University.
- Steel, M. A. 2011b, Petrophysical modelling using self-organising maps, Curtin University.
- Stefano, M., F. Andreasi, S. Re, M. Virgilio, and F. Snyder. 2011, Multiple-domain, simultaneous joint inversion of geophysical data with application to subsalt imaging. *Geophysics*, **76**, no. 3,R69-R80. doi: doi:10.1190/1.3554652.
- Sun, J., and Y. Li. 2011, Geophysical inversion using petrophysical constraints with application to lithology differentiation, *Expanded Abstracts* 2644-2648.
- Sun, J., and Y. Li. 2013a, A general framework for joint inversion with petrophysical information as constraints, *Expanded Abstracts* 3093-3097.
- Sun, J., and Y. Li. 2013b, Petrophysically constrained geophysical inversion using Parzen window density estimation, *Expanded Abstracts*. 3051-3056.
- Sun, J., and Y. Li. 2013c, Petrophysically constrained geophysical inversion using Parzen window density estimation. 83rd Annual International Meeting, SEG, *Expanded Abstracts*,3051-3056.
- Sun, J., and Y. Li. 2014, Exploration of a sulfide deposit using joint inversion of magnetic and induced polarization data, *SEG Technical Program Expanded Abstracts 2014*. 1780-1784.
- Sun, J., and Y. Li. 2015, Multidomain petrophysically constrained inversion and geology differentiation using guided fuzzy c-means clustering. *Geophysics*, **80**, no. 4,ID1-ID18. doi: doi:10.1190/geo2014-0049.1.
- Sun, J., and Y. Li. 2016, Joint inversion of multiple geophysical data using guided fuzzy c-means clustering. *Geophysics*, **81**, no. 3,ID37-ID57. doi: doi:10.1190/geo2015-0457.1.
- Takougang, E. M. T., B. Harris, A. Kepic, and C. V. A. Le. 2015, Cooperative joint inversion of 3D seismic and magnetotelluric data: With application in a mineral province. *Geophysics*, **80**, no. 4,R175-R187. doi: doi:10.1190/geo2014-0252.1.
- Tarantola, A., and B. Valette. 1982, Inverse problems= quest for information. *J. geophys*, **50**, no. 3,150-170.
- ten Kroode, F., S. Bergler, C. Corsten, J. de Maag, F. Strijbos, and H. Tijhof. 2013, Broadband seismic data — The importance of low frequencies. *Geophysics*, **78**, no. 2, WA3-WA14. doi: doi:10.1190/geo2012-0294.1.
- Teranishi, Y., H. Mikada, T. Goto, and J. Takekawa. 2013, Three-dimensional joint inversion of gravity and magnetic anomalies using fuzzy c-means clustering. Paper read at 75th EAGE Conference & Exhibition incorporating SPE EUROPEC 2013.
- Vozoff, K., and D. L. B. Jupp. 1975, Joint Inversion of Geophysical Data. *Geophysical Journal of the Royal Astronomical Society*, **42**, no. 3,977-991. doi: 10.1111/j.1365-246X.1975.tb06462.x.
- Wang, S., T. Kalscheuer, M. Bastani, A. Malehmir, L. B. Pedersen, T. Dahlin, and N. Meqbel. 2017, Joint inversion of lake-floor electrical resistivity tomography and boat-towed radio-magnetotelluric data illustrated on synthetic data and an application from the Äspö Hard Rock Laboratory site, Sweden. *Geophysical Journal International*,ggx414-ggx414. doi: 10.1093/gji/ggx414.
- Wang, Z. 2001, Fundamentals of seismic rock physics. *GEOPHYSICS*, **66**, no. 2,398-412. doi: doi:10.1190/1.1444931.
- Ward, W. O. C., P. B. Wilkinson, J. E. Chambers, L. S. Oxby, and L. Bai. 2014a, Distribution-based fuzzy clustering of electrical resistivity tomography images for

- interface detection. *Geophysical Journal International*, **197**, no. 1, 310-321. doi: 10.1093/gji/ggu006.
- Ward, W. O. C., P. B. Wilkinson, J. E. Chambers, L. S. Oxby, and L. Bai. 2014b, Distribution-based fuzzy clustering of electrical resistivity tomography images for interface detection. *Geophysical Journal International*, **197**, no. 1, 310-321. doi: 10.1093/gji/ggu006.
- Wu, K.-L. 2012, Analysis of parameter selections for fuzzy c-means. *Pattern Recognition*, **45**, no. 1, 407-415. doi: 10.1016/j.patcog.2011.07.012.
- Xie, X. L., and G. Beni. 1991a, A validity measure for fuzzy clustering. *Pattern Analysis and Machine Intelligence, IEEE Transactions on*, **13**, no. 8, 841-847. doi: 10.1109/34.85677.
- Xie, X. L., and G. Beni. 1991b, A validity measure for fuzzy clustering. *Pattern Analysis and Machine Intelligence, IEEE Transactions on*, **13**, no. 8, 841-847. doi: 10.1109/34.85677.
- Zadeh, L. A. 1965, Fuzzy sets. *Information and Control*, **8**, no. 3, 338-353. doi: 10.1016/S0019-9958(65)90241-X.
- Zadeh, L. A. 1978, Fuzzy sets as a basis for a theory of possibility. *Fuzzy Sets and Systems*, **1**, no. 1, 3-28. doi: 10.1016/0165-0114(78)90029-5.
- Zadeh, L. A. 1994, Fuzzy logic, neural networks, and soft computing. *Communications of the ACM*, **37**, no. 3, 77-85.
- Zhang, F., R. Dai, and H. Liu. 2014, Seismic inversion based on L1-norm misfit function and total variation regularization. *Journal of Applied Geophysics*, **109**, no. 0, 111-118. doi: 10.1016/j.jappgeo.2014.07.024.
- Zhang, H., Z. Shang, and C. Yang. 2007, A non-linear regularized constrained impedance inversion. *Geophysical Prospecting*, **55**, no. 6, 819-833. doi: 10.1111/j.1365-2478.2007.00637.x.
- Zhang, J., and A. Revil. 2015, 2D joint inversion of geophysical data using petrophysical clustering and facies deformation. *Geophysics*, **80**, no. 5, M69-M88. doi: 10.1190/geo2015-0147.1.
- Zhou, J., A. Revil, and A. Jardani. 2016, Stochastic structure-constrained image-guided inversion of geophysical data. *Geophysics*, **81**, no. 2, E51-E63. doi: 10.1190/geo2014-0569.1.
- Zhou, J., A. Revil, M. Karaoulis, D. Hale, J. Doetsch, and S. Cuttler. 2014, Image-guided inversion of electrical resistivity data. *Geophysical Journal International*, **197**, no. 1, 292-309. doi: 10.1093/gji/ggu001.
- Ziramov, S., A. Dzunic, and M. Urosevic. 2015, Kevitsa Ni-Cu-PGE deposit, North Finland - A seismic case study. *ASEG Extended Abstracts*, **2015**, no. 1, 1-4. doi: 10.1071/ASEG2015ab122.
- Zoveidavianpoor, M. 2014, A comparative study of artificial neural network and adaptive neurofuzzy inference system for prediction of compressional wave velocity. *Neural Computing and Applications*, **25**, no. 5, 1169-1176. doi: 10.1007/s00521-014-1604-2.
- Zoveidavianpoor, M., A. Samsuri, and S. R. Shadizadeh. 2013, Adaptive neuro fuzzy inference system for compressional wave velocity prediction in a carbonate reservoir. *Journal of Applied Geophysics*, **89**, 96-107. doi: 10.1016/j.jappgeo.2012.11.010.

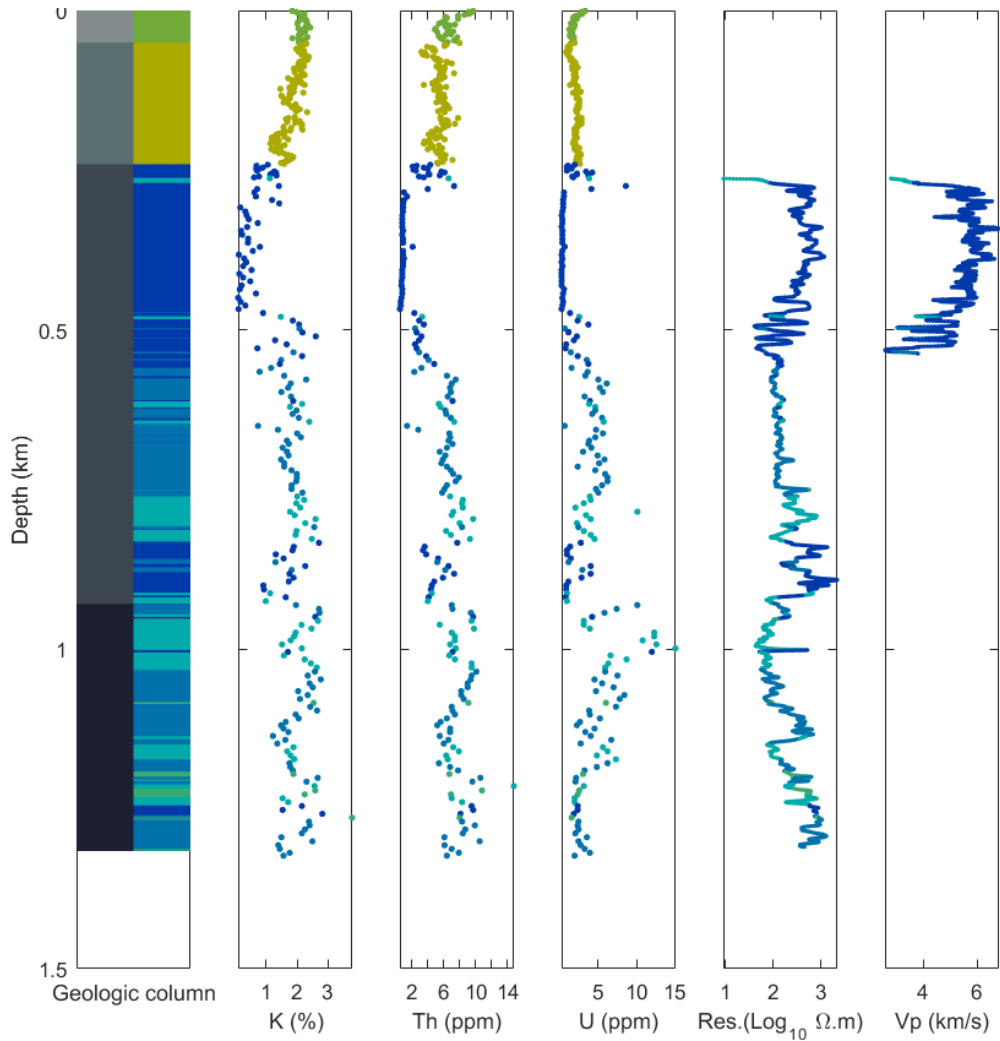
APPENDICES

Appendix A: Borehole data used in Chapter 4

The dataset was acquired in the Carlin-style gold districts, Nevada, the USA by Barrick Gold Corporation. The geological information is provided by Barrick Gold Corporation and referred from the work of Cline et al. (2005). The assay data is available from surface, but downhole geophysical data was only acquired below sedimentary cover layers at depth of about 500 m for hole W1 and 260m for hole W2. And the sonic logs in hole W2 is gathered at the depth from 260 to 530 m.



Hole W2



Legend

Formation keys

QAL	Quaternary alluvium
TC	Tertiary Carlin
OV	Ordovician Valmy
OC	Ordovician Comus

Lithology keys

QAL	Alluvium
TG	Rhyodacite volcanic-tuffaceous silt and clay
TS	Tuffaceous silt
TV	Glassy volcanic
TUF	Tuff, lapilli tuff marker bed
SBM	Siliceous mudstone, siliceous mudstone with tuff
BMT	Mudstone, mudstone with tuff, limestone
QTZ	Quartzite
BAS	Basalt

Data keys

K	- Potassium	Th	- Thorium	U	- Uranium
Res.	- Wireline logs of 64" Normal Resistivity				
Vp	- Full wave form sonic logs of P-wave velocity				

Figure A-1: The borehole data is coded by the colour of lithology. Note that the log data are smoothed by a low-pass filter with window of 0.6096 m (21 data points of interval 0.1ft).

Appendix B: Borehole data analysis used in Chapter 4

The optimal values of cluster number and fuzziness

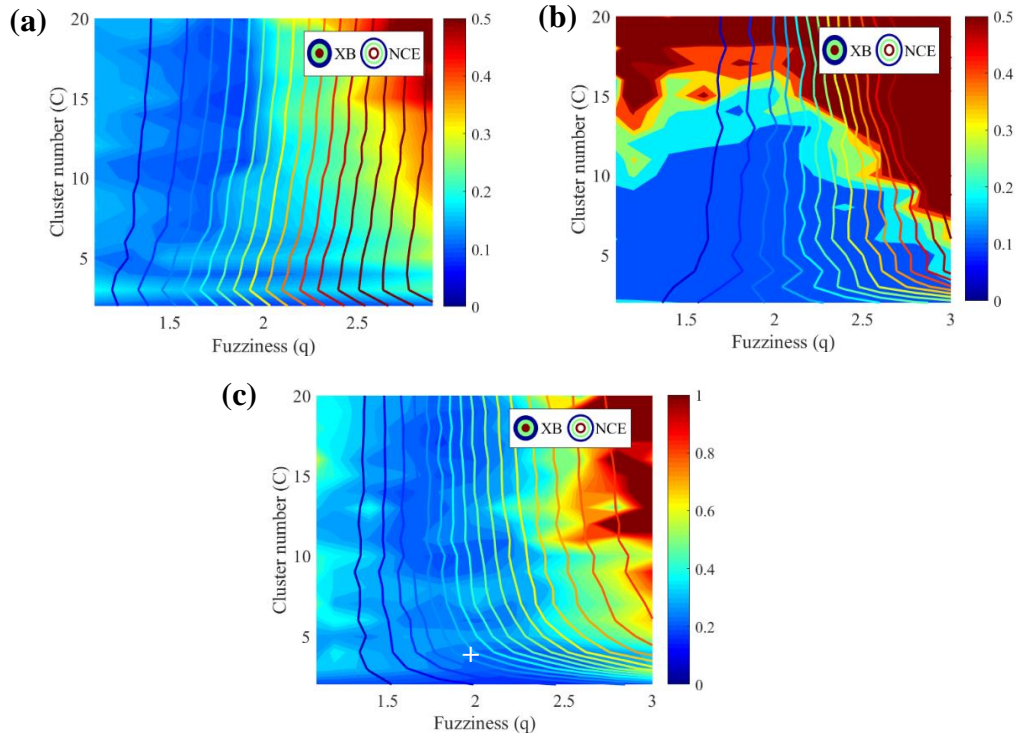


Figure B-1: Variation of the factors XB and NCE with cluster number C and fuzziness q . The input data is (a) resistivity, (b) V_p and (c) both resistivity and V_p . The white cross marks the optimal values of a cluster number of 4, and fuzziness of 2.

The number of clusters and fuzziness can be defined by analysing cluster validity indexes such as XB (Xie and Beni 1991b), and the normalised classification entropy (NCE) (Roubens 1982). Smaller indexes indicate a better clustering result. I analyse three cases of input data: resistivity, P-wave velocity (V_p), and resistivity + V_p , which correspond to the three inversion processes: MT inversion, seismic inversion and co-operative inversion of MT and seismic data (Figure B-1). I then choose the optimal values of C and q as 4 and 2 respectively. This value of fuzziness is also widely used in fuzzy c-means clustering applications (Bezdek, Ehrlich, and Full 1984b, Sun and Li 2015). The fuzziness values and cluster number result in acceptably small values of XB and NCE indexes in all the three cases. Moreover, two clusters can give the smallest values of XB and NCE indexes, but this number is too restrictive and as a

result, the inversions are unstable. If the cluster number is larger than 4, it causes complexity for the inversion particular with the co-operative inversion.

Relationship between acoustic impedance and P-wave velocity

The conversion between acoustic impedance (AI) and P-wave velocity (Vp) can be defined by a cross correlation function of core measurement data (Figure B-2).

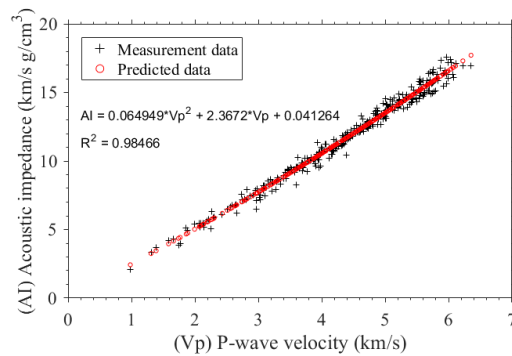


Figure B-2: The function relating AI and Vp from core measurement. This function is used to convert between AI and Vp in my work.

Relationship between resistivity and acoustic impedance

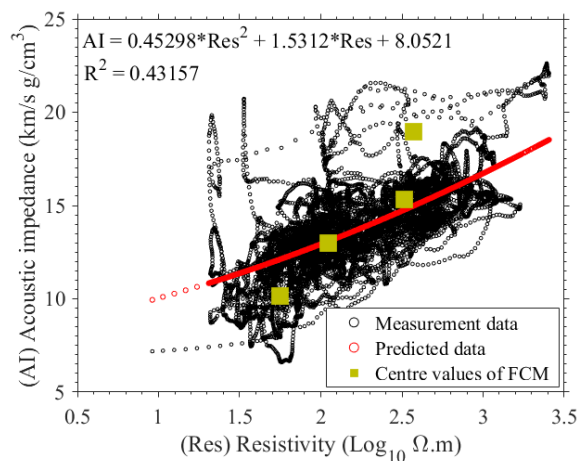


Figure B-3: Cross plot between resistivity (Res) and AI of the borehole data (black circles). The red circles show the calculation using the equation between AI and Res. The square misfit (R^2) of this function shows that the correlation between AI and Res is not high. The yellow squares mark the four centres of fuzzy c-means clustering result. These centres illustrate the positive relation between AI and Res.

The relationships between AI and resistivity used in Chapter 4 is defined by the cross plot function (Figure B-3) and fuzzy c-means clustering (Figure B-4) from the borehole data. The exchange between AI and resistivity of the borehole data W1 (Figure B-4) demonstrates that the use of FCM clustering is more robust than the cross plot method.

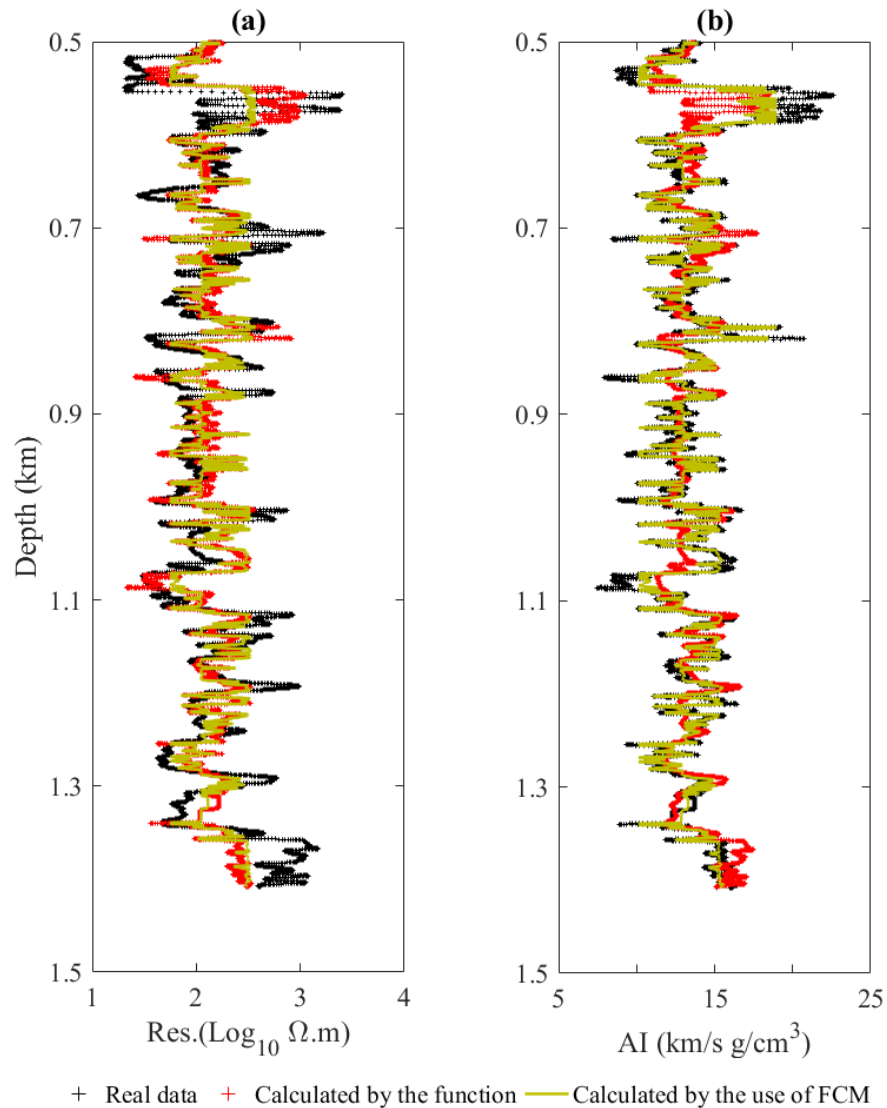


Figure B-4: Comparison between calculation data using the correlation function and FCM clustering in the hole W1. (a) Calculated resistivity (Res.) from AI. (b) Calculated AI from resistivity. Using FCM clustering to exchange the data is better than when using the empirical function, in particular, conversion of AI from resistivity.

Appendix C: Data and misfit of the MT inversion in Chapter 4

MT data

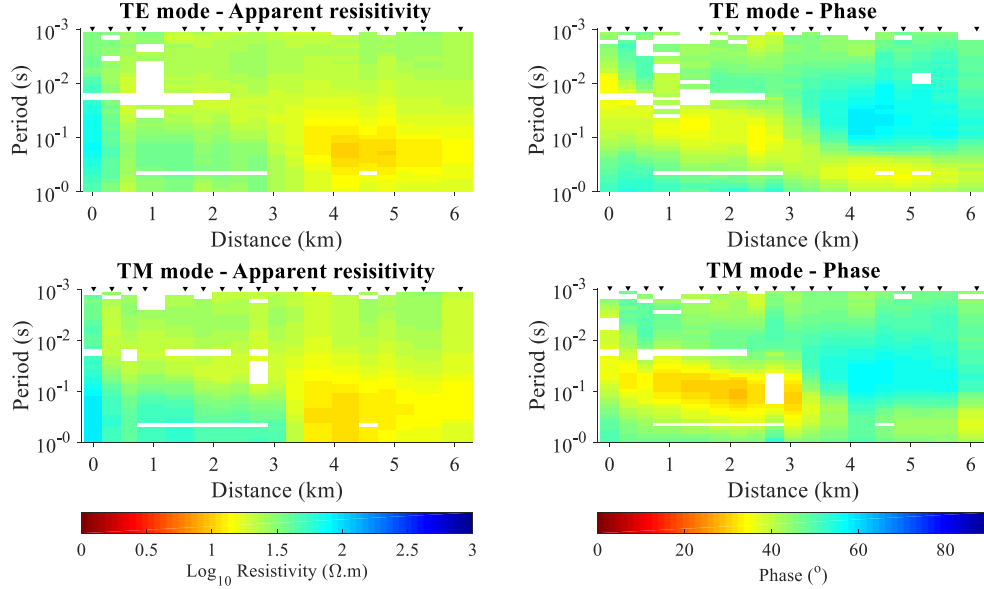


Figure C-1: The apparent resistivity and phase data for the MT profile displayed as pseudo-sections. Triangles show MT stations on the profile.

Misfit of MT inversions

The misfit is illustrated in (Figure C-2). I use the misfit calculation as in (Lee et al. 2009), which measures the difference between real and synthetic data. Generally, the misfit steadily decrease with iterations demonstrating convergence of the inversions.

The relative error is calculated as follows:

$$e_i = 100\% \frac{d_i - s_i}{d_i}, \quad (2.11)$$

where d_i and s_i are real and synthetic data at the i th frequency, apparent resistivity is in logarithmic scale.

Here, I present the relative error of the inversion with only cluster number constraint (Figure C-3), the relative error of other inversions are almost similar. The error is higher at the stations on the left hand side of the profile, particularly stations 6 to 12.

The anisotropy and the 3D effects on the 2D MT inversion caused by the main fault in this area may result the higher error of these stations. The high error level also appears along with fault zones in the results of 3D MT inversion (Le et al. 2016).

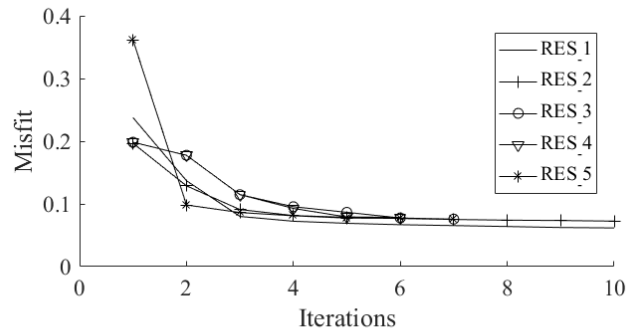


Figure C-2: Misfit of MT inversions. The misfit of sequential co-operative inversion (Table 4-1), from RES_1 to RES_4 correspond constraints of cluster number, petrophysics, petrophysics + boundary from seismic, and petrophysic + seismic inverted model, respectively. RES_5 is the misfit of parallel co-operative inversion.

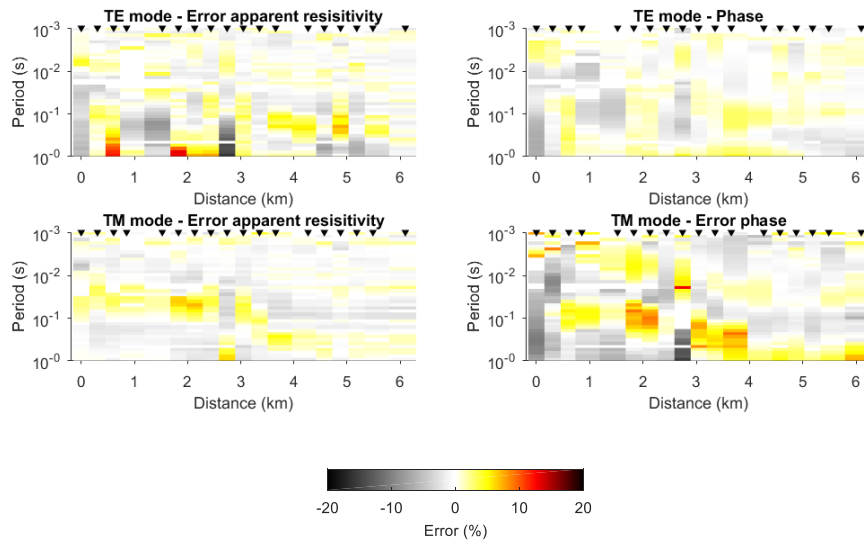


Figure C-3: Relative error of inversion using fuzzy c-means as an added constraint. The best (station 18) and the worst (station 9) misfit between real data and synthetic data of inversion RES_1 using only cluster number constraint. The highest error at the station 5 where the fault presents, this result is consistent with the work of Le et al. (2016).

Appendix D: Error data of seismic inversion in Chapter 4

The seismic data error is calculated by absolute difference between synthetic and real data. Generally, the error is small. It closes to zeros almost everywhere in the section, except at very strong signal location, for instance along boundary between cover layers and the basement.

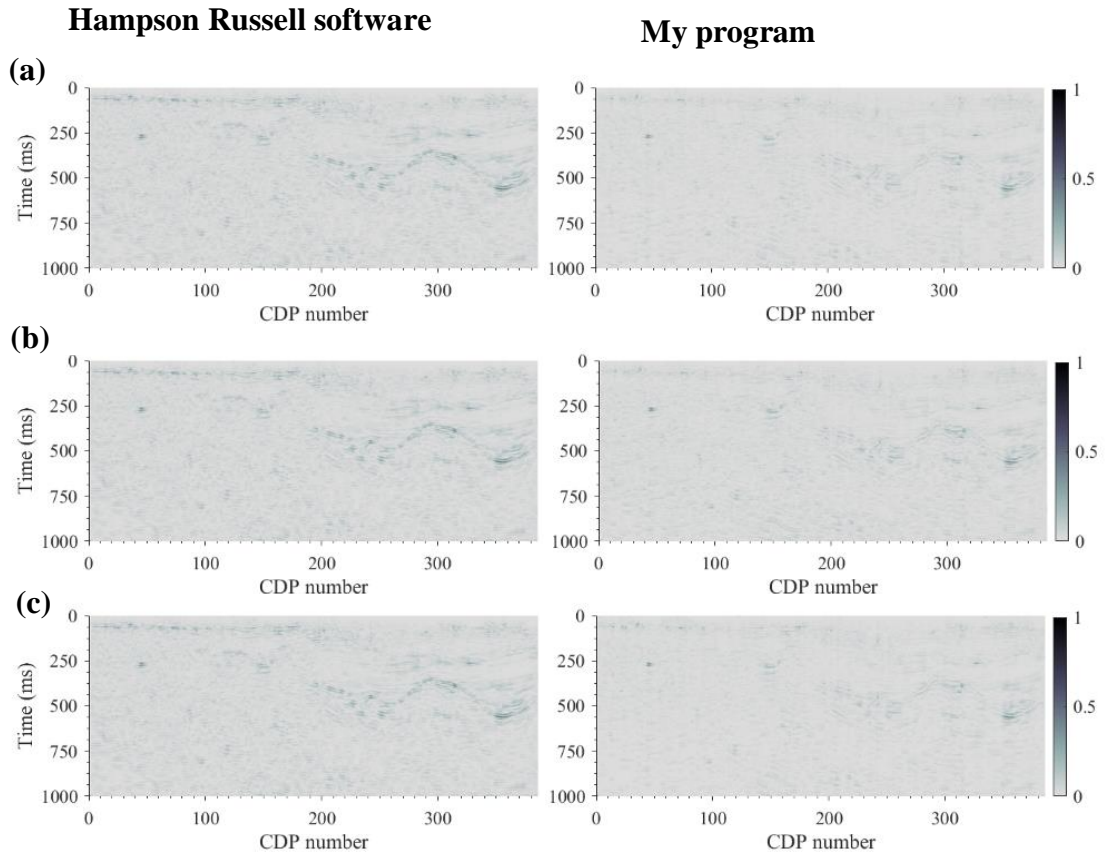


Figure D-1: The error between real data and synthetic data from inverted models using different initial models: (a) borehole data; (b) migrated velocity model; and (c) MT model.

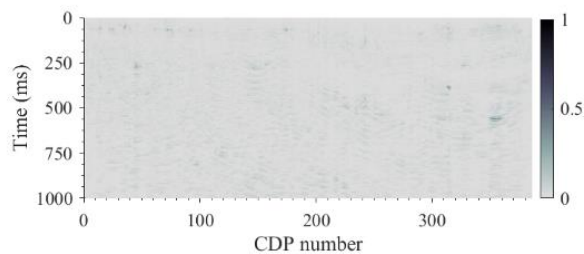


Figure D-2: The error between real data and synthetic data from parallel co-operative inversion.

Appendix E: Lithology in Chapter 5

The lithology from all holes with interval of 1 m. The abbreviations of lithology are presented in the table below.

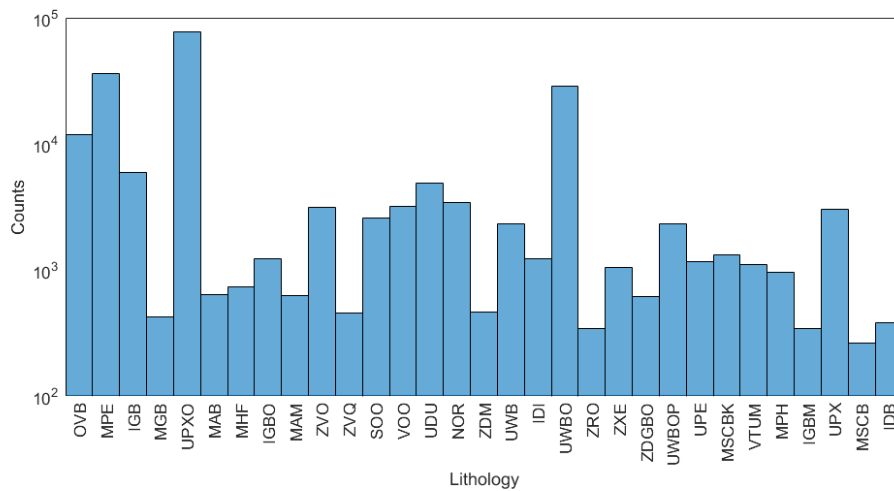


Figure E-1: Histogram of lithological units (interval of 1m) from all holes. The abbreviations are shown in Table E- 1.

Table E-1: Abbreviations of lithology used in Chapter 5

Description	Abbreviation	Description	Abbreviation
overburden	OVB	websterite	UWB
serpentinite, meta peridotite	MPE	granite	IDI
gabbro, micro gabbro, uranite gabbro	IGB	olivine websterite	UWBO
meta-gabbro	MGB	fracture zone	ZRO
olivine pyroxenite	UPXO	xenolith	ZXE
albitite	MAB	dyke - olivine gabbro diabase	ZDGBO
hornfels	MHF	plagioclase bearing olivine websterite komatiite, ultramafic - undifferentiated, peridotite	UWBOP
olivine gabbro	IGBO		UPE
mylonite, hornblendite, amphibolite	MAM	schist - black schist, schist - felsic	MSCBK
vein	ZVO	tuff	VTUM
quartzite	ZVQ	carbonaceous phyllite	MPH
breccia: hydrothermal, hydrothermal, undifferentiated	SOO	magnetite gabbro	IGBM
volcanic: felsic, mafic, undifferentiated	VOO	pyroxenite	UPX
dunite	UDU	phyllite, schist - mafic	MSCB
no recovery, insufficient sample	NOR	diabase	IDB
dyke: amphibole, felsic, mafic	ZDM		

Appendix F: Prediction of sonic velocities, Kevitsa mine, Northern Finland ¹

The sonic velocities can be estimated by using empirical relationships with other rock properties; V_p is a function of density (Brocher 2005) and a function of the composition (Behn and Kelemen 2003). In addition, the velocity depends on many other factors such as porosity, pressure, temperature, saturation, texture, and lithology (Huenges 1997, Wang 2001, Schmitt et al. 2003). The interrelationship of these rock properties causes non-linear and complicated relations between them and the sonic velocities. As a result, conventional models using regression analysis may be insufficient to describe these relations. In recent years, innovative approaches in the fields of fuzzy logic, artificial intelligence and machine learning show promising results for prediction of missing values (Rajabi, Bohloli, and Gholampour Ahangar 2010, Zoveidavianpoor, Samsuri, and Shadizadeh 2013, Zoveidavianpoor 2014).

Fuzzy logic or fuzzy set theory is a concept where the boundaries between subsets of data can be fuzzy (not sharp) (Zadeh 1965). Algorithms based on this concept can deal with the ambiguous data that is common in geoscience. Neuro-fuzzy is a combination of fuzzy logic and neural networks referred to as soft computing (Zadeh 1994). One of the subbranches of the neural network approach are artificial neural networks that are often applied to parameter prediction. The basic idea of using such techniques is to split the complex model of the relationships between the predicted attributes and other properties into a numbers of simple rules. This method is complemented by fuzzy logic to form an approach that may help to tackle the uncertainty associated with geoscientific data. Soft computing has been applied in many areas of the oil industry. Aminzadeh (2004), Aminzadeh and De Groot (2004), Aminzadeh and Wilkinson (2004) applied soft computing to analyse seismic data and to predict reservoir properties. Ahmadi et al. (2013) used artificial neural networks to predict the permeability of a reservoir.

A number of studies showed how artificial intelligence systems can predict the sonic wave velocities from other borehole data. Cranganu and Breaban (2013) predicted the sonic log from the gamma ray- and deep resistivity log using support vector

¹ This is a part of a manuscript that was submitted to a peer-review journal: Kieu D. T., M. C. Kitzig, A. Kopic, Prediction of sonic velocities from other borehole data: An example from the Kevitsa mine site, Northern Finland.

regression. Rezaee, Kadkhodaie Ilkhchi, and Barabadi (2007) utilised fuzzy logic, neuro-fuzzy and artificial neural network approaches to predict Vs from conventional log data in a sandstone reservoir. Asoodeh and Bagheripour (2012) proposed the concept of a committee machine that uses the combined outputs of fuzzy logic, neuro-fuzzy and artificial neural networks to calculate an overall output (prediction). Their work demonstrated that the prediction of compressional, shear and stoneley wave velocity from porosity, resistivity, bulk density and shale volume using committee machines is superior to using the individual techniques alone. Another tool is the adaptive neuro-fuzzy inference system (ANFIS) (Jang 1993) that combines fuzzy models with artificial neural networks; this method outperforms other networks (Singh, Sinha, and Singh 2007, Singh, Vishal, and Singh 2012). ANFIS is also a better predictor compared to multiple linear regression (Rajabi, Bohloli, and Gholampour Ahangar 2010, Zoveidavianpoor, Samsuri, and Shadizadeh 2013, Zoveidavianpoor 2014). The disadvantage of ANFIS is that it uses a large number of rules, which can result in longer computational time. Kisi and Zounemat-Kermani (2016) proposed to embed fuzzy c-means (FCM) into adaptive neuro-fuzzy inference systems. Their work shows, that the ANFIS-FCM model obtained better results in less time, compared to the classical ANFIS model. Pedrycz and Izakian (2014) use FCM clustering to build the functional rules for cluster centric fuzzy modelling.

The prediction of the sonic velocities in carbonate reservoirs was demonstrated in several studies (Rezaee, Kadkhodaie Ilkhchi, and Barabadi 2007, Rajabi, Bohloli, and Gholampour Ahangar 2010, Asoodeh and Bagheripour 2012, Cranganu and Breaban 2013, Zoveidavianpoor, Samsuri, and Shadizadeh 2013, Maleki et al. 2014, Bagheripour et al. 2015), but studies applying this method to hard rock environments are sparse. In crystalline rock, the correlation between the sonic velocities and other logs is likely to be poor. The velocities are generally higher and vary quickly in space due to the complexity of the geological conditions. In this work, we attempt to predict Vp from other borehole data on an example of the Kevitsa Ni-Cu-PGE deposit. Data from a large number of boreholes is available in this area, but sonic logs were acquired in only a few of them (Steel 2011b). 2D and 3D seismic surveys were carried out over the area and the processed and interpreted results described in several studies (e.g.: Malehmir et al. (2012), Koivisto et al. (2015), Ziramov, Dzunic, and Urosevic (2015), Kieu and Kepic (2015a)). However, these studies only utilized data from boreholes

that include sonic logs. These results may be improved if we can exploit the data from all boreholes for seismic processing and acoustic impedance inversion.

In general, the relationship between the sonic velocities and other rock properties is a localised model and different rock units may show different relationships. One approach to form a local relationship between these parameters is to first separate the rocks into groups, where each group shows a clear relation among these parameters. A powerful tool to group data based on similarities of the rock properties is fuzzy clustering. In the following, we describe a fuzzy modelling approach (Pedrycz and Izakian 2014) to predict Vp from other geophysical borehole data for the Kevitsa mine site. We compare our results to the commonly used multiple linear regression method.

Multiple Linear Regression

Multiple linear regression (MLR) uses linear relationships between a dependent variable and multiple independent variables. We assume that the sonic velocity $y=f(x_1, x_2, x_3, x_4)$ is the linear function of other features, in which the independent variables are density (x_1), natural gamma (x_2), magnetic susceptibility (x_3) and resistivity (x_4). We trialled four models for the prediction, namely: linear (F.1), interaction (F.2), quadratic (F.3) and pure quadratic (F.4).

$$y = a_0 + a_1x_1 + a_2x_2 + a_3x_3 + a_4x_4, \quad (F.1)$$

$$y = a_0 + a_1x_1 + a_2x_2 + a_3x_3 + a_4x_4 + a_5x_1x_2 + a_6x_1x_3 + a_7x_1x_4 + a_8x_2x_3 + a_9x_2x_4 + a_{10}x_3x_4, \quad (F.2)$$

$$y = a_0 + a_1x_1 + a_2x_2 + a_3x_3 + a_4x_4 + a_5x_1x_2 + a_6x_1x_3 + a_7x_1x_4 + a_8x_2x_3 + a_9x_2x_4 + a_{10}x_3x_4 + a_{11}x_1^2 + a_{12}x_2^2 + a_{13}x_3^2 + a_{14}x_4^2, \quad (F.3)$$

$$y = a_0 + a_1x_1 + a_2x_2 + a_3x_3 + a_4x_4 + a_5x_1^2 + a_6x_2^2 + a_7x_3^2 + a_8x_4^2, \quad (F.4)$$

where y is the predicted variable, a_0, a_1, \dots, a_{14} are model parameters those are defined in the training process, x_1, x_2, x_3, x_4 are the independent variables.

Cluster-centric fuzzy modeling

A fuzzy ‘input-output’ model for estimation of the sonic logs and other borehole data is built using the fuzzy clustering technique (Pedrycz and Izakian 2014). In this method, the fuzzy clustering is used to define the functional modules (rule base) of the model. Suppose the sonic velocity is $\mathbf{y}=(y_j, j=1, \dots, N)$ and other features are $\mathbf{x}=(x_j, j=1, \dots, N)$, N is a number of samples, the model of input-output is formed as a summation of linearized function:

$$\mathbf{y} = \mathbf{y}_0 + \mathbf{P}\boldsymbol{\delta}, \quad (\text{F.5})$$

where $\mathbf{y}_0=(y_{0j}, j=1, \dots, N)$ and $\boldsymbol{\delta} = (\delta_j, j = 1, \dots, N)$ are defined as following:

$$y_{0j} = \sum_{i=1}^c a_{ji} w_i, \quad (\text{F.6})$$

$$\delta_j = \sum_{i=1}^c a_{ji} (x_j - v_i). \quad (\text{F.7})$$

Output of the model can be calculated as:

$$y_j = \sum_{i=1}^c a_{ji} [w_i + p_i (x_j - v_i)]. \quad (\text{F.8})$$

In equation (F.6), (F.7) and (F.8), C is a number of rules (or number of clusters). The parameters $\mathbf{P}=(\mathbf{p}_i, i=1, \dots, C)$, $\mathbf{W}=(\mathbf{w}_i, i=1, \dots, C)$, and $\mathbf{V}=(\mathbf{v}_i, i=1, \dots, C)$ are defined by training section. \mathbf{P} is model parameter, \mathbf{W} and \mathbf{V} are centre values of the FCM clusters of the predicted and known variables respectively. The firing strength $\mathbf{A}=(a_{ji}, j=1, \dots, N, i=1, \dots, C)$ is defined by membership degree from fuzzy c-means clustering of known variables.

Both cluster-centric fuzzy modeling and multiple linear regression methods use linear relationships between known and unknown variables. However, they differ in the way the prediction model is build. Multiple linear regression applies a single model to the whole dataset, while cluster-centric fuzzy modeling uses multiple linear functions to create the model, which allows this method to deal with a more complex data structure. In this regard, cluster-centric fuzzy modelling is similar to the adaptive neuro-fuzzy inference systems modeling method.

Performance evaluation

The relative root means square error (RMSE) and the accumulated time difference are indicators to evaluate the success of the prediction. These parameters are calculated as follows:

$$RMSE = 100\% \sqrt{\frac{1}{N} \sum_{i=1}^N \frac{(d_i - e_i)^2}{d_i^2}}, \quad (F.9)$$

$$\Delta t = t_d - t_e, \quad (F.10)$$

where \mathbf{d} is measured data; \mathbf{e} is estimated data. t_d and t_e are converted depth to two-way time along borehole trajectory using measured and predicted Vp respectively.

For the sake of performance evaluation, we assume that the measured sonic velocities are correct, despite the fact that they are likely to be corrupted by noise or other measurement errors (as is true for most natural data). RMSE is used to evaluate the difference between measured and predicted data, where smaller values of RMSE point to a better estimation. For seismic imaging, the seismic data is usually transformed from the depth to the time domain. Therefore, seismic events at a particular depth are shifted upward or downward in the time domain if Vp is under- or over-estimated by the prediction. The accumulated time difference shows the level shift of seismic events from their actual position after converting the data from depth-to-time using the predicted Vp. It is a measure of distortion of the image, where a greater values mean higher distortion. We set a threshold value of 2ms. This threshold value is based on the assumption that the dominant frequency of the seismic data is 50Hz, and the average Vp is 6.5 km/s. If the absolute values of accumulated time difference are less than 2ms, the distortion of the seismic image is negligible and the Vp prediction can be used for seismic imaging purposes.

Data sets

We apply MLR and CFM methods to data from five boreholes (H1-H5) from the Kevitsa Ni-Cu-PGE deposit in northern Finland. The five holes are located in different geologic environments (Figure 5-1) to ensure that our model can be applied to the whole Kevitsa dataset. The dataset includes geophysical downhole logs of P-wave velocity (V_p), density (SG), natural gamma (NG), magnetic susceptibility (MS) and resistivity (RES). For each prediction, the data from four different holes is divided into training (70%) and parameter checking (30%), and the resulting model is tested on the remaining hole (five combinations with four holes as input and the remaining as output).

Table F-1: Combination of data sets used for the prediction

Combination	Dataset
C1	Density and natural gamma
C2	Density, natural gamma, and magnetic susceptibility
C3	Density, natural gamma, and resistivity
C4	Density, natural gamma, magnetic susceptibility, and resistivity

To choose the best subset of features (variables), we tested the prediction success on various combinations of input features. It is worth noting that there is no meaningful correlation between the sonic logs and the other measurements, except for SG and NG, which show a moderate correlation (Steel 2011b). The density and natural gamma logs are therefore more important for the prediction process than the magnetic susceptibility and resistivity logs. We performed the prediction with four different input data combinations C1-C4 summarised in Table F-1.

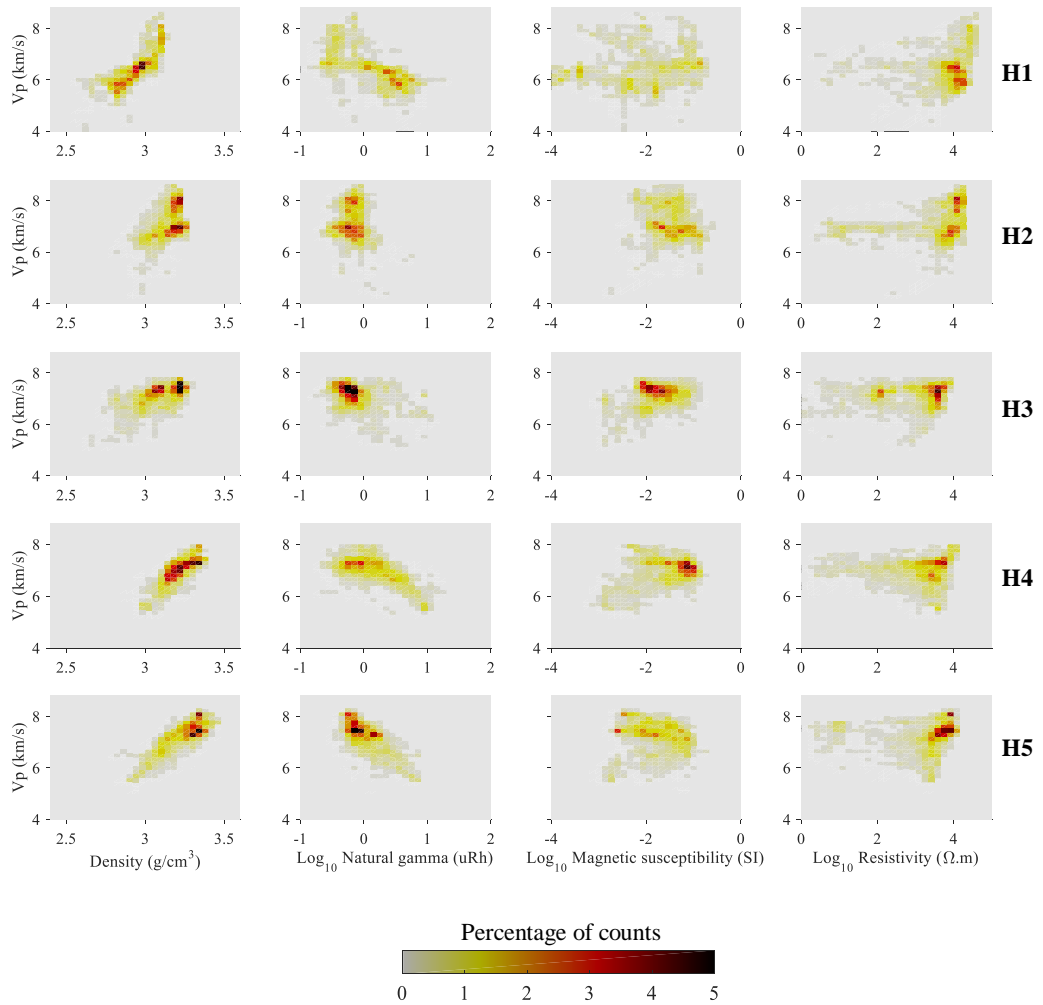


Figure F-1: From left to right, the panels show cross plot V_p versus density, natural gamma, magnetic susceptibility, and resistivity of the five holes from H1 to H5 (from top to bottom). The colour legend represents the data density.

Prediction of V_p using multiple linear regression

We apply the linear, interactions, quadratic, and pure quadratic multiple linear regression to the four data sets C1, C2, C3 and C4 using MATLAB built in routines. The RMSE is calculated to evaluate the accuracy of prediction. The linear function is the best model for V_p estimation. It produces the smallest error for the three data sets C1, C2, and C4 but the error of C3 is slightly larger than from the interaction model . Using the dataset C3 to predict V_p is the best option because the RMSE is smallest in all four models.

Figure F-2 illustrates a comparison between estimated and measured Vp. The estimations of holes H1 and H2 show the worst results, in contrast, the best results are in the hole H4 and H5. The largest RMSE of Vp prediction is in the hole H2.

Table F-2: Average RMSE of the five holes for the different multiple linear regression models for Vp estimation. The linear model (bold) seems to give an overall good result with all data combinations C1-C4. The errors for all models are smallest for the C3 data (red) indicating that this combination might be best suited for training.

Model	Data sets			
	C1	C2	C3	C4
Linear	6.04	6.01	6.01	6.05
Iterations	6.11	6.08	5.89	6.01
Quadratic	6.12	6.28	5.92	6.08
Pure Quadratic	6.10	6.10	6.06	6.26

Table F-3: RMSE of fuzzy cluster modeling for Vp. The data combination C3 yields the smallest average RMSE (red).

Holes	Data sets			
	C1	C2	C3	C4
H1	7.03	7.90	6.40	7.12
H2	7.88	8.03	7.28	7.65
H3	6.18	6.51	6.09	6.80
H4	3.99	3.94	4.12	4.24
H5	4.21	4.31	4.24	4.40
Average	5.86	6.14	5.63	6.04

Prediction of Vp using cluster fuzzy modeling

Cluster fuzzy modeling (CFM) method is applied to the four data sets C1, C2, C3, and C4. CFM parameters are defined by training procedure on data of four holes first, and then the model is validated on the remainder hole. The RMSE of Vp predictions is shown in Table F-3. The RMSE of the five holes is smallest for the data combination C3 and the best prediction was obtained for holes H4, and H5. Figure F-2 presents comparisons between estimated and measured Vp. The prediction in holes H4 and H5 achieve the best results, but the overall trend matches well in all holes.

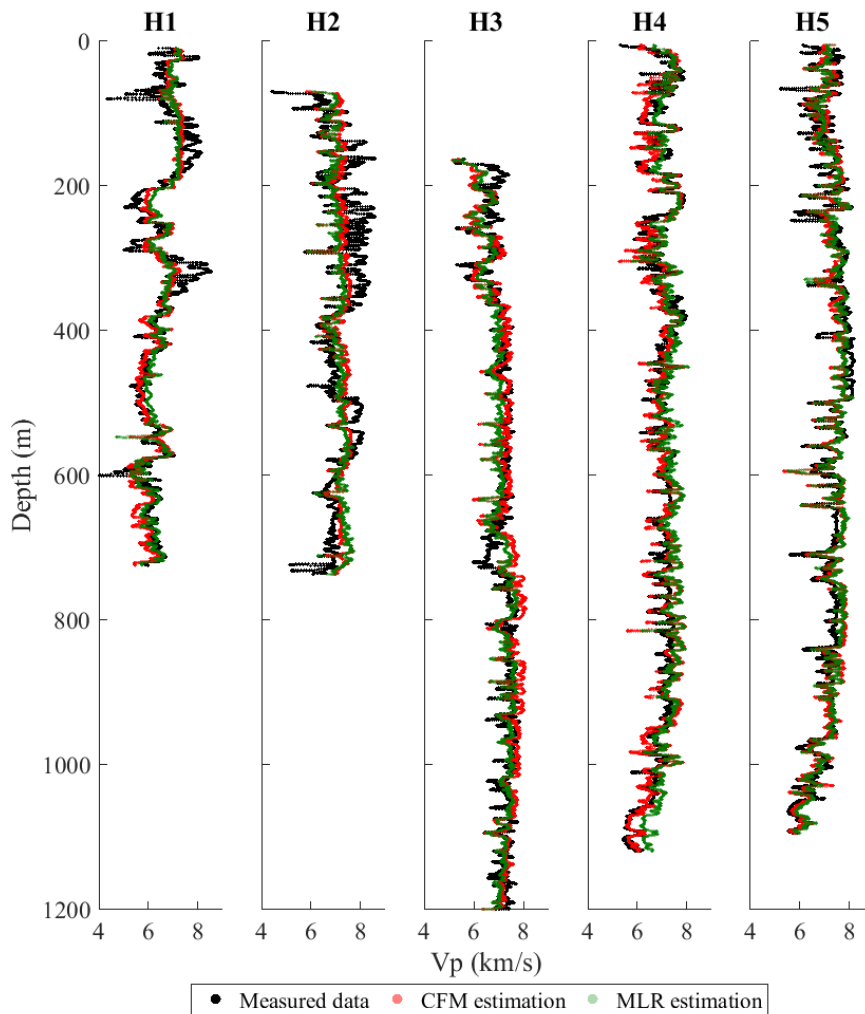


Figure F-2: Comparison between measured (black) and estimated Vp from cluster centric fuzzy modeling (CFM, red) and from the linear case of the multiple linear regression model (MLR, green) for the C3 data combination (density, natural gamma and resistivity).

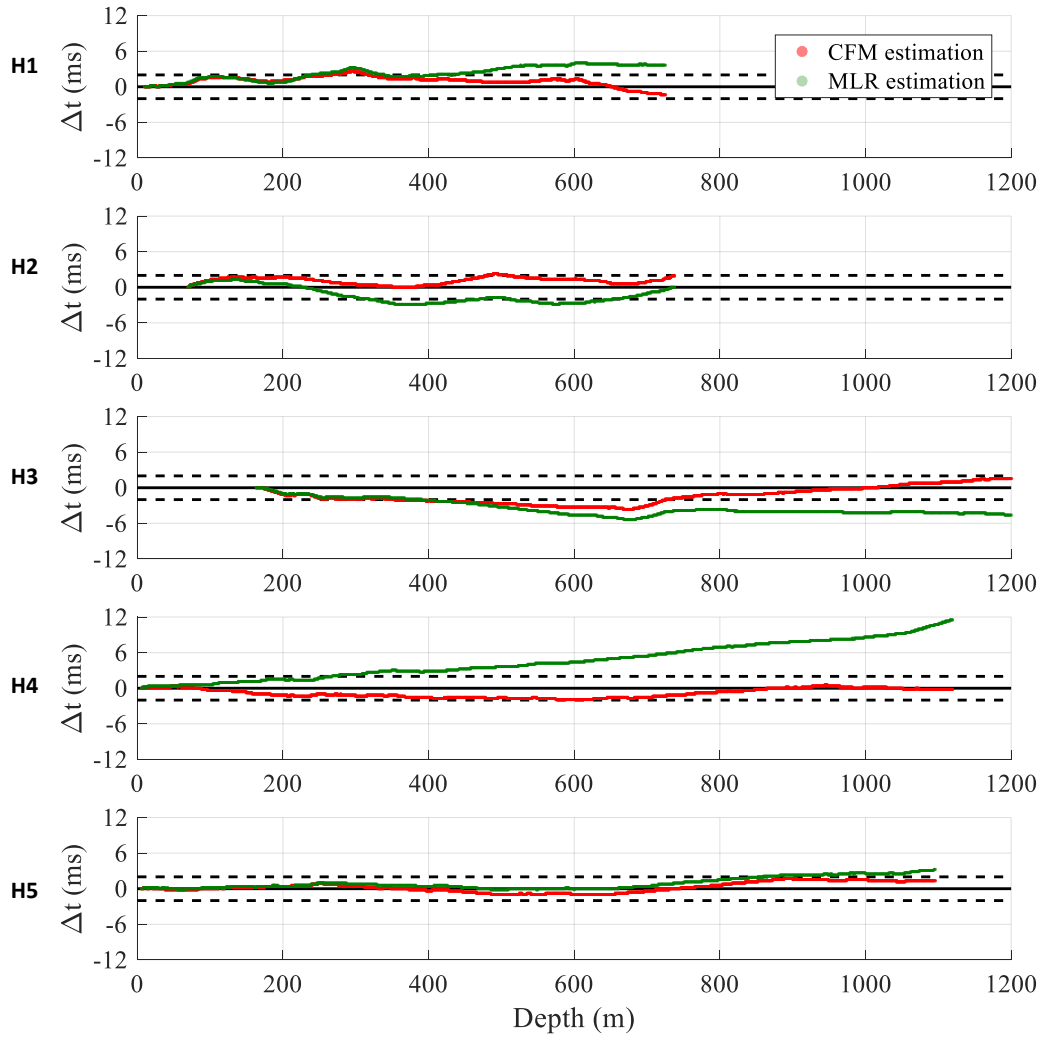


Figure F-3: Comparison between the accumulated time differences calculated from V_p estimation from cluster-centric fuzzy modeling (CFM, red lines) and multiple linear regression (MLR, green lines). The black dashed lines present the threshold values of $\pm \epsilon$ ms. Accumulated time differences closer to zero indicate better performance. V_p prediction using the cluster-centric fuzzy model is superior to the multiple linear regression method in almost all cases (except for borehole H2).

V_p prediction for seismic imaging and inversion

The primary objective of our work was to demonstrate that V_p predicted from other borehole data can be used in seismic imaging and inversion. Therefore, the predictions are evaluated in regards to these processes. In seismic imaging, the depth-to-time conversions should be based on velocities that cause as little accumulation of time difference (travel time error) as possible. In a seismic inversion, the V_p is used to build an initial model that reconstructs the low-frequency data-band that is missing

in seismic reflection data. The process of seismic impedance inversion will use the reflection data to refine the model to include the local variations that provide reflectivity. Thus, it is important that the velocity (V_p) prediction follows trend rather than fitting local fluctuations. Figure F-3 shows that the accumulated time difference (from cluster-centric modeling) stays mostly within the notional threshold of ± 2 ms tolerance; the placement of seismic events can thus be done with little error and the estimated V_p can be used for seismic imaging purposes, such as stacking velocities or robust starting V_p models for pre-stack migration.

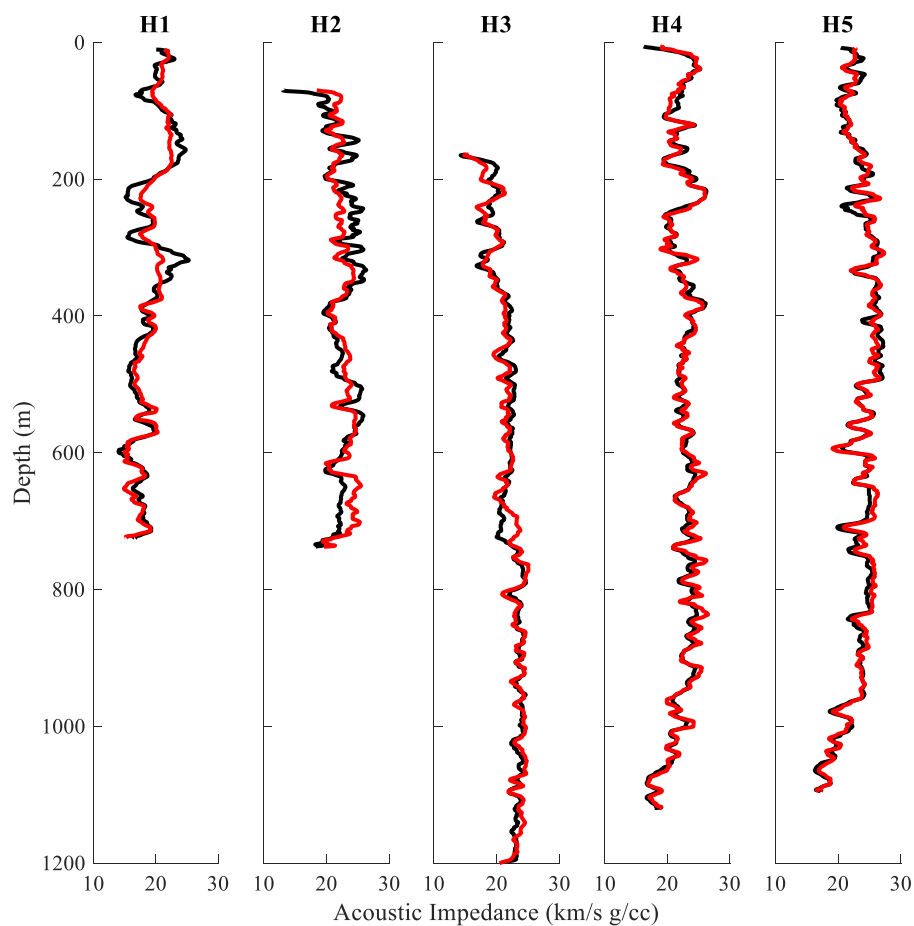


Figure F-4: Comparison between smoothed estimated (red lines) and measured (black lines) acoustic impedance for the five holes (H1-H5, where the other four holes were used for training) from dataset C3. All the data is smoothed by averaging over 10 m. Generally, the predicted acoustic impedance is best fit with measured data in holes H3, H4 and the shallow part of H5, however, it shows difference in H1, H2 and the proportion from depth of 600 to 1000 m of H5. More importantly, most peaks and troughs are appropriately estimated.

Figure F-4 shows the smoothed acoustic impedance product of the estimated and measured Vp and density logs. The data is smoothed by applying a 10 m moving average window. The trends (troughs and peaks), as well as the absolute values are in very good agreement, suggesting that the predicted Vp can be used for seismic (acoustic impedance) inversion. The seismograms (Figure F-5) calculated from estimated Vp support this argument.

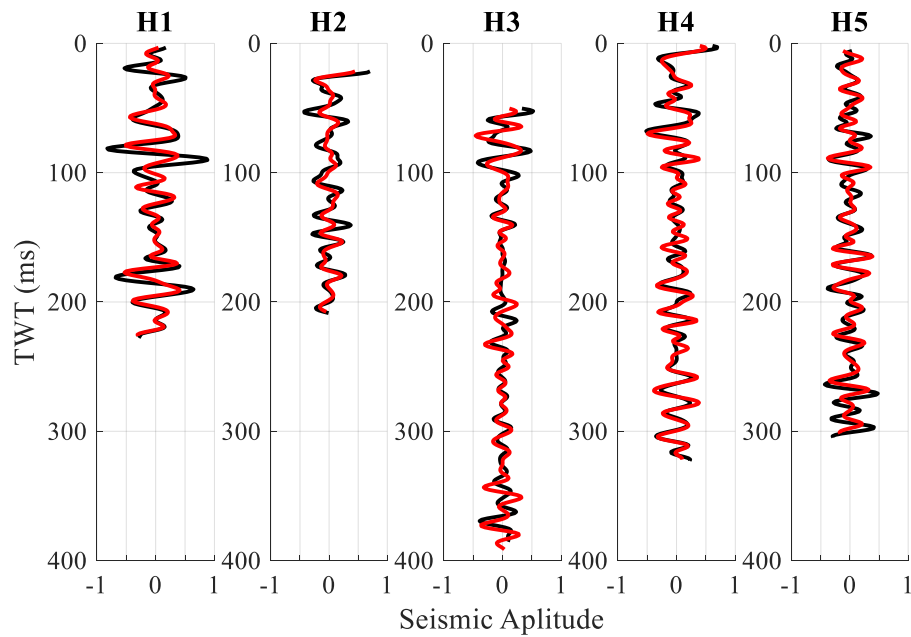


Figure F-5: Comparison seismic seismogram in time domain between estimated data (red lines) and measured data (black lines). The seismogram is formed by convoluting reflectivity and a Ricker wavelet, dominant frequency 50Hz. The reflectivity is calculated from acoustic impedance (Figure F-4).

Appendix G: Filling missing values of the whole boreholes

Since the borehole data is incomplete, the missing values need to be filled. In this work, I use fuzzy c-means clustering process to fill the missing values. The basic idea is to assign the weighted average of the cluster to the missing values. Thus, this method is robust if the missing samples are not too many and not all the features of the samples are missed. For the features acquired in the few holes, such as P-wave velocity, I use the prediction program described in Appendix F.

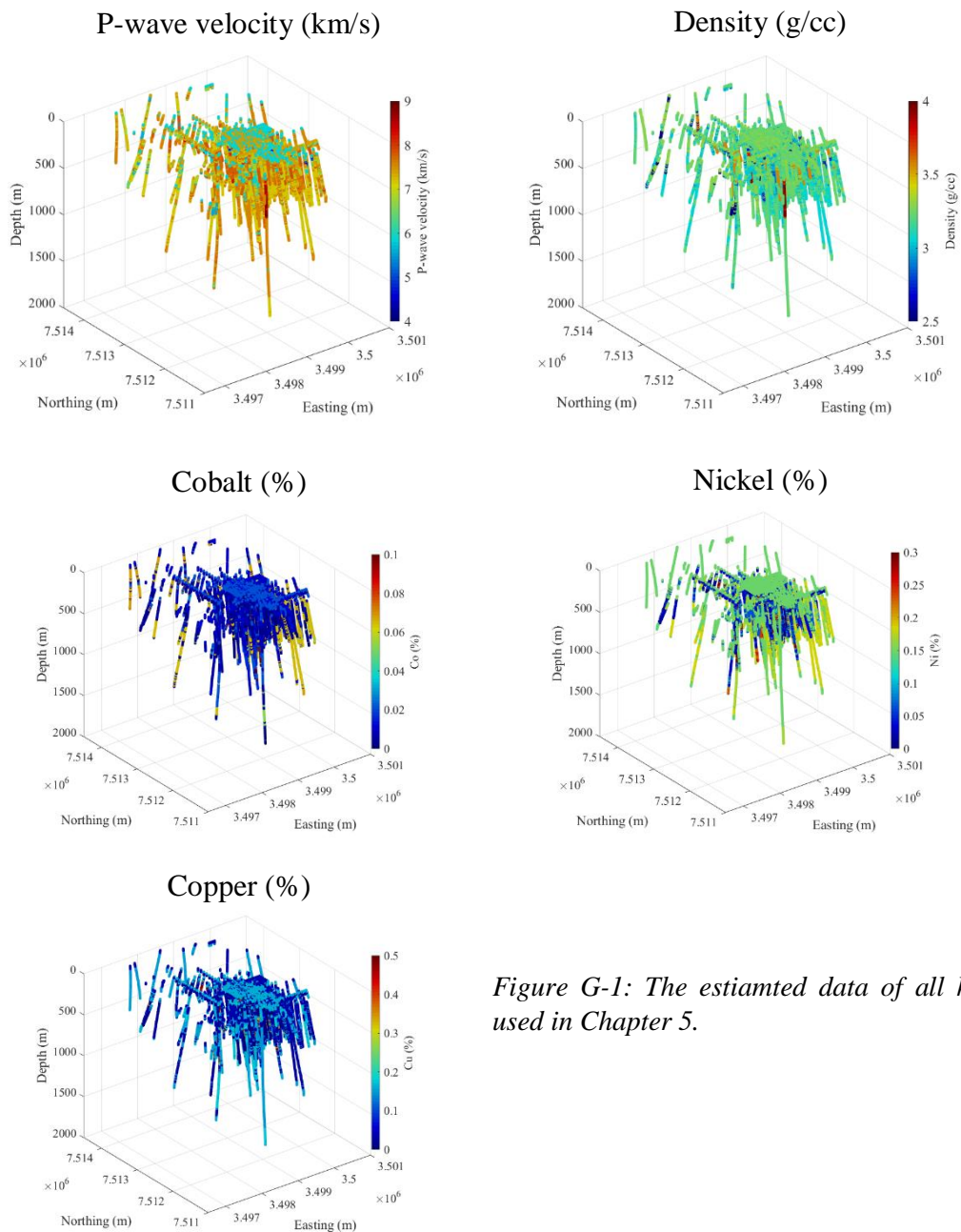


Figure G-1: The estimated data of all holes used in Chapter 5.

Appendix H: Open source code used in this thesis

MT2DInvMatlab (Lee et al. 2009). This package is used for 2D MT inversion. I modified the inversion process based on my algorithms, but the forward modelling is kept. I also modified some plotting functions that are used in Chapter 3 and 4.

I used Matlab function of SeisLab 3.01 package

(<https://au.mathworks.com/matlabcentral/fileexchange/15674-seislab-3-01>):

read_seg_y_file.m, to read seismic SEG-Y files and s_wplot.m to plot seismic trace.

Appendix I: Copyright consent

Permission 1

Permission for using published material in PhD thesis

Thomas Beentje <tbe@eage.org>

Wed 19/07/2017 8:11 PM

To: Duy Thong Kieu

Dear Duy Thong Kieu,

We grant your permission to republish these papers, if they are given proper acknowledgement of being published before by EAGE.

Good luck with your thesis and kind regards,

Thomas Beentje
Media Production Coordinator

EAGE Europe
PO Box 59
3990 DB Houten
The Netherlands
Tel.: [+31 88 9955055](tel:+31889955055)
www.eage.org

From: Duy Thong Kieu [mailto:duythong.kieu@postgrad.curtin.edu.au]

Sent: dinsdag 18 juli 2017 9:55

To: EagePublications <EagePublications@eage.org>

Subject: Permission for using published material in PhD thesis

Dear **publisher**,

It is my understanding that EAGE is the copyright holder of the following material:

1- Kieu, D. T., A. Kepic, and V. A. C. Le. 2016, **Fuzzy Clustering Constrained Magnetotelluric Inversion-Case Study over the Kevitsa Ultramafic Intrusion, Northern Finland**. In Near Surface Geoscience 2016-First Conference on Geophysics for Mineral Exploration and Mining. Barcelona, Spain: EAGE.

2- Kieu, D. T., M. C. Kitzig, and A. Kepic. 2016, **Estimation of P-wave Velocity from Other Borehole Data**. In Near Surface Geoscience 2016 - First Conference on Geophysics for Mineral Exploration and Mining. Barcelona, Spain: EAGE.

I would like to reproduce these works in my doctoral thesis which I am currently undertaken at Curtin University in Perth, Western Australia. Once completed, the thesis will be made available in a hard-copy form in the Curtin library and in a digital form via the Australian Digital Thesis Program. I would be most grateful for your consent to the copying and communication of the work as proposed.

I look forward to hearing from you and thank you in advance for your consideration of my request.

Yours sincerely

Duy Thong Kieu

PhD Student

Curtin University

Department of Exploration Geophysics

GPO BOX U1987, PERTH WA 6845

Permission 2

EXtended abstracts in PhD thesis

Mark Lackie <mark.lackie@mq.edu.au>

Wed 19/07/2017 10:01 AM

To: Duy Thong Kieu

Action Items

Hi Duy,

there is no problem with you doing that. Please reference the abstracts to reflect the original publication (as you have already done). Good luck with your thesis.

cheers Mark
Editor-in-charge Exploration Geophysics

Hi ASEG Webmaster,

A contact enquiry has been made on the ASEG website.

The details of the enquiry are as follows:

Name: Duy Thong Kieu

Contact Number: 0415444830

Email Address: duythong.kieu@postgrad.curtin.edu.au

Message:

Dear publisher,

It is my understanding that ASEG is the copyright holder of the following material:

Kieu, T. D., and A. Kopic. 2015, Seismic Impedance Inversion with Petrophysical Constraints via the Fuzzy Cluster Method. In 24th International Geophysical Conference and Exhibition. Perth, Australia: ASEG.

Kieu, T. D., A. Kopic, and C. Kitig. 2015, Classification of Geochemical and Petrophysical Data by Using Classification of Geochemical and Petrophysical Data by Using Fuzzy Clustering. In 24th International Geophysical Conference and Exhibition. Perth, Australia: ASEG.

Kieu, D. T., A. Kopic, and A. M. Pethick. 2016, Inversion of Magnetotelluric Data with Fuzzy Cluster Petrophysical and Boundary Constraints. In 25th International Geophysical Conference and Exhibition. Adelaide, Australia: ASEG.

I would like to reproduce these works in a doctoral thesis which I am currently undertaken at Curtin University in Perth, Western Australia. Once completed, the thesis will be made available in a hard-copy form in the Curtin library and in a digital form via the Australian Digital Thesis Program. I would be most grateful for your consent to the copying and communication of the work as proposed.

I look forward to hearing from you and thank you in advance for your consideration of my request.

Yours sincerely
Duy Thong Kieu
PhD Student, Curtin University

Dr Mark Lackie
Senior Lecturer in Geophysics
Department of Earth and Planetary Sciences
Macquarie University
North Ryde NSW 2109
Ph 61-2-9850 8377 Mob 0425 237 899
Fx 61-2-9850 6904
WW12 (E7A) Level 1, Room 108

Permission 3

Secretariat EGU Office <secretariat@egu.eu>

Mon 24/07/2017 7:28 PM

To:

Duy Thong Kieu

Action Items

Dear Duy Thong Kieu,

Thanks for your message.

The copyright is retained by the authors. Please see here the licence and copyright agreement:

https://www.egu2015.eu/abstract_management/licence_and_copyright.html

Best regards

Simone Aechter

Secretary

European Geosciences Union (EGU)
EGU Executive Office
Luisenstrasse 37
D-80333 MUNICH (Germany)

Phone: +49 (0)89 2180-6549

Fax: +49 (0)89 2180-17855

E-mail: secretariat@egu.eu

Find out the latest in geoscience research on:

- GeoLog (<http://geolog.egu.eu/>)
- The EGU Blog Network (<http://blogs.egu.eu/>)

You can follow the EGU on:

- Twitter at <https://twitter.com/EuroGeosciences>
- Facebook at <https://www.facebook.com/EuropeanGeosciencesUnion>

Check out the new Imaggero at <http://imaggero.egu.eu/>

EGU General Assembly 2018

Vienna, Austria 8 - 13 April

Am 18.07.2017 um 10:20 schrieb noreply@egu.eu:

Hi,

You have receive a contact request.

Name: Duy Thong Kieu

Email: duythong.kieu@postgrad.curtin.edu.au

Topic: Publications

Dear publisher,

It is my understanding that EGU is the copyright holder of the following material:

Kieu, T. D., and A. Kepic. 2015, A new co-operative inversion strategy via fuzzy clustering technique applied to seismic and magnetotelluric data. EGU General Assembly Conference.

I would like to reproduce this work (abstract and presentation) in a doctoral thesis which I am currently undertaken at Curtin University in Perth, Western Australia. Once completed, the thesis will be made available in a hard-copy form in the Curtin library and in a digital form via the Australian Digital Thesis Program. I would be most grateful for you consent to the copying and communication of the work as proposed.

I look forward to hearing from you and thank you in advance for your consideration of my request.

Yours sincerely

Duy Thong Kieu

PhD student, Curtin University

Permission 4

Permission of using published material in PhD thesis

Ted Bakamjian <Tbakamjian@seg.org>

Tue 18/07/2017 9:39 PM

To: Duy Thong Kieu

Cc: Permissions <permissions@seg.org>

Dear Duy Thong Kieu,

You have SEG permission to reproduce this work in your doctoral thesis, as described in SEG policies on these pages:

<http://seg.org/Publications/Policies-and-Permissions/Permissions>

<http://seg.org/Publications/Policies-and-Permissions/Open-Access-Policy>

Please follow the guidance offered.

Thank you for publishing with SEG.

Sincerely,

Ted

Ted Bakamjian, IOM, CAE | Associate Executive Director, Knowledge Management
+1.918.497.5506 direct

[Society of Exploration Geophysicists \(SEG\)](http://www.seg.org)

8801 South Yale Avenue, Suite 500 Tulsa, OK 74137-3575 USA

On Jul 18, 2017, at 3:12 AM, Duy Thong Kieu
<duythong.kieu@postgrad.curtin.edu.au> wrote:

Dear **publisher**,

It is my understanding that SEG is the copyright holder of the following material:

Kieu, T. D., and A. Kopic. 2015, **Incorporating Prior Information into Seismic Impedance Inversion Using Fuzzy Clustering Technique**. In SEG International

Exhibition and Annual Meeting. New Orleans, USA: Society of Exploration Geophysicists.

I would like to reproduce this work in a doctoral thesis which I am currently undertaken at Curtin University in Perth, Western Australia. Once completed, the thesis will be made available in a hard-copy form in the Curtin library and in a digital form via the Australian Digital Thesis Program. I would be most grateful for you consent to the copying and communication of the work as proposed.

I look forward to hearing from you and thank you in advance for your consideration of my request.

Yours sincerely

Duy Thong Kieu

PhD Student

Curtin University

Department of Exploration Geophysics

GPO BOX U1987, PERTH WA 6845